Air Interface for Next Generation Mobile Communication Networks: Physical Layer Design

A LTE-A Uplink Case Study

Berardinelli, Gilberto

Publication date:
2010

Document Version
Publisher's PDF, also known as Version of record

Air interface for next generation mobile communication networks: Physical Layer Design

A LTE-A Uplink Case Study

Gilberto Berardinelli
Aalborg University
Denmark

A Dissertation submitted for the degree of
Doctor of Philosophy
June 2010

Supervisors:
Troels B. Sørensen, PhD,
Associate Professor, Aalborg University, Denmark.
Preben Mogensen, PhD,
Professor, Aalborg University, Denmark.

Assessment Committee:
Olav Tirkkonen, PhD,
Professor, Helsinki University of Technology, Finland.
Hyung G. Myung, PhD,
Senior Engineer, Qualcomm, USA.
Bernard Fleury, PhD,
Professor, Aalborg University, Denmark.

To my family

"What saves a man is to take a step. Then another step.
It is always the same step, but you have to take it."
Antoine de Saint-Exupéry

"Roads? Where we are going
we don't need roads..."
Emmett Brown in *Back to the future*

Summary

The ambitious data rate target of the 4th generation mobile communication systems can only be achieved by using an efficient air interface, advanced Multiple Input Multiple Output (MIMO) antenna techniques, and wide spectrum allocation. Orthogonal Frequency Division Multiplexing (OFDM) has been selected as air interface for the downlink of the Long Term Evolution - Advanced (LTE-A) systems given its flexibility and its multipath mitigation capability, while Single Carrier Frequency Division Multiplexing (SC-FDM) has been selected for the uplink. The low Peak-to-Average Power Ratio (PAPR) property of the latter guarantees higher power efficiency and extended coverage. Furthermore, a multiple component carrier (CC) structure has been agreed as a solution to cope with the wide spectrum requirement of the LTE-A systems. While the application of MIMO to OFDM is a widely researched topic, the impact of advanced schemes such as transmit diversity or precoding on a SC-FDM air interface is still disregarded.

This thesis deals with the air interface design for the uplink of 4th generation systems based on SC-FDM technology. The interaction of MIMO with SC-FDM is investigated in terms of link performance as well as its effects on the transmit waveforms. Enhancement mechanisms such as fast link adaptation and Hybrid Automatic Repeat Request (HARQ) are also included. It is known from the MIMO theory that spatial multiplexing can boost the throughput, while transmit diversity solutions improve the robustness of the data. A transmit diversity space frequency coding (SFC) algorithm where the Alamouti encoding is performed over adjacent subcarriers is shown to compromise the single carrier nature of the uplink signals. Space Time Coding (STC) has therefore to be preferred for a SC-FDM radio interface, despite of a lower flexibility. An

SFC scheme which does not increase the PAPR of the transmit waveform is also derived. Performance results obtained with Monte Carlo simulations show its effectiveness for small transport data blocks. The precoding operation, which can further enhance the spectral efficiency at low speed by exploiting array gain at the transmitter, also compromises the PAPR of SC-FDM signals, especially when it is applied on a Resource Block (RB) basis. Since wideband precoding has to be considered for SC-FDM, the precoded transmission is more advantageous in case of low frequency selective channels. A codebook of precoding matrices allowing obtaining the same link performance as the one adopted for LTE downlink while keeping the single carrier property of the uplink signals is also proposed. Regarding the comparison with the downlink, SC-FDM is outperformed by OFDM when linear receivers are used. This is due to its higher sensitivity to the noise. Receiver algorithms based on iterative detection are proposed for both cases of single stream and multi-stream transmission. Simulation results show that, the iterative detection can considerably enhance the spectral efficiency of both OFDM and SC-FDM and especially in multi-stream case, due to the removal of the interstream interference. Moreover, the iterative detection is more beneficial for SC-FDM, thus allowing to overcome the performance gap with OFDM when also receive diversity is considered. As a final topic, the transmission over multiple CCs is investigated. NxDFT-s-OFDM, which is the solution for adapting SC-FDM to a multiple CC system, is shown to preserve some PAPR gain over OFDM. The wide spectrum allocation leads to an increase of the feedback overhead which is needed to properly setup the transmission depending on the instantaneous channel conditions: the bundling of link adaptation, HARQ and precoding parameters over frequency resources is foreseen to reduce this signaling overhead and make it comparable with a single CC technology as LTE. A codeword (CW) mixing strategy across multiple CCs is therefore proposed with the aim of boosting the spectral efficiency performance when link parameters bundling is applied. The performance results show the effectiveness of such technique.

The investigations carried out in this thesis confirm SC-FDM as a valid air interface for the uplink of LTE-A; with a careful design of the transceiver chain, it can achieve indeed the same link performance of OFDM, while keeping the remarkable advantage of a higher power amplifier efficiency.

Dansk Resumé

(Abstract in Danish)[1]

Det ambitiøse mål for data raten i fjerde generations mobilkommunikationssystemer kan kun virkeliggøres ved brug af et effektivt air interface, avancerede Multiple Input Multiple Output (MIMO) antenne teknikker, og ved allokering at et bredt frekvens spektrum. Orthogonal Frequency Division Multiplexing (OFDM) er blevet valgt som air interface for downlink i Long Term Evolution - Advanced (LTE-A) systemer pga. dets fleksibilitet og evne til at reducere multipath effecter, og Single Carrier Frequency Division Multiplexing (SC-FDM) er valgt til uplink. Sidstnævntes lave Peak-to-Average Power Ratio (PAPR) egenskaber garanterer højere effektivitet og udvidet dækning. Endvidere er en multiple component carrier (CC) struktur blevet valgt som løsning på det brede spektrum krav i LTE-A. Anvendelsen af MIMO i OFDM er et udbredt forskningsemne, hvorimod effekten af avancerede teknikker såsom transmit diversity og pre-kodnings i SC-FDM air interfacet ikke er undersøgt før nu.

Denne tese beskæftiger sig med design af air interfacet for uplink delen af et fjerde generations system baseret på SC-FDM teknologi. Samspillet mellem MIMO og SC-FDM undersøges i form af link performance og påvirkningen af de transmitterede signaler. Mekanismer til forbedringer såsom fast link adaptation og Hybrid Automatic Repeat Request (HARQ) er også inkluderet. Fra MIMO teori er det kendt at rumlig multiplexing kan øge overførselshastigheden og at transmit diversity løsninger øger dataens robusthed. Det vises at en transmit diversity space frequency coding (SFC) algoritme, hvor Alamouti kodning anvendes på nærliggende subcarriers, kompromitterer de ønskede egenskaber

[1] translation by Mads Lauridsen and Anders Riis Jensen, Department of Electronics Systems, Aalborg University, Denmark

fra single carrier uplink signalet. Derfor foretrækkes Space Time Coding (STC) i et SC-FDM radio interface på trods af lavere fleksibilitet. En SFC teknik som ikke øger PAPR for det transmitterede signal udledes også. Performance resultater opnået vha. Monte Carlo simuleringer viser teknikkens effektivitet for små transport-data blokke. Pre-kodnings operationen, som yderligere kan øge den spektrale effektivitet ved lave hastigheder, ved at udnytte array gain i transmitteren, kompromitterer også SC-FDM signalets PAPR, specielt når den anvendes på Resource Block (RB) niveau. Da wideband pre-kodning skal anvendes i SC-FCM er pre-kodede transmissioner mere fordelagtige for kanaler med lav frekvens-selektivitet. Der foreslåes også en kodebog indeholdende pre-kodnings matricer, som medfører den samme link performance som i LTE downlink samtidig med at uplink signalets single carrier egenskaberne bibeholdes. Mht. en sammenligning med downlink bliver SC-FDM overgået af OFDM når lineærer modtagere anvendes. Det skyldes den højere støj-følsomhed. Der foreslåes modtage-algoritmer, baseret på iterativ detektering, for både single- og multi-stream transmissioner. Simuleringsresultater viser at den iterative dekodning kan forbedre den spektrale effektivitet markant for både OFDM og SC-FDM og specielt i multi-stream tilfældet pga. interstream interferensen fjernes. Endvidere er den iterative dekodning mere fordelagtig for SC-FDM og dermed overvindes performance forskellen ift. OFDM når også receive diversity anvendes. Endeligt undersøges transmission via flere CCs også. Det vises at NxDFT-s-OFDM, som er metoden hvormed SC-FDM kan adapteres til et system med flere CCs, bevarer en del af PAPR fordelen over OFDM. Wide spectrum allokering medfører et øget feedback overhead, hvilket er nødvendigt for at opsætte transmissionen, som afhænger af de øjeblikkelige kanalforhold: det forudses at bundtningen af link adaptation, HARQ og pre-kodnings parametre over frekvensresourcerne reducerer signal overhead og gør det sammenligneligt med en single CC teknologi som LTE. Derfor foreslås en codeword (CW) mixing strategi over flere CCs, hvor målet er at øge den spektrale effektivitet når link parameter bundling anvendes. Resultaterne viser denne tekniks effektivitet.

Undersøgelserne, som er foretaget i denne tese, viser at SC-FDM er et valid air interface for LTE-A uplink: med en omhyggeligt designet transceiver kæde kan man bestemt opnå den samme link performance som i OFDM samtidig med at de bemærkelsesværdige fordele af en højere energi effektivitet bibeholdes.

Preface and Acknowledgements

This dissertation is the result of a three years research project carried out at Radio Access Technology Section (RATE), Department of Electronic Systems, Aalborg University, Denmark, under the supervision and guidance of Associate Professor Troels B. Sørensen and Professor Preben Mogensen. This PhD research project has been sponsored by Aalborg University and Nokia Siemens Networks R&D, Aalborg, Denmark.

I would like to express my sincere gratitude to my supervisors. Their guidance has been fundamental for accomplishing the tasks of this project, and their encouragement as well as their entusiastic mood have brought invaluable energy to my daily work. I would also like to thank Kari Pajukoski from Nokia Siemens Networks, Oulu, Finland, for the interest he has always expressed towards my work, and the useful insights that have helped to lead this project in the right direction. I'm sincerely grateful to the members of the assessment committee, whose detailed comments helped in the clarification of the text throughout this dissertation.
I would like to thank the secretaries Lisbeth Schiønning Larsen and Jytte Larsen for having made the bureaucratic side of my PhD studies so easy, as well as their patience for my usual delays in handing in administrative documents.
Deep gratitude goes to Luis Ángel Maestro Ruiz de Temiño; I had the pleasure of working together with him during the first year of my PhD studies, and his professionalism has definitely contributed in speeding up this project.
It is important for me to thank Simone Frattasi and Mohammed Imadur Rahman; they have co-supervised my work for a short time, which was sufficient to

give me the “fever” of publishing papers.
Many thanks to Basuki Endah Priyanto and Carles Navarro Manchón for having been so helpful in the early stages of my work, when I started dealing with LTE related issues and with the link level simulator.
I would also like to thank my colleagues at Aalborg University and Nokia Siemens Networks for the friendly and relaxed environment, the help and the interesting technical discussions, the amazing travel experiences I shared with many of them. In no specific order, I would like to thank Luis Guilherme Uzeda Garcia, Yuanye Wang, Sanjay Kumar, Naizheng Zheng, Francesco Davide Calabrese, Gilbert Micallef, Guillaume Monghal, Oumer Teyeb, Anders Riis Jensen, Mads Lauridsen, Liu Zhen, Fan Sun, Troels Kolding, Istvan Kovacs, Hung Tuan Nguyen, Christian Rom, Daniela Laselva, Gustavo Wagner Oliveira da Costa, Viviane Silva Teixeira, Claudio Rosa, Klaus Pedersen, Andrea Cattoni, Oscar Tonelli, Claudio Coletti, Michele Polignano, Malek Boussif Celier, Hua Wang, Niels Jørgensen.
I’m grateful to the amazing international community I had the pleasure of joining, which made my stay in Aalborg so pleasant and stimulating; being in contact with so many different cultures has definitely opened up my mind and broadened my horizons. It would be nice to mention one-by-one all my international friends, but I believe it would take at least half of this report.
Most importantly, I would like to sincerely thank my family, in particular my parents Giovanna and Luigi and my sister Antonella, for their encouragement and endless love. They deserve the dedication of this thesis.
Last but not least, I would like to thank Italy, my beautiful and sick country, that pushed me not to be closed to any challenge and to look at the world with critical and uncompromising eyes.

Aalborg, June 2010

Gilberto Berardinelli

Contents

List of Figures

List of Tables

Notation

Abbreviations and mathematical conventions used in the thesis are listed below for quick reference. The abbreviations are additionally defined at their first occurrence.

Abbreviations

3GPP	3rd Generation Partnership Project
ACLR	Adjacent Channel Leakage Ratio
AGI	Antenna Gain Imbalance
AMC	Adaptive Modulation and Coding
AWGN	Additive White Gaussian Noise
BER	Bit Error Rate
BLER	Block Error Rate
BPSK	Binary Phase-Shift Keying
BS	Base Station
BW	Bandwidth
CAZAC	Constant Amplitude Zero Autocorrelation
CC	Component Carrier

CCDF	Complementary Cumulative Distribution Function
CCo	Chase Combining
CDF	Cumulative Distribution Function
CDMA	Code Division Multiple Access
CG-CAZAC	Computer Generated - Constant Amplitude Zero Autocorrelation
CM	Cubic Metric
CoMP	Coordinated Multi-Point
CP	Cyclic Prefix
CQI	Channel Quality Indicator
CRC	Cyclic Redundancy Code
CW	Codeword
DC	Direct Current
DFT	Discrete Fourier Transform
DL	Downlink
EA-STC	Extended Alamouti - Space Time Coding
EESM	Exponential Effective SIR Mapping
EVM	Error Vector Magnitude
FDD	Frequency Division Duplex
FDM	Frequency Division Multiplexing
FFT	Fast Fourier Transform
FS-STC	Frequency Switch - Space Time Coding
FSU	Flexible Spectrum Usage
GB	Guard Band
GSM	Global System for Mobile Communications
HARQ	Hybrid Automatic Repeat Request
HSDPA	High Speed Downlink Packet Access

HSPA+	High Speed Packet Access evolution
HSUPA	High Speed Uplink Packet Access
ICI	Inter-Carrier Interference
IDFT	Inverse Discrete Fourier Transform
IFFT	Inverse Fast Fourier Transform
IP	Internet Protocol
IR	Incremental Redundancy
ISI	Inter-Symbol Interference
ITU	International Telecommunication Union
LTE	Long Term Evolution
LTE-A	Long Term Evolution - Advanced
MAC	Medium Access Control
MAP	Maximum A Posteriori
MCS	Modulation and Coding Scheme
MIMO	Multiple Input Multiple Output
ML	Maximum Likelihood
MMSE	Minimum Mean Square Error
MRC	Maximum Ratio Combining
MU	Multi-User
NB	Narrow Band
OFDM	Orthogonal Frequency Division Multiplexing
OFDMA	Orthogonal Frequency Division Multiple Access
OL	Open Loop
OLLA	Outer Loop Link Adaptation
PACE	Pilot Assisted Channel Estimation
PAPR	Peak-to-Average Power Ratio
PDP	Power Delay Profile

PIC	Parallel Interference Cancellation
PS-STC	Phase Shifted - Space Time Coding
PUCCH	Physical Uplink Control Channel
PUSCH	Physical Uplink Shared Channel
QAM	Quadrature Amplitude Modulation
QoS	Quality of Service
QPSK	Quadrature Phase-Shift Keying
RAN	Radio Access Network
RB	Resource Block
RF	Radio Frequency
RME	Recursive Maximum Expansion
RRM	Radio Resource Management
Rx	Receiver
SAW	Stop And Wait
SC-FDM	Single Carrier Frequency Division Multiplexing
SC-FDMA	Single Carrier Frequency Division Multiple Access
SCM	Spatial Channel Model
SER	Symbol Error Rate
SFC	Space Frequency Coding
SIC	Successive Interference Cancellation
SIMO	Single Input Multiple Output
SISO	Single Input Single Output
SM	Spatial Multiplexing
SNR	Signal-to-Noise Ratio
SRS	Sounding Reference Signal
STC	Space Time Coding
SU	Single User

SVD	Singular Value Decomposition
TBS	Transport Block Size
TDD	Time Division Duplex
TDM	Time Division Multiplexing
Tx	Transmitter
UCI	Uplink Control Information
UE	User Equipment
UL	Uplink
UMTS	Universal Mobile Terrestrial Access
WB	Wide Band
WF	Wiener Filter
WG	Working Group
WI	Work Item
XPD	Cross-Polarization Discrimination
ZF	Zero Forcing

Mathematical Conventions

The following mathematical conventions are used throughout the thesis:

$\mathbf{A}$	Bold upper case indicates a matrix.
$\mathbf{a}$	Bold lower case indicates a matrix.
A, a	Non-bold indicates a scalar.
$E(x)$	Expected value of random variable x.
$(\cdot)^*$	Complex conjugate.
$(\cdot)^T$	Transpose.
$(\cdot)^H$	Hermitian, *i.e.* complex conjugate transpose.
$(a)^x$	a to the power of x.
$\lvert\cdot\rvert$	Absolute value.
$\lVert\cdot\rVert$	Euclidean norm.
$\lVert\cdot\rVert_F$	Frobenius norm.
$min(a)$	Minimum value of a.
$max(a)$	Maximum value of a.
$diag(\cdot)$	Square diagonal matrix.
$log_a(x)$	Logarithm of x to the base a.
$ln(x)$	Natural logatithm.
$mod\, N$	Modulo N in modular arithmetic.

Chapter 1

Introduction

The advent of the wireless communication technology on the mass market has widely affected the daily life, with deep social implications. The possibility of communicating with voice services while being on the move, which was given by the second generation mobile networks [1], is however obsolete nowadays. The parallel growth of the data communication, driven by the Internet phenomenon, has progressively raised the customer demand for high data rate services as well as the expectations in terms of quality of service (QoS). The synergy between broadband data traffic and mobile communication technology is therefore foreseen to match with the mass market demand. *Always get connected* has to be considered as the new paradigm for the modern wireless networks, which are expected to deliver high data rate to the end user to supply the demand of fast browsing as well as multimedia communication. Providing high data rate services through the wireless medium is however much more challenging than in traditional wireline mode. The air interface of the modern wireless system has to be designed by taking into account the inter-user orthogonality as well as the counteraction of the negative effects of the wireless channel; furthermore, multiple antenna elements might be needed to boost the throughput. Given the hardware limitation in the handeld devices, the complexity of the algorithms for the wireless signal generation as well as the data detection has to be kept limited while still ensuring high performance. In case of uplink transmission, low power consumption and therefore longer terminal standby time is a further constraint to be taken into account in the practical design.

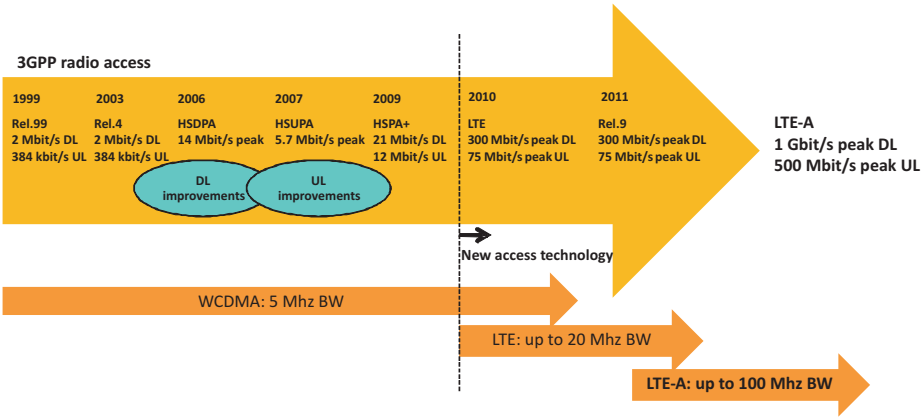

Figure 1.1: Evolution of the 3GPP radio access technologies.

In the last decade several evolutions of mobile systems standards have tried to progressively cope with the increasing demand of data services. For instance, the 3rd Generation Partnership Project (3GPP) has been defining the specifications of the wireless communication systems within the scope of the International Mobile Telecommunications-2000 project of the International Telecommunication Union (ITU). Its work is based on evolved Global System for Mobile Communications (GSM) specifications, and the aim is to include high data rate transmission with high mobility besides traditional voice services [2]. The timeline evolution of the 3GPP radio access technology is shown in Figure 1.1. The first Release 99 specified the 3rd Generation Universal Mobile Terrestrial Access (UMTS) radio networks, based on Code Division Multiple Access (CDMA) air interface [3], targeting peak data rates of 2 Mbit/s in the downlink and 384 kbit/s in the uplink [4]. While the successive Release 4 only added specific all-IP Core Network features, Release 5 defined the specifications of High Speed Downlink Packet Access (HSDPA), which delivers higher downlink data rate by exploiting advanced features such as adaptive modulation and coding (AMC), fast packet scheduling and link layer retransmissions [5]. Release 6 also boosts the uplink performance by specifying the High Speed Uplink Packet Access (HSUPA) requirements. High Speed Packet Access evolution (HSPA+) exploits Multiple Input Multiple Output (MIMO) antenna technology as well as the option of an all-IP architecture. The Long Term Evolution (LTE) standard further pushes the upper data rate and is based on a novel radio technology [6]. LTE has to be considered as the last step towards the 4th generation, the LTE-Advanced standard, that will fully overcome the performance gap with the traditional broadband wireline connection in a user perspective [7].

1.1 From LTE to LTE-A

The first release (Release 8) of LTE has been frozen in December 2008 [8]. The next Release 9 mostly focuses on some minor enhancement as well as LTE/UMTS interoperability, while the specification of LTE-A is currently being elaborated in Release 10. LTE supports peak data rates of 300 Mbit/s in the downlink and 75 Mbit/s in the uplink to be achieved within a 20 MHz bandwidth, as well as user plane latency of 10 ms and control plane latency of less than 100 ms [8].

LTE-A aims to further enhance these targets, in order to ensure long term competiveness in mobile broadband communication [7]. The peak data rates are here set to 1 Gbit/s in the downlink and 500 Mbit/s in the uplink. The peak spectral efficiency target is set to 30 bits/s/Hz in the downlink and 15 bits/s/Hz in the uplink. Also average spectrum efficiency and cell edge throughput targets for different scenarios have been defined, as well as mobility support up to 350 kmph. The control plane latency has to be decreased to 50 ms in the transition from Idle mode to Connected mode, and to 10 ms in the transition from a dormant state to Connected mode. Similarly, also the user plane latency has to be reduced in situations where the user has not a valid scheduling assignment, or it needs to synchronize and obtain a scheduling assignment. For further details, we refer to [7]. The possibility of delivering the promised high data rates of LTE-A can be accomplished only by exploiting several advanced technical features. In the following subsections, we will briefly introduce the main link layer characteristics of LTE-A.

1.1.1 Air interface: OFDMA and SC-FDMA

Orthogonal Frequency Division Multiple Access (OFDMA), which is based on Orthogonal Frequency Division Multiplexing (OFDM)[1], has been selected as the downlink multiple access scheme since Release 8 [8]. In OFDM the data symbols are mapped over narrowband subcarriers which are transmitted in parallel over the wireless channels [9]. Furthermore, a guard band is added at the beginning of each OFDM symbol to remove the effect of the intersymbol interference. This leads to an efficient mitigation of the negative effects of the multipath fading channel. High flexibility in the resource allocation is also ensured by the orthogonality of the subcarriers, since each user accesses disjoint sets of

[1] throughout this report, we refer to Orthogonal Frequency Division Multiplexing (OFDM) to denote the signal generation, and to Orthogonal Frequency Division Multiple Access (OFDMA) to denote the multiplexing of OFDM signals by several users. The same denomination holds for SC-FDM/SC-FDMA.

them. Nevertheless, the time domain superposition of narrowband signals can generate large envelope variations in the resultant waveform: highly dynamic power amplifiers at the transmitter are necessary to cope with the high Peak-to-Average Power Ratio (PAPR) of the OFDM signals in order to avoid distortion due to the incurring of non linearities. This makes OFDM unsuitable for the uplink transmission, where Single Carrier Frequency Division Multiple Access (SC-FDMA) has been selected. SC-FDMA is based on Single Carrier Frequency Division Multiplexing (SC-FDM) and exploits similar benefits as OFDM, at the same time keeping low power envelope fluctuations since the data symbols are sent serially in the time domain [10]. The baseline principles of OFDM and SC-FDM are illustrated in Figure 1.2. In January 2009, both OFDMA and SC-FDMA have been also confirmed as multiple access schemes for LTE-A [11].

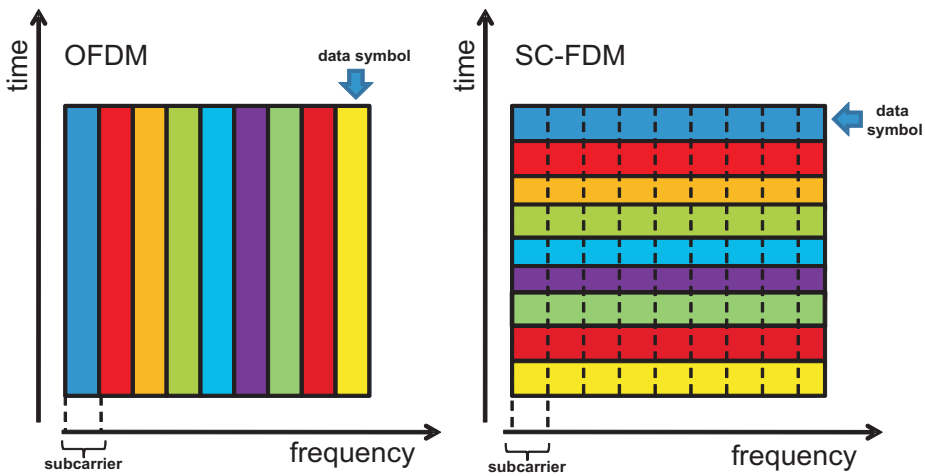

Figure 1.2: OFDM and SC-FDM principles.

1.1.2 MIMO

The achievement of the downlink data rate target of LTE makes essential the usage of Multiple Input Multiple Output (MIMO) antenna techniques [12]. Intuitively, when multiple antennas are available on both transmitter and receiver side, it becomes possible to enhance the capacity of the wireless link since multiple data streams can be sent over the same time-frequency resources (spatial multiplexing) [13]. At the same time, the multiple antennas can offer additional degrees of freedom to enhance the reliability of a single data stream (transmit diversity)[14]: this results to be particularly advantageous in case of poor radio link conditions. Furthermore, the MIMO performance can be further enhanced

when some channel state information is available at the transmitter, through a channel-aware *precoding* of the data streams [15]. In most of the cases the channel state information at the transmitter can be achieved only by using feedback signaling. We therefore refer to closed loop MIMO in case of availability of a feedback channel, while open loop MIMO solutions typically do not exploit any channel state information.

Table 1.1 shows the LTE and LTE-A antenna configurations. In LTE downlink up to 4 transmit antennas are to be supported, while in LTE uplink only single transmit antenna schemes have been standardized [8]. The higher target data rate of LTE-A leads to an extension of the downlink MIMO configuration up to 8x8, while also MIMO solutions are to be applied in the uplink.

In order to justify the MIMO adoption in LTE-A uplink, let us elaborate on the achievable spectral efficiency in this standard. The frame duration in LTE-A is fixed at 1 ms and consists of 14 OFDM/SC-FDM symbols [8]. By assuming the following notation:

- N_T: number of transmit antennas;
- N_{sub}: number of user subcarriers;
- B_{sel}: number of bits per symbol for the highest order modulation and coding scheme;
- ECR_{sel}: coding rate for the highest order modulation and coding scheme;
- T_F: frame duration;
- N_{sym}: number of OFDM/SC-FDM symbols in a frame;
- W: transmission bandwidth in Hz;
- Ov: fractional overhead due to the pilots for the channel estimation [8];

the maximum spectral efficiency is therefore given by

$$S_{max} = \frac{N_T \times N_{sub} \times B_{sel} \times ECR_{sel} \times N_{sym} \times (1 - Ov)}{T_F \times W} \tag{1.1}$$

Assuming no pilot overhead and 64QAM with coding rate 4/5 as the highest order modulation and coding scheme, it can be easily shown that a maximum spectral efficiency of 16.128 bits/s/Hz is achievable with 4 transmit antennas, thus overcoming the LTE-A uplink target. However, usually the 4th and the 11th

Table 1.1: LTE/LTE-A antenna configurations

LTE		LTE-A	
downlink	uplink	downlink	uplink
SISO	SISO	SISO	SISO
1x2	1x2	1x2	1x2
1x4	1x4	1x4	1x4
2x2	-	2x2	2x2
2x4	-	2x4	2x4
4x4	-	4x4	4x4
-	-	4x8	-
-	-	8x8	-

symbol of the frame are dedicated to the pilot symbols for channel estimation at the receiver. This results in an overhead equal to 14.29%, which lowers the maximum spectral efficiency to 13.824 bits/s/Hz. The LTE-A uplink spectral efficiency target cannot therefore be achieved when pilot symbols for channel estimation are sent in each frame. However, if the channel is slowly variant, the constraint of estimating its frequency response at each frame can be relaxed. Assuming that only a frame out of 3 carries pilots, the resultant upper spectral efficiency is equal to 15.36 bits/s/Hz. A solution for achieving higher spectral efficiency while keeping pilot symbols in each frame would be, of course, increasing the coding rate: with 64QAM 7/8 we obtain a maximum value of 15.12 bits/s/Hz. Note that both spatial multiplexing and transmit diversity modes, as well as open/closed loop options, have to be considered to cope with a wide range of user conditions.

1.1.3 Transmission over multiple component carriers

The LTE bandwidth (20 MHz) is not sufficient to achieve the ambitious data rate target of LTE-A. In principle, an upper data rate of 1 Gbit/s could be supported by a bandwidth extension up to 40 MHz. However, the necessity of ensuring high data rates to a number of users within the cell to enhance also cell capacity and coverage further boosts the bandwidth requirement: it has been therefore agreed that LTE-A has to support a system bandwidth up to 100 MHz [7]. Furthermore, LTE-A has to be backwards compatible with the previous LTE to ensure coexistence of both technologies, at the same time minimizing the standardization efforts. As shown in Figure 1.3, the 100 MHz bandwidth

is therefore divided in 5 Component Carriers (CCs), each of them keeping the LTE numerology for what concerns subcarrier spacing as well as number of subcarriers. An LTE-A terminal can access contiguous CCs or non contiguous CCs depending on flexible spectrum usage policies as well as scheduling decisions, while any LTE terminal can access a single CC only.

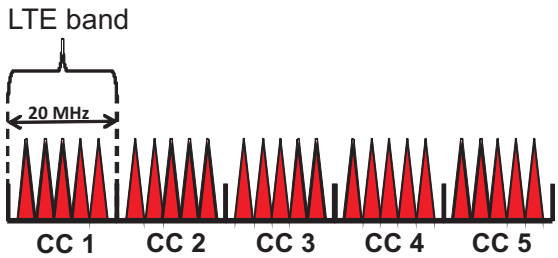

Figure 1.3: LTE-A bandwidth structure.

1.1.4 Advanced Link Layer Features

In both LTE and LTE-A, high spectral efficiencies can be achieved by using a wide set of link layer features aiming to dynamically adapt the transmission parameters to the average or instantaneous radio link conditions. The most common link level techniques are described in the following:

- **AMC**. Various modulation schemes (QPSK, 16QAM, 64QAM) with different coding rates are supported by LTE and LTE-A. The transmitter should dynamically apply at each transmission the Modulation and Coding Scheme (MCS) leading to highest expected throughput given the average or instantaneous channel conditions [16]. AMC increases therefore the signaling overhead since the proper MCS has to be selected at the receiver, and its index fed back to the transmitter. Updating the MCS at each frame can be therefore very demanding in terms of signaling, but necessary to cope with channels having wide Signal-to-Noise ratio (SNR) dynamics. On the contrary, for channels having low SNR dynamics the selection of the MCS can be done over the average channel conditions, thus relaxing the feedback requirements.

- **Adaptive transmission bandwidth**. The width and the position in the spectrum of the transmission band can be updated in each frame. The decision is usually taken by the scheduler, which locates the users in the spectrum with the aim of enhancing the maximum or the average cell throughput. The scheduling decisions are tipically based on a Proportional

Fair (PF) metric [17], aiming at maximizing the throughput while keeping some degrees of fairness among the users. Also QoS policies might affect the scheduling decisions. The transmitter should be therefore able to dynamically locate the portion of data to be sent across the whole system bandwidth.

- **Hybrid Automatic Repeat Request (HARQ)**. It is basically a fast link level retransmission strategy [18]. It requires a feedback message to inform the transmitter whether the previously sent data block has been successfully detected. A predefined number of attempts for the transmission of each data block is allowed. HARQ combines the received data block in a next attempt with the previous one to increase the reliability of the delivered data stream. The fact that this operation is carried out at the physical layer of the protocol stack reduces the latency with respect to traditional ARQ protocols at Medium Access Control (MAC) layer.

1.2 Towards an LTE-A Uplink link layer interface design

An uplink LTE-A transmitter is adopting the SC-FDM technology, whose main selling point is the low PAPR of the transmit signals [10]. The PAPR of the transmit waveforms determines the bias point and the efficiency of the power amplifier: for a given output power, a low PAPR requires a small input backoff, with remarkable benefits in terms of reduced power consumption. That makes the SC-FDM technology extremely advantageous for the uplink transmission, given the battery limitations in the user equipment. Furthemore, the low PAPR property of the uplink signals can extend the cell coverage. This is because in poor radio link conditions (i.e., user at the cell edge), the transmitter can generate waveforms having higher average power without incurring signal distortion.

However, it has been shown that OFDM generally outperforms SC-FDM in terms of spectral efficiency when linear receivers are used [19]; this is because SC-FDM systems suffer from an effect called “noise enhancement”, which degrades the estimation of the data symbols in the receiver. The “noise enhancement” of the SC-FDM technology leads to lower cell throughput in the uplink direction than in the downlink when the allocated resources are the same. Smarter receiver algorithms are therefore to be designed to overcome the noise enhancement issue while keeping reasonable complexity.

It has been mentioned that the LTE-A uplink air interface is expected to support different MIMO algorithms. Spatial multiplexing, transmit diversity and

precoding solutions are to be included, in both open loop and closed loop modes. This allows to achieve high performance at different SNRs as well as different mobility conditions. The suitability of the known MIMO algorithms for LTE-A uplink has therefore to be evaluated by assuming the SC-FDM radio interface. While in open loop spatial multiplexing mode the data streams are sent over the channel without any manipulation on the transmit waveforms, in more advanced schemes such as transmit diversity and precoding the MIMO encoder can affect the low PAPR property of the SC-FDM signal. For instance, in open loop transmit diversity mode, the MIMO encoder modifies the position of the frequency samples to be sent over each antenna, thus altering the signal properties in the time domain. Similarly, in precoded transmission the data streams are multiplied by a complex matrix, which performs a linear combination of the original signals. Furthermore, in most of the cases precoded transmission requires a feedback channel to inform the transmitter on the precoding matrix to be used. The performance of precoding techniques is depending on the number of available matrices; obiously, the wider the set of precoding matrices, the better is the expected performance since the matrix which better matches with the instantaneous channel conditions can be selected. However, a wide set of precoding matrices affects both the size of the feedback message, which should be kept small, and the complexity of the algorithm for the matrix selection. A smart design has therefore to deal with a tradeoff between feedback overhead and achievable performance.

The feedback signaling is expected to dramatically increase also when transmission over multiple CCs occurs. This is because the parameters which are needed to properly setup the communication chain (i.e., MCS index, HARQ ACK/NACK messages, precoding matrices) are now to be sent per each CC. Of course, these parameters can be bundled across multiple CCs, but this comes at the expense of lower throughput since the adaptation towards the channel conditions is partly lost. Solutions aiming to keep low feedback overhead while still providing high spectral efficiency are definitely appealing in a practical design. Note that the transmission over multiple CCs also affects the PAPR of the transmit signals, since their single carrier property is lost. The suitability of a SC-FDM based air interface in such situations is therefore to be evaluated.

1.3 Thesis objectives

This PhD project aims at designing the transceiver chain of a MIMO system based on SC-FDM technology. The work is phrased in the context of the upcoming LTE-A uplink standard in order to ensure the suitability of the discussed concepts in a real system. The work-scope is illustrated in Figure 1.4. The

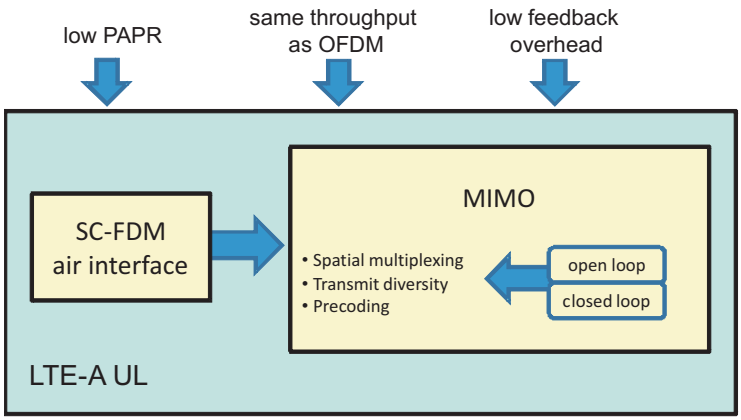

Figure 1.4: Work scope of the research project.

design of MIMO solutions for LTE-A uplink raises further issues with respect to the downlink, which has already been faced in the LTE standard. It would not be possible to blindly apply in the uplink design the MIMO features included in the LTE downlink standard, since they were not optimized for a SC-FDM-based radio interface. This means, the existing solutions might have a different impact on a SC-FDM-based system than on a OFDM-based one. Furthermore, they might affect the low PAPR property of the uplink signals, thus reducing the main benefit of SC-FDM technology.

The suitability of the existing MIMO techniques for a SC-FDM based radio interface is therefore to be evaluated. The main performance targets are the spectral efficiency and the power envelope fluctuations of the transmit signals. The achievement of high spectral efficiency involves both the transmitter and the receiver design, since the transmit signals can be shaped in a way to cope with the experienced link conditions, and smart detection algorithms in the receiver can counteract the detrimental effect of the wireless channel. For instance, the noise enhancement issue of the SC-FDM technology should be overcome at the receiver, in order to obtain the same performance of the OFDM-based downlink transmission. Realistic constraints as channel estimation errors and radio frequency impairments have to be taken into account in order to ensure the feasibility for the practical implementation.

In case the existing approaches have limited impact when applied in a MIMO SC-FDM system or they modify the nature of the single carrier signals, new solutions have to be designed to cope with such flaws. Note that the new solutions should be easily compatible with the concepts of the previous LTE Release 8, in order to minimize the standardization efforts. The reasonable

complexity of the algorithms for the signal generation as well as for the detection is a further constraint to be considered.

To sum up, the PhD project has the following main objectives:

- investigate the suitability of known MIMO schemes for LTE-A uplink;
- optimize the performance of open/closed loop MIMO transmission assuming the SC-FDM technology;
- enhance the SC-FDM performance by exploiting advanced solutions in the receiver side for both single and multiple stream transmission;
- keep low feedback overhead in case of closed loop transmission as well as transmission over multiple CCs.

This PhD work is well aligned with the 3GPP standardization, which is currently evaluating and defining techniques and algorithms to be adopted in LTE-A uplink.

1.4 Scientific Methodology

The project involves both transmitter and receiver design and optimization, and therefore several branches of the wireless physical layer research area. Since a complete analytical investigation would be unfeasible given the complexity of the system as well as the number of involved parameters, a detailed link level simulator for LTE-A uplink has been developed by extending the work of former PhD students, and the presented algorithms are evaluated via Monte Carlo simulations. The simulator is calibrated according with the 3GPP specifications concerning layer 1 multiplexing and channel coding [20]. The simulation parameters (e.g., bandwidth configurations, channel models, ...) are also set to be compliant with the standard specifications. Each of the research subareas involved in this PhD project will be approached by following the same methodology, described in the following steps:

- Survey on state-of-the-art about the problem and theoretical study of the solutions already proposed in literature.
- Selection of the most promising solution(s) for the specific case of a LTE-A uplink system.

- Analytical modeling of the solution(s) found in step 2.
- Implementation and performance evaluation of the solution(s).
- Research and development of new or modified approaches that can overcome the flaws of the previously studied ones, optimizing the performance for the LTE-A uplink case.
- Implementation and performance evaluation of new solutions.
- Dissemination to industry of the results obtained in order to get feedback on the practicality of the proposed solutions.

1.5 Outline of the dissertation and contributions

This dissertation consists of 8 chapters. A general overview of each chapter is presented here, and the main contributions are highlighted in relation to this.

Chapter 2 introduces OFDM and SC-FDM and provides some baseline link level performance results. Issues related to the resource allocation in multi-user scenarios are described. A scheduling algorithm which assumes localized allocation in the spectrum of the user data is proposed for SC-FDMA.

Contributions: Derivation of the analytical expression of the SC-FDM time domain signal. Modeling of the OFDM/SC-FDM transceiver chain and link level evaluation. Development of a simplified multi-user simulator. Design and implementation of a new scheduling algorithm for SC-FDMA.

Chapter 3 introduces the MIMO concept in a theoretical framework, and discusses its implementation in LTE-A uplink. The transceiver chain for open loop spatial multiplexing is presented and evaluated, also considering constraints as real channel estimation and radio frequency impairments. Advanced features as fast link adaptation and HARQ are also presented and included in the evaluation.

Contributions: Optimization of the linear receiver to remove the bias introduced by the Minimum Mean Square Error (MMSE) equalizer. Definition of the fast link adaptation strategy for SC-FDM. Design of a channel estimator suitable for a pilot pattern based on Constant Amplitude Zero Autocorrelation (CAZAC) sequences. Extensive link evaluation of open loop MIMO solutions.

Chapter 4 deals with open loop transmit diversity solutions for LTE-A uplink. Approaches based on Space Frequency Coding (SFC) and Space Time Coding

(STC) are presented and evaluated in terms of link performance as well as their effect on the envelope of the trasmit signals. Further SFC solutions are derived starting from the single carrier sequences in the time domain.

Contributions: Implementation of traditional SFC/STC. Design and evaluation of SFC solutions keeping the low PAPR property of the SC-FDM waveforms. Evaluation of further transmit diversity solutions for 4 transmit antennas.

Chapter 5 focuses on the design of precoded MIMO solutions for LTE-A, considering both Frequency Division Duplex (FDD) and Time Division Duplex (TDD) modes. Ideal solutions based on the singular value decomposition (SVD) of the channel are taken as an upper bound for more realistic approaches based on a limited codebook of precoding matrices. The performance of the codebook adopted in LTE downlink is presented and a new codebook which does not increase the PAPR of the transmit signals is designed and evaluated for different antenna patterns.

Contributions: Derivation of an SVD-based codebook based on the quantization of the right singular vectors of the channel matrix. Extensive link evaluation of the performance of the LTE codebook. Design and evaluation of a low-PAPR codebook specific for SC-FDM air interface. Design and evaluation of a precoding pilots - based algorithm to be adopted in TDD mode.

Chapter 6 faces the design of advanced receivers based on iterative detection with the aim of enhancing the SC-FDM performance and thus overcoming the performance gap with OFDM. Solutions for single and multiple data stream transmission are proposed.

Contributions: Design of a new single stream turbo receiver with adaptive coefficients. Implementation of MIMO turbo receiver with parallel and successive interference cancellation. Definition of a new turbo processing strategy with limited complexity merging both single and multiple stream detection.

Chapter 7 deals with the transmission over multiple CCs. The focus is on the bundling of the link level parameters across multiple CCs, in order to reduce the feedback overhead and make it comparable with the one of Release 8. Two codeword mixing strategies with the aim of reducing the performance losses due to the link parameters bundling are proposed and evaluated.

Contributions: Evaluation of the power envelope fluctuations of uplink signals generated over multiple CCs. Optimization of the link adaptation when link parameters bundling is considered. Optimization of turbo receiver with HARQ bundling. Design and evaluation of two new codeword mixing strategies aiming

at improving the spectral efficiency performance with link parameters bundling.

Finally, Chapter 8 summarizes the main achievements and states the future work.

1.6 Publications

The following articles (in chronological order) have been authored or co-authored during the PhD studies:

- G. Berardinelli, B. E. Priyanto, T. B. Sørensen, and P. Mogensen, "Improving SC-FDMA performance by Turbo Equalization in UTRA LTE uplink," IEEE 67th Vehicular Technology Conference, pp.2557-2561, May 2008.
- L. A. Maestro Ruiz de Temiño, G. Berardinelli, S. Frattasi, P. Mogensen, "Channel aware scheduling algorithms for SC-FDMA in LTE," IEEE 19th International Symposium on Personal, Indoor and Mobile Radio Communications, pp.1-6, September 2008.
- G. Berardinelli, L. A. Maestro Ruiz de Temiño, S. Frattasi, M. Imadur Rahman, P. Mogensen, "OFDMA vs. SC-FDMA: performance comparison in Local Area IMT-A Scenarios," Special Issue of IEEE Wireless Communications Magazine on Recent Advances and Evolution of WMAN and WLAN Standards, pp.64-82, October 2008.
- L. A. Maestro Ruiz de Temiño, G. Berardinelli, S. Frattasi, K. Pajukoski, P. Mogensen, "Single-User MIMO for LTE-A Uplink: performance evaluation of OFDMA vs. SC-FDMA," IEEE Radio and Wireless Symposium, pp.304-307, January 2009.
- B. E. Priyanto, G. Berardinelli, T. B. Sørensen, "Single-Carrier Transmission for UTRA-LTE Uplink," Handbook of Long Term Evolution of 3GPP Radio/Cellular Technology, pp.181-212, Borko Furht, Syed A. Ahson, Boca Raton, Florida: CRC Press, April 2009.
- G. Berardinelli, L. A. Maestro Ruiz de Temiño, S. Frattasi, T. B. Sørensen, P. Mogensen, K. Pajukoski, "On the Feasibility of Precoded Single User MIMO for LTE-A Uplink," Journal on Communications, Special Issue on Wireless Gigabit Technologies, pp.155-163, April 2009.
- G. Berardinelli, C. Navarro Manchón, L. Deneire, T. B. Sørensen, P. Mogensen, K. Pajukoski, "Turbo Receivers for Single User MIMO LTE-A Uplink", IEEE 69th Vehicular Technology Conference, pp.1-5, April 2009.

- G. Berardinelli, T. B. Sørensen, P. Mogensen, K. Pajukoski, "Precoded multirank transmission with linear receivers for LTE-A uplink," IEEE 70th Vehicular Technology Conference, pp.1-5, September 2009 (nominated for the Best Student Paper Award).
- G. Berardinelli, T. B. Sørensen, P. Mogensen, K. Pajukoski, "SVD-based vs. Release 8 codebooks for Single User MIMO LTE-A Uplink," in the Proc. of IEEE 71th Vehicular Technology Conference, May 2010.
- G. Berardinelli, T. B. Sørensen, P. Mogensen, K. Pajukoski, "Link parameters bundling across multiple Component Carriers in LTE-A Uplink," in the Proc. of IEEE 71th IEEE Vehicular Technology Conference, May 2010.
- G. Berardinelli, T. B. Sørensen, L. A. Maestro Ruiz de Temiño, P. Mogensen, K. Pajukoski, "Open Loop Transmit Diversity solutions for LTE-A Uplink," in the Proc. of 2010 European Signal Processing Conference, August 2010.
- G. Berardinelli, T. B. Sørensen, P. Mogensen, K. Pajukoski, "Transmission over Multiple Component Carriers in LTE-A Uplink," IEEE Wireless Communication Magazine, to be published.
- G. Berardinelli, T. B. Sørensen, P. Mogensen, K. Pajukoski, "Low Cubic Metric Codebook for MIMO SC-FDM," IEEE Wireless Communication Magazine, planned for submission.

Chapter 2

OFDM(A) and SC-FDM(A) principles and baseline evaluation

2.1 Introduction

Modern wireless networks aim at achieving high data rate transmission by/to several users sharing a limited pool of physical resources and experiencing different SNR conditions. This can be obtained by establishing efficient rules for multiplexing the users along the available resources, as well as by designing signal waveforms which are robust to the negative effects of the multipath channel.

Third generation networks are based on Code Division Multiple Access (CDMA) [3]. In this scheme, users share the same time-frequency slots and are multiplexed in the code domain. By defining families of orthogonal codes, it would possible in principle to resolve the signals of different users in the receiver. However, the lack of fully-orthogonal codes leads to an inter-user interference which increases with the number of users. This may reduce the overall capacity of the cellular network.

Orthogonal Frequency Division Multiple Access (OFDMA), which is based on

Orthogonal Frequency Division Multiplexing (OFDM), has been instead adopted for the downlink in the 4th generation mobile communication systems. In this scheme, the users are transmitting in dedicated frequency resources as in traditional frequency division multiplexing (FDM) mode. However, the user signal is generated as a superposition in the time domain of the narrowband waveforms generated in fractions of the spectrum. This allows to convert the high data rate transmission in parallel low data rate transmissions, with remarkable benefits in terms of multipath mitigation [9]. Furthermore, the orthogonality in the frequency domain allows to exploit flexible channel dependent scheduling algorithms. As a drawback, the time domain superposition of narrowband signals may generate large envelope variations in the resultant waveform. This leads to the necessity of applying a large backoff at the input of the power amplifier in order to avoid signal distortions.

The reduced efficiency due to the large backoff in the power amplifiers can be a severe constraint in case of limited power supply. Single Carrier Frequency Division Multiple Access (SC-FDMA), which is based on Single Carrier Frequency Division Multiplexing (SC-FDM), has been therefore adopted for the uplink of LTE and LTE-A given the power constraints in the user equipment (UE). In this scheme, the data symbols are transmitted serially in the time domain as in traditional single carrier systems, thus avoiding wide envelope variations [10]. Furthermore, the SC-FDM signal can be generated as a modified form of the OFDM signal [19], thus exploiting similar benefits in terms of flexibility and robustness to the multipath.

In this chapter, OFDM(A) and SC-FDM(A) are introduced and compared in terms of link performance as well as flexibility in the resource allocation. Advantages and disadvantages of both solutions are widely discussed. The aim is to provide the baseline results which will be used as the reference for the next chapters dealing with MIMO transmission.

The chapter is structured as follows. Section 2.2 describes the generation of OFDM and SC-FDM signals. Section 2.3 presents two widely used measures of the OFDM/SC-FDM power envelope fluctuations. A detailed link level evaluation is carried out in Section 2.4, while issues related to the bandwidth allocation among several users are faced in Section 2.5. Finally, the summary is given in Section 2.6.

2.2 OFDM and SC-FDM signal generation

In OFDM the data symbols modulate narrowband subcarriers, which are transmitted in parallel over the wireless channel. An analog realization of the OFDM modulator would therefore consist of N sinusoidal generators oscillating at different frequencies, where N is the number of data symbols to be sent. This complex solution can be efficiently replaced by an Inverse Fast Fourier Transform (IFFT) block, which generates digitally the time domain waveform. In SC-FDM, the data symbols are transmitted instead in the time domain. However, the SC-FDM signal can be generated by using the same transmitter chain of OFDM.

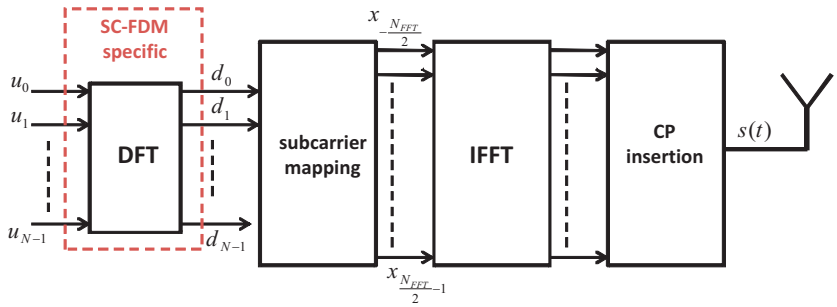

Figure 2.1: OFDM/SC-FDM signal generation.

The baseband OFDM/SC-FDM signal generation is shown in Figure 2.1. For SC-FDM, an additional Discrete Fourier Transform (DFT) block is present. This block spreads each symbol belonging to the N-size data vector $\mathbf{u}$ over the whole used subcarrier set. The elements of the output vector $\mathbf{d}$ can be therefore expressed as:

$$\mathbf{d}(i) = \frac{1}{\sqrt{N}} \sum_{k=0}^{N-1} \mathbf{u}(k) e^{-j\frac{2\pi k i}{N}} \tag{2.1}$$

for $i = 0, \cdots, N-1$.

For OFDM instead, $\mathbf{d} = \mathbf{u}$. The vector $\mathbf{d}$ is then mapped on the $\mathbf{x}$ vector which adapts the size of $\mathbf{d}$ to the IFFT size. Assuming $\mathbf{m}$ as the vector of the positions of the samples of $\mathbf{d}$ in $\mathbf{x}$, the elements of the latter can be written as:

$$\mathbf{x}(q) = \begin{cases} \mathbf{d}(I(q)), & \text{if } q \in \mathbf{m} \\ 0, & \text{otherwise} \end{cases} \tag{2.2}$$

for $q = -\frac{N_{FFT}}{2}, \cdots \frac{N_{FFT}}{2} - 1$, where $I(q)$ returns the index of the vector $\mathbf{m}$ where q is mapped, and N_{FFT} is the IFFT size. For SC-FDM, only the following subcarrier mapping modes are defined:

1. *localized mode*:
$$\mathbf{m} = p : 1 : (p + N - 1) \tag{2.3}$$
where p is the index of $\mathbf{x}$ where the first element of $\mathbf{d}$ is mapped. The elements of $\mathbf{d}$ are therefore located in a contiguous portion of the bandwidth.

2. *distributed mode*:
$$\mathbf{m} = p : S : (p + S \cdot N) \tag{2.4}$$
where S is a predefined spreading factor. The elements of $\mathbf{d}$ are here located in periodic positions on the available bandwidth.

Even though the distributed mode achieves higher frequency diversity, it results to be highly sensitive to the frequency offset between different users [21]. Throughout this dissertation, we will only consider SC-FDM with localized mode.

By assigning subcarrier blocks on a user basis, it is possible to achieve inter-user orthogonality. The samples $\mathbf{x}$ passes through the IFFT block, and finally, a Cyclic Prefix (CP) is added at the beginning of the symbol by copying the last N_{CP} samples of the output vector.

The resultant OFDM/SC-FDM continuous-time signal can be expressed as:

$$s(t) = \frac{1}{\sqrt{N}} \sum_{k=-\frac{N_{FFT}}{2}}^{\frac{N_{FFT}}{2}-1} \mathbf{x}(k) e^{j2\pi k \frac{t - T_{CP}}{T_S N_{FFT}}} \tag{2.5}$$

for $0 \leq t \leq T_{OFDM}$, where T_S is the sampling period of the system, $T_{CP} = N_{CP} \cdot T_S$ and $T_{OFDM} = N_{FFT} \cdot T_S + T_{CP}$.

Since the samples $\mathbf{x}$ are transmitted in parallel in the time domain, they are expected to experience flat fading, provided the subcarrier bandwidth $\Delta f = 1/(T_S N_{FFT})$ is smaller than the coherence bandwidth of the channel. This allows the use of a simple one-tap-equalizer in the frequency domain.

Furthermore, the insertion of the CP allows to remove the residual intersymbol interference (ISI) as well as the intercarrier interference (ICI) at the expense of

some spectral efficiency loss. Note that, since the CP is generated as a cyclic copy of the last part of the OFDM/SC-FDM time symbol, the orthogonality between subcarriers is preserved [9].

2.3 Envelope fluctuations in OFDM/SC-FDM

Since the OFDM signal is generated as a superposition of narrowband sinusoidal waveforms, its envelope may show wide variations with respect to the average power. This is because the sinusoidal signals on each subcarrier can be added coherently, resulting in high peaks of the instantaneous power. The large envelope fluctuations can introduce distortions in the signal sent over the air when exceeding the linear region of the power amplifier. The easiest way to avoid this distortion is to introduce an input backoff to the power amplifier. This however reduces its power efficiency, measured as the ratio of the transmitted power to the power dissipated in direct current (DC). Several further solutions based on clipping and filtering the resultant waveform have been developed to reduce the power amplitude of the OFDM signal and thereby avoid undesired distortions [22]. However, they come at the expense of poorer spectral efficiency performance, as well as increased out of band emissions [23].

Regarding SC-FDM, it can be shown that its time domain samples can be written as:

$$\mathbf{s}(i) = \tilde{\mathbf{v}}(i) e^{j\frac{2\pi i p}{N_{FFT}}} \tag{2.6}$$

for $i = -\frac{N_{FFT}}{2}, \cdots, \frac{N_{FFT}}{2} - 1$, where

$$\tilde{\mathbf{v}}(i) = \frac{1}{\sqrt{N}} \sum_{z=0}^{N-1} \mathbf{d}(z) e^{j\frac{2\pi i z}{N_{FFT}}} = \frac{1}{N} \sum_{z=0}^{N-1} \sum_{q=0}^{N-1} \mathbf{u}(q) e^{-j\frac{2\pi z(qN_{FFT} - iN)}{N_{FFT}N}} \tag{2.7}$$

It can be easily verified that

- for $q = i\frac{N}{N_{FFT}}$,

$$\tilde{\mathbf{v}}(i) = \mathbf{u}\left(i\frac{N}{N_{FFT}}\right); \tag{2.8}$$

- for $q \neq i\frac{N}{N_{FFT}}$

$$\tilde{\mathbf{v}}(i) = \sum_{q=0}^{N-1} \mathbf{u}(q)\xi\left(q,i\right) \tag{2.9}$$

where

$$\xi\left(q,i\right) = \frac{1}{N}\frac{sin\left(\frac{\pi(iN-qN_{FFT})}{N_{FFT}}\right)}{sin\left(\frac{\pi(iN-qN_{FFT})}{N_{FFT}N}\right)}e^{j\frac{\pi\left(iN-qN_{FFT}\right)(N-1)}{N_{FFT}N}}. \tag{2.10}$$

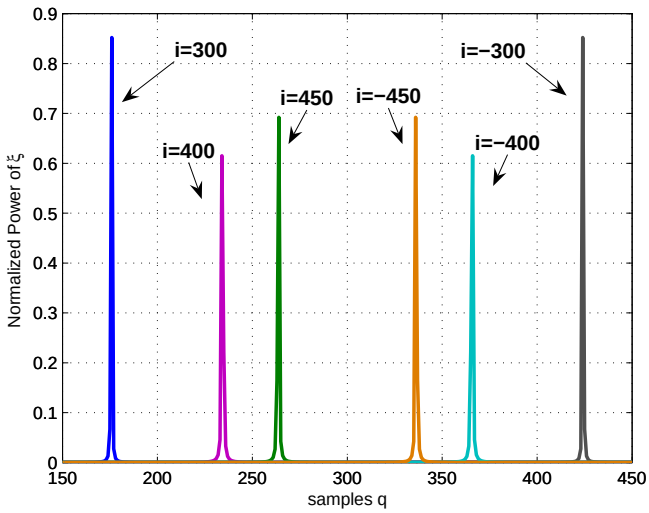

Figure 2.2: Power amplitude of the sequence ξ as a function of q, assuming $N = 600$ and $N_{FFT} = 1024$.

The samples $\tilde{\mathbf{v}}$ are therefore copies of the data symbols $\mathbf{u}$ in the positions corresponding to the integer multiples of N/N_{FFT}, while in the other positions they correspond to a weighted sum of the $\mathbf{u}$ samples. Figure 2.2 shows the power of the sequence ξ as a function of q. It can be noticed that, for a given i, the sequence ξ has visible power amplitude over a very limited range of q samples; this means, only very few data symbols $\mathbf{u}(q)$ contribute to the sum in Eq.(2.9) for a given i. Lower power envelope fluctuations with respect to OFDM are therefore expected.

The main used metric for the measure of the amplitude of the power envelope fluctuations are introduced below:

1. Complementary Cumulative Distribution Function (CCDF) of the Peak-to-Average Power Ratio (PAPR). It can be expressed as follows:

$$CCDF(P_t) = Prob\left(\frac{P_t}{P_a} > P_G\right) \tag{2.11}$$

   where P_t is the instantaneous power of the signal, P_a is the average transmit power, and P_G is the power threshold of the signal. Values of the order of 10^{-3} of the CCDF of the PAPR are usually considered for the comparison of different signals.

2. Cubic metric (CM). It refers to the third power term of the voltage signal, which is known to be the main cause of intermodulation distortions in the amplification process [24]. The third power term of the instantaneous voltage is compared with the power of the CDMA voice reference signal. The CM can be expressed as follows:

$$CM = \frac{20log_{10}\left\{E\left[\frac{|s|}{\sqrt{E(|s|^2)}}\right]^3\right\} - 20log_{10}\left\{E\left[\frac{|r_v|}{\sqrt{E(|r_v|^2)}}\right]^3\right\}}{K} dB \tag{2.12}$$

   where s is the instantaneous signal in the time domain, r_v is the CDMA voice reference signal, and K is an empirical slope factor which depends on the radio technology. For multicarrier signal, it has been shown to be equal to 1.56. It can be also shown that

$$20log_{10}\left\{E\left[\frac{|r_v|}{\sqrt{E\left(|r_v|^2\right)}}\right]^3\right\} = 1.524\, dB \tag{2.13}$$

While the PAPR is the most intuitive metric of the envelope signal fluctuations and still widely used in academia, the CM has been agreed in standardization as a valid predictor of the power derating which is needed in the power amplifier to avoid distortions [25].

In Figure 2.3, the CCDF of the PAPR of OFDM and SC-FDM is shown for various modulation schemes. A total of 600 subcarriers is assumed, which in the LTE terminology corresponds to a 10 MHz transmission bandwidth. Results have been obtained over a set of 40000 symbols. OFDM results not to be sensitive to the modulation scheme; however, its PAPR is around 2 dB higher

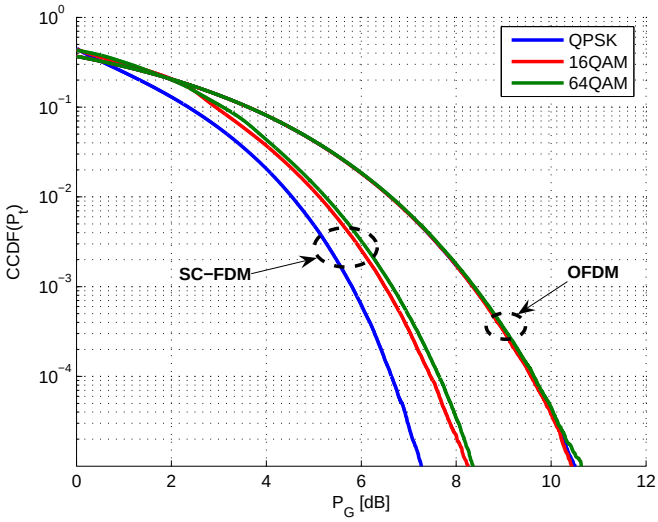

Figure 2.3: CCDF of the PAPR of OFDM and SC-FDM signals.

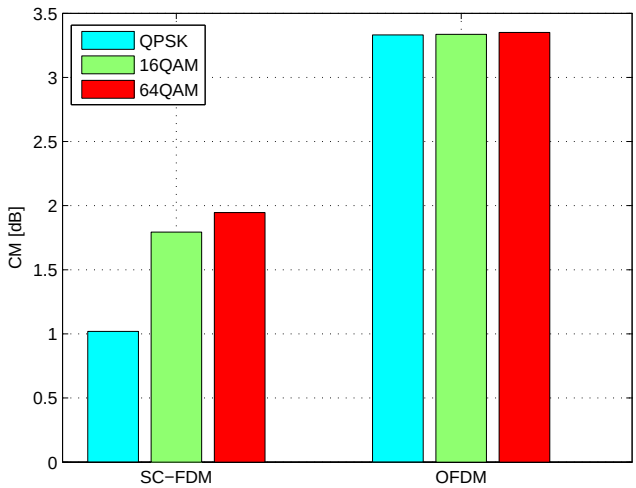

Figure 2.4: CM of OFDM and SC-FDM signals.

Table 2.1: LTE physical parameters

System BW (MHz)	1.25	2.5	5	10	15	20
Frame duration (ms)	1	1	1	1	1	1
Subcarrier spacing (kHz)	15	15	15	15	15	15
Sampling frequency(MHz)	1.92	3.84	7.68	15.36	23.04	30.72
FFT size	128	256	512	1024	1536	2048
Number of subcarriers	75	150	300	600	900	1200

than SC-FDM with 64QAM. According to the CM results (see Figure 2.4), OFDM would need a power backoff of around 3.3 dB to avoid intermodulation distortion, while in SC-FDM the power backoff does not exceed 2 dB, even for 64QAM.

Further improvements on the PAPR of SC-FDM can be achieved by applying pulse shaping in the frequency domain; however, this solution requires a bandwidth expansion which results in lower throughput [23]. In the prosecution of the thesis, we will not consider the effect of the pulse shaping on SC-FDM.

2.4 Link level analysis for LTE Uplink

OFDM and SC-FDM have been selected as downlink and uplink modulation and coding schemes for LTE, respectively [7]. In this section, we perform a baseline evaluation of their link level performance considering one transmit antenna, as agreed for the uplink of LTE. Basic LTE physical parameters are shown in Table 2.1, for different bandwidth configurations. Our aim is to highlight the main link level characteristics of SC-FDM before discussing the issues concerning its adoption in MIMO LTE-A, that will be widely treated in the following chapters.

The simplified baseband OFDM/SC-FDM transceiver chain with N_R receive antennas is shown in Figure 2.5. We consider one Codeword (CW), whose infomation bits are turbo-encoded with rate 1/3 and punctured, according to the LTE specifications [20]. The resultant bit stream enters the modulator block, which maps them to data symbols belonging to a predefined constellation. The OFDM/SC-FDM signal is then generated as discussed in Section 2.2. Note that the size of the data vector corresponds to the number of subcarriers where the symbols are mapped, i.e. $N = N_{sub}$ according to the definition given in Section 1.1.2.

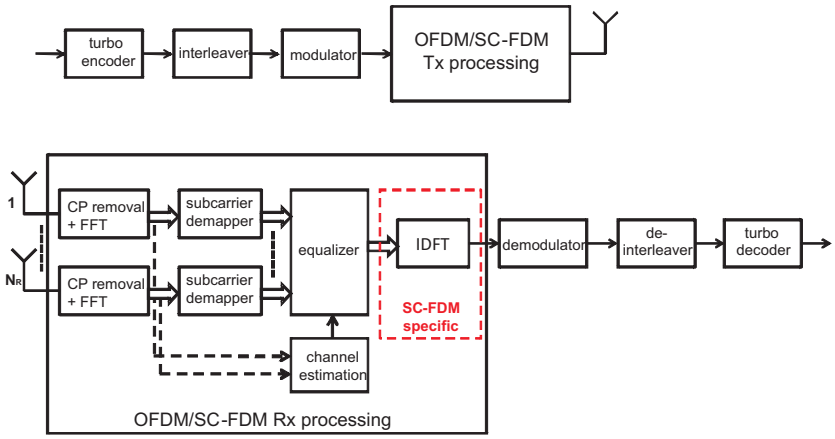

Figure 2.5: OFDM/SC-FDM transceiver chain.

At the receiver side, the CP is removed from the time symbols at each antenna and the time symbols are converted to the frequency domain by an FFT. Assuming that the CP is longer than the maximum excess delay of the channel, the signal received at the ith antenna in subcarrier k after the subcarrier de-mapping can be expressed as [9]:

$$\mathbf{r}_i(k) = \mathbf{h}_i(k)\mathbf{d}(k) + \mathbf{w}_i(k) \tag{2.14}$$

for $k = 0, \cdots, N_{sub} - 1$, where $\mathbf{h}_i(k)$ is the channel frequency responses and $\mathbf{w}_i(k)$ is the additive white gaussian noise (AWGN) with $E(\mathbf{w}_i(k)\mathbf{w}_i^*(k)) = \sigma_w^2$, for $i = 1, \cdots, N_R$.

Frequency domain one-tap equalization is performed to remove the effects of the fading channel. To do so, an estimate of the channel frequency response is provided by the channel estimation block. Firstly, let us consider a simple Zero Forcing (ZF) equalizer [19]. In Single-Input-Single-Output (SISO) mode (i.e., $N_R = 1$), the equalized signal in subcarrier k is given by

$$\mathbf{r}_{eq}(k) = \frac{\mathbf{r}_1(k)}{\mathbf{h}_1(k)} \tag{2.15}$$

The resultant instantaneous noise power in subcarrier k (and therefore in the

data symbol mapped on it) can be therefore expressed as:

$$W_k = \frac{|\mathbf{w}_1(k)|^2}{|\mathbf{h}_1(k)|^2} \tag{2.16}$$

From Eq.(2.16) it results that, in case the channel gain in a certain subcarrier is very low, the noise at that frequency can dramatically increase.

SC-FDM spreads each data symbol over the whole subcarrier set, and it therefore achieves higher frequency diversity than OFDM. On the other side, in SC-FDM an estimate of the data symbol is available after the IDFT block, which reverts the DFT spreading applied in the transmitter. The resultant instantaneous noise power affecting the generic q^{th} data symbol can be approximated as follows:

$$W_q \approx \frac{1}{N} \sum_{i=0}^{N-1} \frac{|\mathbf{w}_1(i)|^2}{|\mathbf{h}_1(i)|^2} \tag{2.17}$$

While in OFDM a deep fade in the channel frequency response impacts only the symbol(s) mapped over the subcarrier(s) experiencing the fade, in SC-FDM it affects any data symbol. This means, the frequency localized enhanced noise is here spread over the whole symbol set. A Minimum Mean Square Error (MMSE) equalizer [26] is therefore commonly adopted for SC-FDM for the purpose of limiting this noise enhancement. Its output can be expressed as:

$$\mathbf{r}_{eq}(k) = \frac{\mathbf{h}_1^*(k)}{|\mathbf{h}_1(k)|^2 + \frac{\sigma_w^2}{\sigma_d^2}} \mathbf{r}_1(k) \tag{2.18}$$

where with $\sigma_d^2 = E[\mathbf{d}_i(k)\mathbf{d}_i^*(k)]$ (typically, $\sigma_d^2 \approx 1$). It is worth to notice that the MMSE equalizer introduces a scaling factor on the estimated frequency samples $\mathbf{r}_{eq}$. An optimization of the MMSE equalizer for removing this bias will be discussed in the following Chapter.

In case of $N_R > 1$, the ZF equalizer takes the form of Maximal Ratio Combiner (MRC) [27], which can be expressed as:

$$\mathbf{r}_{eq}(k) = \frac{\sum_{i=1}^{N_R} \mathbf{h}_i^*(k)\mathbf{r}_i(k)}{\sum_{i=1}^{N_R} |\mathbf{h}_i(k)|^2} \tag{2.19}$$

Similarly, the output of the MMSE equalizer can be written as:

$$\mathbf{r}_{eq}(k) = \frac{\sum_{i=1}^{N_R} \mathbf{h}_i^*(k)\mathbf{r}_i(k)}{\sum_{i=1}^{N_R} |\mathbf{h}_i(k)|^2 + \frac{\sigma_w^2}{\sigma_d^2}} \tag{2.20}$$

The resultant symbol estimates are demodulated to generate a *soft* estimate of the transmitted bits, which are de-interleaved, de-punctured and turbo decoded to estract the original information bit stream.

2.4.1 Performance results

The performance of the baseline OFDM/SC-FDM transceiver chain has been evaluated by Monte Carlo simulations. An overview of the used link simulator is given in Appendix A. We use as a reference 5 MHz LTE configuration parameters (see Table 2.1). The main simulation parameters are gathered in Table 6.2. A Typical Urban channel model is used [28]. The channel models used in this dissertation are described in Appendix B. Each data frame has a duration of 1 ms, and is formed by 14 OFDM/SC-FDM symbols. It is assumed that the 4th and the 11th symbols are dedicated to the pilots which enable the channel estimation at the receiver, while the remaining 12 symbols carry data. Note that the size of the CW has to match to the amount of data to be mapped over 12 OFDM/SC-FDM time symbols. In this study, we assume full channel knowledge at the receiver, therefore the presence of the pilots only represents a dummy overhead of 14.29%. At the receiver, ZF equalizer is used for OFDM and MMSE equalizer for SC-FDM. It has to be mentioned that in a real LTE uplink system, the 14 time symbols of the frame carry the Physical Uplink Shared Channel (PUSCH) [6], where the data can be frequency multiplexed with uplink control information (UCI) such as Channel Quality Indicator (CQI) or ACK/NACK messages. When no data transmission occurs, the control informations are instead mapped over the Physical Uplink Control Channel (PUCCH).

Figure 2.6 shows the uncoded BER of both OFDM and SC-FDM, assuming a single receive antenna. SC-FDM clearly outperforms OFDM for QPSK. This is due to the higher frequency diversity gain of SC-FDM; since each data symbol is spread over the whole transmission bandwidth, it becomes possible to retrieve the information even in presence of localized deep fades of the channel. On the other hand, also the noise is spread over the whole bandwidth by the IDFT block in the receiver; for a more noise-sensitive modulation scheme (16QAM), OFDM shows lower BER than SC-FDM in low SNR region.

Table 2.2: Simulation parameters for baseline LTE link level evaluation

Carrier frequency	2 GHz
Sampling frequency	7.68 MHz
Number of subcarriers	300
FFT size	512
CP length	$5.2^a/4.68^b$ μs
Frame duration	1 ms
Antenna Configurations	SISO(1x1), 1x2, 1x4
Channel model	Typical Urban
User speed	3 kmph
Pilot Overhead (Ov)	14,29%
Channel Estimation	Ideal
MCS settings	QPSK: 1/2, 2/3 16QAM: 1/2, 2/3, 3/4
Channel Coding	3GPP Rel.8 compliant Turbo code with basic rate 1/3
Turbo decoder iterations	8

[a] 1st and 8th OFDM/SC-FDM symbol in a frame.
[b] $2^{th} - 7^{th}$ and $9^{th} - 14^{th}$ OFDM/SC-FDM symbols in a frame.

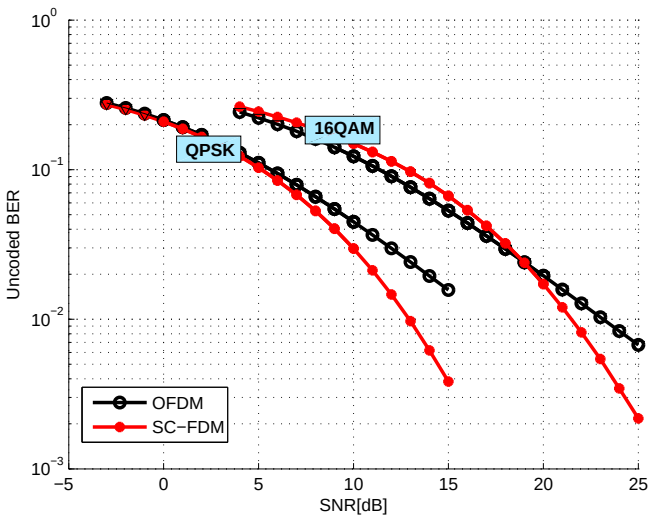

Figure 2.6: Uncoded BER performance of OFDM/SC-FDM for SISO.

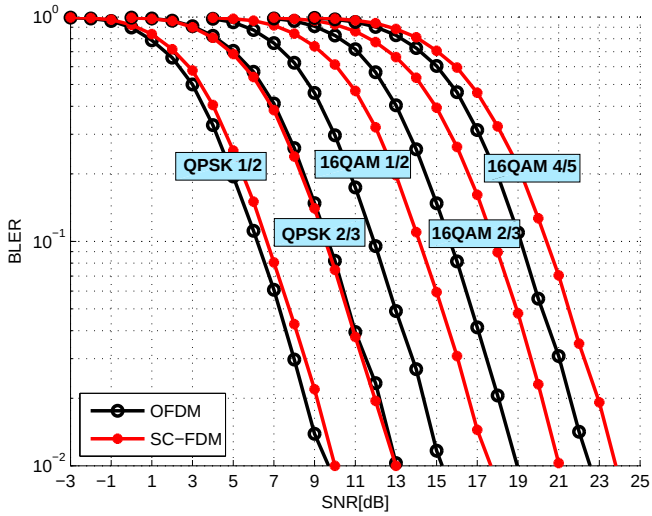

Figure 2.7: BLER performance of OFDM/SC-FDM for SISO.

The noise spreading in SC-FDM leads to distributed errors on the demodulated bit stream. It is well known that the turbo decoder shows better performance in presence of localized errors rather than distributed errors. This explains the behaviour of the Block Error Rate (BLER) results in Figure 2.7. Here, OFDM clearly outperforms SC-FDM for 16QAM. For QPSK with coding rate 2/3, the performance is instead approximately the same. This is due to the higher sensitivity to the coding gain of OFDM [29].

In Figure 2.8 the BLER performance for 2 receive antennas is shown. From the comparison with Figure 2.7 it can be seen that the performance of both OFDM and SC-FDM is improved. Furthermore, the gap between them is visibly reduced. This is because the presence of multiple receive antennas allows to average the channel seen at the receiver, thus smooting the deep fades which are the main reason of the noise enhancement of SC-FDM. The addition of receive antennas further reduces the spectral efficiency gap between OFDM and SC-FDM, as shown in Figure 2.9. Note that the spectral efficiency is calculated as follows:

$$S_{eff} = (1 - BLER) \cdot S_{max} \tag{2.21}$$

where S_{max} is defined as in Eq.(1.1).

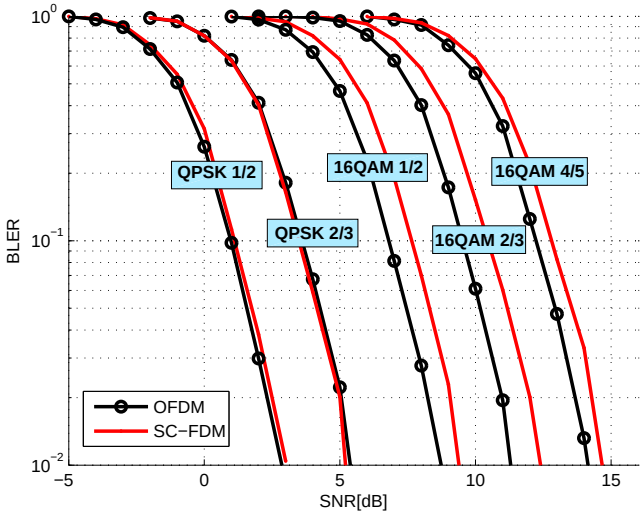

Figure 2.8: BLER performance of OFDM/SC-FDM for SIMO 1x2.

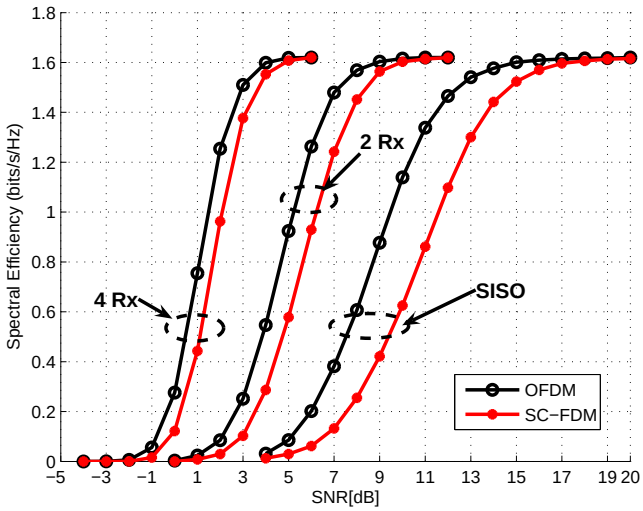

Figure 2.9: Spectral efficiency performance of OFDM/SC-FDM for different numbers of receive antennas.

2.5 Considerations on the resource allocation

In the previous section a baseline link level evaluation of OFDM/SC-FDM has been carried out. Here we extend our analysis to a multi-user scenario, where each user is transmitting or receiving OFDM/SC-FDM signals over a portion of the available bandwidth. In a practical scenario, each user may experience different conditions in terms of speed, path loss and shadowing. Furthermore, users can have different requirements in terms of Quality of Service (QoS). A smart design of the network should take into account the different user conditions and provide fairness among them. This should be made without a drastic reduction of the total cell throughput. Furthermore, when the bandwidth is shared among many users, few resources are given to each of them and therefore the user throughput is reduced. Nevertheless, in an adaptive OFDMA/SC-FDMA based system, the overall cell throughput increases with the number of users. This effect is called multi-user diversity gain and becomes possible due to the orthogonality of OFDM time-frequency resources [30]. The multi-user diversity gain is mainly due to the increase of the total received power at the base station with the number of users as well as the possibility of assigning resources to the user who can utilize them best. It can be exploited by adopting a Channel Dependent Scheduling. The rough idea is to allocate blocks of subcarriers, commonly named Resource Blocks (RBs) to the users experiencing better channel conditions in those frequency positions. However, a fundamental distinction exists between OFDMA and SC-FDMA. While in OFDMA each user can transmit over RBs which are randomly distributed over the available bandwidth, in SC-FDMA the RBs should be located in a contiguous manner. This is done at the purpose of preserving the single carrier property of the uplink signal. The difference is shown in Figure 2.10.

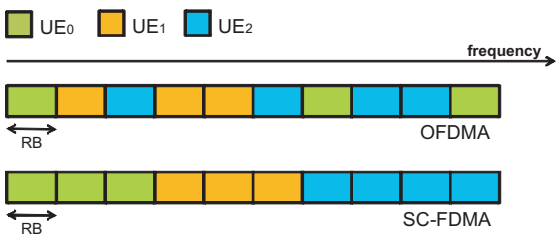

Figure 2.10: Resource allocation in OFDMA and SC-FDMA.

Of course, the constraint of SC-FDMA reduces its scheduling flexibility with respect to OFDMA. A relatively low complex channel aware scheduling algorithm for SC-FDMA is proposed in Appendix C, where a simplified semi-analytic approach for the evaluation of the maximum achievable cell spectral efficiency is also presented.

Table 2.3: Simulation Parameters for simplified multi-user evaluation

Cell radius	250 m
Minimum BS-UE distance	15 m
Carrier frequency	2 GHz
Antenna scheme	SISO
Number of users	1-40
Total number of subcarriers	1200 (100 RBs)
UE speed	3 kmph
Simulated slots	2000
Maximum transmitted power per user	24 dBm
Noise power	-160 dBm/Hz
Channel model	C1NLOS Classical Doppler [31]
PathLoss and shadowing models	from Winner II project [31]
Access schemes	OFDMA, SC-FDMA
Scheduling metric	Channel Blind, PF

Note that, in a real system, the scheduler design faces a number or realistic constraints including feedback signaling, corrupted channel status reports or power control. The aim of this section is however to compare the maximum achievable spectral efficiency of the discussed access technologies, thus neglecting the implementation issues.

Table 2.3 shows the main parameters of the MATLAB simulator, which has been developed according to the mentioned semi-analytical approach. The investigated scenario is an isolated cell with no surrounding interferer cells, where propagation and channel models are taken from [31]. We consider a fully loaded scenario in terms of bandwidth usage. The simulator generates a predefined number of users and uniformly distributes them within the cell. The average spectral efficiency is obtained after a simulation time equal to 2000 slots.

In Figure 2.11 the maximum achievable spectral efficiency for both OFDMA and SC-FDMA is shown as a function of the number of users in the cell. A simple channel blind scheduler, which equally divides the frequency resources among the users, is considered together with the channel aware scheduling solutions proposed in Appendix C. A Proportional Fair (PF) metric is used in the scheduler [17]. For both the multiple access schemes, the spectral efficiency increases with the number of users because of the multi-user diversity gain of OFDMA/SC-FDMA systems. It can be seen that OFDMA outperforms SC-FDMA, especially for low number of users. This is due to the combination of 2 factors:

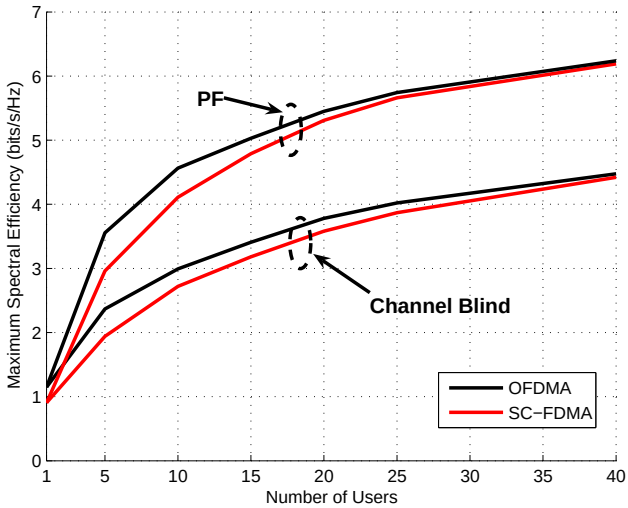

Figure 2.11: OFDMA vs. SC-FDMA comparison in multiuser scenario with different scheduling metrics.

1. the inherent lower capacity of SC-FDMA, due to the constraint of having an unique MCS over the whole transmission bandwidth (see Appendix C).
2. the higher flexibility of OFDMA in the resource allocation.

As the number of users increases, few resources are located to each of them, and therefore the gain due to the flexibility of OFDMA is reduced. Note that, for both OFDMA and SC-FDMA, channel dependent scheduling with PF metric improves up to 40% the spectral efficiency obtained with the channel blind scheduler.

2.6 Summary

In this chapter, we have introduced OFDM(A) and SC-FDM(A), which have been agreed as multiple access schemes for the upcoming LTE and LTE-A systems because of their flexibility as well as their capability to efficiently cope with the frequency selective channel. OFDM and SC-FDM signals can be generated by using the same transmitter chain, including for SC-FDM an additional DFT block. OFDM waveforms have been shown to have large power envelope fluc-

tuations in the time domain, which results in reduced power efficiency. This is because a large input backoff is needed in the power amplifier to avoid distortions and therefore lower link performance. SC-FDM can operate with smaller input backoff given its lower PAPR; it results therefore to be particularly suitable for the uplink given the power supply limitations in the user equipment. A baseline link level evaluation has shown that SC-FDM allows to achieve for QPSK better uncoded BER results than OFDM since it exploits inherent frequency diversity. However, the behavior of the coded results turns to be the opposite for high order modulation and coding schemes, since the IDFT block in the SC-FDM receiver spreads the noise contribution on the faded subcarriers over the whole bandwidth, and the turbo decoder fails in recovering such distributed errors. The noise enhancement of SC-FDM can be partly compensated by adding receive antennas, since the spatial diversity allows to smooth the deep fades of the equivalent channel seen at the receiver.

Both OFDMA and SC-FDMA allow to increase the cellular throughput with the number of users because of the increase of the total received power as well as the possibility of exploiting channel dependent scheduling. SC-FDMA shows however lower flexibility than OFDMA in the resource allocation since the RBs have to be located to each user in a contiguous way, and this results in lower maximum spectral efficiency. However, for high number of users in the cell the performance gap becomes negligible.

Chapter 3

Open Loop MIMO for LTE-A uplink

3.1 Introduction

In the last fifteen years, Multiple Input Multiple Output (MIMO) antenna techniques have drawn enormous attention by both industry and academia because of their promised benefits in the data rate increase as well as the link quality improvement, which do not come at the expense of additional bandwidth or transmit power [32].

When multiple transmit antennas are available at both ends of the transceiver chain, it becomes possible to send multiple data streams over the same time-frequency resources, provided the receiver is able to remove their mutual interference. This allows to improve the maximum data rate with respect to single transmit antenna solutions. On the other hand, multiple transmit antennas can be used to enhance the reliability of the data streams in case of poor radio link conditions by exploiting redundancy in the spatial domain. Furthermore, when some *apriori* knowledge of the channel is available at the transmitter side, it becomes possible to further improve the robustness of the data to be sent and/or enhance the received signal power.

MIMO schemes are particularly suitable to be combined with OFDM because of the capability of this scheme to convert the frequency-selective channel in multiple flat channels [33]. Upcoming 4th generation mobile communication systems are therefore expected to exploit MIMO algorithms to achieve the promised data rates.

Regarding 3GPP radio networks, in LTE multiple antenna solutions have been included for the downlink, while only single transmit antenna schemes have been defined for the uplink [8]. However, the upcoming LTE-A standard will definitely include MIMO solutions even in the uplink to achieve the ambitious target of 15 bits/s/Hz [7]. MIMO schemes have to be combined with advanced features like fast link adaptation [16] and Hybrid Automatic Repeat Request (HARQ) [18] to further boost the transceiver performance. Furthermore, since the promised spectral efficiency can be achieved provided the receiver is able to correctly recover the channel state information, an efficient channel estimator has to be designed.

In this chapter the open loop MIMO spatial multiplexing design for LTE-A uplink is discussed. The performance of SC-FDM is compared with OFDM to highlight the difference with the downlink when the same multiple antenna scheme is set. The chapter aims also at introducing some of the baseline features of the LTE-A link layer interface, which will be further elaborated and optimized in the following parts of this thesis.

The chapter is outlined as follows. Section 3.2 introduces a baseline classification of the MIMO schemes, highlighting their main gain mechanisms. Section 3.3 presents a theoretical discussion on the MIMO capacity. The implementation of MIMO solutions to the LTE-A uplink standard is presented in Section 3.4, while in Section 3.5 the transceiver chain for the specific case of spatial multiplexing is described in details. A channel estimator based on the usage of time domain orthogonal pilot sequences is proposed in Section 3.6. An extensive link performance evaluation is carried out in Section 3.7. Finally, Section 3.8 gives a summary of the contents of the chapter.

3.2 Baseline classifications of the MIMO schemes

The degrees of freedom that multiple transmit antenna systems offer can be exploited to achieve different goals depending on factors such as user position or instantaneous channel conditions. The main gain mechanisms which can be obtained in MIMO transmission mode are mentioned below [34]:

1. *Array gain.* If multiple antennas are available on the receiver side, it becomes possible to recover several versions of the same signal and combine them to increase the total received power. To obtain array gain even on the transmitter side, some degree of channel knowledge is needed.
2. *Diversity gain.* Since multiple antennas are expected to see independent versions of the fading channel, the receiver combining allows to smooth the deep fades and therefore minimize the signal level variability. In case of single transmit antenna and N_R uncorrelated receive antennas, the diversity order is N_R.
3. *Multiplexing gain.* It denotes the increase of the data rate due to the transmission of several streams over the same bandwidth. By using a smart detection algorithm, it is possible indeed to recover the multiple streams by removing their mutual interference contribution.
4. *Interference Rejection.* Cellular networks with frequency reuse are likely to experience co-channel interference. The multiple antennas can be used to detect and remove the interferer signals from the desired signals. The interference rejection is therefore analogous to the multiplexing gain, where the difference is that not all the detected streams are the desired ones.

Depending on the gain mechanism they are exploiting and the processing being applied at the transmitter side, it is possible to classify the MIMO schemes in 3 main categories:

1. *Spatial multiplexing.* The transmit antennas are used to send multiple data streams over the channel. These data streams can belong to the same CW or to different CWs. Spatial multiplexing schemes aim hence at increasing the data rate.
2. *Transmit diversity.* The N_T transmit antennas are used to send a single data stream over the channel. Transmit diversity techniques aim therefore at improving the reliability of the data stream by exploiting redundancy in the spatial domain. This results to be particularly suitable in low SNR conditions (e.g.,users at the cell edge), since the data stream can be made more robust to the noise and to the channel fades.
3. *Precoding.* When some degree of channel knowledge is available on the transmitter side, it is possible to apply weights on the data streams to be transmitted in order to counteract the negative effect of the channel and enhance the received signal power.

All the mentioned MIMO categories have to be supported in a modern wireless communication network, so that the throughput of users which are close to

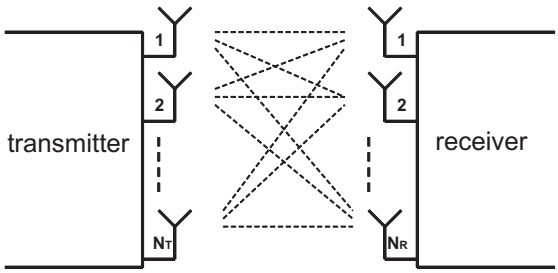

Figure 3.1: Generic MIMO system with N_T transmit antennas and N_R receive antennas.

the base station can be leveraged, and at the same time the coverage can be extended for users at the cell edge with more robust transmission.

Regarding precoding, schemes that rely on the availability of a feedback message to retrieve some channel state information are often reffered as *Closed Loop MIMO*. Schemes which do not make use of such feedback information are instead referred as *Open Loop MIMO*. It is worth to mention that the distinction between *Open Loop MIMO* and *Closed Loop MIMO* can appear misleading since in a real system feedback signaling is needed to properly setup the parameters of the communication chain even in open loop mode; within 3GPP, it has been however agreed that the denomination *Closed Loop MIMO* refers exclusively to the feedback information for the precoding task.

Depending on the physical location of the transmit antennas, we can also distinguish between:

- Single User MIMO (SU-MIMO): the data streams are communicated from (or to) a single UE;

- Multi User MIMO (MU-MIMO): the data streams are communicated from (or to) distinct UEs, in order to enhance the overall communication capabilities.

Of course, MU-MIMO raises further issues at network layer, since smart algorithms for the selection of the UEs to be coupled over the same physical resources have to be designed. However, this is out of scope of this dissertation.

3.3 Capacity of MIMO channels

It has been shown that the maximum achievable spectral efficiency of a MIMO system with N_T transmit antennas and N_R receive antennas, as depicted in Figure 3.1, can be written as [13]:

$$S_{MIMO} = log_2 \left[det \left(\mathbf{I}_{N_R} + \mathbf{HQH}^H \right) \right] \tag{3.1}$$

where $\mathbf{I}_{N_R}$ is the $N_R \times N_R$ identity matrix, $\mathbf{H}$ is the $N_R \times N_T$ channel matrix, and $\mathbf{Q}$ is the covariance matrix of the transmit signal vector. When the channel is unknown at the transmitter and the channel entries are gaussian [35], the spectral efficiency is maximized by assuming equal power distribution among the transmit antennas, i.e.

$$\mathbf{Q} = \frac{\rho}{N_T} \mathbf{I}_{N_T} \tag{3.2}$$

where ρ is the SNR at each receive antenna. In this case, Eq.(3.1) can be re-written as:

$$S_{MIMO} = \sum_{i=1}^{min(N_T, N_R)} log_2 \left(1 + \rho \lambda_i\right) \tag{3.3}$$

where λ_i is the ith eigenvalue of the matrix $\mathbf{HH}^H$. S_{MIMO} grows linearly with $min\left(N_T, N_R\right)$. The maximum spectral efficiency can be achieved by assuming that the transmit signals can be retrieved without interference.

When the channel is known at the transmitter, it is theoretically possible to enhance the spectral efficiency by distributing the transmit power according to the waterfilling algorithm [13]. The resultant maximum spectral efficiency can be expressed as:

$$S_{MIMO} = \sum_{i=1}^{min(N_T, N_R)} log_2 \left(\mu \lambda_i\right)^+ \tag{3.4}$$

where μ is chosen so that

$$\rho = \sum_{i=1}^{min(N_T,N_R)} \left(\mu - \frac{1}{\lambda_i}\right)^+ \tag{3.5}$$

and "+" takes into account only the positive terms.

In a practical system, full channel knowledge at the transmitter is impossible to obtain. Therefore, Eq.(3.1) is of higher practical importance. The spectral efficiency values in Eq.(3.1) cannot however be achieved due to several implementation issues. In [36] the following modified upper spectral efficiency formula has been defined for the specific case of LTE systems:

$$S_{MIMO} = \bar{B}\varrho log_2\left(1 + \frac{\rho}{\rho_\eta}\right) \tag{3.6}$$

where the term $\bar{B}$ considers the system bandwidth efficiency, ρ_η is the SNR efficiency and ϱ is a correction factor. The bandwidth efficiency is usually reduced by factors such as practical filter implementations, pilot and cyclic prefix overheads. On the other side, full SNR efficiency is practically not possible due to the limited code block length, the limited set of modulation and coding schemes, and the non-idealities in the transceiver design. This reduces the effective capacity of the MIMO channel from its nominal value.

3.4 MIMO implementation in LTE-A Uplink

As mentioned in the introduction, MIMO solutions for the uplink were discarded in LTE work item, while they are definitely taking place in LTE-A to achieve the more ambitious spectral efficiency target. Both spatial multiplexing and transmit diversity modes are to be included in order to enhance maximum data rate and coverage. Also both open loop and closed loop transmission are to be considered.

It has been shown by straightforward calculations that a minimum 4x4 MIMO configuration is needed to achieve the LTE-A uplink target of 15 bits/s/Hz. Both 2 and 4 transmit antenna solutions are therefore to be included in the standard. Since the early stages of the LTE-A work item, it has been agreed to use a maximum of 2 CWs in the uplink [37]. This decision has been made to avoid

Table 3.1: Transport Block Sizes in LTE-A Uplink

R	2Tx		4Tx	
	TBS CW1	TBS CW2	TBS CW1	TBS CW2
1	TBS_{ref}	-	TBS_{ref}	-
2	TBS_{ref}	TBS_{ref}	TBS_{ref}	TBS_{ref}
3	-	-	TBS_{ref}	$2TBS_{ref}$
4	-	-	$2TBS_{ref}$	$2TBS_{ref}$

the use of 4 CWs in 4 transmit antenna mode, that would increase the overall complexity. Moreover, CWs having wider size can boost the turbo decoder performance [38]. In case of spatial multiplexing mode with 2 transmit antennas (2Tx), each CW can be directly mapped over one transmit antenna, while with 4 transmit antennas (4Tx) each CW has to be split onto 2 layers. Diversity gain can be obtained by adopting a number of effective data streams, ofter referred as transmission *rank (R)*, which is lower than the number of transmit antennas. Note that the effective data streams can belong to the same CW or the different CWs.

The amount of bits of each CW which enters the turbo encoder depends on the transmission rank. According to the formalism defined in Section 1.1.2, let us define a reference Transport Block Size (TBS) as follows:

$$TBS_{ref} = N_{sub} \times B_{sel} \times ECR_{sel} \times N_{sym} \times (1 - Ov) \tag{3.7}$$

Table 3.1 shows the TBSs for each of the ranks for 2Tx and 4Tx, respectively; they represent the number of information bits to be sent by each CW per time slot. The transmission rank R also defines the number of *layers* where the data streams have to be mapped. The CW-to-layer mapper is shown in Figure 3.2. Note that, for $R < N_T$, some manipulation on the layers must be performed to adapt them to the number of transmit antennas. In case of precoded transmission, this can be obtained by multiplying the layers by a $N_T \times R$ channel-aware matrix. For open loop transmit diversity, the single layer has to be further encoded to match with N_T.

It is worth to notice that, from a pure physical layer point of view, the design of SU-MIMO and MU-MIMO solutions can be seen as equivalent problems. The concept is shown in Figure 3.3. The spatial multiplexing 2x2 scheme can be seen

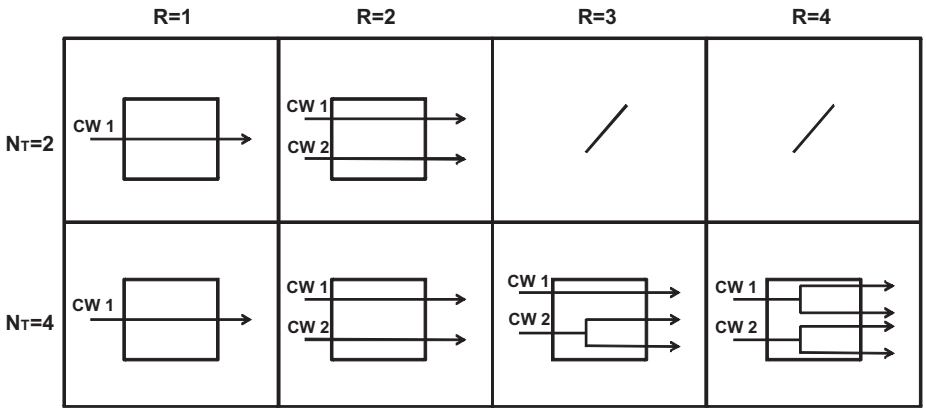

Figure 3.2: CW-to-layer mapping in LTE-A uplink.

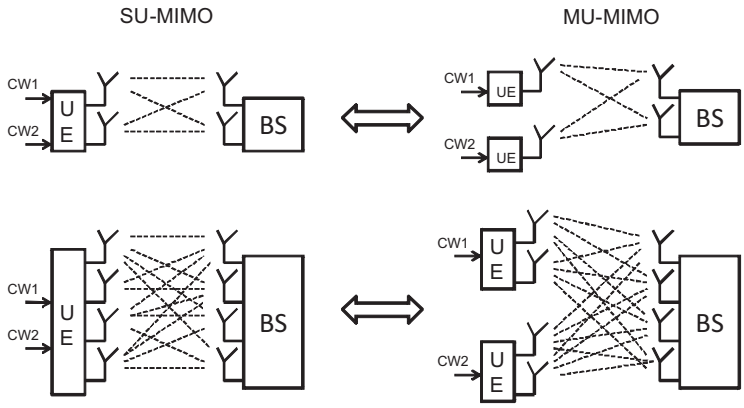

Figure 3.3: Equivalence between SU-MIMO and MU-MIMO.

as equivalent to the case of 2 users transmitting with a single antenna in the same time-frequency resources; similarly, the 4x4 rank 2 SU-MIMO problem can be seen as equivalent to the 2x2 rank 1 MU-MIMO problem with 2 users. Whether not differently specified, throughout this thesis we will refer to SU-MIMO.

Both open loop transmit diversity and precoded transmission will be widely discussed in the next chapters. For the rest of the chapter we will keep our focus on the open loop spatial multiplexing mode ($R = N_T$).

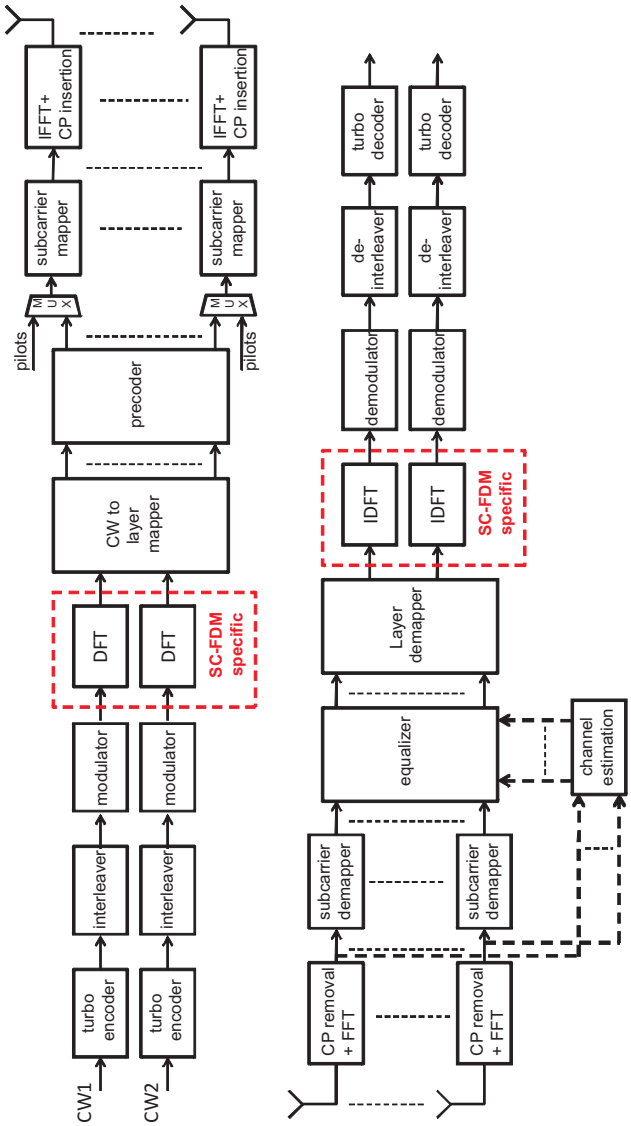

Figure 3.4: MIMO transceiver chain for LTE-A uplink.

3.5 Transceiver chain for spatial multiplexing

The simplified baseband transceiver chain for a generic LTE-A MIMO system is depicted in Figure 3.4. The bits of the two CWs are independently encoded, punctured, interleaved and mapped in QPSK/M-QAM symbols as described in Section 2.4. Note that, for SC-FDM, the size of the DFT must be set equal to the number of symbols to be sent by each antenna; in spatial multiplexing mode, it is therefore straightforward to notice that:

$$N_{DFT} = \begin{cases} N, & \text{for 2Tx} \\ \frac{N}{2}, & \text{for 4Tx} \end{cases} \tag{3.8}$$

where N is the number of encoded data symbols. Of course, $N_{DFT} = N_{sub}$. The symbol vectors $\mathbf{d}_i, i = 1, 2$, which correspond to the data symbols for OFDM and to the output of the DFT block for SC-FDM, are then fed to the CW-to-layer mapper, as shown in Figure 3.2, and afterwards to the precoder block. The output of the precoder for each subcarrier k can be expressed as:

$$\mathbf{q}[k] = \mathbf{F}[k]\tilde{\mathbf{d}}[k] \tag{3.9}$$

where $\tilde{\mathbf{d}}[k] = [\tilde{\mathbf{d}}_1(k), \tilde{\mathbf{d}}_2(k), \ldots, \tilde{\mathbf{d}}_R(k)]^T$ is a vector containing the encoded MIMO complex transmit symbols at subcarrier k, and $\mathbf{F}[k]$ is a $N_T \times R$ complex precoding matrix. The power delivered to layer n is given by

$$P_n^{lay} = \sigma_d^2 \|\mathbf{F}_{:,n}\|^2 \tag{3.10}$$

for $n = 1, \cdots, R$, where σ_d^2 is defined as in Section 2.4, $\|\cdot\|$ denotes the euclidean norm, and $\mathbf{F}_{:,i}$ is the ith column of $\mathbf{F}$. The power per antenna q is given by

$$P_q^{ant} = \sigma_d^2 \|\mathbf{F}_{q,:}\|^2 \tag{3.11}$$

for $q = 1, \cdots, N_T$, where $\mathbf{F}_{q,:}$ is the qth row of $\mathbf{F}$. When no channel knowledge is available at the transmitter, the spectral efficiency can be maximized by equally dividing the transmit power among the layers and the transmit antennas (see Section 3.3), i.e.

$$\mathbf{F} = \sqrt{\frac{1}{N_T}}\mathbf{I}_{N_T} \tag{3.12}$$

Next, pilot symbols are inserted in predefined subcarrier positions at each transmit antenna in order to enable channel estimation at the receiver. The frequency samples on each antenna are then converted to the time domain by the IFFT. A CP is added over each antenna, and the resultant signals are sent over the channel. Assuming that the CP is longer than the maximum excess delay introduced by the channel, the received signal in subcarrier k after FFT and CP removal can be expressed as [9]:

$$\mathbf{r}[k] = \mathbf{H}[k]\mathbf{q}[k] + \mathbf{w}[k] \tag{3.13}$$

where $\mathbf{w}[k] = [\mathbf{w}_1(k), \mathbf{w}_2(k), \ldots, \mathbf{w}_{N_R}(k)]^T$ is the additive white Gaussian noise (AWGN) vector with autocorrelation given by $E[\mathbf{w}_i(k)\mathbf{w}_i(k)^H] = \sigma_w^2$ and

$$\mathbf{H}[k] = \begin{bmatrix} h_{11}(k) & \ldots & h_{1N_T}(k) \\ \vdots & \ddots & \vdots \\ h_{N_R1}(k) & \ldots & h_{N_RN_T}(k) \end{bmatrix} \tag{3.14}$$

is the channel transfer function matrix at subcarrier k. $h_{ij}(k)$ denotes the complex channel gain from the transmit antenna j to the receive antenna i.

The signal $\mathbf{r}$ is then fed to the equalizer block. While in single transmit antenna mode the equalizer compensates the amplitude and phase distorsions introduced by the channel, in MIMO spatial multiplexing mode it also aims at reducing the interstream interference. A MIMO ZF detector removes the interstream interference but also enhances the noise. It has been shown in [39] that a MIMO MMSE detector outperforms a MIMO ZF one because of its noise mitigation capability, even though some residual interstream interference persists. We will therefore consider an MMSE detector for both OFDM and SC-FDM in MIMO mode.

The output of the MMSE detector in subcarrier k can be written as follows:

$$\mathbf{r}_{eq}[k] = \mathbf{R}_{dd}\mathbf{H}[k]^H \left(\mathbf{H}[k]\mathbf{R}_{dd}\mathbf{H}^H[k] + \sigma_w^2\mathbf{I}_{N_R}\right)^{-1}\mathbf{r}[k] \tag{3.15}$$

with

$$\mathbf{R}_{dd} = diag(P_1^{ant}, ..., P_{N_T}^{ant}), \tag{3.16}$$

where $diag\,(\cdot)$ denotes a square diagonal matrix.

Since the total transmit power is equally split among the antennas, Eq.(3.15) can be expressed as:

$$\mathbf{r}_{eq}[k] = \mathbf{H}[k]^H \left(\mathbf{H}[k]\mathbf{H}^H[k] + N_T \frac{\sigma_w^2}{\sigma_d^2} \mathbf{I}_{N_R} \right)^{-1} \mathbf{r}[k] \tag{3.17}$$

The rest of the receiver chain performs the reverse operations of the transmitter.

3.5.1 Optimization of MMSE equalizer and demodulator

Here we elaborate more on the design of equalizer and demodulator. Defining the MMSE gain matrix $\mathbf{G}$ in subcarrier k as follows:

$$\mathbf{G}[k] = \mathbf{H}[k]^H \left(\mathbf{H}[k]\mathbf{H}^H[k] + N_T \frac{\sigma_w^2}{\sigma_d^2} \mathbf{I}_{N_R} \right)^{-1} \mathbf{H}[k] \tag{3.18}$$

and neglecting the residual mutual interference terms arising from the off-diagonal terms of $\mathbf{G}$, the output of the MMSE equalizer can be expressed as:

$$\mathbf{r}_{eq,i}(k) = \mathbf{g}_{ii}(k)\mathbf{q}_i(k) + \tilde{\mathbf{w}}_i(k) \tag{3.19}$$

for $i = 1, \cdots, N_T$, where $\mathbf{g}_{ii}(k)$ is the ith element on the diagonal of $\mathbf{G}[k]$, and $\tilde{\mathbf{w}}_i(k)$ is the residual noise. The MMSE equalizer introduces therefore a scaling factor on each subcarrier of the equalized signal. This can be particularly critical since the estimate of each symbol may be corrupted. In OFDM the MMSE scaling factor in subcarrier k can be easily removed by dividing $\mathbf{r}_{eq,i}$ per $\mathbf{g}_{ii}$, i.e.

$$\hat{\mathbf{u}}_i(k) = \frac{\mathbf{r}_{eq,i}(k)}{\mathbf{g}_{ii}(k)} \tag{3.20}$$

for $i = 1, \cdots, N_T$.

However, the removal of the scaling factor per subcarrier might result in a noise enhancement in case of channel fades. This can be critical for SC-FDM, since the noise will be spread over the whole bandwidth. The MMSE bias for SC-FDM should be therefore removed after the IDFT. By exploiting the properties

of the IDFT operation, the estimate of the pth data symbol[1] before scaling factor removal can be written as:

$$\tilde{\mathbf{u}}_i(p) = \sum_{l=0}^{N_{DFT}-1} \tilde{\mathbf{q}}_i(l) \sum_{\eta=-\infty}^{+\infty} \mathbf{v}_{p-l-\eta N_{DFT}} \tag{3.21}$$

for $p = 0, \cdots, N_{DFT}-1$, where $\{\tilde{\mathbf{q}}_i(l)\}_{l=0}^{N_{DFT}-1} = IDFT\{\mathbf{q}_i\}$, and $\{\mathbf{v}_l\}_{l=0}^{N_{DFT}-1} = IDFT\{\mathbf{g}_{ii}\}$. Note that the sequence $\mathbf{v}$ is defined as 0 outside $[0, N_{DFT}-1]$. Eq.(3.21) can be easily expressed in matricial form:

$$\begin{bmatrix} \tilde{\mathbf{u}}_i(0) \\ \tilde{\mathbf{u}}_i(1) \\ \vdots \\ \tilde{\mathbf{u}}_i(N_{DFT}-1) \end{bmatrix} = \begin{bmatrix} \mathbf{v}_0 & \mathbf{v}_{N_{DFT}-1} & \cdots & \mathbf{v}_1 \\ \mathbf{v}_1 & \mathbf{v}_0 & \cdots & \mathbf{v}_2 \\ \vdots & \ddots & \ddots & \vdots \\ \mathbf{v}_{N_{DFT}-1} & \mathbf{v}_{N_{DFT}-2} & \cdots & \mathbf{v}_0 \end{bmatrix} \cdot \begin{bmatrix} \tilde{\mathbf{q}}_i(0) \\ \tilde{\mathbf{q}}_i(1) \\ \vdots \\ \tilde{\mathbf{q}}_i(N_{DFT}-1) \end{bmatrix} \tag{3.22}$$

Since for realistic SNR values $\mathbf{g}_{ii}(k) \approx 1$, most of the energy is located on the diagonal of the first matrix of the product in Eq.(3.22). The MMSE bias on the pth data symbol can be therefore removed as follows:

$$\hat{\mathbf{u}}_i(p) = \frac{\tilde{\mathbf{u}}_i(p)}{\mathbf{v}_0} \tag{3.23}$$

Note that $\mathbf{v}_0 = \{IDFT\{\mathbf{g}_{ii}\}\}_0 = E\{\mathbf{g}_{ii}\}$.

The estimated symbols are then fed to the demodulator, which computes *soft* estimates of the coded bits in the form of likelihood ratios. By using the well known max-log approximation [27], for OFDM the likehood ratio of the jth bit associated to the pth transmit data symbol ($b_{p,j}$) can be expressed as:

$$L(b_{p,j}) = \sigma_{s,p}^2 \left\{ max_{u^m:\tilde{b}_{m,j}=1} \left(-\frac{|\mathbf{r}_{eq}(p) - \mathbf{g}_{ii}(p)u^m|^2}{\sigma_w^2} \right) + \right.$$
$$\left. -max_{u^m:\tilde{b}_{m,j}=0} \left(-\frac{|\mathbf{r}_{eq}(p) - \mathbf{g}_{ii}(p)u^m|^2}{\sigma_w^2} \right) \right\} \tag{3.24}$$

[1] the residual noise component is here neglected

where u^m denotes the mth symbol of the constellation, $\tilde{b}_{m,j}$ is the jth bit of u^m and $\sigma^2_{s,p}$ can be computed as [40]

$$\sigma^2_{s,p} = \frac{\sigma^2_w}{\mathbf{g}_{ii}(p) - \mathbf{g}^2_{ii}(p)} \tag{3.25}$$

From Eq.(3.20) it follows that

$$L\left(b_{p,j}\right) = \sigma^2_{s,p}\mathbf{g}^2_{ii}(p)\cdot \left\{ max_{u^m:\tilde{b}_{m,j}=1}\left(-\frac{|\hat{\mathbf{u}}_i(p) - u^m|^2}{\sigma^2_w}\right) - max_{u^m:\tilde{b}_{m,j}=0}\left(-\frac{|\hat{\mathbf{u}}_i(p) - u^m|^2}{\sigma^2_w}\right)\right\} \tag{3.26}$$

Similarly, for SC-FDM we have:

$$L\left(b_{p,j}\right) = \frac{1}{N_{DFT}}\left(\sum_{p=0}^{N_{DFT}-1}\sigma^2_{s,p}\mathbf{g}^2_{ii}(p)\right)\cdot \cdot\left\{ max_{u^m:\tilde{b}_{m,j}=1}\left(-\frac{|\hat{\mathbf{u}}_i(p) - u^m|^2}{\sigma^2_w}\right) - max_{u^m:\tilde{b}_{m,j}=0}\left(-\frac{|\hat{\mathbf{u}}_i(p) - u^m|^2}{\sigma^2_w}\right)\right\} \tag{3.27}$$

The performance improvements due to the removal of the MMSE scaling factor is shown in Figure 3.5, assuming 2x2 antenna configuration and 16QAM 1/2. The simulation assumptions are in line with Table 3.3, and will be further presented in the following. The improvement in terms of uncoded BER is of around 0.5 dB for both OFDM and SC-FDM, and also reflects to the BLER performance.

3.6 Channel estimation design

In the 3GPP radio networks channel knowledge at the receiver, which is needed to perform the equalization task as well as advanced Radio Resource Management (RRM) techniques, can be achieved through pilot assisted channel estimation (PACE) [41]. In LTE downlink a pattern of pilots is multiplexed in

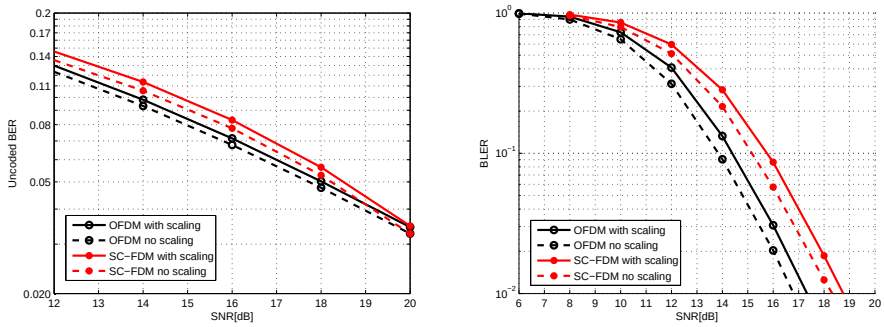

(a) uncoded BER (b) BLER

Figure 3.5: Link performance improvements due the the removal of the MMSE scaling factor for 2x2 antenna configuration and 16QAM 1/2.

time and frequency with data, so that the receiver can estimate the channel in the pilot positions and apply some interpolation algorithm to get the channel response over the whole bandwidth [8]. Since the pilot allocation as defined in LTE downlink would break the low PAPR property of SC-FDM, in LTE uplink it has been agreed to multiplex the pilot symbols with data only in the time direction. As mentioned in Chapter 2, in the uplink the pilots are located in the 4th and 11th symbol of the frame. This section deals with the design of a practical channel estimation technique suitable for MIMO LTE-A uplink. The basic pilot sequences are presented and a simple channel estimator is proposed.

3.6.1 Cyclically extended Constant Amplitude Zero Autocorrelation (CAZAC) sequences

Constant amplitude zero autocorrelation (CAZAC) sequences have been adopted as basic family for the pilots generation in LTE uplink [20]. The kth entry of the nth sequence having length L, where n is relatively prime with L is given by:

$$c_n(k) = \begin{cases} e^{\frac{j2n\pi}{L}\left(k+k\frac{k+1}{2}\right)} & \text{if L is odd} \\ e^{\frac{j2n\pi}{L}\left(k+k^2\right)} & \text{if L is even} \end{cases} \tag{3.28}$$

for $k = 0, \cdots, L-1$. The CAZAC sequences have drawn enormous interest because of the following properties [42]:

- zero autocorrelation;
- cross-correlation limited to $\sqrt{L}$;
- constant amplitude in time and frequency domain.

In order to get an high number of sequences, L must be a prime number. Selecting L as a prime number guarantees indeed $L-1$ sequences with limited cross-correlation between any pair of them. The length of the CAZAC sequences has however to be adapted to the UE bandwidth, so that each entry can be mapped over one subcarrier. The UE bandwidth comprises M RBs, and therefore the number of subcarriers is multiple of 12 [8]. Furthermore, few sequences with short length would be available: that makes CAZAC sequences not suitable for users with small transmission bandwidth ($M < 3$). For $M > 3$, the base pilot sequence for LTE uplink has been therefore defined as the cyclic extension of a CAZAC sequence, i.e.

$$\tilde{c}_n(k) = c_n\left(k \, mod \, L_{RB}\right) \tag{3.29}$$

for $k = 0, \cdots, N_{sub} - 1$, where L_{RB} is the biggest prime number lower than N_{sub}. Note that $N_{sub} = 12 \cdot M$. For $M < 3$, the base sequence is instead defined as the Computer Generated CAZAC (CG-CAZAC) sequence:

$$\tilde{c}_n(k) = e^{j\frac{\varphi(k)}{4}} \tag{3.30}$$

for $k = 0, \cdots, N_{sub} - 1$, where $\varphi(n)$ values are defined in [20].

The base sequences c_n are divided in 30 groups with $n = 0, \cdots, 29$. Each cell can use sequences belonging to one group, or sequences belonging to different groups when a *group hopping* strategy is enabled. For further details, we refer to [20].

Whitin a cell, additional reference sequences can be obtained by applying a linear phase rotation α in the frequency domain to the same base sequence, as follows:

$$\tilde{c}_n^{\alpha}(k) = e^{j\alpha k}\tilde{c}_n(k) \tag{3.31}$$

for $k = 0, \cdots, N_{sub} - 1$.

The phase rotation translates to a cyclic shift in the time domain waveforms. This allows to obtain channel state information from users sharing the same frequency resources, e.g. in MU-MIMO mode.

Note that the usage of superimposed pilots among several users in the frequency domain allows a better intercell interference rejection than frequency multiplexed dedicated pilots, since the higher length of the sequence translates in higher processing gain for the interference removal [43]. This is the reason why the frequency division multiplexing has been discarded in the LTE work item as option for the uplink pilot allocation.

For SU-MIMO LTE-A uplink, a different phase rotated version of the same cyclically extended CAZAC sequence can be used as pilot sequence over each transmit antenna. To ensure the orthogonality in the time domain, we can select:

$$\alpha = \begin{cases} m\pi, & m = 0, 1 \quad \text{for } N_T = 2 \\ m\frac{\pi}{2}, & m = 0, 1, 2, 3 \quad \text{for } N_T = 4 \end{cases} \tag{3.32}$$

The resultant time domain waveforms are shown in Figure 3.6.

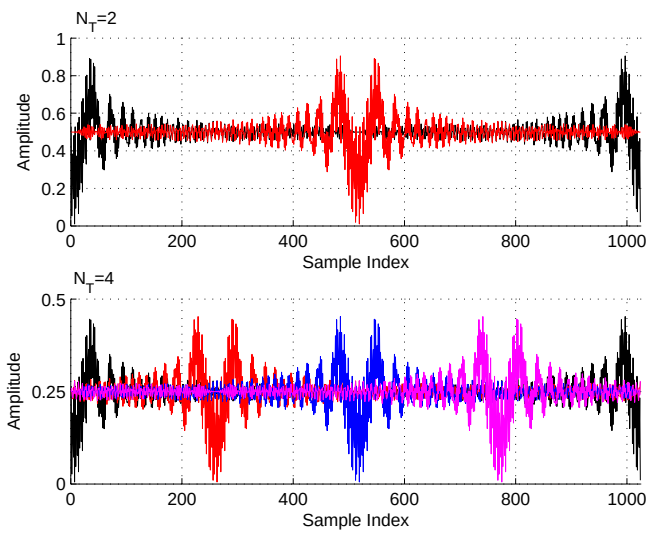

Figure 3.6: Time domain waveforms for cyclically extended CAZAC sequences, assuming $N_{FFT} = 1024$. The different colors refer to signals over different antennas.

Table 3.2: Maximum number of UEs using the same cyclically extended CAZAC sequences

N_T	number of UEs
1	12
2	6
4	3

Note that the selection of α as in Eq.(3.32) can be easily relaxed, since a time shift which is longer than the delay spread of the channel would ensure orthogonality of the resultant channel impulse responses. Assuming the CP duration as minimum time shift, up to 12 orthogonal reference signals can be theorically obtained from the same basic ciclically extended CAZAC sequence. Table 3.2 denotes the maximum number of UEs which can simultaneously use the same cyclically extended CAZAC sequence in MU-MIMO mode by applying different phase shifts.

It is worth to notice that different CAZAC sequences should not be used simultaneously in the same cell because of their non-zero crosscorrelation.

3.6.2 Proposed channel estimator

The proposed channel estimator for the generic receive antenna r_i is shown in Figure 3.7. The received signal in the pilot symbols is converted to the frequency domain by the FFT block, afterwards it is multiplied on a tap basis by a local copy of the pilot sequence used at the transmitter. By denoting $\mathbf{p}$ as the pilot sequence and $\mathbf{r}_p$ as the received frequency samples in the pilot positions, the overall channel frequency response is therefore extracted as follows:

$$\tilde{\mathbf{h}}_i(k) = \mathbf{r}_p(k)\mathbf{p}^*(k) \tag{3.33}$$

for $k = 0, \cdots, N_{sub} - 1$. Then, an IFFT is applied to obtain the channel impulse responses from each of the transmit antennas. By assuming the α values as in Eq.(3.32), the centers of the time responses result to be spaced of a number of samples equal to $\tilde{T} = \frac{N_{FFT}}{N_T}$. The separation of the time response for each

antenna can be easily obtained by taking the following group of samples:

$$\left[\tilde{T}(i-1) : \tilde{T}(i-1) + N_{CP} - 1\right] \cup \left[N_{FFT} - \tilde{T}(i-1) - \kappa : N_{FFT} - \tilde{T}(i-1)\right] \tag{3.34}$$

for $i = 1, \cdots, N_T$, with κ integer, and padding with zeros the remaining samples. Note that the second part of the union in Eq.(3.34) contains the energy samples due to the power leakage of the channel impulse response. They are generated because of the mismatch between the length of the pilot sequence and the IFFT size ($N_{sub} < N_{FFT}$). In our simulations, we will consider $\kappa = N_{CP}/3$. The resultant vectors are then converted to the frequency domain to extract the channel frequency response between the N_T transmit antennas and the receive antenna r_i. A Wiener filter [44] is applied to each of the frequency responses to improve the quality of the estimate by mitigating the residual noise contribution. Finally, a linear time domain interpolation is applied between the 4th and the 11th time symbols in order to extract the channel response over the whole frame duration.

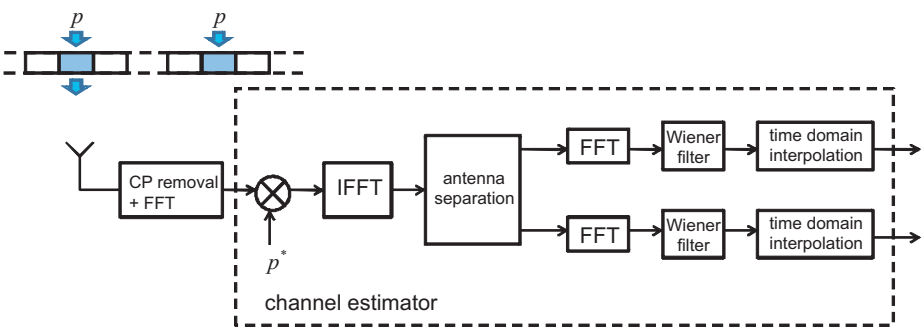

Figure 3.7: Proposed channel estimator for LTE-A uplink.

3.7 Performance evaluation

The LTE-A uplink MIMO performance is evaluated in this section by assuming a Typical Urban channel with uncorrelated antennas [28]. The main simulation parameters are shown in Table 3.3. When fast link adaptation is used (see Appendix A), we assume a 5 ms delay between the selection of the MCS to be used in the receiver and its application in the transmitter.

The fast link adaptation differentiates from the long term link adaptation, where

Table 3.3: Simulation parameters for open loop MIMO evaluation

Carrier frequency	2 GHz
Sampling frequency	15.36 MHz
Number of subcarriers	600
FFT size	1024
CP length	$5.2^a/4.68^b$ μs
Frame duration	1 ms
Antenna configurations	2x2, 2x4, 4x4
Channel model	Typical Urban
User speed	3 kmph
Pilot Overhead (Ov)	14,29%
Channel Estimation	ideal based on WF
MCS settings	QPSK: 1/3, 1/2, 2/3 16QAM: 1/2, 2/3, 4/5 64QAM: 1/2, 2/3, 4/5
Channel Coding	3GPP Rel.8 compliant Turbo code with basic rate 1/3
Turbo decoder iterations	8
BLER Target	1% without HARQ 10% with HARQ
HARQ retransmission strategy	IR
HARQ Max. number of retransmissions	4
HARQ SAW channels	6

[a] 1st and 8th OFDM/SC-FDM symbol in a frame.
[b] $2^{th} - 7^{th}$ and $9^{th} - 14^{th}$ OFDM/SC-FDM symbols in a frame.

the selection of the MCS is based on long term channel statistics. Since long term link adaptation requires lower feedback overhead, it has been shown to be more advantageous in case of highly frequency selective channels, where the dynamic range of the post-detection instantaneous SNR is limited [45]. Fast link adaptation results to be therefore useful in case of low frequency selective channels, e.g. flat channel.

The validity of the fast link adaptation algorithm presented in Appendix A is shown in Figure 3.8 for a 2x2 antenna configuration, where also the spectral efficiency curves of the single MCSs are shown. It is assumed full channel knowledge and no HARQ. Note that the envelope of the spectral efficiency curves of all the MCSs represents the long term link adaptation curve, which is based on the selection of the MCSs depending on the average SNR value. The fast link adaptation curve hence lies partly on the long term link adaptation curve,

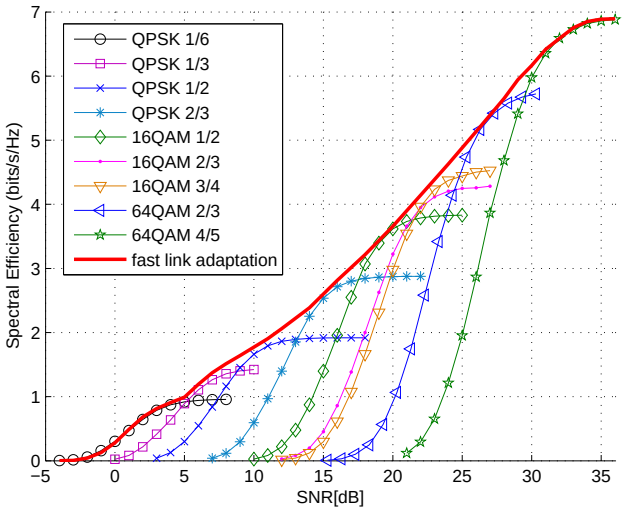

Figure 3.8: Long term link adaptation and fast link adaptation for SC-FDM 2x2.

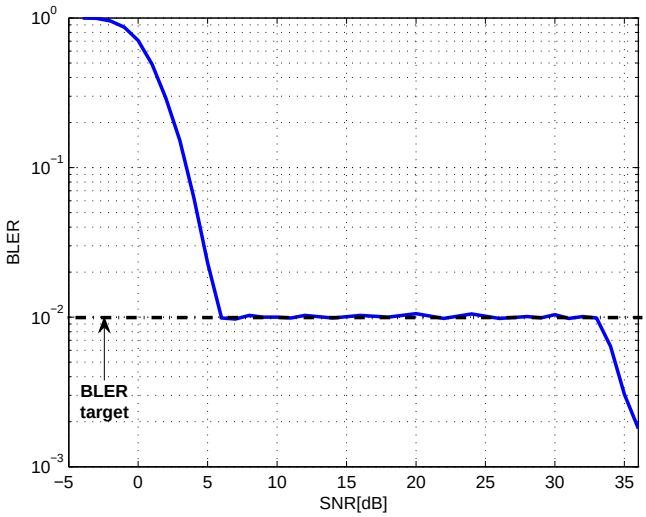

Figure 3.9: BLER performance of SC-FDM 2x2 with fast link adaptation.

but also offering some gain in the transition regions of different MCSs. This is due to its capability to instantaneously cope with the variations of the SNR. As mentioned above, the fast link adaptation gain is expected to be higher for flat channels, given the higher post detection SNR variability.

As shown in Figure 3.9, the fast link adaptation algorithm allows to fulfill the BLER target requirement in the medium SNR region, while in the low and high SNR regions the performance is obiouvsly dominated by the lowest and highest order MCS, respectively.

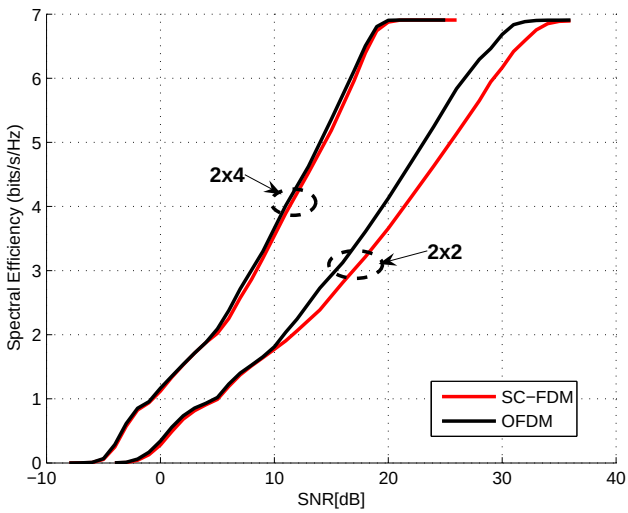

Figure 3.10: OFDM vs. SC-FDM: performance comparison for 2x2 and 2x4 antenna configurations.

In Figure 3.10, the performance of SC-FDM is compared with OFDM, for both 2x2 and 2x4 configuration and still assuming fast link adaptation. As expected, in a 2x2 configuration OFDM clearly outperforms SC-FDM in medium and high SNR region because of the noise enhancement issue in SC-FDM. They perform instead approximately the same in low SNR region, where low order MCSs are typically used, which are robust to the noise. The gap is however pretty reduced in a 2x4 configuration, because of the positive effect of the increase of the diversity branches on the SC-FDM performance.

The results obtained with a 4x4 configuration are shown in Figure 3.11. The 2x4 result for SC-FDM is also included for the purpose of comparison. Again, OFDM outperforms SC-FDM. Note that the fast link adaptation curve of SC-FDM 2x4 configuration follows the shape of the OFDM 4x4 in the medium SNR

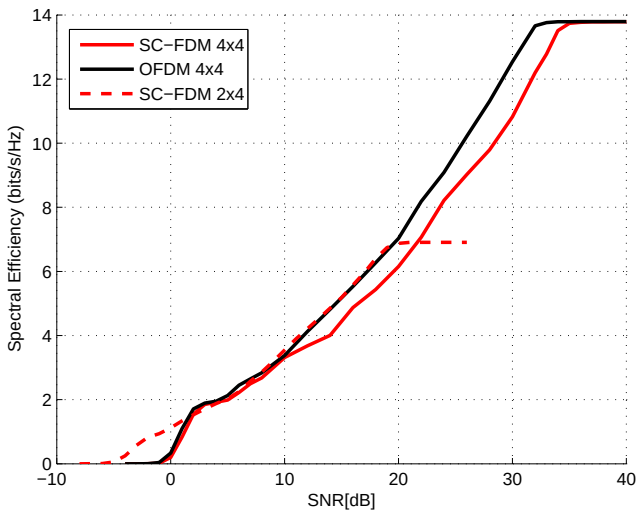

Figure 3.11: OFDM vs. SC-FDM: performance comparison with 4x4 antenna configuration.

region, thus overcoming SC-FDM 4x4. Again, this is due to the diversity gain in 2x4 configuration. Given the reduced complexity in the spatial processing of 2x4 configuration, spatial multiplexing 4x4 shall be used only in high SNR region.

The HARQ impact on the performance is shown in Figure 3.12. Note that the BLER target is set to 0.1 when HARQ is applied. This is made accoding with the 3GPP specifications, since the usage of HARQ allows a more aggressive selection of the MCSs [46]. In both 2x2 and 2x4 cases, HARQ leads to higher gain in low SNR region. This is because at low SNRs the possibility of exploiting retransmissions is more beneficial for increasing the throughput. Note that, in a 2x4 configuration, the benefits of HARQ are negligible at high SNRs.

The losses due to the real channel estimation are shown in Figure 3.13, assuming 16QAM 1/2. For 2x2 transmission the degradation with respect to SISO is very small. The SNR loss increases instead in a 4x4 configuration. This is mainly due to the lower transmit power per antenna in this configuration, and hence bigger influence from noise. The maximum degradation is limited to around 0.3 dB. Figure 3.14 shows the fast link adaptation results. As expected, the performance degradation due to the real channel estimation is more visible in a 4x4 configuration, especially at very low SNR.

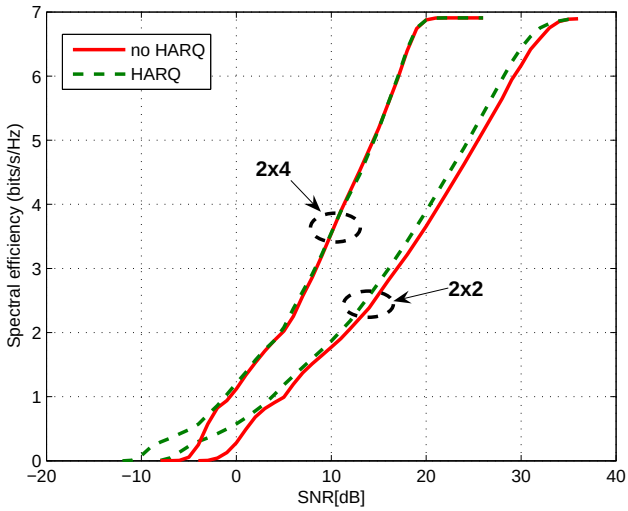

Figure 3.12: Fast link adaptation performance of SC-FDM with HARQ.

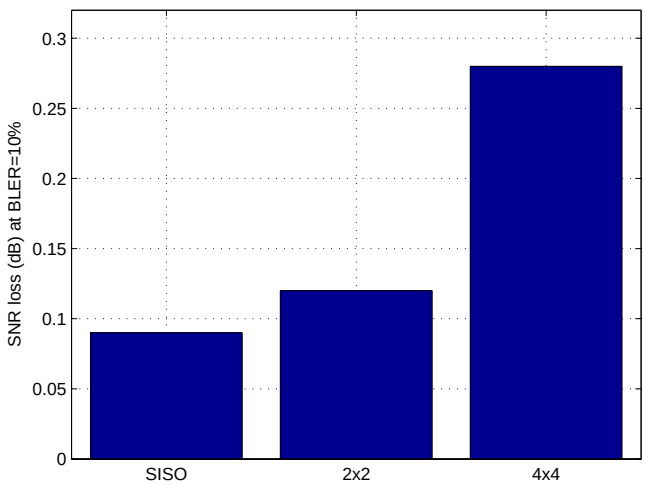

Figure 3.13: SNR losses due to real channel estimation for 16QAM 1/2.

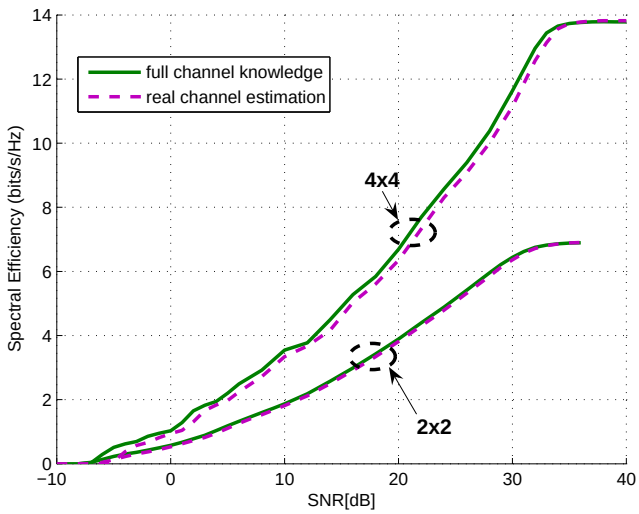

Figure 3.14: Fast link adaptation performance of SC-FDM with real channel estimation.

Finally, the spectral efficiency losses in the fast link adaptation due to the RF impairments modeled with the white noise source generator as described in Appendix A are shown in Figure 3.15. An EVM value of 5% is assumed. The degradation is negligible in 2x2 configuration, while it becomes visible in 4x4 configuration, especially in high SNR region, where high order MCSs are typically selected.

3.8 Summary

In this chapter, we have introduced the principles of MIMO transmission and in particular we have discussed the design of open loop spatial multiplexing for LTE-A uplink. A detailed description of the transceiver chain is provided. The SC-FDM air interface is compared with OFDM to highlight the performance difference with the downlink. Most of the results are obtained with fast link adaptation, allowing to select the MCS which better copes with the instantaneous channel conditions. OFDM has been shown to outperform SC-FDM because of the noise enhancement issue of the latter in 2x2 and 4x4 configurations; however, the increase of the diversity branches allows to considerably reduce the performance gap. HARQ allows to further boost the spectral effi-

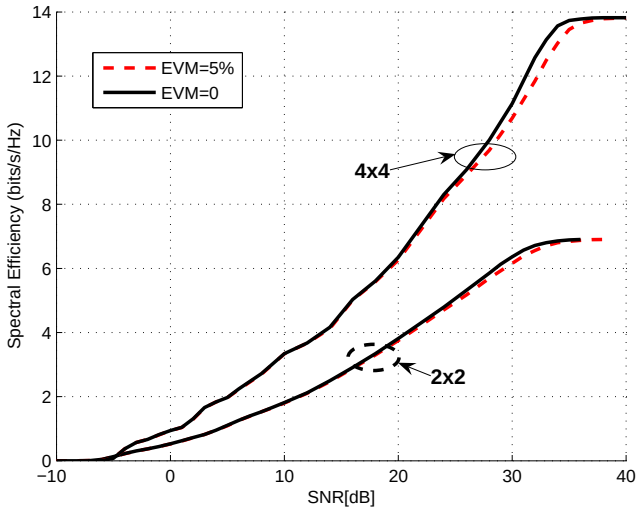

Figure 3.15: Effect of the RF impairments at the transmitter on the spectral efficiency performance.

ciency performance, especially in the low SNR region where retransmissions of the same CW are more likely to happen. An efficient channel estimator which exploits the orthogonality in the time domain of the cyclically extended phase-shifted CAZAC sequences is proposed. The pilot-assisted channel estimation leads inevitably to some SNR loss with respect to the ideal case of full channel knowledge at the receiver. At 3 kmph, the SNR losses with respect to the full channel knowledge have been shown to be negligible in 2x2 mode and limited to around 0.3 dB in 4x4 transmission. The radio frequency impairments at the transmitter end (modeled as an equivalent white noise source and assuming an EVM value of 5%) lead to some spectral efficiency losses in the high SNR region, especially in a 4x4 antenna configuration.

Chapter 4

Transmit diversity solutions for LTE-A uplink

4.1 Introduction

Transmit diversity techniques exploit redundancy across various domains (e.g., time and frequency) with the aim of improving the reliability of the information transfer data. The spatial domain introduced by the MIMO transmission can also be capitalized to obtain diversity gain while saving other physical resources. This is particularly advantageous in poor radio channel conditions, where spatial multiplexing is not beneficial. MIMO transmit diversity solutions improve the cell edge performance, thus extending the coverage. While closed loop techniques exploit some degree of channel knowledge at the transmitter, open loop transmit diversity solutions do not make use of such information. They are therefore particularly suitable for high speed, where the reliability of the channel state information provided by a feedback message is inevitably compromised.

In this chapter, we focus on open loop transmit diversity techniques for the uplink of LTE-A. Several solutions for both cases of 2 and 4 transmit antenna are discussed and evaluated in terms of link performance as well as CM of the transmit signals. The aim is to identify among the known approaches the most

suitable ones for a MIMO SC-FDM-based air interface.

The chapter is structured as follows. Section 4.2 presents a short state of the art in the MIMO spatial diversity design. Section 4.3 and 4.4 introduce and evaluate transmit diversity solutions for 2 and 4 transmit antennas, respectively. Finally, a summary is given in Section 4.5.

4.2 MIMO spatial diversity

Open loop MIMO transmit diversity techniques capitalize on the spatial domain to achieve diversity gain. The aim of spatial diversity is to consider the multiple antennas as degrees of freedom for sending a unique data stream. Of course, the data stream has to be encoded in a way that exploits such redundancy. In particular, in Space Time coding (STC) the time domain is exploited together with the spatial one to achieve diversity gain, while in Space Frequency Coding (SFC) the frequency domain is used. The seminal paper of Alamouti [47] proposed a simple encoding scheme for 2 transmit antennas which achieves full diversity order and rate one transmission. This means, each data symbol is weighted by all the complex coefficients in the channel matrix, and one symbol is transmitted per each channel use. Moreover, the Alamouti scheme assumes a simple MRC receiver. This is its main advantage with respect to Space Time Trellis codes [48], that provide also coding gain at the expense of an exponentially growth of the decoder complexity with the size of the symbol constellation. The simplicity of the Alamouti principle, which can be applied for both STC and SFC, motivated the search of similar solutions for more than 2 transmit antennas. Tarokh et al. applied the theory of orthogonal designs to create analogs of the Alamouti scheme for 4 transmit antennas [49]; howewer, they have shown that full diversity cannot be achieved with such configurations without sacrificing the full transmission rate. They therefore proposed full diversity codes with fractional rate for the 4 transmit antenna case. On the other hand, rate one transmission can be obtained by sacrificing the full diversity concept: quasi orthogonal codes have been therefore derived by Jafarkhani in [50]. It has been recently shown in [51] that rate one transmission and full diversity for high number of transmit antennas can be in principle achieved by relying on a feedback message which informs the transmitter on the strongest channel eigenvalue; however, this solution breaks the open loop transmission principle. All the proposed techniques are sensitive to the delay spread, and therefore result to be suitable for flat fading environments. Since OFDM-based radio interfaces can convert frequency selective channels into multiple flat subchannels, the matching between MIMO OFDM and STC/SFC solutions is foreseen.

4.3 Open Loop transmit diversity solution for 2 transmit antennas

Transmit diversity solutions are to be included in LTE-A uplink to boost the link performance in difficult radio conditions. In this section, some known and new solutions are evaluated for the 2 transmit antenna case, which is agreed as basic MIMO option in LTE-A Uplink. With reference to the baseband system model presented in Figure 3.4, we consider a single CW and replace the precoder block with the transmit diversity encoder, which applies the Alamouti principle over both time and frequency domain. Both link performance and effect of the transmit diversity encoder on the time domain signals are evaluated.

4.3.1 Space Time Coding (STC)

In the STC scheme, symbols are coded in both space and time to add redundancy. If the transmit diversity encoding is performed in frequency domain, the Alamouti scheme is applied to the whole subcarriers'set to emulate a time-domain Alamouti operation. The dimension of the set corresponds to the DFT size. By assuming that the subcarriers belonging to two adjacent time symbols are numerated from 0 to $2N_{sub} - 1$, the output of the encoder for the same subcarrier k over the two time symbols can be expressed as:

$$\begin{bmatrix} \mathbf{q}_1(k) & \mathbf{q}_1(k+N_{sub}) \\ \mathbf{q}_2(k) & \mathbf{q}_2(k+N_{sub}) \end{bmatrix} = \frac{1}{\sqrt{2}} \cdot \begin{bmatrix} \mathbf{d}(k) & \mathbf{d}(k+N_{sub}) \\ -\mathbf{d}^*(k+N_{sub}) & \mathbf{d}^*(k) \end{bmatrix} \tag{4.1}$$

for $k = 0, \cdots, N_{sub} - 1$, where $\mathbf{d}$ is the original frequency domain sequence, and with subindices on q referring to the 2 antennas. Note that each group of N_{sub} subcarriers forms a SC-FDM symbol after the IFFT operation.

Of course, the CM of the signals over both antennas is not modified by the encoding since the conjugating operation is performed over the whole subcarriers' set; this means, it only provides a phase shift on the corresponding time domain waveforms.

Assuming that the channel remains approximately constant over the same subcarrier in the two adjacent time symbols, an estimate of the transmit frequency samples can be obtained with the MMSE equalizer in Eq.(3.17), by considering

the following receive vector:

$$\mathbf{r}[u] = \left[\mathbf{r}_{1:N_R}(u) \;\; \mathbf{r}^*_{1:N_R}(v)\right]^T \tag{4.2}$$

with $u = k$, $v = k + N_{sub}$, and the equivalent channel matrix given by:

$$\mathbf{H}[u] = \begin{bmatrix} h_{:,1}(u) & -h_{:,2}(u) \\ h^*_{:,2}(u) & h^*_{:,1}(u) \end{bmatrix} \tag{4.3}$$

where $h_{:,t}$ denotes the $N_R \times 1$ vector of the channel coefficients between the tth transmit antenna and the N_R receive antennas. It is worth to mention that in the MMSE detector the expression $\mathbf{H}[u]\mathbf{H}^H[u]$ reduces to $\sum_{i=1}^{N_R} |h_{i,1}|^2 + |h_{i,2}|^2$, thus avoiding the cumbersone matrix inversion.

Note that STC requires an even number of time symbols in the SC-FDM frame: this reduces the flexibility of this scheme since in a real implementation some of the time symbols may be occupied by sounding reference signals (SRSs) or physical control channels instead of data [52].

4.3.2 Space Frequency Coding (SFC)

The SFC scheme provides redundancy by exploiting both frequency and space domains. The output of the transmit diversity encoder in the two neighbouring subcarriers $(k, k+1)$ can be written as follows:

$$\begin{bmatrix} \mathbf{q}_1(k) & \mathbf{q}_1(k+1) \\ \mathbf{q}_2(k) & \mathbf{q}_2(k+1) \end{bmatrix} = \frac{1}{\sqrt{2}} \begin{bmatrix} \mathbf{d}(k) & \mathbf{d}(k+1) \\ -\mathbf{d}^*(k+1) & \mathbf{d}^*(k) \end{bmatrix} \tag{4.4}$$

for k odd.

Note that the signal sent over antenna 1 is unmodified by the encoding.

In this case, the MMSE detector works with the assumption that the channel remains constant over two neighbouring subcarriers. The equivalent receive vector and channel matrix can be written as in Eq.(4.2) and Eq.(4.3), respectively, assuming $u = k$, $v = k + 1$.

Since the transmit diversity encoder scrambles the order of the frequency samples to be transmitted by the second antenna, the low CM property of SC-FDM can be affected. Figure 4.1 shows the CM of the transmit signals on the second antenna when SFC scheme is used. Results are presented for different modulation schemes. OFDM SISO performance is also included for the sake of comparison. It has to be mentioned that, for OFDM, the CM of the time domain signals is not affected by the modulation or the encoding scheme. SFC leads to a penalty which is more evident for QPSK and decreases for higher order modulations. Even though a gain of around 1.2 dB over OFDM is preserved even for 64QAM, the CM increase results to be here particularly critical since transmit diversity techniques are usually adopted in power limited scenarios.

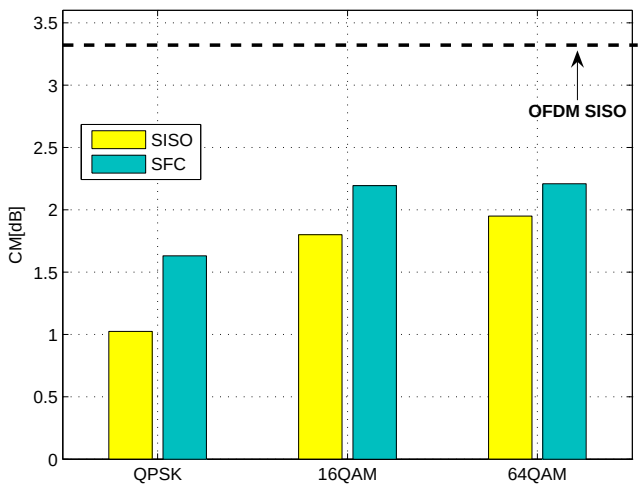

Figure 4.1: CM performance of SFC vs. SISO.

4.3.3 Derivation of low CM SFC schemes

In the previous subsections the most known approaches to perform Alamouti encoding across time or frequency domains have been presented. SFC results to be more flexible than STC since it does not require any assumption on the number of time symbols in a frame. However, the low CM of the transmit signals is compromised since their single carrier property is lost. Note that a time domain sequence can be considered as a *single carrier sequence* if the power amplitude of the samples corresponds to the one of a known data symbol constellation.

In this section, we elaborate on the design of space frequency coding solutions starting from the single carrier sequences in the time domain. Our aim is to obtain a scheme which does not compromise the low CM property of the uplink signals.

In order to facilitate the discussion, let us define the following two criteria:

- *Alamouti criterion.* Given two complex sequences $\mathbf{a} = \left[a_0, a_1, \cdots, a_{\bar{N}-1}\right]$ and $\mathbf{b} = \left[b_0, b_1, \cdots, b_{\bar{N}-1}\right]$, we claim that they fulfill the Alamouti criterion if and only if $\forall i \in \left\{0, 1, \cdots, \bar{N}-1\right\}$ there is always $j \in \left\{0, 1, \cdots, \bar{N}-1\right\} - \{i\}$ so that the matrix

$$\begin{bmatrix} a_i & a_j \\ b_i & b_j \end{bmatrix} \tag{4.5}$$

  is an orthogonal matrix.

- *Contiguity criterion.* Given the previously defined complex sequences $\mathbf{a}$ and $\mathbf{b}$, we claim that they fulfill the contiguity criterion if and only if

$$b_i = a^*_{\left(\bar{N}-i-q\right) mod \bar{N}} e^{j\phi(i)}, \quad \text{for } i = 0, \cdots, \bar{N}-1 \tag{4.6}$$

  or

$$b_i = a^*_{\left(i-\bar{N}-q\right) mod \bar{N}} e^{j\phi(i)}, \quad \text{for } i = 0, \cdots, \bar{N}-1 \tag{4.7}$$

  where $\phi(i)$ is a linear function of i and q is a generic integer number. It is worth to notice that in Eq.(4.6) the samples b_i conjugate and revert the order of the samples a_i, while in Eq.(4.7) the samples b_i conjugate and cyclically shift the positions of a_i.

Of course, space frequency coding can be performed over frequency sequences fulfilling the Alamouti criterion.

It can be shown that, given the two time domain single carrier sequences $\mathbf{u}$ and $\tilde{\mathbf{u}}$, the necessary condition so that the corresponding frequency domain sequences respect the Alamouti criterion is that $\mathbf{u}$ and $\tilde{\mathbf{u}}$ follow both the Alamouti and the contiguity criteria.

If $\mathbf{u}$ corresponds to a vector of data symbols, according to the contiguity criterion the sequence $\tilde{\mathbf{u}}$ is simply a conjugate, sample and phase shifted version of $\mathbf{u}$.

In the following, we elaborate on the sequence $\tilde{\mathbf{u}}$ which in our framework represents the generated time domain sequence over the second antenna, while the sequence $\mathbf{u}$ over the first antenna is unmodified. For simplicity, we assume that the sequence $\tilde{\mathbf{u}}$ has length N_{sub}, hence corresponding to the equivalent pre-DFT signal (see Figure 2.5). However, as shown in Section 2.3, the power fluctuations of the effective time domain samples are not significantly affected by the different sequence length (N_{FFT}).

According to Eq.(4.6) and Eq.(4.7), let us consider the following two cases:

- *Conjugated cyclically reverted samples.* In this case, the generic element of the sequence $\tilde{\mathbf{u}}$ can be written as:

$$\tilde{\mathbf{u}}(i) = \mathbf{u}^* \left((N_{sub} - i - q) \, mod N_{sub} \right) e^{j\phi(i)} \tag{4.8}$$

  for $i = 0, \cdots, N_{sub}-1$. It can be easily verified that, by assuming $\phi(i) = \pi i$ and q odd, the sequences $\mathbf{u}$ and $\tilde{\mathbf{u}}$ also respect the Alamouti criterion. The correspondent frequency domain samples on the second antenna, obtained by applying a DFT operation over $\tilde{\mathbf{u}}$, are given by:

$$\tilde{\mathbf{d}}(k) = (-1)^{N_{sub}-q+1} \, e^{-j\frac{2\pi}{N_{sub}}(N_{sub}-q)k} \mathbf{d}^* \left(\left(k - \frac{N_{sub}}{2} \right) mod N_{sub} \right) \tag{4.9}$$

  for $k = 0, \cdots, N_{sub}-1$. It can be noticed that the position of the frequency samples on the second antenna does not depend on the value q of the time domain shift, which is absorbed in a phase term. The Alamouti coding in the frequency domain results to be applied over samples having constant distance equal to $N_{sub}/2$ subcarriers. This can severely affect the performance of the MMSE detector in case of a frequency selective channel.

- *Conjugated cyclically shifted samples.* The generic element of the sequence $\tilde{\mathbf{u}}$ can in this case be expressed as:

$$\tilde{\mathbf{u}}(i) = \mathbf{u}^* \left((i - N_{sub} - q) \, mod N_{sub} \right) e^{j\phi(i)} \tag{4.10}$$

  for $i = 0, \cdots, N_{sub}-1$. The Alamouti criterion between sequences $\mathbf{u}$ and $\tilde{\mathbf{u}}$ is fulfilled by assuming $q = N_{sub}/2$ and $\phi(i) = \pi \left(N_{sub} - M + 1 + 2\frac{i(N_{sub}-M)}{N_{sub}} \right)$, with M odd integer. The correspondent frequency domain sequence is given by:

$$\tilde{\mathbf{d}}(k) = (-1)^{N_{sub}-M+1} \, e^{j\pi(N_{sub}-M-k)} \mathbf{d}^* \left((N_{sub} - M - k) \right) \tag{4.11}$$

for $k = 0, \cdots, N_{sub} - 1$. Here, the sequences $\mathbf{d}$ and $\tilde{\mathbf{d}}$ always fulfill the Alamouti criterion. By selecting $M = N_{sub}/2 + 1$, we obtain the following compact expression for the sequence $\tilde{\mathbf{d}}$:

$$\tilde{\mathbf{d}}(k) = (-1)^{k+1} \mathbf{d}^* \left(\left(\frac{N_{sub}}{2} - k - 1 \right) mod N_{sub} \right) \tag{4.12}$$

It is worth to notice that Eq.(4.12) leads to the lowest average distance between the frequency samples where the Alamouti principle is applied. The frequency distance is indeed comprised between 1 to $N_{sub}/2 - 1$ samples, thus in any case lower than in Eq.(4.9).

In the numerical evaluation we will only consider the solution in Eq.(4.12) as low CM SFC scheme because of its lower average distance between coupled Alamouti frequency samples. The output of the MMSE detector can be written as for SFC assuming $u = (o-1)\frac{N_{sub}}{2} + i, v = o\frac{N_{sub}}{2} - i - 1$, with $o = 1, 2$ and $i = 1, \cdots, \frac{N_{sub}}{4} - 1$.

4.3.4 Performance evaluation

The proposed open loop diversity schemes with 2 transmit antennas have been evaluated with our LTE-compliant MATLAB simulator. The main simulation parameters are shown in Table 4.1. Two different channel models are considered: Typical Urban and urban micro spatial channell (SCMD), with coherence bandwidths of 375 kHz and 1 MHz, respectively (see Appendix B). Each data frame has a duration of 1 ms, and is formed by 14 SC-FDM time symbols. As usual, it is assumed that the 4th and the 11th symbol carry the pilots which enable the channel estimation at the receiver.

In Figure 4.2, the original SFC and STC are compared with single transmit antenna, for Typical Urban channel and a transmission bandwidth of 5 MHz, corresponding in the LTE numerology to 25 RBs. It is further assumed 16QAM with coding rate 2/3, low speed (3 kmph) and full channel knowledge at the receiver. The additional diversity gain provided by SFC with respect to 1x2 and 1x4 configurations is evident from the slope of the BLER curves. The gain over single transmit antenna schemes is up to 2.5 dB in 2x2 case and 1.5 dB in 2x4 case. No relevant performance difference is visible between SFC and STC, since the frequency separation between adjacent subcarriers is much lower than the coherence bandwidth of the Typical Urban channel, and at low speed the channel does not change significantly between adjacent time symbols. The MMSE detector can therefore work properly for both SFC and STC schemes.

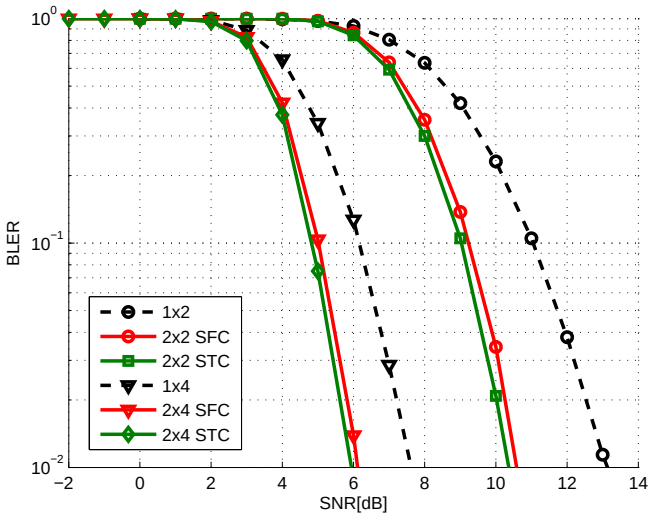

Figure 4.2: SFC/STC performance for low speed.

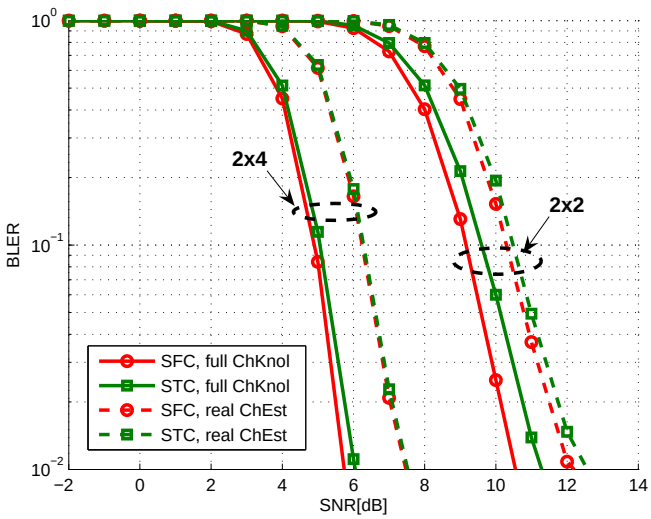

Figure 4.3: SFC/STC performance for high speed: full channel knowledge (full chKnol) vs. real channel estimation (real ChEst).

Table 4.1: Simulation parameters for open loop transmit diversity evaluation

Carrier frequency	2 GHz
Sampling frequency	7.68 MHz
Number of subcarriers	300, 12, 36
FFT size	512
CP length	$5.2^a/4.68^b$ μs
Frame duration	1 ms
Antenna Configurations	1x2, 2x2, 1x4, 2x4, 4x4
Channel Models	Typical Urban, SCMD
User Speed	3 kmph, 150 kmph
Pilot Overhead (Ov)	14,29%
Channel estimation	ideal, based on WF
MCS settings	QPSK: 1/6, 1/3, 1/2, 2/3 16QAM: 1/2, 2/3, 3/4 64QAM: 2/3, 4/5
Channel Coding	3GPP Rel.8 compliant Turbo code with basic rate 1/3
Turbo decoder iterations	8

[a] $1^{st}, 8^{th}$ SC-FDM symbol in a frame.
[b] $2^{th} - 7^{th}$,$9^{th} - 14^{th}$ SC-FDM symbol in a frame.

For high speed (150 kmph), SFC outperforms STC in the 2x2 case (see Figure 4.3) by around 0.5 dB as the channel response changes significantly between adjacent time symbols. However, when real channel estimation is considered, the performance gap between SFC and STC scheme is negligible. For channel estimation based on Wiener Filter (WF) [44] in the frequency domain and linear interpolation in the time domain (between the responses obtained from the 4th and the 11th time symbols), the error due to estimation in frequency direction at high speeds results to be more critical than the error in the time direction. This is because of the incurring of ICI, which leads to higher losses for SFC compared to STC when real channel estimation is considered. Note that in 2x4 case both schemes perform equivalently thanks to the higher diversity gain of the 4 receive antennas.

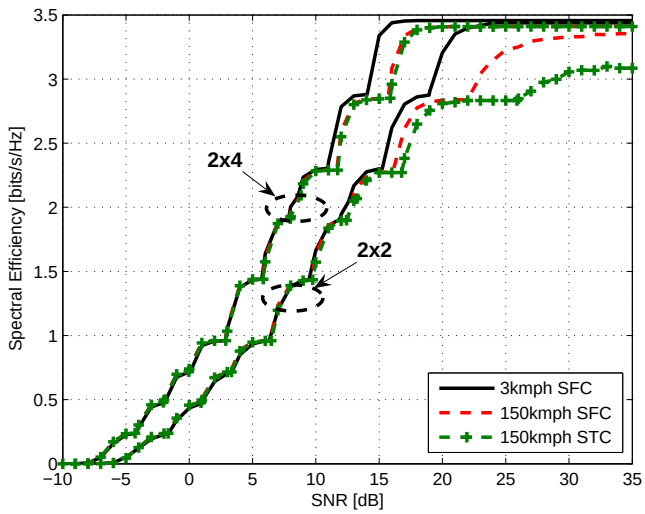

Figure 4.4: Long Term link adaptation curves for SFC/STC with 2x2 and 2x4 configurations.

The performance results over the whole SNR range are shown in Figure 4.4 in terms of long term link adaptation curves, obtained as the envelope of the spectral efficiency curves for several MCSs. The high speed case leads to some performance loss at high SNR region because of the sensitivity of the high order MCSs to ICI, but, as expected, STC performs worse than SFC. However, both transmit diversity solutions are effective in low-medium SNR region, where these techniques are more likely to be used. Furthermore, the increase of diversity in the 2x4 configuration allows to reduce the gap for the 3 kmph case, and at the same time makes the two techniques have the same performance.

In the Typical Urban scenario the low CM SFC scheme derived in Section 4.3.3 fails completely with an UE bandwidth of 25 RBs (BLER equal to 1 over the whole SNR range). This is a result of the frequency separation (up to 149 subcarriers) between the samples being encoded in the Alamouti operation, a frequency separation which is much wider than the coherence bandwidth of the Typical Urban channel.

The suitability of the low CM SFC scheme is therefore evaluated by assuming a very small user bandwidth to reduce the frequency separation between the paired subcarriers. Figure 4.5(a) shows the results obtained assuming the UE moving at 150 kmph and transmitting over 1 RB (12 subcarriers). In this scenario the low CM SFC scheme still provides some gain over 1x2 configuration

at high SNR (around 1 dB at 10% BLER). However, a bandwidth allocation of 3 RBs (36 subcarriers) is enough to make the scheme fail (see Figure 4.5(b)). The performance of low CM SFC is also evaluated for the SCMD channel (see Figure 4.6), having lower frequency selectivity than the Typical Urban channel. In 1 RB case, low CM SFC slightly outperforms STC in a 2x2 configuration. For an UE transmitting over 3 RBs, STC overcomes low CM SFC, though their gap is below 0.4 dB. Note that a gain up to 1.8 dB over 1x2 and 1x4 is preserved in either case.

Therefore, low CM SFC scheme can still provide additional SNR gain with respect to single transmit antenna solutions without incurring a CM penalty and avoiding the STC's constraint of having an even number of time symbols. Given that its suitability is restricted to very small bandwidth allocations, it can be considered a solution for the transmission of Uplink Control Information (UCI), which in LTE/LTE-A is frequency multiplexed with data in the Physical Uplink Shared Channel (PUSCH) [6].

4.4 Open loop transmit diversity solutions for 4 transmit antennas

It is known that full diversity and full rate transmission cannot be obtained simultaneously in a 4 transmit antenna system [49] when no feedback is assumed [51]. It is known that in a practical LTE-A system different transmission rates are achieved by using different MCSs; in order not to affect the complexity of the link adaptation algorithm, it is worth to consider as a constraint the full rate transmission and therefore sacrificing the full diversity concept. In this section, some open loop transmit diversity solutions for 4 transmit antennas are presented and evaluated.

4.4.1 Extended Alamouti Space-Time Coding (EA-STC)

It represents the most intuitive solution for applying the Alamouti principle to a 4 transmit antenna system. The equivalent of the Alamouti matrix in a 4x4 dimension can be obtained with a recursive construction procedure as shown in [53]. The resultant output of the encoder for the same subcarrier belonging to four adjacent time symbols can be expressed as:

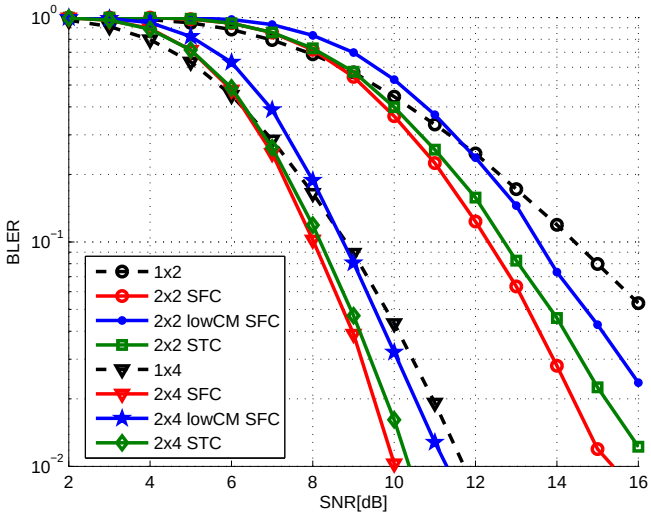

(a) 1 RB

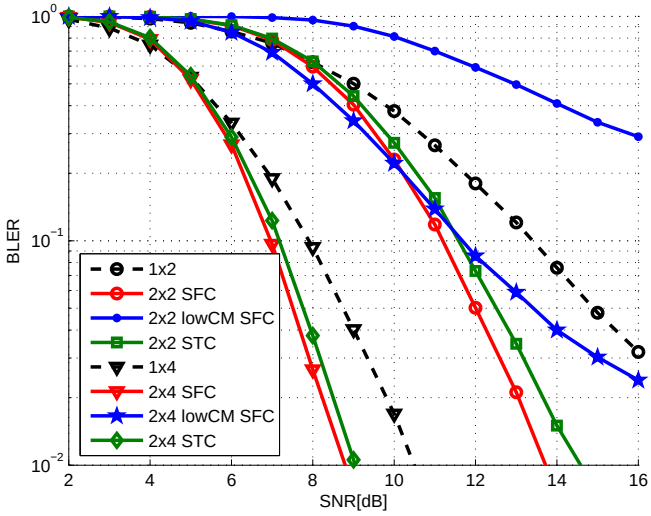

(b) 3 RBs

Figure 4.5: BLER performance of STC, SFC and low CM SFC with Typical Urban channel.

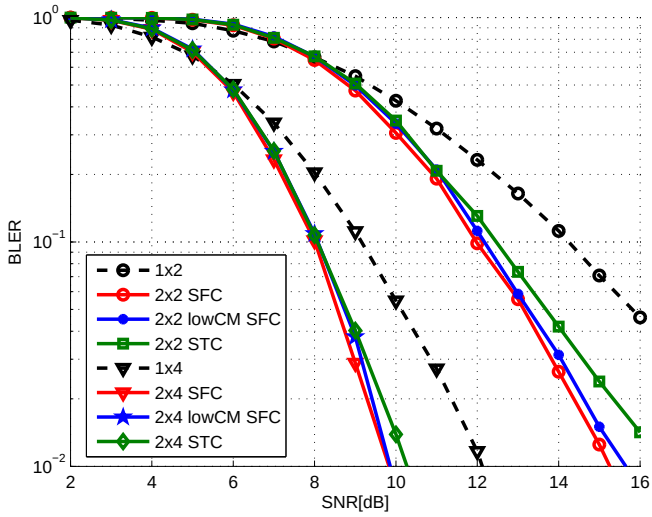

(a) 1 RB

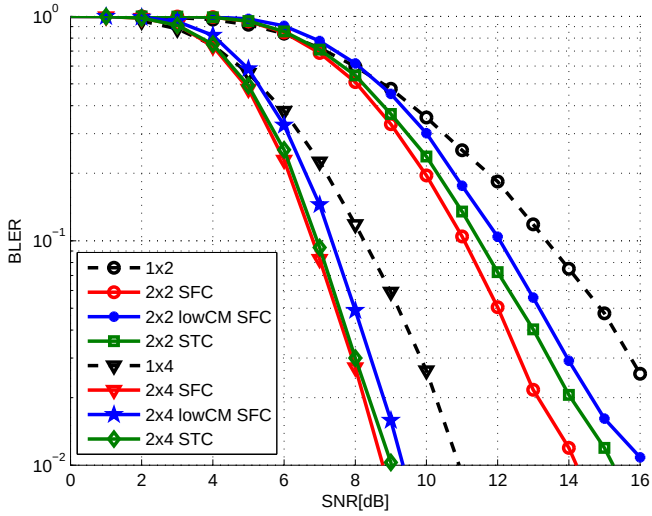

(b) 3 RBs

Figure 4.6: BLER performance of STC, SFC and low CM SFC with SCMD channel.

$$\begin{bmatrix} \mathbf{q}_1(k) & \mathbf{q}_1(k+N_{sub}) & \mathbf{q}_1(k+2N_{sub}) & \mathbf{q}_1(k+3N_{sub}) \\ \mathbf{q}_2(k) & \mathbf{q}_2(k+N_{sub}) & \mathbf{q}_2(k+2N_{sub}) & \mathbf{q}_2(k+3N_{sub}) \\ \mathbf{q}_3(k) & \mathbf{q}_3(k+N_{sub}) & \mathbf{q}_3(k+2N_{sub}) & \mathbf{q}_3(k+3N_{sub}) \\ \mathbf{q}_4(k) & \mathbf{q}_4(k+N_{sub}) & \mathbf{q}_4(k+2N_{sub}) & \mathbf{q}_4(k+3N_{sub}) \end{bmatrix} = \frac{1}{2} \cdot$$
$$\cdot \begin{bmatrix} \mathbf{d}(k) & \mathbf{d}(k+N_{sub}) & \mathbf{d}(k+2N_{sub}) & \mathbf{d}(k+3N_{sub}) \\ -\mathbf{d}^*(k+N_{sub}) & \mathbf{d}^*(k) & -\mathbf{d}^*(k+3N_{sub}) & \mathbf{d}^*(k+2N_{sub}) \\ -\mathbf{d}^*(k+2N_{sub}) & -\mathbf{d}^*(k+3N_{sub}) & -\mathbf{d}^*(k) & \mathbf{d}^*(k+2N_{sub}) \\ \mathbf{d}(k+3N_{sub}) & -\mathbf{d}(k+2N_{sub}) & -\mathbf{d}(k+N_{sub}) & \mathbf{d}(k) \end{bmatrix} \tag{4.13}$$

for $k = 0, \cdots, N_{sub} - 1$. Again, the MMSE detector has the form in Eq.(3.17) by assuming the following equivalent channel matrix on each subcarrier:

$$\mathbf{H}[k] = \begin{bmatrix} h_{:,1}(k) & -h_{:,2}(k) & -h_{:,3}(k) & h_{:,4}(k) \\ h^*_{:,2}(k) & h^*_{:,1}(k) & -h^*_{:,4}(k) & -h^*_{:,3}(k) \\ h^*_{:,3}(k) & -h^*_{:,4}(k) & h^*_{:,1}(k) & -h^*_{:,2}(k) \\ h_{:,4}(k) & h_{:,3}(k) & h_{:,2}(k) & h_{:,1}(k) \end{bmatrix} \tag{4.14}$$

where $h_{:,t}$ denotes the 4×1 vector of the channel coefficients between the tth transmit antenna and the 4 receiving antennas, and

$$\mathbf{r}[u] = [\mathbf{r}_{1:4}(u) \;\; \mathbf{r}^*_{1:4}(v) \;\; \mathbf{r}^*_{1:4}(w) \;\; \mathbf{r}_{1:4}(z)]^T \tag{4.15}$$

with $u = k$, $v = k+N_{sub}$, $w = k+2N_{sub}$, $z = k+3N_{sub}$, and $k = 0, \cdots, N_{sub}-1$.

4.4.2 Phase Shifted - Space Time Coding (PS-STC)

The previous EA-STC requires the channel to be constant over 4 time symbols to properly perform the detection task. This constraint can be very restrictive for high mobility. The PS-STC scheme has similar requirement of STC with 2 transmit antennas, i.e. the channel needs to be constant over 2 time symbols only. The main idea of PS-STC is that a subset of the transmit antennas sends a phase shifted version of the signals sent by another subset of antennas. Let us assume that antenna 1 and 2 deliver the same output of STC. The frequency

domain signals sent over antenna 3 and 4 can be therefore expressed as:

$$\mathbf{q}_3(k) = \mathbf{q}_1(k) \cdot e^{jk\theta} \tag{4.16}$$

$$\mathbf{q}_4(k) = \mathbf{q}_2(k) \cdot e^{j(k\theta+\upsilon)} \tag{4.17}$$

for $k = 0, \cdots, N_{sub} - 1$, where θ and υ are fixed angular values. In this case the equivalent channel matrix to be used in the MMSE detector is:

$$\mathbf{H}[k] = \begin{bmatrix} h_{1,:}(k) + h_{3,:}(k)e^{jk\theta} & -h_{:,2}(k) - h_{:,4}e^{j(k\theta+\phi)} \\ h^*_{:,2}(k) + h^*_{:,4}e^{-j(k\theta+\phi)} & h^*_{:,1}(k) + h^*_{:,3}(k)e^{-jk\theta} \end{bmatrix} \tag{4.18}$$

where $h_{:,r}$ denotes the 1×4 vector of the channel coefficients between the 4 transmit antennas and the rth receive antenna. The vector of the received samples can be written as:

$$\mathbf{r}[u] = [\mathbf{r}_{1:4}(u) \;\; \mathbf{r}^*_{1:4}(v)]^T \tag{4.19}$$

with $u = k$, $v = k + N_{sub}$, and $k = 0, \cdots, N_{sub} - 1$.

4.4.3 Frequency Switch - Space Time Coding (FS-STC)

An alternative solution consists in dividing the data stream in 2 substreams and applying the STC Alamouti scheme per antenna couple. Of course, each substream has to be mapped over different sets of subcarriers. The output of the encoder can be therefore written as follows:

$$\begin{bmatrix} \mathbf{q}_1(k) & \mathbf{q}_1(k+\frac{N_{sub}}{2}) & \mathbf{q}_1(k+N_{sub}) & \mathbf{q}_1(k+3\frac{N_{sub}}{2}) \\ \mathbf{q}_2(k) & \mathbf{q}_2(k+\frac{N_{sub}}{2}) & \mathbf{q}_2(k+N_{sub}) & \mathbf{q}_2(k+3\frac{N_{sub}}{2}) \\ \mathbf{q}_3(k) & \mathbf{q}_3(k+\frac{N_{sub}}{2}) & \mathbf{q}_3(k+N_{sub}) & \mathbf{q}_3(k+3\frac{N_{sub}}{2}) \\ \mathbf{q}_4(k) & \mathbf{q}_4(k+\frac{N_{sub}}{2}) & \mathbf{q}_4(k+N_{sub}) & \mathbf{q}_4(k+3\frac{N_{sub}}{2}) \end{bmatrix} = \frac{1}{\sqrt{2}} \cdot$$
$$\cdot \begin{bmatrix} \mathbf{d}(k) & 0 & \mathbf{d}(k+N_{sub}) & 0 \\ -\mathbf{d}^*(k+N_{sub}) & 0 & \mathbf{d}^*(k) & 0 \\ 0 & \mathbf{d}\left(k+\frac{N_{sub}}{2}\right) & 0 & \mathbf{d}\left(k+\frac{3N_{sub}}{2}\right) \\ 0 & -\mathbf{d}^*\left(k+\frac{3N_{sub}}{2}\right) & 0 & \mathbf{d}^*\left(k+\frac{N_{sub}}{2}\right) \end{bmatrix} \tag{4.20}$$

for $k = 0, \cdots, N_{sub}/2 - 1$. Note that, to preserve the single carrier property of the transmit signals, the DFT in the transmitter has here to be applied at each substream, i.e., the DFT size is reduced at $N_{sub}/2$. It is straightforward to notice that the transmit frequency samples can be estimated by applying over disjoint sets of subcarriers the same detector of traditional STC.

4.4.4 Performance evaluation

The proposed algorithms are evaluated by assuming a Typical Urban channel. The simulation assumptions are still as in Table 4.1. Results obtained with ideal channel estimation are shown in Figure 4.7, for both low and high speed. The 4 transmit antennas algorithms are compared with STC 2x4. At 3 kmph, STC 2x4 slightly outperforms EA-STC at low SNR, while the behaviour turns to be the opposite at higher SNR. This is because, in low SNR region, STC 2x4 benefits from having the transmit power split over only 2 antennas. Among the described 4 transmit antenna schemes, PS-STC performs the best. However, its SNR gain over STC 2x4 is limited to around 0.5 dB at 10% BLER. This gain is further reduced at 150 kmph, up to 0.2 dB. Note that at high speed EA-STC fails dramatically, since the condition of stationarity of the channel response over 4 time symbols is inevitably lost.

The impact of the real channel estimation on the performance is shown in Figure 4.8. Here, STC 2x4 tends to outperform all the 4 transmit antenna schemes for both low and high speed. Only PS-STC shows some SNR gain at low BLER values. This is due to the higher channel estimation error in 4 transmit antenna mode (see Section 3.6), which reduces the already poor SNR gain of the discussed schemes over STC 2x4.

4.5 Summary

In this chapter, the suitability of several open loop transmit diversity schemes is evaluated for an LTE-A uplink air interface, based on SC-FDM technology.

In 2 transmit antenna mode, both SFC and STC approaches based on Alamouti encoding are considered. SFC suffers from a CM penalty, whereas STC has reduced flexibility due to the rigid time domain encoding. Both approaches show about the same performance at low speed. At high speed SFC overcomes STC in a 2x2 antenna configuration, and especially for high order MCSs, but with increased diversity (2x4) their performance is again the same. A new SFC

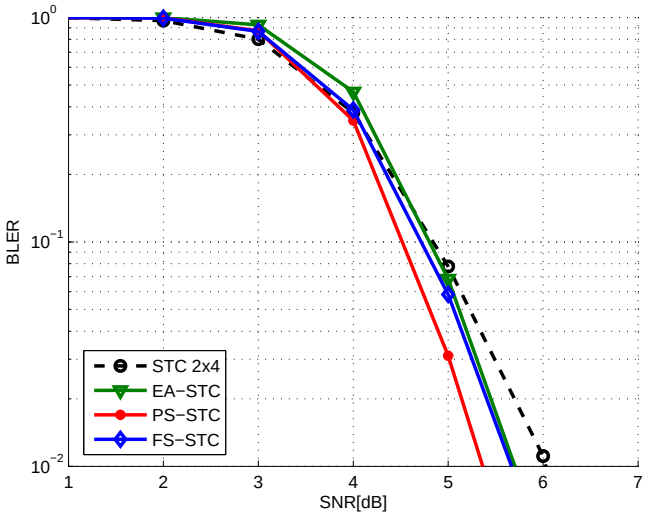

(a) 3 kmph

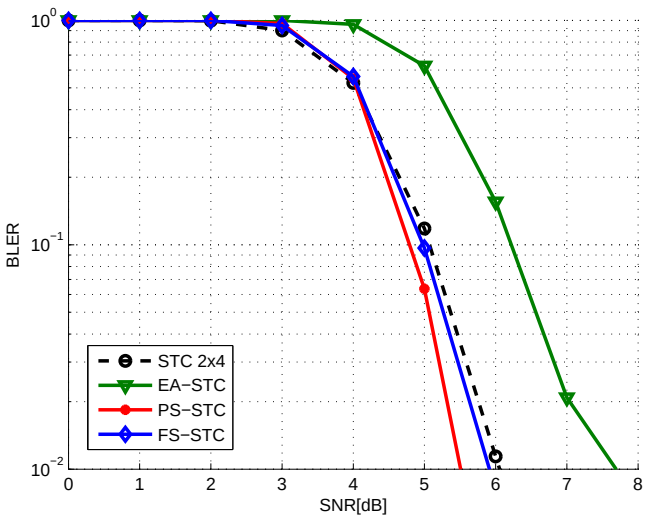

(b) 150 kmph

Figure 4.7: 4x4 transmit diversity scheme performance assuming full channel knowledge at the receiver.

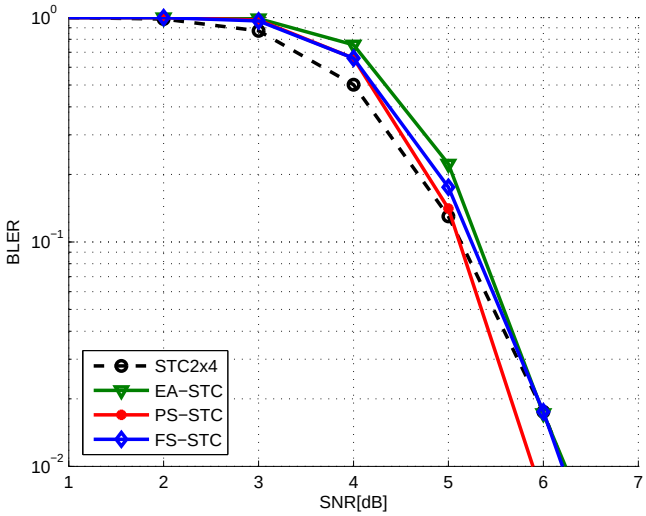

(a) 3 kmph

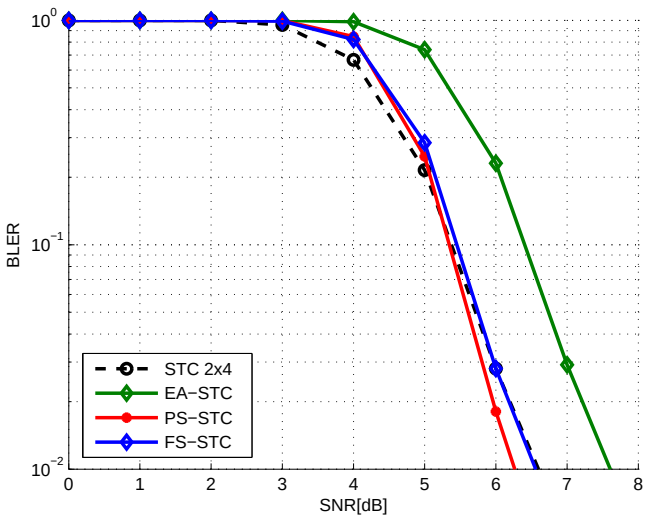

(b) 150 kmph

Figure 4.8: 4x4 transmit diversity scheme performance assuming real channel estimation at the receiver.

scheme which preserves the low CM property of the SC-FDM signals has been derived starting from a conjugated and cyclically reverted version of the original single carrier signal; however, this solution results to be valid for UEs transmitting a small amount of data, and can be therefore considered a candidate for the transmission of UCI.

In 4 transmit antenna mode, the achievement of full diversity is mathematically not possible in case the rate one transmission has to be preserved. An extended Alamouti approach has been tested and compared to further solutions based on phase shift of the same transmit signals or frequency shift over different subcarrier sets. The extended Alamouti solution is shown to be very sensitive to the UE's speed and therefore not suitable for a practical implementation. The other algorithms provide a limited gain with respect to the 2 transmit antenna solutions when full channel knowledge and 4 receive antennas are assumed. Moreover, this gain is lost when real channel knowledge is considered, due to the higher error in the channel estimation process for 4 transmit antennas compared to 2 transmit antennas. We therefore do not see any reason for moving towards a 4 transmit antenna open loop transmit diversity scheme definition in the upcoming LTE-A uplink standard: for high speed and/or difficult channel conditions, we suggest to convey the total transmit power over 2 transmit antennas where a STC/SFC solution can be applied.

Chapter 5

Precoded MIMO design for LTE-A uplink

5.1 Introduction

In a MIMO transceiver chain, the acquisition of channel knowledge in the receiver is necessary to correctly recover the data streams by compensating the amplitude and phase distorsion and/or reduce the mutual interference contributions. MIMO performance can be further leveraged when some degrees of channel knowledge are also available at the transmitter [13]. In case of full channel state information at the transmitter, it would be possible indeed to send data over the strongest eigenmodes of the channel, with remarkable advantages in terms of throughput. Channel knowledge at the transmitter is however much more challenging to be achieved. In Time Division Duplex (TDD) mode, where UE and BS operate over the same band in different time instants, the channel information acquired in reception mode can be exploited to match the streams to be sent to the channel eigenmodes, provided the channel is slowly variant. This is done by multiplying the data streams by a *precoding* matrix. In Frequency Division Duplex (FDD) mode, where UE and BS send data at the same time over independent bands, there is no way to achieve such channel knowledge but using some feedback signaling. This feedback message has however limited size and the resolution of the channel state information is reduced.

A codebook-based approach is usually adopted to deal with limited feedback capacity in FDD mode. In the receiver a matrix belonging to a predefined collection is selected, and its index is fed back to the transmitter for precoding the data streams. The matrix in the codebook can be selected as the one which maximizes the expected capacity, or that better matches with the channel eigenmodes, or depending on SNR metrics [54].

Precoded MIMO is to be included in LTE-A uplink to further boost the spectral efficiency performance at low speed. Its design has to deal with a number of constraints such as reduced complexity of the algorithms for the precoder selection, limited feedback size, outdated channel state information, and backwards compatibility with the previous LTE Release 8. Furthemore, in a LTE-A air interface the precoder should preserve the single carrier property of the uplink signals to avoid undesired CM increase.

This chapter focuses on the design of precoded MIMO solutions for LTE-A uplink. Ideal solutions are initially evaluated in order to establish an upper bound when more realistic assumptions are taken. The aim is to discuss the suitability of the precoded MIMO solutions for the upcoming standard. Even though the main focus is on FDD mode with limited feedback, some insights for the specific case of TDD mode are also provided.

The chapter is structured as follows. Section 5.2 presents the ideal precoding with full channel knowledge at the transmitter. Section 5.3 deals with Singular Value Decomposition (SVD) based precoding assuming unquantized and limited feedback. Section 5.4 discusses the criteria for the design of an universal codebook of precoding matrices. Section 5.5 presents and evaluates the codebook already adopted in LTE downlink. Section 5.6 discusses the design of a low CM codebook for LTE-A uplink and lastly, some optimizations for TDD mode are presented in Section 5.7. Finally, the summary is given in Section 5.8.

5.2 Ideal precoding based on known channel

To define the ideal precoding matrix, let us introduce the time dimension in the analytical model presented in Section 3.3. Here, we assume to perfectly know the channel state at the transmitter. A common way to express the channel matrix at time instant t_{α_0} in subcarrier k is through its SVD [55], as follows:

$$\mathbf{H}_{t_{\alpha_0}}[k] = \mathbf{U}_{t_{\alpha_0}}[k]\mathbf{\Sigma}_{t_{\alpha_0}}[k]\mathbf{V}^H_{t_{\alpha_0}}[k] \tag{5.1}$$

where $\mathbf{U}_{t_{\alpha_0}}[k]$ is the $N_R \times N_R$ matrix having as columns the eigenvectors of $\mathbf{H}^H_{t_{\alpha_0}}[k]\mathbf{H}_{t_{\alpha_0}}[k]$, $\mathbf{V}_{t_{\alpha_0}}[k]$ is the $N_T \times N_T$ matrix having as columns the eigenvectors of $\mathbf{H}^H_{t_{\alpha_0}}[k]\mathbf{H}_{t_{\alpha_0}}[k]$, and $\mathbf{\Sigma}_{t_{\alpha_0}}[k]$ can be expressed as[1]:

$$\mathbf{\Sigma}_{t_{\alpha_0}}[k] = \begin{bmatrix} \bar{\mathbf{\Sigma}}_{t_{\alpha_0}}[k] \\ \mathbf{0}_{N_R-K,N_T} \end{bmatrix} \tag{5.2}$$

where K is the rank of the matrix $\mathbf{H}_{t_{\alpha_0}}[k]$, $\mathbf{0}_{a,b}$ denotes the $a \times b$ zero matrix and

$$\bar{\mathbf{\Sigma}}_{t_{\alpha_0}}[k] = [diag\,(\lambda_1, \cdots, \lambda_K)\ \mathbf{0}_{K,N_T-K}] \tag{5.3}$$

where $\lambda_1, ..., \lambda_K$ are the singular values of $\mathbf{H}^H_{t_{\alpha_0}}[k]\mathbf{H}_{t_{\alpha_0}}[k]$. Note that $\mathbf{U}_{t_{\alpha_0}}[k]$ and $\mathbf{V}_{t_{\alpha_0}}[k]$ are unitary matrices (i.e., $\mathbf{U}_{t_{\alpha_0}}[k]\mathbf{U}^H_{t_{\alpha_0}}[k] = \mathbf{U}^H_{t_{\alpha_0}}[k]\mathbf{U}_{t_{\alpha_0}}[k] = \mathbf{I}_{N_R}$, and $\mathbf{V}_{t_{\alpha_0}}[k]\mathbf{V}^H_{t_{\alpha_0}}[k] = \mathbf{V}^H_{t_{\alpha_0}}[k]\mathbf{V}_{t_{\alpha_0}}[k] = \mathbf{I}_{N_T}$). Let us define now the following precoding matrix:

$$\mathbf{F}[k] = \mathbf{F}_{t_{\alpha_0}}[k] = \sqrt{\mathbf{R}_{dd}}\bar{\mathbf{V}}_{t_{\alpha_0}}[k] \tag{5.4}$$

where $\bar{\mathbf{V}}_{t_{\alpha_0}}[k]$ denotes the matrix containing the first R columns of $\mathbf{V}_{t_{\alpha_0}}[k]$, with R equal to the transmission rank, and $\mathbf{R}_{dd}$ is defined as in Eq.(3.16).

It can be easily shown that, if the $\bar{\mathbf{U}}^H_{t_{\alpha_0}}[k]$ matrix is used as a matched filter at the receiver, where $\bar{\mathbf{U}}_{t_{\alpha_0}}[k]$ denotes the matrix containing the first R columns of $\mathbf{U}_{t_{\alpha_0}}[k]$, the MIMO channel can be decomposed in R independent spatial channels, whose gains are given by $\lambda_1^2, ..., \lambda_R^2$.

Since $\mathbf{V}_{t_{\alpha_0}}[k]$ is an unitary matrix, in case of full rank transmission (i.e., $R = K = N_T$) the power is equally distributed among the layers and the transmit antennas (see Section 3.5). It is worth to notice that the ideal precoding leads to a performance imbalance between the streams for $R > 1$ when equal power allocation is considered. This is due to the different gains of the channel eigenmodes where the streams are matched. It is known from the MIMO theory that the upper spectral efficiency when full channel knowledge is available at the transmitter can be obtained by dividing the power among the antennas according to the waterfilling algorithm (see Section 3.3). A proper weighting of the transmit power among the antennas can be also optimal for a number of criteria including

[1] here we assume $N_R \geq N_T$

QoS and equal error rate among the streams, as shown in [56] and [57]. Nevertheless the waterfilling solution, which assigns higher power to the antennas transmitting over the strongest eigenmode, fails in a practical system with limited MCS set [58]. This is because higher power over the strongest eigenmodes does not lead to any benefit once the associated streams reach their maximum spectral efficiency value. In our paper [59], we have proposed to weight the transmit power on each antenna depending on some critical parameter at the receiver, e.g., the joint uncoded Symbol Error Rate (SER). This solution tends to enhance the transmit power on the weaker eigenmodes at high SNRs. Given the practical difficulties in the computation of the optimal power vector for each frame, we will not consider the impact of the weighted power allocation in the prosecution of this thesis.

5.3 SVD precoding based on feedback

The performance of the precoded transmission is obviously dependent on the resolution of the channel state information at the transmitter. In FDD mode, the channel knowledge can only be achieved through feedback signaling, whose capacity should be kept reasonably low. The aim of this section is to elaborate on the SVD-based precoding in a real LTE-A uplink system. We consider the case of precoding with unquantized feedback as an upper bound for the more realistic case of precoding with limited feedback.

5.3.1 Precoding with unquantized feedback

Here, we assume a feedback channel with infinite capacity. This means, the BS can inform the UE about the optimal precoding matrix to adopt with infinite resolution. Note that this case is however different from the ideal precoding described in the Section 5.2. This is because the transmitter is not aware of the channel state at time instant t_{α_0} on which it is going to send the data, and therefore it cannot compute $\mathbf{F}_{t_{\alpha_0}}$. Nevertheless, the precoding matrix can be computed at the receiver by SVD of the estimated channel frequency response, and fed back to the transmitter, which uses it for the following transmission. The procedure is explained in the following steps:

- At time instant t_{α_0}, the BS estimates the channel frequency response $\mathbf{H}_{t_{\alpha_0}}$ based on pilot information;
- the BS computes the precoding matrix $\mathbf{F}_{t_{\alpha_0}}$ from $\mathbf{H}_{t_{\alpha_0}}$ as in Eq.(5.4), and

send it back to the UE;

- the UE precodes the data stream(s) as in Eq.(3.9) by using $\mathbf{F}_{t_{\alpha_0}}$, and sends them to the channel at instant $t_{\alpha_1} = t_{\alpha_0} + \Delta t$.
- The BS estimates $\mathbf{H}_{t_{\alpha_1}}$ from the received pilots and uses an MMSE detector to recover the data. According with the formalism of Section 3.5, the output of the MMSE detector at subcarrier k can be written as follows:

$$\mathbf{r}_{eq}[k] = \mathbf{F}_{t_{\alpha_0}}[k]^H \mathbf{H}_{t_{\alpha_1}}[k]^H \left(\mathbf{H}_{t_{\alpha_1}}[k] \mathbf{F}_{t_{\alpha_0}}[k] \mathbf{F}_{t_{\alpha_0}}[k]^H \mathbf{H}_{t_{\alpha_1}}[k]^H + N_T \frac{\sigma_w^2}{\sigma_d^2} \mathbf{I}_{N_R} \right)^{-1} \mathbf{r}[k] \tag{5.5}$$

Therefore, both UE and BS agree on the precoding matrix, even though this is outdated with respect to the channel state on which the transmission is performed. This approach could be considered close to the ideal solution if slow variation of the channel in the time interval Δt is assumed.

5.3.2 Precoding with limited feedback

The most intuitive way to reduce the feedback overhead in the SVD-based precoding approach is to quantize the right singular vectors of the channel matrix. In [60], an efficient method for the derivation of a codebook of unitary matrices based on the iterative Lloyd algorithm [61] is proposed. In this way, it is possible to select as a precoder the unitary matrix belonging to the codebook which is closer to the $\mathbf{V}[k]$ matrix. The following selection criterion can be adopted:

Select

$$\mathbf{F}_s = arg\, min_{\hat{\mathbf{F}} \in C_u} \left\| \mathbf{V}[k]\mathbf{D}[k] - \hat{\mathbf{F}} \right\|_F \tag{5.6}$$

where C_u is the codebook of unitary matrices, $\|\cdot\|_F$ denotes the Frobenius norm, and $\mathbf{D}$ is defined as:

$$\mathbf{D}[k] = diag\left(-\phi_1, \cdots, -\phi_R\right) \tag{5.7}$$

with $\phi_i = \hat{\mathbf{F}}_{:,i}^H \mathbf{V}_{:,i}[k]$ for $i = 1, \cdots, R$, where $\hat{\mathbf{F}}_{:,i}$ and $\mathbf{V}_{:,i}[k]$ denote the i-th column of the $\hat{\mathbf{F}}$ and the $\mathbf{V}[k]$ matrices, respectively. The matrix $\mathbf{D}[k]$ resolves the ambiguity of the non-univocity of the SVD decomposition [55].

Since it may be impractical sending a feedback message for each subcarrier, the selection of the codebook element is generally done over a group of N_s subcarriers, i.e.

Select

$$\mathbf{F}_s = arg\,min_{\hat{\mathbf{F}} \in C_u} \frac{1}{N_s} \sum_{k=0}^{N_s-1} \left\| \mathbf{V}[k]\mathbf{D}[k] - \hat{\mathbf{F}} \right\|_F \tag{5.8}$$

In the following, we will refer to narrowband (NB) precoding when the precoding matrix is selected on a RB basis, and to wideband (WB) precoding when it is selected over the whole transmission bandwidth.

It is worth to notice that the SVD-based precoding should only be used for $R = 1$ when weighted power allocation is not applied. This is because for $R > 1$ the performance imbalance among the streams may lead to floor and ceiling effects in low and high SNR region, respectively [58]. The main advantage of the SVD-based approach for the codebook generation is its simple scalability; codebooks of larger size can be easily obtained with the Lloyd algorithm by performing a more accurate quantization of the $\mathbf{V}$ matrix.

It can be shown that, for $R = 1$, the power distribution among the antennas may change at each transmission, while the total power is unchanged. This power imbalance can be avoided by forcing the entries of the precoding matrix to be constant modulus, i.e.

$$\tilde{\mathbf{F}}_s = \frac{\mathbf{F}_s}{\|\mathbf{F}_s\|} \tag{5.9}$$

In this way, the precoding matrix only provides a phase shift on the frequency samples.

5.4 Practical codebook design

Given the unfeasibility of SVD based precoding for high rank transmission, many contributions in literature addressed the issue of the codebook design concerning a number of criteria. A well known approach considers the codebook design as equivalent to the mathematical problem of subspace packing in the Grassmannian manifold, for both space-time coding [62] and spatial multiplexing [63], assuming identically distributed Rayleigh fading matrix channels.

(a) linear array (b) dual polarized

Figure 5.1: 4x4 antenna configurations.

Closed form subspace packings are only available for certain values of R and N_T [64]. For instance, for $R = 1$ and $N_T = 2$, the Grassmanian manifold is isomorphic with the two-dimensional sphere [65], thus allowing to identify the codebook elements as the vertices of deformed Platonic solids [66]. In most of the cases, vector quantization techniques are however still required. In [67] a design criterion based on the minimization of the BER is considered, while in [68] a column by column quantization approach is proposed for large number of transmit antennas. Even though the cited papers offer deep comprehension of the issue and valid analytical solutions, they do not take into account non identically distributed statistics of the Rayleigh channels. In [69], codebook obtained as spherical caps on che Grassmanian manifold are derived for the specific case of correlated channels. Nevertheless, the codebook is dynamically chosen from a predefined codeset, leading to high sensitivity to feedback errors [70]. Furthermore, practical transceiver constraints are typically not considered.

The codebook to be used in a real transceiver chain should be universal, i.e. it has to show good performance in a number of propagation conditions and at the same time be easily manageble. In [71], a number of criteria for the design of universal practical codebooks are proposed. The main criteria are the following:

1. Maximization of the minimum chordal distance between the matrices of the codebook. The chordal distance between the elements $\mathbf{F}_a$ and $\mathbf{F}_b$ of the codebook is defined as:

$$d\left(\mathbf{F}_a, \mathbf{F}_b\right) = \frac{1}{\sqrt{2}} \left\| \mathbf{F}_a \mathbf{F}_a^H - \mathbf{F}_b \mathbf{F}_b^H \right\|_F \tag{5.10}$$

   The chordal distance is the most common metric used in the problem of finding good packings in the Grassmannian manifold. Furthermore, it has been shown to be an optimal design metric when a post MMSE selection criterion for the codebook element is adopted [63]. A high minimum chordal distance in the codebook ensures indeed a good representation of the Grassmannian manifold.

2. High performance in single-polarized channels. They assume antenna elements located over a linear array, as shown in Figure 5.1(a). The elements of the codebook should preserve high gain response over all directions of departure of the transmit signals. In [71] a design criterion related to the maximization of the minimum of the gain response of the array over all direction of departures is proposed, assuming rank 1 transmission as well as highly correlated channels. However, in the uplink high correlation at the transmit array is quite unlikely. Throughout this chapter, we will therefore evaluate the suitability of the proposed codebooks in single polarized channels through simulations.

3. High performance for dual polarized channels. Two couples of orthogonal polarized antennas, as shown in Figure 5.1(b), are assumed. This configuration results to be particularly suitable for the uplink, since it offers a compact antenna realization. An adequate precoder for such channels would be given by a block diagonal matrix. A further rotation matrix has to be applied in case of a $\pi/4$ rotation with respect of the vertical setting. For further details, we refer to [71]. It is worth to mention that a $\pm\pi/4$ slant allows to exploit the symmetry in reflections off the earth's surface for both polarizations, which is not the case for other polarization configurations such as $(0, \pi/2)$ [72]. Again, the suitability of a codebook in such scenarios will be here evaluated through simulations.

4. Simple matrix selection. For instance, the nested property between ranks could be considered; this means, the lower rank precoder is part of the precoder used for larger rank. This allows to re-use the calculation of the lower rank precoder for the larger rank in case of rank overriding. Furthermore, the entries of each of the codebook's matrices can be constrained to the set $\left\{\pm 1, \pm j, \frac{\pm 1 \pm j}{2}\right\}$. It can be shown [73] that this property reduces the number of matrix-vector operations for the matrix selection.

5. Equal power per antenna. It is preferable that the codebook does not introduce power imbalance between the antennas, so that all the power amplifiers can be equally utilized. This can be obtained by forcing the codebook entries to be constant modulus.

Starting from these criteria, in [71] a generation metodology is proposed. The aim is starting from the design of rank 1 codebook and obtaining the higher rank codebooks by permuting its entries while respecting all the design criteria. In this way, the nested property is also satisfied.

Table 5.1: Feedback overheads with Release 8 codebook (bits per time frame)

MIMO configuration	NB precoding	WB precoding
2Tx rank 1	75	3
4Tx each rank	100	4

5.5 LTE downlink codebook

The aforementioned criteria have been taken into account by the 3GPP in the design of codebooks for 2Tx and 4Tx in LTE Release 8 downlink [8].

For 2Tx case, a set of 6 vectors with dimension 2×1 and large chordal distance (1.4142) has been defined for rank 1 transmission. The codebook for rank 2 transmission is obtained by permuting the couples of vectors of the codebook for rank 1 which keep the unitary property of the precoding matrix. However, in March 2009 in the work item (WI) for LTE-A it has been agreed to remove the codebook for rank 2 transmission and replace it with the identity matrix $\mathbf{I}_2$ [74]. This is because precoded transmission with full rank does not provide sufficient array gain.

The codebooks for 4Tx transmission are obtained by permuting the columns of the 4×4 Householder matrix [75]. The codebook for each rank R, with $R = 1, 2, 3, 4$ consists of 16 precoding matrices with dimension $4 \times R$. The bigger size of 4Tx codebook compared to the 2Tx one allows to cope with a wider range of propagation conditions (e.g., single and dual polarized antenna pattern) which the 4Tx transmission offers. This codebook has also been shown to fulfill the requirements of large chordal distance (0.7071, 1 and 0.7071 for rank 1, 2 and 3, respectively). Again, it has been recently decided to replace the rank 4 codebook with the identity matrix $\mathbf{I}_4$ [74].

All the entries in the matrices of the LTE downlink codebook belong to the set $\left\{\pm 1, \pm j, \frac{\pm 1 \pm j}{2}\right\}$, thus allowing to reduce the computational complexity in the calculation of Eq.(5.11). In the SVD-based codebook instead, the entries of the matrices are random-like, and therefore the complexity for the selection of the precoding matrix is expected to be higher. Furthermore, in the LTE downlink codebook the lower rank precoder is part of the precoder used for larger rank, hence fulfilling the nested property. Also the equal power per antenna property holds, with the exception of two vectors in the 2Tx rank 1 codebook. Finally, the LTE downlink codebook distributes equally the power among the layers.

The selection of the precoding matrix can be based on a number of criteria including instantanous capacity, maximization of the minimum receive vector distance, or maximization of the minimum singular value of the equivalent channel matrix [63]. Here, we propose to select the matrix which maximizes the desired power per frequency sample after the MMSE filtering. This criterion can be expressed as follows:

Select

$$\mathbf{F}_s = arg\,max_{\hat{\mathbf{F}} \in C^{N_T}_{R,Rel8}} \sum_{i=1}^{R} \frac{\mathbf{g}_{ii}^{\hat{F}[k]}}{1 - \mathbf{g}_{ii}^{\hat{F}[k]}} \cdot \sigma_w^2 \tag{5.11}$$

where $\mathbf{g}_{ii}^{\hat{F}[k]}$ is the ith element of the diagonal of the $\mathbf{G}$ matrix expressed as in Eq.(3.18) but substituing $\mathbf{H}[k]$ with $\mathbf{H}_{eq}[k] = \hat{\mathbf{F}}[k]\mathbf{H}[k]$, and $C^{N_T}_{R,Rel8}$ is the Release 8 codebook for N_T transmit antennas and rank R. It can be easily shown that the expression in Eq.(5.11) corresponds to the sum of the equivalent channel gains for the R layers.

Again, to reduce the feedback overhead the selection of the precoding matrix is generally done over a set of N_s subcarriers, i.e.

Select

$$\mathbf{F}_s = arg\,max_{\hat{\mathbf{F}} \in C^{N_T}_{R,Rel8}} \frac{1}{N_s} \sum_{k=0}^{N_s-1} \sum_{i=1}^{R} \frac{\mathbf{g}_{ii}^{\hat{F}[k]}}{1 - \mathbf{g}_{ii}^{\hat{F}[k]}} \cdot \sigma_w^2 \tag{5.12}$$

The feedback overhead of the Release 8 downlink codebook for both NB precoding and WB precoding are shown in Table 5.1, assuming an UE transmitting over 5 MHz.

5.5.1 Link performance evaluation

The behaviour of the codebook defined for LTE downlink is here evaluated in a LTE-A uplink air interface (i.e. for SC-FDM) and compared with the SVD-based one as well as with open loop solutions. The simulation parameters are gathered in Table 5.2. Both cases of NB precoding and WB precoding are considered. A 5 ms delay is assumed between the precoding matrix computation in the BS and its application in the UE. As shown in [45], the precoded transmission is feasible only for very low speed (below 10 kmph) and we will therefore assume 3 kmph as a default UE speed.

Figure 5.2 shows the BLER results obtained with 2x2 antenna configuration

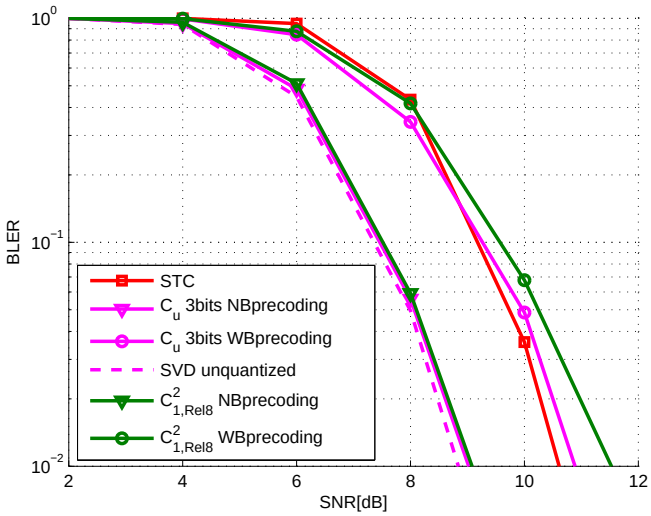

Figure 5.2: BLER performance of precoding with limited feedback for 2x2 rank 1 and Typical Urban channel.

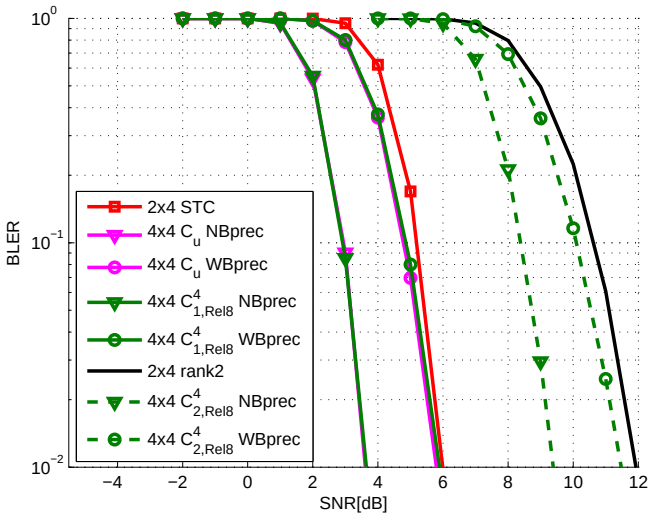

Figure 5.3: BLER performance of precoding with limited feedback for 4 transmit antennas and Typical Urban channel.

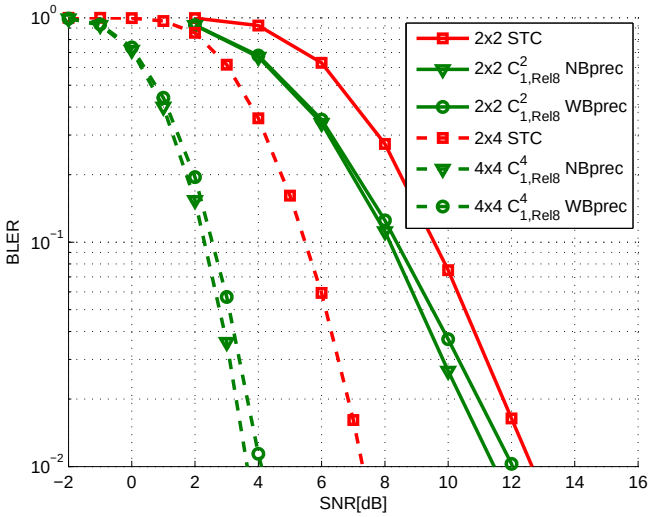

Figure 5.4: BLER performance of precoding with limited feedback assuming Indoor office channel, 4x4 and 2x2 antenna configurations and rank 1 transmission.

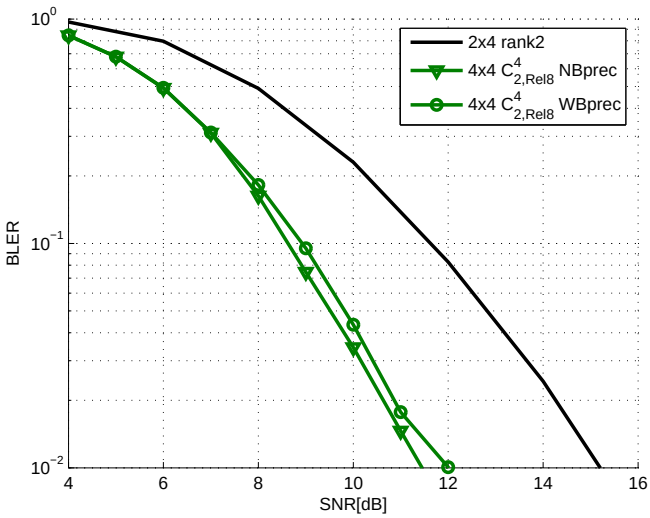

Figure 5.5: BLER performance of precoding with limited feedback assuming Indoor office channel, and 4x4 rank 2 transmission.

Table 5.2: Simulation parameters for precoded MIMO evaluation

Carrier frequency	2 GHz
Sampling frequency	7.68 MHz
Number of subcarriers	300
FFT size	512
CP length	$5.2^a/4.68^b$ μs
Frame duration	1 ms
Antenna configurations	2x2, 2x4, 4x4
Channel Models	Typical Urban Indoor Office
User speed	3 kmph
Pilot Overhead (Ov)	14,29%
Channel Estimation	based on WF
MCS setting	16QAM 2/3
Channel Coding	3GPP Rel.8 compliant Turbo code with basic rate 1/3
Turbo decoder iterations	8

[a] 1st and 8th OFDM/SC-FDM symbol in a subframe.
[b] $2^{th} - 7^{th}$ and $9^{th} - 14^{th}$ OFDM/SC-FDM symbols in a subframe.

and rank 1 transmission, assuming a Typical Urban channel and 16QAM with coding rate 2/3. STC result is also included for the purpose of comparison. In case of SVD-based precoding, a codebook C_u with 8 matrices (thus requiring 3 bits for indexing), has been designed. The codebook with 8 matrices ensures therefore a fair comparison with the LTE downlink codebook for 2x2 rank 1 ($C^2_{1,Rel8}$), which requires the same feedback overhead. C_u with NB precoding leads to high performance gain, which is however much reduced in case of WB precoding. This is obviously due to the loss of resolution when the precoding matrix is computed over a transmission bandwidth which is much larger than the coherence bandwidth of the Typical Urban channel (see Appendix B). No significant difference with STC is indeed visible for WB precoding. Note that SVD-based codebook with 8 matrices allows to obtain the same performance of precoding with unquantized feedback, therefore a wider extension of the codebook is not required. $C^2_{1,Rel8}$ shows approximately the same performance of C_u in both WB precoding and NB precoding cases.

The performance results obtained with 4x4 antenna configuration are shown in

Figure 5.3. Again, results are compared with STC. The gain of NB precoding is up to 2.5 dB over STC 2x4, and is considerably reduced for WB precoding. Similar considerations can be drawn for the case of rank 2. Note that some array gain is here lost due to the increase of the multiplexing branches. The gain of WB precoding over 2x4 rank 2 is limited to around 0.6 dB. Note that in 2x4 rank 2 case no precoding is performed, i.e. $\mathbf{F}_s = \sqrt{\frac{1}{2}}\mathbf{I}_2$, as mentioned above. It is worth to mention that, even though precoded transmission requires a feedback channel and no evident gain is visible, it is still preferable to STC since it does not assume any constraint on the number of time symbols in a frame.

The SNR loss due to the WB precoding is however much reduced when an Indoor office channel model [31] is assumed (see Figure 5.4 and Figure 5.5). This is due to the wider coherence bandwidth of this channel (up to 12 MHz), so that a single precoding matrix still matches with the overall channel response. Here, the gain of $C^2_{1,Rel8}$ over STC is around 1.7 dB. In 4x4 configuration, the SNR gain increases up to 3.4 dB for rank 1 and 2.7 dB for rank 2 at 10% BLER.

5.5.2 Effect of the antenna correlation

In real propagation scenarios antenna correlation is likely to appear given constraints in terms of physical antenna realization as well as the presence of low scattering environments. Here we evaluate the impact of the antenna correlation on the precoded transmission assuming single and double polarized antennas, as already described in Section 5.4.

In case of single polarized antennas, the correlation can be easily modeled with the known Kronecher approach [76]. By defining the transmit and receive antenna correlation matrices as follows:

$$\mathbf{R}_{tx} = \begin{bmatrix} 1 & r_{tx} & r_{tx}^2 & \cdots & r_{tx}^{N_T-1} \\ r_{tx} & 1 & r_{tx} & \ddots & \vdots \\ r_{tx}^2 & r_{tx} & 1 & \ddots & r_{tx}^2 \\ \vdots & \ddots & \ddots & \ddots & r_{tx} \\ r_{tx}^{N_T-1} & \cdots & r_{tx}^2 & r_{tx} & 1 \end{bmatrix} \tag{5.13}$$

$$\mathbf{R}_{rx} = \begin{bmatrix} 1 & r_{rx} & r_{rx}^2 & \cdots & r_{rx}^{N_R-1} \\ r_{rx} & 1 & r_{rx} & \ddots & \vdots \\ r_{rx}^2 & r_{rx} & 1 & \ddots & r_{rx}^2 \\ \vdots & \ddots & \ddots & \ddots & r_{tx} \\ r_{rx}^{N_R-1} & \cdots & r_{rx}^2 & r_{rx} & 1 \end{bmatrix} \tag{5.14}$$

where r_{tx} and r_{rx} are the correlation coefficients of the transmit and receive antennas, respectively, the spatial correlation matrix of the MIMO radio channel can be expressed as:

$$\mathbf{R} = \mathbf{R}_{tx} \otimes \mathbf{R}_{rx} \tag{5.15}$$

where $\otimes$ denotes the Kronecher product. The $N_R N_T \times 1$ column vector of the correlated channel coefficients can be obtained as [76]:

$$\mathbf{h}_{corr} = \mathbf{B} \cdot \tilde{\mathbf{h}} \tag{5.16}$$

where $\mathbf{B}$ results from the Choleski factorization of $\mathbf{R}$ [55] and $\tilde{\mathbf{h}}$ is the $N_R N_T \times 1$ column vector of the identically distributed channel coefficients. Note that the Kronecker model is only valid if the transmit correlation coefficients are independent in magnitude from the corresponding receive antenna, and vice versa [32].

For dual polarized antennas (see Figure 5.1(b)), both spatial and polarization domains may affect the performance. A well known indicator of the channel ability of separating two orthogonal polarizations is the cross-polarization discrimination (XPD) factor [77], defined as follows:

$$XPD = \frac{E\left\{\left|h_{+\frac{\pi}{4},-\frac{\pi}{4}}\right|^2\right\}}{E\left\{\left|h_{+\frac{\pi}{4},+\frac{\pi}{4}}\right|^2\right\}} = \frac{E\left\{\left|h_{-\frac{\pi}{4},+\frac{\pi}{4}}\right|^2\right\}}{E\left\{\left|h_{-\frac{\pi}{4},-\frac{\pi}{4}}\right|^2\right\}} \tag{5.17}$$

where $h_{a,b}$ denotes the channel response between the slant a and the slant b. A simple Kronecker model for 2 couples of cross-polarized antennas has been proposed within 3GPP [78]. This model derives from the necessity of simplifying

the spatial channel model (SCM) for practical simulations by identifying a few representative scenarios. The resultant covariance matrix is given by:

$$\mathbf{R} = \begin{bmatrix} 1 & r_{tx} \\ r_{tx}^* & 1 \end{bmatrix} \otimes \mathbf{\Xi} \otimes \begin{bmatrix} 1 & r_{rx} \\ r_{rx}^* & 1 \end{bmatrix} \tag{5.18}$$

where $\mathbf{\Xi}$ is the polarization covariance matrix, which can be written as:

$$\mathbf{\Xi} = E\left[\mathbf{h}_v \cdot \mathbf{h}_v^H\right] \tag{5.19}$$

with $\mathbf{h}_v = \left[h_{+\frac{\pi}{4},+\frac{\pi}{4}}\ h_{+\frac{\pi}{4},-\frac{\pi}{4}}\ h_{-\frac{\pi}{4},+\frac{\pi}{4}}\ h_{-\frac{\pi}{4},-\frac{\pi}{4}}\right]^T$.

By normalizing to 1 the power of the co-polarized channel components (i.e., $E\left\{\left|h_{+\frac{\pi}{4},+\frac{\pi}{4}}\right|^2\right\} = E\left\{\left|h_{-\frac{\pi}{4},-\frac{\pi}{4}}\right|^2\right\} = 1$) , the polarization covariance matrix can be expressed as:

$$\mathbf{\Xi} = \begin{bmatrix} 1 & t_p & r_p & t_p r_p \\ t_p^* & XPD & t_p^* r_p & r_p \\ r_p^* & t_p r_p^* & XPD & t_p \\ t_p^* r_p^* & r_p^* & t_p^* & 1 \end{bmatrix} \tag{5.20}$$

where t_p and r_p are the cross-correlation values, i.e.

$$\begin{aligned} t_p &= E\left(h_{+\frac{\pi}{4},+\frac{\pi}{4}} h^*_{+\frac{\pi}{4},-\frac{\pi}{4}}\right) = E\left(h_{-\frac{\pi}{4},-\frac{\pi}{4}} h^*_{-\frac{\pi}{4},+\frac{\pi}{4}}\right) \\ r_p &= E\left(h_{+\frac{\pi}{4},+\frac{\pi}{4}} h^*_{-\frac{\pi}{4},+\frac{\pi}{4}}\right) = E\left(h_{-\frac{\pi}{4},-\frac{\pi}{4}} h^*_{+\frac{\pi}{4},-\frac{\pi}{4}}\right) \end{aligned} \tag{5.21}$$

Note that both models might not be accurate to describe the effect of the correlation in real scenarios. However, they result to be useful tools to explicitely evaluate its impact on the link performance.

Let us consider now the following cases:

- linear array, with spatial correlation equal to 0.2 at the UE and 0.6 at the BS;
- linear array, with spatial correlation equal to 0.3 at the UE and 0.8 at the BS;

- two couples of dual polarized antennas, with XPD=1, $t_p = r_p = 0.2$, and no spatial correlation between the antenna couples;
- two couples of dual polarized antennas, with XPD=0.3, $t_p = r_p = 0.2$, and no spatial correlation between the antenna couples;
- two couples of dual polarized antennas, with XPD=1, $t_p = r_p = 0.2$, and spatial correlation between the antenna couples equal to 0.3 at the UE and 0.8 at the BS.

It is worth to notice that the spatial correlation at the transmitter is always set to be lower than the one at the receiver: this reflects reality where the UE is usually closer to the scattering sources such as buildings, trees, etc. than the BS, and therefore the channel has wider angular spread and lower spatial correlation than in the BS [79]. Note also that the cross-correlation between antennas belonging to the same couple is set to be very low. This is generally consistent with most of the reported measurements [80].

Figure 5.6(a) depicts the BLER performance obtained with the described correlation patterns for different transmission ranks and Indoor office channel. With the exception of rank 4 transmission, where $\mathbf{F} = \frac{1}{2}\mathbf{I}_4$, WB precoding is assumed. Spatial correlation generally leads to a consistent performance loss, which is more evident for high rank. This is because the spatial correlation reduces the diversity gain in interference limited scenarios. However, for rank 1 the spatial correlation leads to better performance than uncorrelated transmission in low SNR region; in noise limited scenarios, focusing the transmit energy over one particular direction results in an SNR increase at the receiver [81]. The impact of the different cross-polarization discrimination factors is limited when no spatial correlation arises. Note that, for rank 1 transmission, a configuration with high XPD leads to a slight performance gain than low XPD. A high XPD factor leads indeed to a polarization diversity which is beneficial for single stream transmission. The configuration *dual polarized, XPD=1, spatial corr. Tx 0.3 Rx 0.8* is shown to outperform *linear, spatial corr. Tx 0.3 Rx 0.8*, even though the spatial correlation is set to be the same. This is because in the first case the spatial correlation arises only between the couples of dual polarized antennas, while each couple can still benefit from the polarization diversity.

Similar conclusions can be drawn for the Typical Urban channel (see Figure 5.6(b)). The impact of the spatial correlation is here slightly reduced with respect to the Indoor office case. At the same time, no degradation is visible for dual polarized antennas without spatial correlation. Moreover, the higher dispersivity of the channel reduces the benefits of spatial correlation in the low SNR region for rank 1 transmission; hence no gains with respect to uncorrelated transmission are visible.

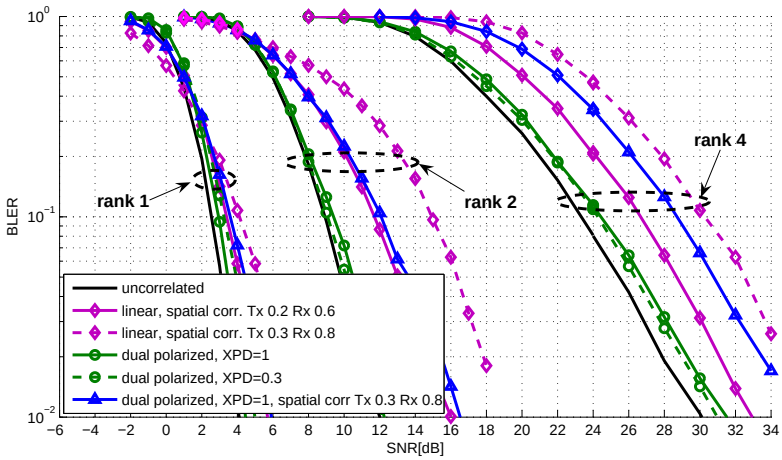

(a) Indoor office

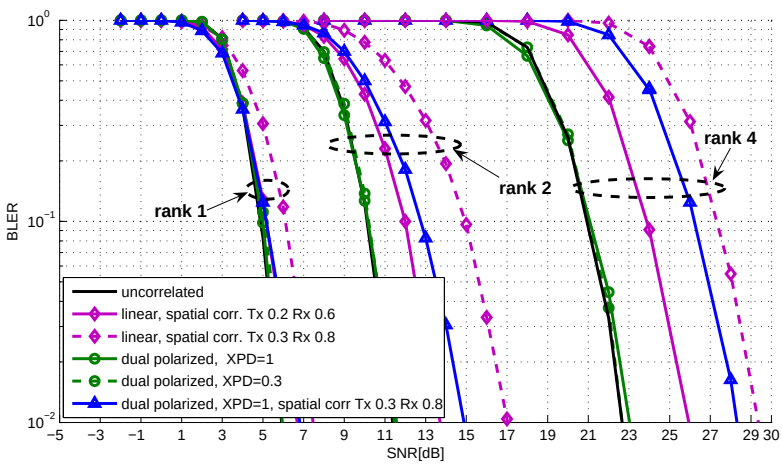

(b) Typical Urban

Figure 5.6: BLER performance of different transmission ranks with different antenna correlation patterns.

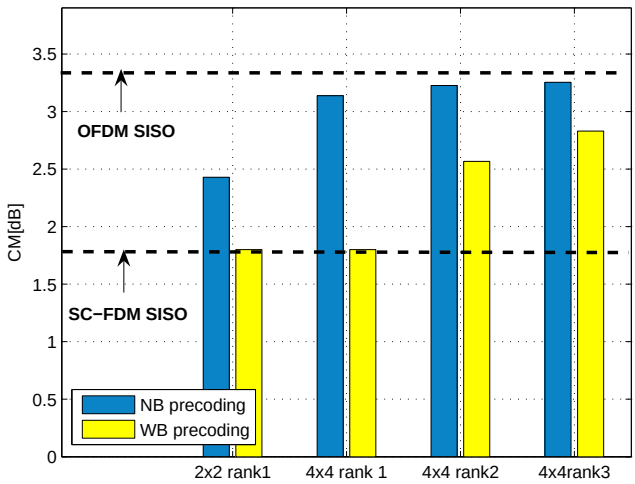

Figure 5.7: CM performance of NB and WB precoding for 16QAM.

5.5.3 CM performance

Finally, let us make some considerations on the nature of the precoded signals. Since the precoding in the frequency domain is equivalent to a convolution and a summation of the data symbols in the time domain, the single carrier property of the transmit waveforms can be affected. In Figure 5.7, the CM of the precoded signals is shown for 16QAM and several precoding configurations. The OFDM and SC-FDM SISO cases are also shown. It has also to be mentioned that the precoding does not affect the CM of the OFDM signals. As a common trend, the NB precoding shows higher CM than WB precoding, and in case of 4x4 rank 3 the gain over OFDM is almost completely lost. However, rank 1 with WB precoding does not lead to any increase of the CM; this is because the precoding vector for rank 1 transmission provides only a phase shift on the time domain signal at each antenna, and therefore does not modify the signal properties when it is applied over a set of subcarriers equal to the DFT-size.

5.6 Low CM codebook design

It has been shown that the LTE downlink codebook provides SNR gain over open loop solutions, but also increases the CM of the transmit signals. The

single carrier property is only preserved for rank 1 transmission when WB precoding is applied. An efficient design of the uplink codebook should therefore include the low CM constraint. In this section, some improvements in the LTE downlink codebook are discussed with the aim of designing feasible solutions for LTE-A uplink. We consider the chordal distance as a main design metric, and evaluate the suitability of the solutions for different antenna patterns through simulations. WB precoding has to be considered as a necessary but not sufficient condition to maintain the single carrier property of the uplink signals. It has been shown that WB precoding reduces dramatically the feedback overhead; on the other hand, it can severely reduce the performance gain in case of highly frequency selective channel. Note that some of the constraints presented in Section 5.4 can be relaxed due to some specific uplink behavior. For instance, antenna gain imbalance (AGI) is quite likely to appear in the UE due, for instance, to the grip of the handeld device [82]. This means, the system performance can benefit by including antenna selection in order to convey the total available power towards the higher gain antenna(s). This sacrifices, of course, the equal power per antenna concept, but limits the options to the on/off alternative.

Note that, for the 2Tx case, only rank 1 is considered for precoded transmission. Since the LTE downlink codebook for rank 1 does not increase the CM of the uplink signals when WB precoding is applied, no modifications are needed for LTE-A uplink. As shown in Section 3.2, the SU-MIMO spatial multiplexing 2x2 scheme can be seen equivalent to the case of 2 users transmitting with a single antenna in the same time-frequency resources. Since it has been agreed not to use any precoding for full rank transmission, also open loop SIMO has to be considered as basic MU-MIMO scheme for 2 UEs.

For the rest of this section, we will focus on the 4Tx case. The proposed codebook breaks the rank overriding property of Release 8 codebook. However, the total number of 64 precoding matrices as agreed for LTE downlink is preserved. The optimizations for rank 1, 2 and 3 are described in the following.

5.6.1 4x4 rank 1

Sinilarly to the 2x2 case, the LTE downlink codebook for 4x4 rank 1 transmission preserves the low CM property when WB precoding is used, and it can therefore be applied also in LTE-A Uplink. It has been mentioned that AGI can easily occur in the UE. Some antenna selection elements should be included in the 4x4 rank 1 codebook, so that some of the antennas can be turned off in case of high

gain imbalance. Let us introduce the following set of vectors:

$$\tilde{C} = \frac{1}{\sqrt{2}} \left\{ \begin{bmatrix} 1 \\ 0 \\ p \\ 0 \end{bmatrix}, \begin{bmatrix} 0 \\ 1 \\ 0 \\ p \end{bmatrix} \right\} \tag{5.22}$$

with $p \in \{\pm 1, \pm j\}$. The extended codebook for LTE-A uplink is given by

$$C^4_{1,ext} = C^4_{1,Rel8} \cup \tilde{C} \tag{5.23}$$

where $C_{1,Rel8}$ is the Release 8 codebook for rank 1. The resultant codebook for rank 1 includes therefore 24 matrices. By including the set $\tilde{C}$, any antenna couple can be eventually turned off during the transmission.

In Figure 5.8 the performance of the new codebook for rank 1 is compared with the Release 8 codebook, assuming Indoor office channel model. In $C^4_{1,Rel8}$, the presence of AGI leads to a consistent SNR loss. The gain due to the turn-off vectors increases with the AGI. For AGI equal to 12 dB, the gain is up to 2 dB. Note that for $C^4_{1,ext}$ the presence of AGI leads to better performance than no AGI in low SNR region: this is due to the possibility of conveying the whole transmit power to a single transmit antenna couple.

5.6.2 4x4 rank 2

The Release 8 codebook for rank 2 transmission performs a complex combination of the frequency samples generated from different CWs. A CM preserving codebook can be designed by including the constraint that each row of the matrices contains only one non-zero element. In this way, when WB precoding is applied, the time domain signal sent by each antenna is simply a phase shifted version of the original SC-FDM signal, thus preserving the low CM property. Let us define the following codebook:

$$C^4_{2,CMpres} = \frac{1}{2} \left\{ \begin{bmatrix} 1 & 0 \\ p & 0 \\ 0 & 1 \\ 0 & q \end{bmatrix} \right\} \tag{5.24}$$

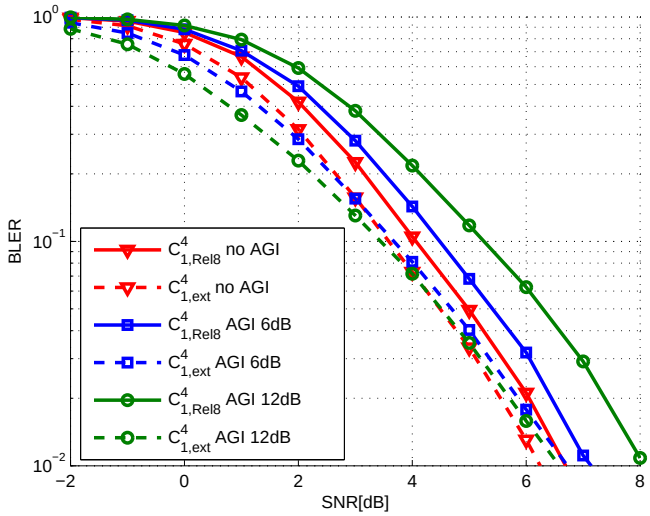

Figure 5.8: BLER performance of the extended codebook for 4x4 rank 1.

for $p, q \in \{\pm 1, \pm j\}$.

It contains 16 matrices and has a minimum chordal distance equal to 0.5. Since each row has only one non-zero element, it fully preserves the single carrier property of the uplink signals.

The performance of the CM preserving codebook for rank 2 with Indoor office channel is shown in Figure 5.9(a). The correlation patterns as defined in subsection 5.5.2 are considered. The CM preserving codebook leads to a slight loss in uncorrelated scenario, turning however in a slight gain when correlation arises. The gain of the proposed codebook in correlated scenarios becomes more evident in Typical Urban channel (see Figure 5.9(b)), where moreover no appreciable degradation for uncorrelated antennas is visible.

The 4x4 rank 2 SU-MIMO problem can be seen as equivalent to the 2x2 rank 1 MU-MIMO problem with 2 users. In this case, precoded transmission is worth to be considered for low dispersive channels. Note that the codebook shown in Eq.(5.24) can also be used in MU-MIMO mode, since the streams transmitted by the antenna couples $\{1, 2\}$ and $\{3, 4\}$ are obtained from the 1st and the 2nd CW, respectively, and can therefore belong to different users.

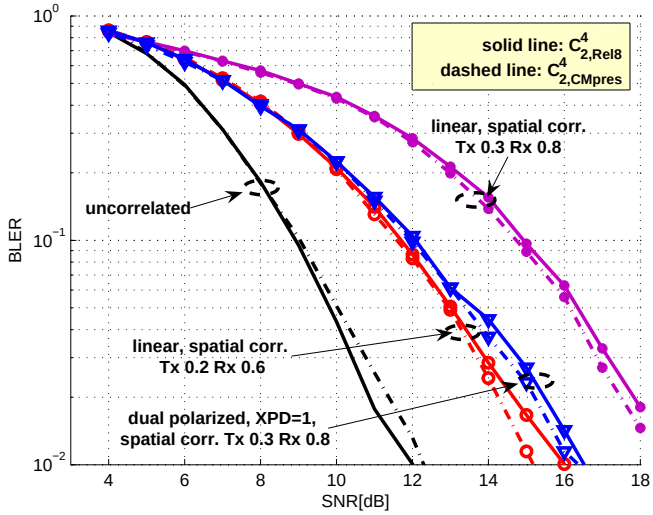

(a) Indoor office

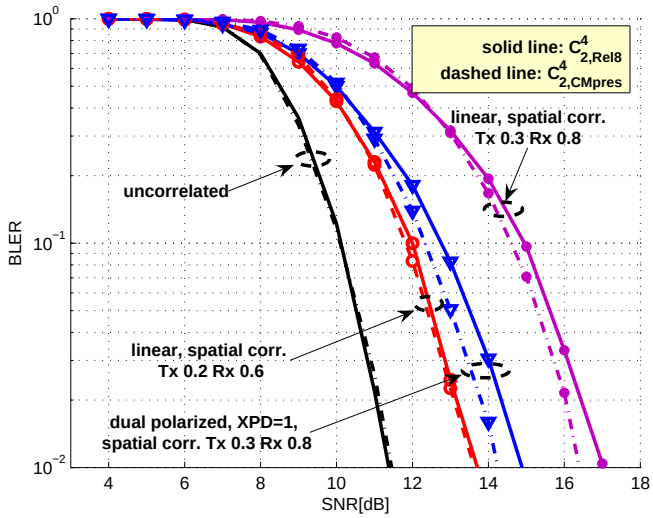

(b) Typical Urban

Figure 5.9: BLER performance of the CM preserving codebook for 4x4 rank 2.

5.6.3 4x4 rank 3

In rank 3 transmission the first CW is mapped over one layer, while the second CW is split over two layers (see Figure 3.2).

Simlarily to the rank 2 case, a CM preserving codebook for rank 3 should cope with the costraint of having a single element different from zero at each row. A potential codebook for rank 3 is the following one:

$$C^4_{3,CMpres} = \frac{1}{2}\left\{ \begin{bmatrix} 1 & 0 & 0 \\ 0 & 1 & 0 \\ 0 & 0 & 1 \\ 0 & 0 & p \end{bmatrix}, \begin{bmatrix} 0 & 1 & 0 \\ 1 & 0 & 0 \\ 0 & 0 & 1 \\ 0 & 0 & p \end{bmatrix}, \begin{bmatrix} 0 & 0 & 1 \\ 0 & 0 & p \\ 1 & 0 & 0 \\ 0 & 1 & 0 \end{bmatrix}, \begin{bmatrix} 0 & 0 & 1 \\ 0 & 0 & p \\ 0 & 1 & 0 \\ 1 & 0 & 0 \end{bmatrix} \right\} \tag{5.25}$$

for $p \in \{1, -1, j, -j\}$. This codebook has chordal distance equal to 0.3536. In this codebook the power is not equally distributed among the layers (see Section 3.5). Equal power per layer can only be obtained by assigning lower power to the antennas transmitting layer 3, i.e. by defining the following codebook:

$$C^{4'}_{3,CMpres} = \Gamma \cdot C_{3,CMpres} \tag{5.26}$$

where $\Gamma = diag\left(\frac{2}{\sqrt{3}}, \frac{2}{\sqrt{3}}, \sqrt{\frac{2}{3}}, \sqrt{\frac{2}{3}}\right)$.

Nevertheless, in this way the antenna power balance, which is desirable to be kept at the transmitter, is lost.

It can be assumed that, for rank 3 transmission, the constraint of having low CM can be partly sacrified, without however incurring in the dramatical CM increase of LTE downlink codebook. This is because rank 3 transmission occurs for non-power limited users [83]. Let us define the following CM friendly codebook:

$$
\begin{aligned}
&C^{4}_{3,CMfriendly} = \frac{1}{2\sqrt{2}} \cdot \\
&\cdot \left\{ \begin{bmatrix} 1 & 1 & 0 \\ -j & 0 & 1 \\ -1 & 0 & j \\ 1 & -1 & 0 \end{bmatrix}, \begin{bmatrix} 1 & 1 & 0 \\ j & 0 & 1 \\ 1 & 0 & j \\ 1 & -1 & 0 \end{bmatrix}, \begin{bmatrix} 1 & 1 & 0 \\ -j & 0 & 1 \\ 1 & 0 & -j \\ -1 & 1 & 0 \end{bmatrix}, \begin{bmatrix} 1 & 1 & 0 \\ j & 0 & 1 \\ 1 & -1 & 0 \\ 1 & 0 & j \end{bmatrix}, \right. \\
&\begin{bmatrix} 1 & 1 & 0 \\ -1 & 1 & 0 \\ j & 0 & 1 \\ -1 & 0 & -j \end{bmatrix}, \begin{bmatrix} 1 & 1 & 0 \\ 1 & -1 & 0 \\ -j & 0 & 1 \\ -1 & 0 & j \end{bmatrix}, \begin{bmatrix} 1 & 1 & 0 \\ -j & j & 0 \\ 1 & 0 & 1 \\ 1 & 0 & -1 \end{bmatrix}, \begin{bmatrix} 1 & 1 & 0 \\ j & -j & 0 \\ -1 & 0 & 1 \\ 1 & 0 & 1 \end{bmatrix}, \\
&\begin{bmatrix} 1 & 1 & 0 \\ j & 0 & 1 \\ j & -j & 0 \\ -j & 0 & 1 \end{bmatrix}, \begin{bmatrix} 1 & 1 & 0 \\ j & 0 & 1 \\ -j & j & 0 \\ j & 0 & -1 \end{bmatrix}, \begin{bmatrix} 1 & 1 & 0 \\ -j & 0 & 1 \\ -j & j & 0 \\ -j & 0 & -1 \end{bmatrix}, \begin{bmatrix} 1 & 1 & 0 \\ -j & 0 & 1 \\ j & -j & 0 \\ j & 0 & 1 \end{bmatrix}, \\
&\begin{bmatrix} 1 & 1 & 0 \\ 1 & 0 & 1 \\ 1 & 0 & -1 \\ j & -j & 0 \end{bmatrix}, \begin{bmatrix} 1 & 1 & 0 \\ 1 & 0 & 1 \\ -1 & 0 & 1 \\ -j & j & 0 \end{bmatrix}, \begin{bmatrix} 1 & 1 & 0 \\ -1 & 0 & 1 \\ 1 & 0 & 1 \\ -j & j & 0 \end{bmatrix}, \begin{bmatrix} 1 & 1 & 0 \\ -1 & 0 & 1 \\ -1 & 0 & -1 \\ j & -j & 0 \end{bmatrix}, \\
&\left. \begin{bmatrix} 1 & 1 & 0 \\ 1 & -1 & 0 \\ j & 0 & 1 \\ 1 & 0 & j \end{bmatrix}, \begin{bmatrix} 1 & 1 & 0 \\ -1 & 1 & 0 \\ -j & 0 & 1 \\ 1 & 0 & -j \end{bmatrix}, \begin{bmatrix} 1 & 1 & 0 \\ -j & j & 0 \\ -1 & 0 & 1 \\ -1 & 0 & -1 \end{bmatrix}, \begin{bmatrix} 1 & 1 & 0 \\ j & -j & 0 \\ 1 & 0 & 1 \\ -1 & 0 & 1 \end{bmatrix} \right\}
\end{aligned}
\tag{5.27}
$$

It achieves minimum chordal distance equal to 0.5, and it guarantees equal power allocation among the antennas.

Equal power per layer at the output of the precoder block can be obtained by defining the following modified codebook:

$$
C^{4,eqPow}_{3,CMfriendly} = C^{4}_{3,CMfriendly} \cdot \Gamma' \tag{5.28}
$$

where $\Gamma' = diag\left(\frac{1}{\sqrt{3}}, \sqrt{\frac{2}{3}}, \sqrt{\frac{2}{3}}\right)$.

Furthermore, it is straightforward to verify that

$$
\left\|\hat{\mathbf{F}}_{1,:}\right\|^2 = \left\|\hat{\mathbf{F}}_{2,:}\right\|^2 = \left\|\hat{\mathbf{F}}_{3,:}\right\|^2 = \left\|\hat{\mathbf{F}}_{4,:}\right\|^2 \tag{5.29}
$$

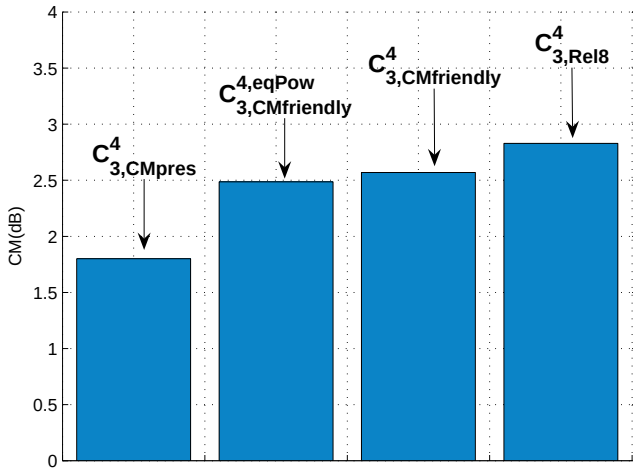

Figure 5.10: CM performance of the 4x4 rank 3 codebooks for 16QAM.

for each $\hat{\mathbf{F}} \in C^{4,eqPow}_{3,CMfriendly}$. Therefore the codebook in Eq.(5.28) also maintains the antenna power balance.

The CM performance of the introduced codebooks is shown in Figure 5.10, assuming 16QAM. The CM increase of the codebooks in Eq.(5.27) and Eq.(5.28) still preserves some gain with respect to the Release 8 one. This is because in the CM friendly codebook the signal sent over each antenna is obtained as a complex linear combination of the samples mapped over 2 layers, instead of 3 layers as in the Release 8 codebook.

Since in rank 3 transmission the transport block sizes for each CW are different (see Table 3.1), the link performance of the presented codebook is evaluated here by considering as a performance metric the spectral efficiency instead of the BLER. The Indoor office channel with the *dual polarized, XPD=1, spatial corr. Tx 0.3 Rx 0.8* configuration is assumed. In case of the CM friendly codebook, both cases of equal power per layer and non-equal power per layer are considered. Figure 5.11(a) shows the spectral efficiency performance for each CW, while in Figure 5.11(b) the cumulative curves are represented. In $C^4_{3,CMpres}$ the 1st CW is clearly penalized with respect of $C^4_{3,Rel8}$. This is because in our CM preserving codebook layer one is only mapped over one antenna, and therefore it does not exploit any array gain. The 2nd CW has instead approximately the same performance of the Release 8 case. $C^{4,eqPow}_{3,CMfriendly}$ performs the same as

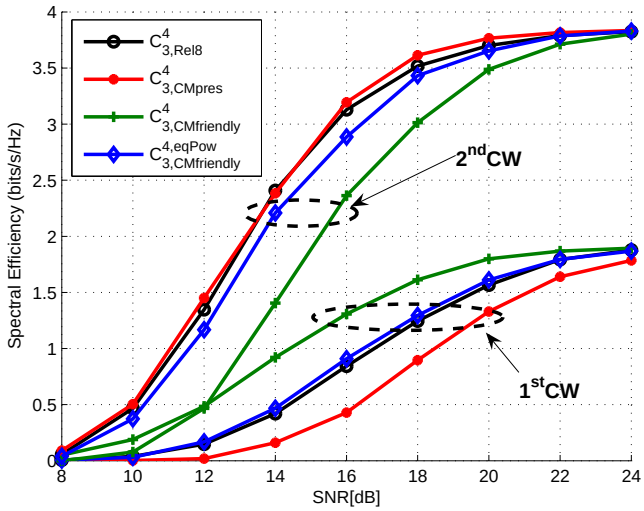

(a) each CW

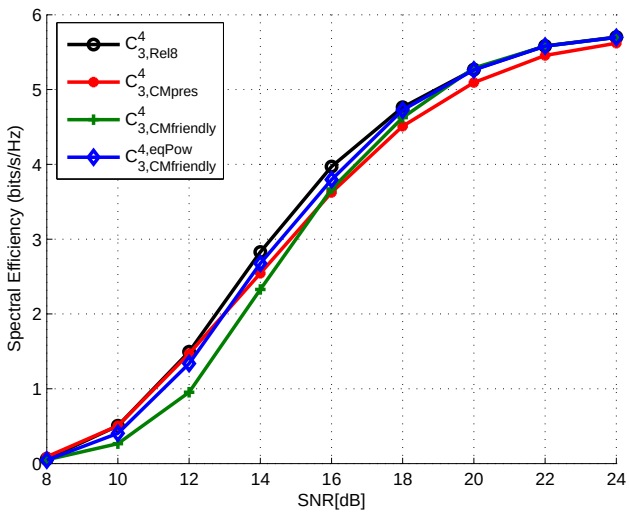

(b) cumulative curves

Figure 5.11: Spectral efficiency performance of the codebooks for 4x4 rank 3.

$C^4_{3,Rel8}$ for the 1st CW and leads to a slight SNR loss for the 2nd CW. When the equal power per layer condition is not fulfilled ($C^4_{3,CMfriendly}$), the losses in the 2nd CW are much more evident, while the 1st CW clearly outperforms the other codebook options. This is because in the CM friendly codebook the 1st CW is mapped over the whole antenna set (see Eq.(5.27)), thus achieving high array gain. The cumulative spectral efficiency curves shown in Figure 5.11(b) evidence the CM friendly codebook with equal power per layer as the approach which performs closer to the Release 8 codebook. Similar results have been obtained by considering different correlation patterns and Typical Urban channel.

5.7 Precoding in TDD mode

In the previous sections, several precoding solutions have been presented for FDD mode, thus assuming that the precoding matrix can only be retrieved by exploiting some feedback signaling. This section deals instead with TDD mode transmission, where UE and BS are transmitting over the same band in different time instants. Hence the channel state information can be obtained in reception mode and exploited when switching to transmission mode. This means, feedback signaling may be in principle avoided, and the channel information may also be more accurate, assuming a slowly variant channel. Two solutions are discussed in this section, one based on blind precoding and another based on precoded pilots.

5.7.1 Blind precoding

It has been shown that the SVD-based precoding provides approximately the same performance of the LTE codebook. The most intuitive way to exploit the channel reciprocity in TDD mode would be to re-derive the precoding matrix at the UE given the estimated channel frequency response. This idea is explained in details in the following:

- At time instant t_{α_0}, the UE receives a data frame and computes $\mathbf{F}_{t_{\alpha_0}}$ from the SVD of the estimated $\mathbf{H}_{t_{\alpha_0}}$. It uses $\mathbf{F}_{t_{\alpha_0}}$ to precode the data streams, which are sent at time instant $t_{\alpha_1} = t_{\alpha_0} + \Delta t$.

- The BS receives the data frame and computes $\mathbf{F}_{t_{\alpha_1}}$ from the estimated $\mathbf{H}_{t_{\alpha_1}}$. In this case, the output of the MMSE detector can be written as follows:

$$\mathbf{r}_{eq}[k] = \mathbf{F}_{t_{\alpha_0}}[k]^H \mathbf{H}_{t_{\alpha_1}}[k]^H \left(\mathbf{H}_{t_{\alpha_1}}[k] \mathbf{F}_{t_{\alpha_1}}[k] \mathbf{F}_{t_{\alpha_1}}[k]^H \mathbf{H}_{t_{\alpha_1}}[k]^H + N_T \frac{\sigma_w^2}{\sigma_d^2} \mathbf{I}_{N_R} \right)^{-1} \mathbf{r}[k] \tag{5.30}$$

The difference with Eq.(5.5) is that here the precoding matrix computed at the base station is updated with respect to the one used at the UE.

Despite of its simplicity, this solution fails in a real system when realistic Δt delays are considered [59]. It has been shown that the time correlation between the columns of the $\mathbf{V}$ matrix drops much faster than the correlation between the elements of the channel matrix [84]; this means that, even though after a certain delay the elements of the $\mathbf{H}$ matrix are still correlated, the corresponding $\mathbf{V}$ matrices obtained by SVD of $\mathbf{H}$ could be substantially different. Thus, the MMSE detector cannot work properly.

5.7.2 Precoded pilots option

In order to avoid the poor performance of blind precoding, both UE and BS should employ the same $\mathbf{F}$ matrix for precoding and detection tasks, respectively. At the same time, the channel reciprocity in TDD mode should be exploited, i.e. no feedback message has to be sent. A possible solution for informing the BS on the precoding matrix used at the transmitter is precoding the pilot symbols [85]. The procedure is described in the following steps:

- at time t_{α_0} the UE receives a data frame and computes $\mathbf{F}_{t_{\alpha_0}}$ from the estimated $\mathbf{H}_{t_{\alpha_0}}$. It uses $\mathbf{F}_{t_{\alpha_0}}$ for precoding both data and pilot symbols. This means, the following equivalent frequency domain pilot symbols are sent over the channel:

  $$\tilde{\mathbf{p}}[k] = \mathbf{F}_{t_{\alpha_0}}[k] \mathbf{p}[k] \tag{5.31}$$

  for $k = 0, \cdots, N_{sub} - 1$.

- at time t_{α_1} the BS receives the data frame and estimates from the pilot symbols the equivalent channel matrix, i.e.

  $$\mathbf{H}_{t_{\alpha_1}, eq}[k] = \mathbf{H}_{t_{\alpha_1}}[k] \mathbf{F}_{t_{\alpha_0}}[k] \tag{5.32}$$

  for $k = 0, \cdots, N_{sub} - 1$. In this way, the same detector of Eq.(5.5) can be adopted.

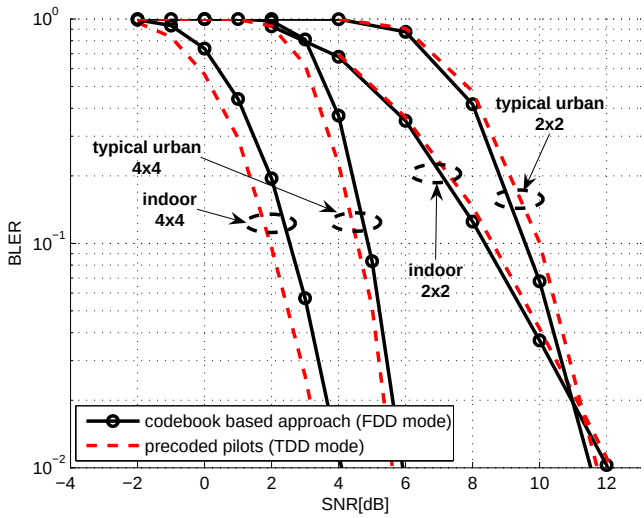

Figure 5.12: BLER performance of the precoded pilots option in TDD mode.

Of course, the best solution for exploiting the channel reciprocity in TDD mode is using the unquantized SVD precoding. However, the proposed low CM codebook can still be used as for FDD mode, in case of high rank transmission.

The performance results of the precoded pilots option for rank 1 are shown in Figure 5.12. The unquantized SVD approach is assumed (see Eq.(5.9)). It has to be mentioned that, in TDD mode, a careful RF calibration procedure is needed since transmission and reception chains use typically different IQ mixers and power amplifiers [86]. The residual calibration error is here modeled as in [87]. Again, a 5 ms delay is assumed between the precoding matrix computation in the receiver and its application in the transmission. Of course, WB precoding is considered in order no to increase the CM of the signals.

In 2x2 rank 1 case, the precoding in TDD mode performs approximately as the codebook based approach in FDD mode for both Typical Urban and Indoor office channels. This is consistent with the observation that, in 2x2 rank 1, the unquantized SVD performs the same as quantized SVD and LTE codebook (see Figure 5.2). The slight loss is due to the calibration error. In 4x4 rank 1 configuration, some SNR gain of the precoded pilot option in TDD mode is evident. However, it is worth to mention that the reliability of the channel information which is needed to perform the precoding can be severely affected by the asymmetry of the interference patterns in uplink/downlink. This has been neglected in our evaluation.

5.8 Summary

In this chapter, we have discussed the precoded MIMO transmission for a SC-FDM based air interface. Solutions based on the SVD of the channel matrix can approach the theoretical MIMO capacity, however they lead to high complexity and power imbalance among the antennas. Several criteria for the design of an universal codebook of precoding matrices are presented, taking into account practical transceiver constraints. The link performance is initially evaluated considering the LTE Release 8 codebook and WB precoding has been identified as a necessary condition to reduce the CM increase. In an Indoor office scenario, the precoded transmission leads to a consistent SNR gain with respect to open loop one; however, no relevant improvement over STC is visible in a Typical Urban channel for rank 1 transmission. Spatial correlation severely affects the performance, especially for Indoor office channel, while the impact of the polarization discrimination in dual polarized channels is limited. A CM preserving codebook is proposed, and has been shown to provide approximately the same gain as the Release 8 one, for both uncorrelated and correlated scenarios, and even better results for rank 1 transmission due to the inclusion of antenna turn-off vectors. Moreover, the codebook proposed for 4x4 rank 2 can also be used in MU-MIMO mode, assuming 2 users transmitting in 2x2 rank 1 configuration.

The channel reciprocity in TDD mode can be exploited to perform precoding without any feedback message. A solution based on precoding the pilot symbols besides the information data has been shown to lead to some SNR gain over the codebook based approach in 4x4 rank 1 transmission case, while no benefit is visible in 2x2 rank 1 mode.

Chapter 6

Turbo receiver design for LTE-A uplink

6.1 Introduction

The throughput performance of the wireless transceiver chain is strongly affected by the detection algorithm at the receiver. The optimal detector, based on an exaustive search of the transmit data vector among all the possible options, is however unfeasible in a practical system because of the huge computational burden. A wide branch of literature focuses therefore to suboptimal approaches having high performance while keeping reasonable complexity.

It has been shown in the previous chapters that the SC-FDM performance is corrupted by a noise enhancement, which affects the estimate of the data symbols in both single and multiple transmit antenna modes. This leads to a spectral efficiency gap with OFDM, lowering the cell throughput in the uplink direction with respect to the downlink, when the allocated physical resources are the same. On the other hand, the link performance results shown in the previous chapters are obtained by assuming a simple MIMO MMSE linear detector, which mitigates the noise but does not completely remove the interstream interference. Of course, this also reduces the throughput.

In this chapter, advanced non-linear receiver solutions are discussed as suitable options for LTE-A Uplink. Our aim is to improve the spectral efficiency performance with manageable additional complexity, at the same time reducing the impact of the noise enhancement of the SC-FDM technology.

The chapter is outlined as follows. Section 6.2 presents a synthetic overview of the main non-linear detection techniques. The proposed single stream and multi-stream turbo receivers are presented and evaluated in Section 6.3 and Section 6.4, respectively. Finally, a summary is given in Section 6.5.

6.2 Principles of the turbo detection

It is known that the optimal receiver is based on the maximum likelihood (ML) detection of the information bits [88], which performs an exaustive search of the transmit sequence over all the possible options. However, this solution is practically unfeasible when both MIMO transmission and coding are combined [40]. Lot of research effort has been spent in developing new methods for achieving high error correction capability while keeping a reasonable computational burden.

A fundamental distinction exists between heuristic methods and formal optimization methods. In the heuristic methods, the information is exchanged between different blocks in the receiver, such as channel estimator, detector and channel decoder. On the other hand, formal optimization methods, such as for instance Bayesian inference methods, provide a framework for the whole optimization of the receiver according to a design principle. Examples of these methods are the use of Factor Graphs [27] or Variational Bayesian inference based on Kullback-Leibler divergence minimization [89].

The sequential nature of the LTE/LTE-A receiver as assumed within 3GPP makes the heuristic approach more suitable for a practical design. Since the feasibility of the formal optimization methods in practical receivers is still being verified, in this thesis we will only focus on heuristic methods.

The most known heuristic approach is definitely the turbo-processing, which consists in an iterative exchange of soft decisions between different stages in the receiver. The turbo processing idea is motivated by the success of the turbo codes, which are capable to approach the Shannon capacity in AWGN channels [90]. The turbo codes use a concatenated encoding strategy at the transmitter, while in the receiver two decoding stages are iteratively exchanging soft information, so that the output of one stage can be seen as *apriori* information for

the other stage. The invention of the turbo codes has immediately raised the research interest in decoding solutions aiming to cope with more realistic channel models than AWGN, by applying the principle of the iterative detection to the whole receiver structure. The algorithm for the turbo decoding has been hence extended to channels affected by intersymbol interference, by considering the channel itself as a further encoder [91]. This approach is known as turbo equalization.

Most of the technical literature dealing with turbo processing distinguishes between the inner and outer decoding processes. The outer decoder aims at recovering the information bits by exploiting the knowledge of the parity bits. The inner decoder aims instead at providing an estimate of all the transmit data bits. The turbo equalizer, for instance, uses the Maximum A Posteriori (MAP) algorithm as inner decoder. Again, the MAP algorithm becomes unfeasible when MIMO transmission occurs, so that further solutions have been proposed. In the sphere detection [92] only a small subset of the possibly transmitted data symbols is considered, so that the complexity of the MAP algorithm is considerably reduced. In the iterative search tree detection [93], the selection of the elements in the subset is improved since the a priori information obtained from the outer decoder is taken into account. In the multilevel bit mapping iterative tree search [93], the detection is performed in steps of 2 bits at a time regardless of the modulation order.

Even though the mentioned solutions considerably reduce the computational load, the most feasible approach for applying the turbo principle in an LTE/LTE-A receiver is conservative with respect of its linear nature. This means, each stage of the turbo detection process consists in linear filtering plus decoding. In this way, the turbo receiver can be easily scaled to the simple linear detector when higher detection capabilities are not requested.

6.3 Single stream turbo receiver

LTE-A uplink air interface is supporting both single and multi-stream transmission. It has been shown in Chapter 2 that the linear receiver performance is affected by a noise enhancement which degrades the estimate of the data symbols. When multiple streams are sent over the channel, also interstream interference occurs. In this section, we focus on the single stream transmission, and propose a solution aiming at reducing the noise enhancement of the SC-FDM technology.

The proposed turbo receiver is shown in Figure 6.1. According to the turbo

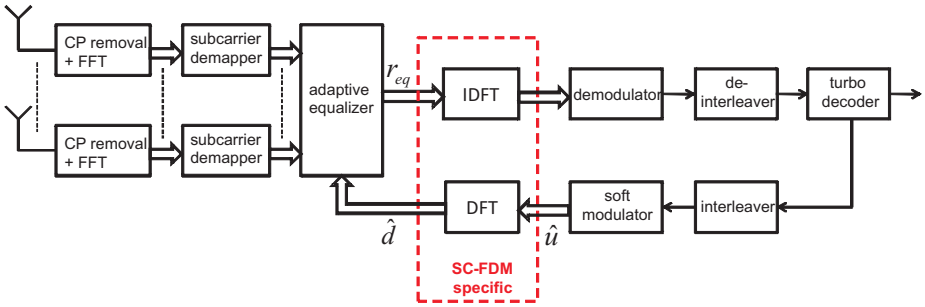

Figure 6.1: Single stream turbo receiver.

principle, equalizer and turbo decoder are joint in a loop and separated by bit-interleavers and bit-deinterleavers: the information produced by one of these blocks at each iteration can be viewed as apriori information for the other one.

The purpose of this receiver is to improve iteratively the reliability of the estimate of the transmitted symbol sequence. In particular, the equalizer coefficients are updated at each iteration depending on this estimate. It is worth to notice that the turbo decoder represents here the outer decoder, while the adaptive equalizer can be seen as the inner decoder. The idea for this adaptive equalizer is taken from [94], where the turbo processing is used with the aim of eliminating the residual ISI. In our case, if the time domain inter-sample interference is fully removed, each of the single carrier time domain data symbol would only be weighted by a single channel coefficient. In this way, the noise enhancement of SC-FDM can be reduced.

At each iteration of the algorithm, the received frequency domain signals at each antenna are multiplied by the forward coefficients $\mathbf{C}_{ff}$ of the adaptive equalizer, which will be discussed in the following subsection. Then, all the sequential linear operation of the SC-FDM detection (i.e., IDFT-spread, demodulation, de-interleaving...) are performed. The log-likelihood ratios of all coded bits are therefore submitted to the turbo decoder. The turbo decoder exploits a soft operation instead of its traditional hard detection task: it computes an improved log-likelihood ratio of all coded bits, taking into account the knowledge of the encoder scheme. This soft output has been obtained modifying the structure of each MAP decoder inside the turbo decoder [95], applying the BCJR algorithm [90] for both the systematic and the parity bits [96].

Considering the feedback from the turbo decoder in Figure 6.1, after the symmetrical interleaving operation, the resulting soft values $L^I(\cdot)$ are grouped in p-length blocks $\left\{\left[L^I(b_{0,1}), ..., L^I(b_{0,p})\right], ..., \left[L^I(b_{N_{sub}-1,1}), ..., L^I(b_{N_{sub}-1,p})\right]\right\}$, where $p = log_2(M)$, with M the number of elements of the considered symbol con-

stellation, and $b_{k,i}$ is the ith bit associated to the kth transmitted symbol. In this way, a $(N_{sub} \times p)$ matrix having in each row the log-likelihood ratios of the bits belonging to each transmitted symbol is obtained. According to the definition of likelihood ratio $\left(L^I\left(b_{k,i}\right) = ln\frac{P(b_{k,i}=1)}{P(b_{k,i}=0)}\right)$, the probability of each bit is computed as follows:

$$P(b_{k,i} = 0) = \frac{1}{1 + e^{(L^I(b_{k,i}))}} \tag{6.1}$$

$$P(b_{k,i} = 1) = \frac{e^{(L^I(b_{k,i}))}}{1 + e^{(L^I(b_{k,i}))}} \tag{6.2}$$

for $k = 0, \cdots, N_{sub} - 1$ and $i = 1, \cdots, p$. Thus, it is possible to calculate the $(N_{sub} \times M)$ apriori symbol probability matrix $\lfloor P_a(\underline{u}_k^m) \rfloor$, having in each row the probability of each symbol u^m of the constellation at frequency k. Assuming independence between the interleaved coded bits, each element of this matrix is given by:

$$P_a(\underline{u}_k^m) = \prod_{q=1}^{p} P(b_{k,q} = \tilde{b}_{m,q}) \tag{6.3}$$

for $k = 0, \cdots, N_{sub} - 1$ and $m = 1, \cdots, M$, where $\tilde{b}_{m,q}$ is the qth bit of u^m. From each row of this matrix a soft estimate of the transmitted symbol vector can be computed as follows:

$$\widehat{\mathbf{u}}(k) = E\left(\underline{u}_k^i\right) = \sum_{i=1}^{M} u^i P_a(\underline{u}_k^i) \tag{6.4}$$

for $k = 0, \cdots, N_{sub} - 1$. So the estimated sequence is converted in frequency domain through a DFT operation. The resultant sequence $\widehat{\mathbf{d}}$ is then submitted to the adaptive equalizer. Note that the usage of soft feedback avoids propagation of errors in the detection loop, which typically occurs when hard estimates are fed back [97]. Moreover, it is worth to mention that the *full* soft decoder information is here fed back and not only the *extrinsic* information as in the traditional turbo equalization. As noticed in [98], the whole soft information consisting of channel and extrinsic information should indeed be fed back in case of linear inner decoder since the latter does not include any channel information.

The turbo receiver exploits the described tasks for a number of iterations; after which, the turbo decoder makes hard decisions about the transmitted bits.

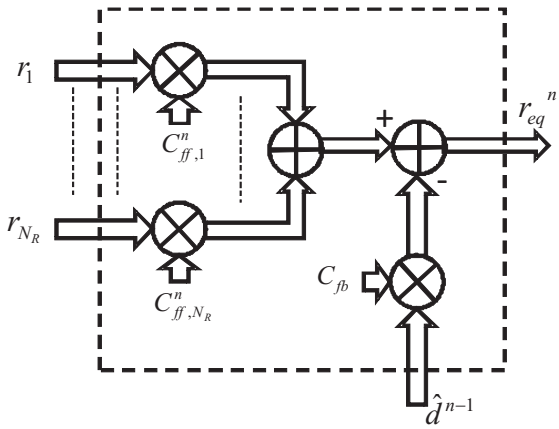

Figure 6.2: Adaptive equalizer.

6.3.1 Adaptive equalizer

As shown in Figure 6.2, the adaptive equalizer uses forward and feedback adaptive coefficients. The analytical derivation of the adaptive equalizer coefficients for SIMO is shown in Appendix D; the extension to other single stream solutions as STC is straightforward. The forward coefficients multiply the received samples at each antenna, and are a function of the variance of the estimated data sequence at the previous iteration. With reference to the SIMO case, the forward coefficient at the ith receive antenna in the nth iteration can be expressed as follows:

$$\mathbf{C}^n_{ff,i}(k) = \frac{\sigma_u^2}{1+\beta\widehat{\sigma}^2_{u,n-1}} \frac{\mathbf{h}_i^*(k)}{\left(\sigma_u^2 - \widehat{\sigma}^2_{u,n-1}\right)\sum_{i=1}^{N_R}\left|\mathbf{h}_i(k)\right|^2 + \sigma_w^2} \tag{6.5}$$

for $k = 0, \cdots, N_{sub}-1$, where $\mathbf{h}$ denotes the channel frequency response, σ_u^2 is the variance of the transmit data vector, $\widehat{\sigma}^2_{u,n-1}$ is the variance of the estimated sequence $\widehat{\mathbf{u}}$ at the $(n-1)$-th iteration, and

$$\beta = \frac{1}{N_{sub}} \sum_{q=0}^{N_{sub}-1} \frac{\sum_{i=1}^{N_R}\left|\mathbf{h}_i(q)\right|^2}{\left(\sigma_u^2 - \widehat{\sigma}^2_{u,n-1}\right)\sum_{i=1}^{N_R}\left|\mathbf{h}_i(q)\right|^2 + \sigma_w^2}. \tag{6.6}$$

Assuming a zero mean transmit data vector, $\widehat{\sigma}^2_{u,n-1}$ can be obtained as follows:

$$\widehat{\sigma}^2_{u,n-1} = \frac{1}{N_{sub}} \sum_{q=0}^{N_{sub}-1} \left|\widehat{\mathbf{u}}^{n-1}(q)\right|^2 \tag{6.7}$$

Note that at the first iteration, when no feedback information is available, $\widehat{\sigma}^2_{u,0} = 0$ and Eq.(6.5) performs as the traditional MMSE equalizer. By increasing the number of iterations, the estimate of the transmit sequence becomes more accurate, and therefore $\widehat{\sigma}^2_{u,n} \to \sigma^2_u$.

The feedback coefficients multiply instead the estimate of the data sequence at the previous iteration, with the aim of reducing the residual noise component. They can be expressed as:

$$\mathbf{C}_{fb}\left(k\right) = \sum_{i=1}^{N_R} \mathbf{h}_i\left(k\right) \mathbf{C}_{ff,i}\left(k\right) - \frac{1}{N_{sub}} \sum_{q=0}^{N_{sub}-1} \sum_{i=1}^{N_R} \mathbf{h}_i(q) \mathbf{C}_{ff,i}\left(q\right) \tag{6.8}$$

for $k = 0, \cdots, N_{sub} - 1$. Therefore the resultant output of the equalizer at subcarrier k is given by:

$$\mathbf{r}^n_{eq}[k] = \mathbf{C}_{ff}[k]\mathbf{r}[k] - \mathbf{C}_{fb}(k)\widehat{\mathbf{d}}^{n-1}(k) \tag{6.9}$$

where $\mathbf{C}_{ff}[k] = [\mathbf{C}_{ff,1}(k), \cdots, \mathbf{C}_{ff,N_R}(k)]$, and $\mathbf{r}[k] = [\mathbf{r}_1(k), \cdots, \mathbf{r}_{N_R}(k)]^T$.

6.3.2 Performance evaluation

The proposed single stream turbo receiver is evaluated by assuming a Typical Urban channel model. The main simulation assumptions are in line with Table 6.1. Ideal channel estimation is assumed. We first consider the 1x2 SIMO case. Also OFDM performance is included. It has to be mentioned that the single stream turbo receiver has not visible impact on the performance, so that only results obtained with linear ZF receiver are shown for OFDM.

Figure 6.3 depicts the BLER performance of the SC-FDM 16QAM system with three different coding rates. Results obtained with turbo receiver, with 2 and 4 iterations of the presented algorithm, are shown. Compared with the linear

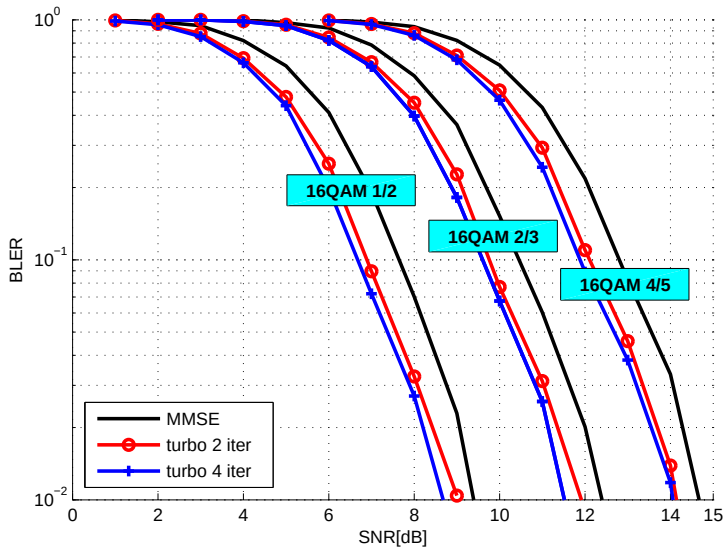

Figure 6.3: Single stream turbo receiver performance for SC-FDM, assuming SIMO 1x2 antenna configuration.

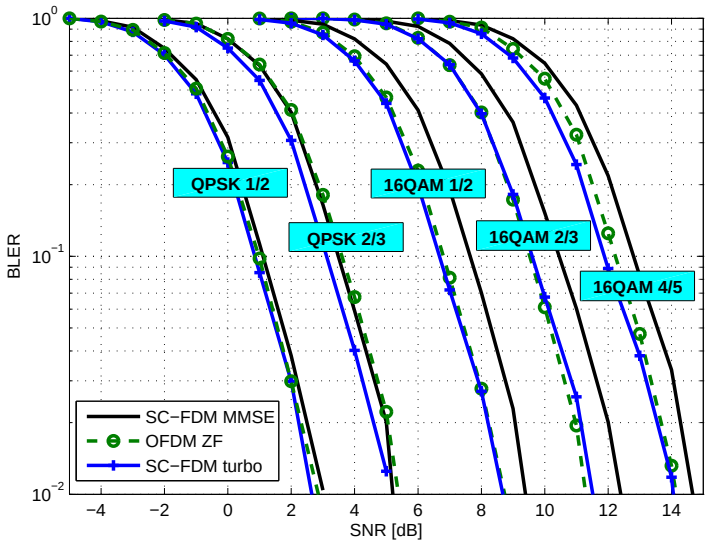

Figure 6.4: BLER performance for SC-FDM with single stream turbo receiver vs. OFDM, assuming SIMO 1x2 antenna configuration.

Table 6.1: Simulation parameters for turbo receiver evaluation

Carrier frequency	2 GHz
Sampling frequency	15.36 MHz
Number of subcarriers	600
FFT size	1024
CP length	$5.2^a/4.68^b$ μs
Frame duration	1 ms
Antenna configurations	1x2, 2x2, 2x4, 4x4
Channel Model	Typical Urban
User speed	3 kmph
Pilot Overhead (Ov)	14,29%
Channel Estimation	ideal based on WF
MCS settings	QPSK: 1/6, 1/3, 1/2, 2/3 16QAM: 1/2, 2/3, 3/4 64QAM: 2/3, 4/5
Channel coding	3GPP Rel.8 compliant Turbo code with basic rate 1/3
Turbo decoder iterations	8
BLER Target	10%
HARQ^c retransmission strategy	IR
HARQ Max. number of retransmissions	4
HARQ SAW channels	6

$^a 1^{st}$ and 8th OFDM/SC-FDM symbol in a subframe.
$^b 2^{th} - 7^{th}$ and $9^{th} - 14^{th}$ OFDM/SC-FDM symbols in a subframe.
^{c}only used with fast link adaptation

MMSE receiver, the turbo receiver shows a gain of around 1 dB. Since according with our assumptions the CP allows complete removal of the ISI, the gain is exclusively due to the reduction of the noise component. Significant gain is already obtained from 2 iterations of the algorithm.

In Figure 6.4 the performance of OFDM has also been included, and the results are shown for both QPSK and 16QAM modulations. The aim is to compare with the SC-FDM turbo receiver performance for 2 iterations of the algorithm.

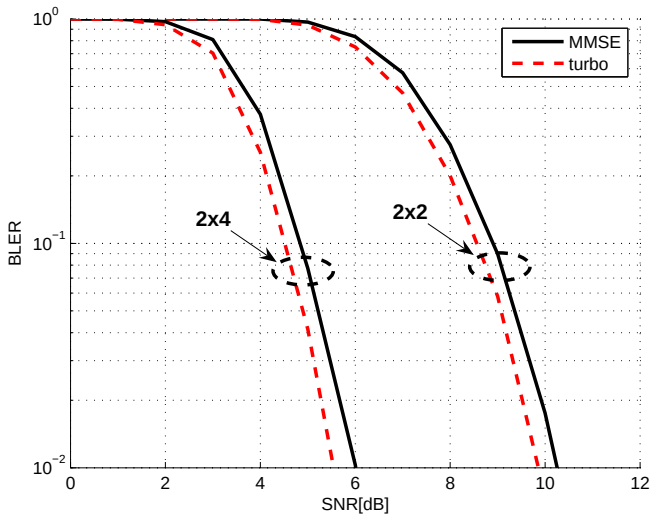

Figure 6.5: BLER performance for SC-FDM with single stream turbo receiver, assuming STC.

The gain of the turbo receiver is evident for 16QAM given its higher sensitivity to the noise, while it is negligible for QPSK. Therefore the turbo receiver should be used only for high order MCSs. It is also clear that the turbo receiver allows to overcome the gap with OFDM, so that both air interfaces show now approximately the same BLER performance.

Results obtained with open loop transmit diversity are depicted in Figure 6.5, assuming STC and 16QAM 1/2. The gain of the turbo receiver with 2 iterations of the algorithm is limited to around 0.4 dB in this case. This is because the high diversity order of STC already provides consistent noise enhancement reduction, thus reducing the benefits of the turbo detection.

6.4 Multi-stream turbo receiver

In spatial multiplexing mode multiple data streams are sent by the UE over the same time frequency resources. The user throughput can be boosted when the interstream interference is eliminated, so that the transmission of the multiple streams can be seen as a combination of independent single transmit antenna transmissions. Unfortunately, when a simple MMSE equalizer is used, some

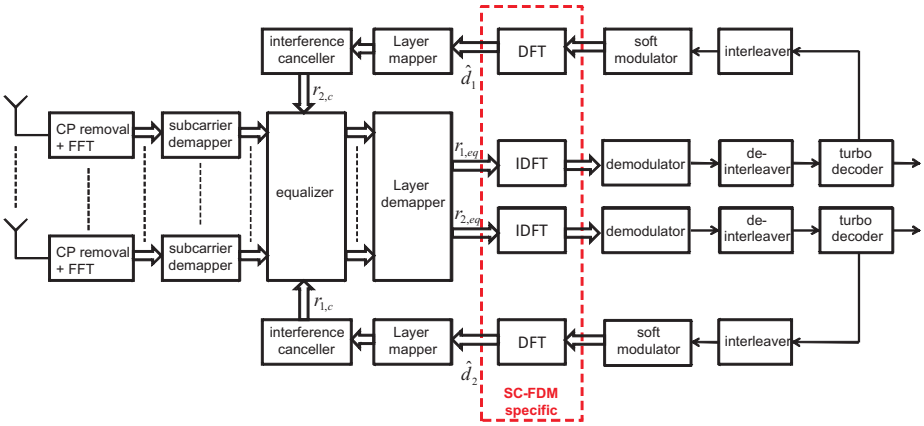

Figure 6.6: Structure of the multi-stream turbo receiver.

residual interstream interference persists. Again, a receiver designed according to the turbo principle is expected to boost the link performance, since the estimates of the data sequences at each iteration can be used to remove the mutual interference contribution. It is worth to notice that, a receiver able to remove the interstream interference allows to fully exploit the diversity gain of the multiple receive antennas; this is particularly beneficial for SC-FDM.

The structure of the considered turbo receiver is shown in Figure 6.6. Again, the equalizer and the turbo decoder are joint in a loop, benefiting from the mutual information exchange. As in the single stream turbo receiver, an estimate of each CW is obtained by re-encoding and modulating the soft output of the turbo decoder. These soft estimates are then fed back to an interference canceller, allowing to progressively remove the mutual interference contribution.

In the following, we present the principles of two widely adopted iterative detection techniques: Parallel Interference Cancellation and Successive Interference Cancellation [99]. In order to keep simple the analytical formalism, we implicitly refer to the full rank transmission; the extension to the multi-rank precoded transmission is straightforward.

6.4.1 Parallel Interference Cancellation (PIC)

In the PIC technique, all the CWs are detected in parallel, interleaved, remodulated and sent back to the interference canceller, whose output for the

m-th CW in the subcarrier k at n-th iteration can be written as follows:

$$\mathbf{r}^n_{m,c}(k) = \mathbf{r}[k] - \mathbf{H}_{Z-\{m\}}[k]\widehat{\mathbf{d}}^{n-1}_{Z-\{m\}}(k) \tag{6.10}$$

where $Z = \{1, 2\}$ is the set of the CWs'indexes, $\mathbf{H}_{Z-\{m\}}$ denotes the column of the MIMO channel matrix $\mathbf{H}$ corresponding to the antennas on which the $(Z - \{m\})$-th CW has been mapped, and $\widehat{\mathbf{d}}^{n-1}_{Z-\{m\}}$ is the frequency domain soft estimate of the $(Z - \{m\})$-th CW, obtained in the previous iteration. The residual error after the interference cancellation has to be taken into account in the equalization. The frequency domain equalization for the m-th CW in subcarrier k can be carried out as follows [100]:

$$\mathbf{r}^n_{m,eq}(k) = \mathbf{H}^H_m[k]\left[\frac{1}{\sigma^2_u}\mathbf{H}[k]\mathbf{Q}_n\mathbf{H}^H[k] + N_T\frac{\sigma^2_w}{\sigma^2_u}\mathbf{I}_{N_R}\right]^{-1}\mathbf{r}^n_{m,c}(k) \tag{6.11}$$

where $\mathbf{Q}_n = diag\,(q_1, \cdots, q_{N_T})$ is the $N_T \times N_T$ diagonal matrix of the residual interference powers, whose j-th element can be expressed as:

$$q_j = \begin{cases} \sigma^2_u, & \text{if } \; j = m \\ \sigma^2_u - \widehat{\sigma}^2_{Z-\{m\},n-1} & \text{if } \; j \neq m \end{cases} \tag{6.12}$$

where $\widehat{\sigma}^2_{Z-\{m\},n-1}$ is the variance of the soft modulated symbols of the $(Z - \{m\})$-th CW at $(n-1)$-th iteration.

Note that at the beginning, when no apriori information is available, $\widehat{\sigma}^2_0 = 0$ and Eq.(6.11) acts as a traditional MIMO MMSE equalizer.

6.4.2 Successive Interference Cancellation (SIC)

In the SIC technique the CWs are first ordered depending on some criterion, and the detection and the decoding processes are performed sequentially. The CWs are usually ordered according to their equivalent channel gain, so that the CW with highest equivalent channel gain is detected first. The equivalent channel gain of the m-th CW at the n-th iteration can be expressed as:

$$\tilde{H}^n_m = \frac{1}{N_{sub}}\sum_{k=0}^{N_{sub}-1}\mathbf{H}^H_m[k]\left[\frac{1}{\sigma^2_u}\mathbf{H}[k]\mathbf{Q}_n\mathbf{H}^H[k] + N_T\frac{\sigma^2_w}{\sigma^2_u}\mathbf{I}_{N_R}\right]^{-1}\mathbf{H}_m[k] \tag{6.13}$$

The selected CW is detected, soft modulated and fed back to the interference canceller, whose output can be written as follows:

$$\mathbf{r}^n_{m,c}(k) = \mathbf{r}[k] - \mathbf{H}_{Z-\{m\}}[k]\widehat{\mathbf{d}}^v_{Z-\{m\}}(k) \tag{6.14}$$

where

$$\begin{array}{ll} v = n & \text{if } Z - \{m\} = argmax_{i=1,2}\tilde{H}^n_i \\ v = n-1 & \text{if } Z - \{m\} \neq argmax_{i=1,2}\tilde{H}^n_i \end{array} \tag{6.15}$$

The equalizer's output for the m-th CW in subcarrier k is given by:

$$\mathbf{r}^n_{m,eq}(k) = \mathbf{H}^H_m[k]\left[\frac{1}{\sigma^2_u}\mathbf{H}[k]\tilde{\mathbf{Q}}_n\mathbf{H}^H[k] + N_T\frac{\sigma^2_w}{\sigma^2_u}\mathbf{I}_{N_R}\right]^{-1}\mathbf{r}^n_{m,c}(k) \tag{6.16}$$

where $\tilde{\mathbf{Q}}_n = diag\left(\tilde{q}_1, \cdots, \tilde{q}_{N_T}\right)$, whose generic i-th element can be written as:

$$\tilde{q}_i = \begin{cases} \sigma^2_u, & \text{if } \ i = m \\ \sigma^2_u - \widehat{\sigma}^2_{Z-\{m\},n} & \text{if } \ i \neq m, j = argmax_{i=1,2}\tilde{H}^n_i \\ \sigma^2_u - \widehat{\sigma}^2_{Z-\{m\},n-1} & \text{if } \ i \neq m, i \neq argmax_{i=1,2}\tilde{H}^n_i \end{cases} \tag{6.17}$$

6.4.3 Turbo processing with limited complexity

An obvious drawback of the iterative detection techniques is their computational complexity with respect to the linear detection, increasing with the number of iterations. However, since an estimate of the transmitted CWs is available at each iteration, the turbo processing presented above is redundant once at least one of them has been correctly detected. In LTE, a Cyclic Redundancy Code (CRC) is appended to the information bits of the CW to check if the detection process has been successful. Here, we propose to use this error-detection capability to reduce the turbo processing complexity. In fact, checking the CRC allows to stop the iterative process once CWs are correctly decoded. Furthermore, we combine in the same process both the interstream interference removal and the noise enhancement reduction for SC-FDM.

Let us suppose to perform the generic n-th iteration of the PIC or SIC algorithm. After both CWs have been detected, their CRC is checked by taking hard decisions on the soft bits. The possible options and the subsequent behaviour to be adopted are the followings:

- Both CWs are not successfully detected. Continue performing PIC or SIC in the *(n+1)*-th iteration.
- Only one CW is successfully detected. In this case, the interstream interference can be fully removed from the wrong CW. Therefore, the MIMO system is virtually reduced to a SIMO one, and the noise enhancement reduction strategy for SC-FDM presented in Section 6.3 can be adopted. To sum up, the following steps have to be performed:
  - *(n+1)*-th iteration: feed back only the correct CW for interstream interference removal and equalization;
  - from *(n+2)*-th iteration: re-modulate the wrong CW obtaining $\widehat{\mathbf{d}}_{wr}^{n+1}$ and use the adaptive equalizer coefficients defined in Section 6.3, that have been shown to reduce the noise enhancement of SC-FDM in a single stream transmission.
- Both CWs are successfully detected: jump to the detection of the next data frame.

The main computational burden of each iteration is due to the calculation of the matrix inverse in the equalizer (e.g., Eq.(6.16)), especially in 4x4 configuration, as well as the turbo decoding process. Several approaches for reducing the complexity of the matrix inversion operation in MMSE-based receivers have been proposed in the literature. The most known approach exploits the matrix inversion lemma [55], while solutions based on QR decomposition and Square Givens rotations have been derived, for instance, in [101] and [102], respectively. Even though the number of required operations can be sensibly reduced (at the expenses of a higher hardware resource usage [103]), the equalization task has still to be considered cumbersome. Developing efficient algorithms for avoiding the matrix inversion in the detector is however out of the scope of this thesis. Here, we simply evaluate the number of occurrences of this operation. In the following, we will assume that an iteration of both PIC and SIC is completed once an estimate of both CWs is available by exploiting the feedback information. The linear MMSE equalization can instead be considered as the 0-*th* iteration of the PIC scheme.

It is easy to notice that, when no CRC-checking is exploited, the total number of matrix inversion operations is given by $2N_{it}$, where N_{it} is the number of outer iterations. This is because in Eq.(6.16) the $\tilde{\mathbf{Q}}_n$ matrix has to be updated with the variance of each estimated CW. Let us elaborate now on the proposed low complexity solution, considering the SIC approach. At the first iteration, 2 matrix inversions are performed. From the 2nd iteration, the possible alternatives and the subsequent number of matrix inversions are shown in Table 6.2, where P_{c_n} denotes the probability that the CW is correctly detected at the nth

Table 6.2: Matrix inversions for $(n+1)^{th}$ iteration $(n \geq 1)$

Case n^{th} iteration	**Probability event**	**Added matrix inversions**
both CWs correct	$P_{c_n}^2$	0
only one CW correct	$2P_{c_n}(1-P_{c_n})$	1
both CWs wrong	$(1-P_{c_n})^2$	2

iteration. It is worth to notice that, if a CW is correctly detected at the nth iteration, no matrix inversion operation is necessary after the $(n+1)^{th}$ iteration given the proposed noise enhancement reduction strategy.

The total number of matrix inversion operations is therefore given by:

$$N_{inv} = 2 + 2\sum_{n=1}^{N_{it}-1} P_{c_n}(1-P_{c_n}) + 2\sum_{n=1}^{N_{it}-1}(1-P_{c_n})^2 \tag{6.18}$$

The effective complexity of the turbo decoder is also strictly dependent on the chosen implementation. In our simulator, we use the max-log approximation [27] for avoiding the exponential operations in the likelihood ratio computation at each decoding stage. The complexity results to be linear with the number of iterations. In the turbo processing, the reduction of the total number of outer decoder iterations is therefore foreseen.

6.4.4 Performance evaluation

The performance of the turbo receiver is evaluated by Monte Carlo simulations. We use as a reference 10 MHz LTE configuration parameters [8]. The main simulation parameters are the same as in Table 6.1. Compared to the evaluation in section 6.3.2, real channel estimation based on WF is assumed.

Figure 6.7 shows the performance of PIC and SIC for a 2x2 rank 2 SC-FDM system in terms of BLER, assuming 16QAM 2/3. Linear MMSE performance and SIMO results with single stream turbo receiver is also included. Both iterative techniques lead to a consistent gain over linear detection, of up to 5 dB with 6 iterations. That limits the gap with SIMO transmission to within 2 dB at 1% BLER. Most of the gain is already obtained after the first iteration. Note that at the first iteration PIC performs better than SIC because in the latter the soft interference is removed only from one CW. However, for higher number of iterations both techniques perform similarly. It can be seen (Figure

6.8) that SIC converges slightly faster than PIC. This is because in SIC one of the soft estimates used in the interference cancellation is obtained in the current iteration, while in PIC both are obtained in the previous iteration.

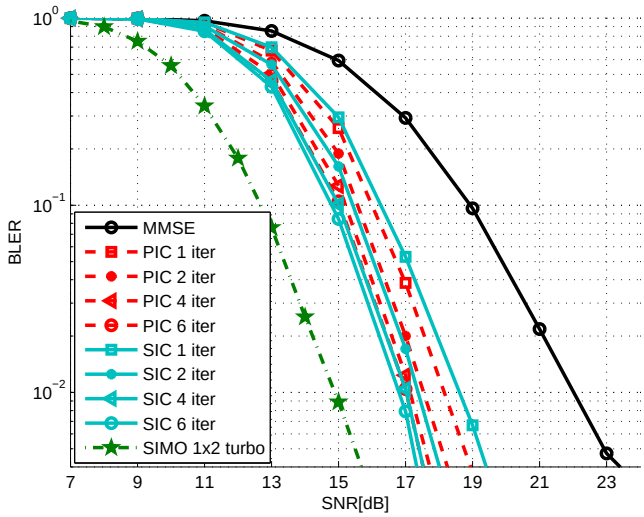

Figure 6.7: BLER performance of SC-FDM in a 2x2 antenna system, with 16QAM 2/3.

Figure 6.9 depicts a comparison between OFDM and SC-FDM for SIC receivers. It can be clearly seen that both air interfaces benefit from the iterative detection. However, for OFDM the gain of SIC with respect to MMSE is limited to 3.5 dB. This allows reducing the performance gap between OFDM and SC-FDM to within 1 dB. The higher relative gain of SC-FDM compared to MMSE is due to the reduction of the noise enhancement provided by the turbo processing. Furthermore, by comparing Figure 6.7 and Figure 6.9, it can also be noticed that the relative gain between different iterations is slightly higher for SC-FDM.

The gap between OFDM and SC-FDM with MMSE is quite reduced with a 2x4 antenna configuration, as presented in Figure 6.10. This is due to the increase of diversity, which averages the channel seen at the receiver. In this way, the deep fades of the channel are smoothed, and therefore the noise enhancement of SC-FDM is reduced. Here, the iterative processing only leads to a gain up to 2 dB for SC-FDM and 1.5 dB for OFDM.

The performance result on the whole SNR range, when fast link adaptation is used, are shown in Figure 6.11. Turbo SIC with 2 iterations is considered, and HARQ is also included. For low SNRs, OFDM performs as good as SC-FDM

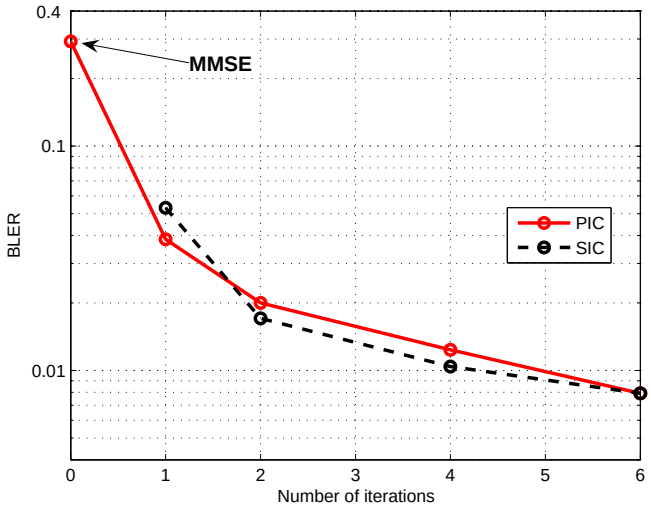

Figure 6.8: SC-FDM PIC vs. SIC, for SNR=18 dB.

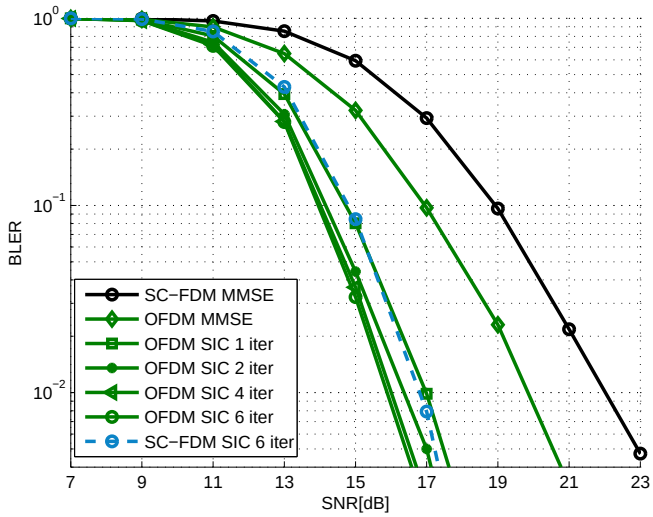

Figure 6.9: Performance comparison between OFDM and SC-FDM in a 2x2 antenna system, with 16QAM 2/3.

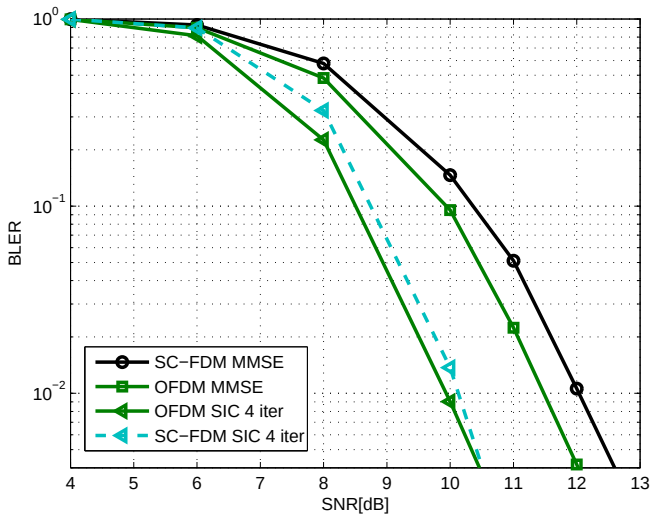

Figure 6.10: Performance comparison between OFDM and SC-FDM in a 2x4 antenna system, with 16QAM 2/3.

for both linear and iterative detection. The performance gap is relevant for high order MCSs, where the higher relative gain of the turbo receiver for SC-FDM is evident. OFDM and SC-FDM tend to perform similarly in a 2x4 antenna system, as suggested by the previous results.

It has been mentioned in Chapter 5 that Antenna Gain Imbalance (AGI) is likely to appear in the UE. In Figure 6.12 the performance of the turbo SIC receiver with AGI is compared with MMSE assuming fast link adaptation and 2x2 configuration. In the MMSE case, the negative effect of the AGI is clearly visible in high SNR region and therefore for high order MCSs, where the spectral efficiency tends to drop. However, the turbo SIC receiver nulls the performance gap irrespective of the different AGI configurations at high SNRs. This is due to nature of the turbo SIC processing, since when AGI is effective the CW transmitted by the high gain antenna is more likely to be correctly decoded with relatively higher effect in removing its interference contribution from the CW transmitted by the low gain antenna. The robustness of the turbo SIC receiver to the AGI makes this solution particularly envisable also in MU-MIMO mode, where power imbalance between the coupled UEs is likely to appear.

Results obtained with 4x4 configuration and different transmission ranks are shown in Figure 6.13, still assuming fast link adaptation. For rank 1 transmission, the single stream turbo receiver is used, while higher transmission ranks

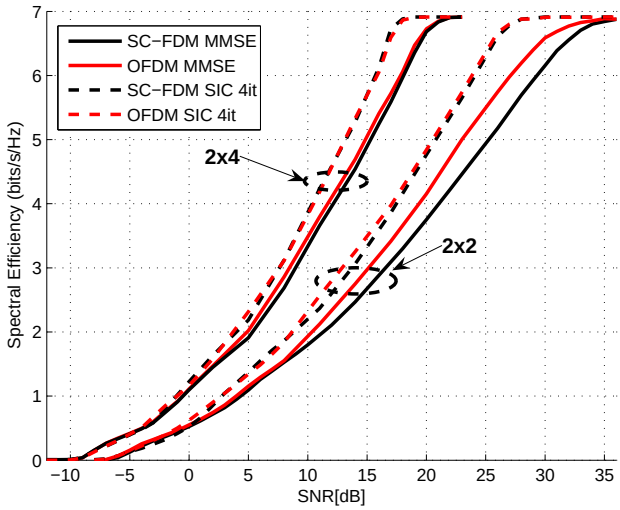

Figure 6.11: Performance comparison between OFDM and SC-FDM with fast link adaptation and turbo SIC receiver.

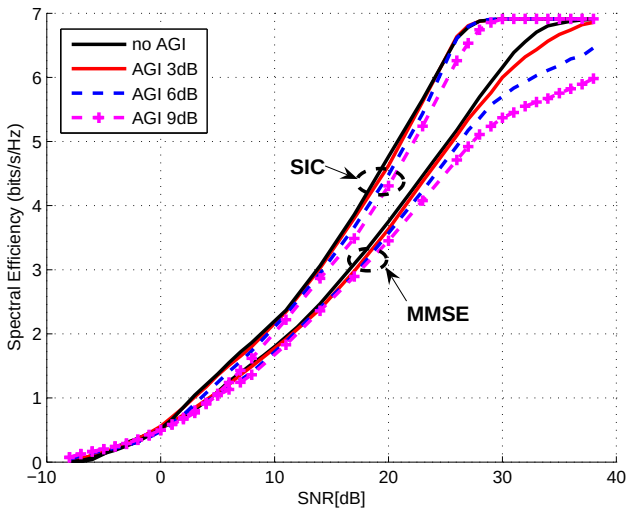

Figure 6.12: Performance of the turbo SIC receiver with AGI.

exploit the MIMO turbo SIC approach. As a common trend, the turbo receiver is effective at high SNR, and therefore for high order MCSs. The usage of single stream turbo receiver shows up to 1 dB of SNR gain, while for higher ranks the performance gain is higher due to the reduction of the interstream interference. The array gain has therefore a similar effect of the receive diversity on the turbo receiver performance; the possibility of exploiting inner gain mechanisms of the MIMO transmission reduces the impact of the turbo processing. Rank 4 transmission achieves the highest gain over linear MMSE, of up to 4 dB.

It has been mentioned in Section 6.4.3 that the main computational burden of the turbo SIC receiver is given by the matrix inversions needed for the equalization as well as the number of turbo decoding iterations. In Figure 6.14 the average number of matrix inversions per subframe is shown as a function of the BLER. Results are obtained assuming a 2x2 configuration and 4 inner iterations. The upper bound of the non-limited complexity solution is also shown. As expected, the number of matrix inversions decreases fast with the BLER decrease due to the higher occurrences of correct CW detections at the first iterations. For very low BLER, all the CWs are correctly retrieved at the first iteration, therefore the number of matrix inversions tends to 2.

All the previous results have been obtained by assuming a number of turbo decoding iterations equal to 8 at each inner iteration, i.e. up to $8N_{it}$ in total. This tends to dramatically increase the computational complexity with respect to linear detection. Here, we set to 8 the total number of turbo decoder iterations, so as to keep the same computational burden of the linear receiver. The impact on the BLER performance is shown in Figure 6.15. In the legend, the expression $[a_1, a_2, \cdots, a_{N_{it}}]$ denotes the number of turbo decoder iterations at the 1st, 2nd, N_{it}^{th} inner iteration. The performance degradation with respect to the $[8, 8]$ and $[8, 8, 8, 8]$ cases is limited to around 0.2 dB for 2 inner iterations, and increases to around 0.5 dB for 4 inner iterations. This means, the gain of using a high number of inner iterations is lost when the number of turbo decoder iterations is limited. In order to avoid undue latency in the detection, the number of inner iterations should therefore be limited when a constraint in terms of turbo decoder iterations is assumed. Note also that no relevant differences are visible among the "cheaper" options.

6.5 Summary

The high sensitivity to the noise of SC-FDM based air interface can be considerably reduced by performing iterative detection. In this way the performance gap with OFDM, and therefore with the downlink transmission, can be overcome at

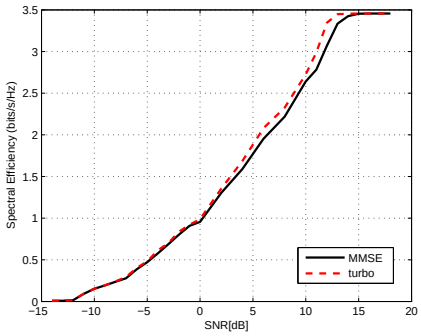

(a) Rank 1

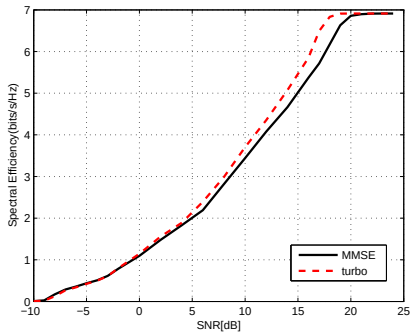

(b) Rank 2

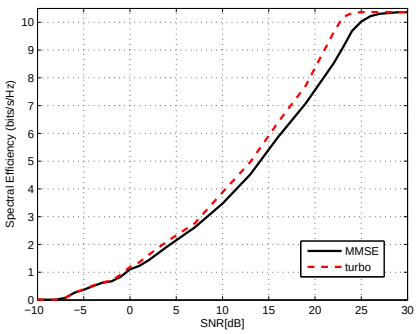

(c) Rank 3

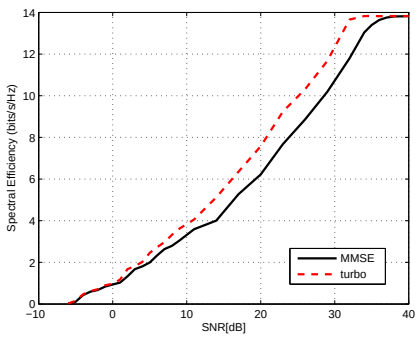

(d) Rank 4

Figure 6.13: Turbo receiver performance in 4x4 configuration.

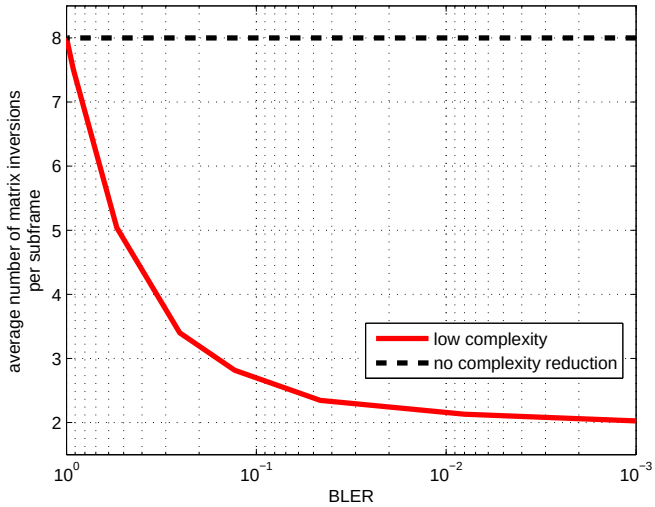

Figure 6.14: Number of matrix inversions, assuming 2x2 configuration, 16 QAM 2/3 and 4 inner iterations.

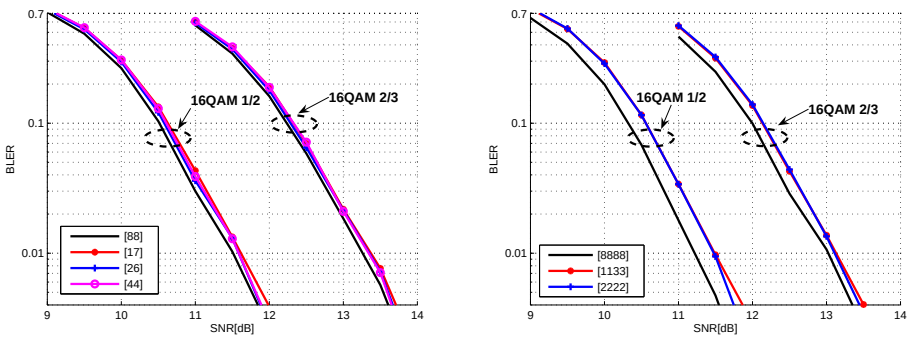

(a) 2 inner iterations

(b) 4 inner iterations

Figure 6.15: Effect of the reduced number of outer iterations on the BLER performance, assuming 2x2 rank 2 configuration.

the cost of an increase in the computational complexity. Solutions for single and multi-stream transmission are proposed. While the single stream turbo receiver simply aims at reducing the noise enhancement of SC-FDM, the multi-stream turbo receiver performs also parallel or successive interstream interference cancellation, thus revealing the potential diversity of the MIMO transmission. This leads to an impressive SNR gain, of up to 5 dB in 2x2 mode. The turbo SIC receiver has been shown to converge slightly faster than turbo PIC. Furthermore, it results to be particularly beneficial when AGI occurs, given the possibility of removing the interference of the CW experiencing high gain, from the low gain CW. The addition of diversity branches, or the array gain at the transmitter in precoded trasmission, reduces the impact of the turbo detection, which therefore results to be more advantageous in 2x2 or 4x4 full rank configurations. The proposed solution based on CRC-checking and noise enhancement reduction considerably reduces the number of cumbersome matrix inversions. Moreover, the total number of turbo decoder iterations can be set to be the same as for the linear receiver, with negligible performance degradation when the number of inner iterations is limited to 2.

Chapter 7

Transmission over multiple component carriers

7.1 Introduction

The achievement of the targeted data rates in LTE-A foresees the usage of a transmission bandwidth up to 100 MHz. Moreover, compatibility between LTE Release 8 and LTE-A is required in order to allow a smooth migration between the two technologies. An LTE terminal should be able to operate in a LTE-A system without dramatically increasing the control signaling or requiring new protocol stacks. That leads to severe constraints for the multiple access.

In the Radio Access Network (RAN) Working Group 1 (WG1) meeting, a multiple component carriers (CCs) solution has been agreed as the underlying structure for the LTE-A spectrum [7]. The 100 MHz bandwidth is divided to 5 chunks, referred as Component Carriers (CCs), each of them keeping the structure of the LTE system bandwidth.

The necessity of being backward compatible with LTE while coping with the multiple CCs structure of the LTE-A spectrum put further constraints in the SC-FDM signal generation. It will not be possible to maintain the single carrier property for a transmission bandwidth larger than 20 MHz because the edges

of each CC have to be reserved for Release 8 Physical Uplink Control Channel (PUCCH) [104]. Therefore further solutions have been proposed and discussed.

The new spectrum configuration opens new challenges in the overall system design. For instance, each cell shold be able to select the frequency chunks to be used depending on the estimated intercell interference conditions (autonomous component carrier selection) [105]. New scheduling algorithms that aim at balacing the load across multiple CCs as well as power control solutions *per CC* are to be designed. The multiple CC structure foresees also a careful design of transmit and receive filters aiming at eliminating the mutual power leakage between adjacent chunks.

However, all the mentioned issues concern system level implementation or radio frequency design, and are therefore out of the scope of this dissertation. In this chapter, we focus on the transmission over multiple CCs for LTE-A uplink in a pure link level perspective; the generation of the uplink signals over wide bandwidth is discussed, as well as the issues of the link adaptation design over the multiple CCs. The wide spectrum allocation leads indeed to an increase of the feedback overhead which is needed to properly setup the transmission depending on the instantaneous channel conditions: *bundling* of link parameters over frequency resources is foreseen to reduce this signaling overhead and make it comparable with LTE Release 8.

The chapter is structured as follows. Section 7.2 introduces the LTE-A spectrum configuration, while the agreed multiple access scheme for the uplink is presented in Section 7.3. The main part of this chapter is dedicated to the CM performance of the signal generated over multiple CCs (Section 7.4) and to the bundling of the main link parameters across multiple CCs (Section 7.5). The summary is finally presented in Section 7.6.

7.2 LTE-A spectrum configuration

The agreed multiple component carrier structure for the LTE-A spectrum is shown in Figure 7.1. In this setup, the bandwidth is divided in 5 CCs, each of them having an effective bandwidth equal to 18 MHz. As mentioned in the introduction, this structure allows the development of “low category” UEs whose reception bandwidth is lower than the maximum, e.g. 18 MHz for LTE UEs. Furthermore, it makes possible the CCs to be controlled by different BSs by exploiting Flexible Spectrum Usage (FSU) techniques [106]. There are two mechanisms to accede the available spectrum:

1. Channel bonding: combining multiple adjacent CCs.
2. Channel aggregation: combining 2 or several totally separate CCs.

A guard band (GB) is assumed between the CCs. This GB exploits a double role:

1. It avoids the interference between adjacent CCs when a Release 8 LTE UE receives in its 18 MHz bandwidth while the BS is also transmitting to LTE-A UEs in the adjacent CCs. It has been shown in [107] that 19 subcarriers (285 kHz) would be sufficient to minimize the interference power, but at the time of this dissertation the GB size has not been defined yet.
2. It satisfies the 100 kHz channel raster condition for each CC. The channel raster condition was specified in the Release 8 LTE and for the existing 3G systems, and forces the center of each CC to be a multiple of 100 kHz [6].

Note that a further GB is left on both sides of the LTE-A spectrum to avoid interference with systems operating on the adjacent bands.

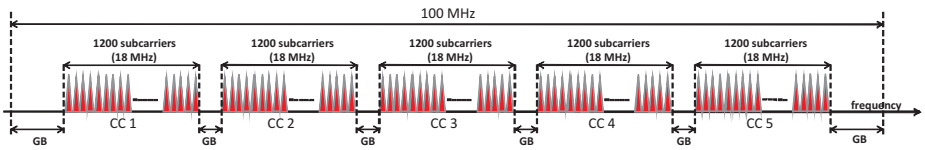

Figure 7.1: Structure of the LTE-A spectrum.

7.3 NxDFT-s-OFDM

The multiple access scheme for the uplink of LTE-A has to cope with the proposed spectrum configuration. That leads to some modifications with respect to the Release 8 signal generation.

The baseband transmitter chain of SC-FDM as adopted in LTE uplink has been shown in Section 2.2. In the LTE-A uplink transmitter, the most intuitive solution to cope with the multiple CC structure is to use a single DFT having dimension equal to the size of the transmit block over the whole used CC set. However, this option (named *clustered* DFT-s-OFDM) has been discarded in the work item (WI), since the larger transmit block with respect to LTE Release 8

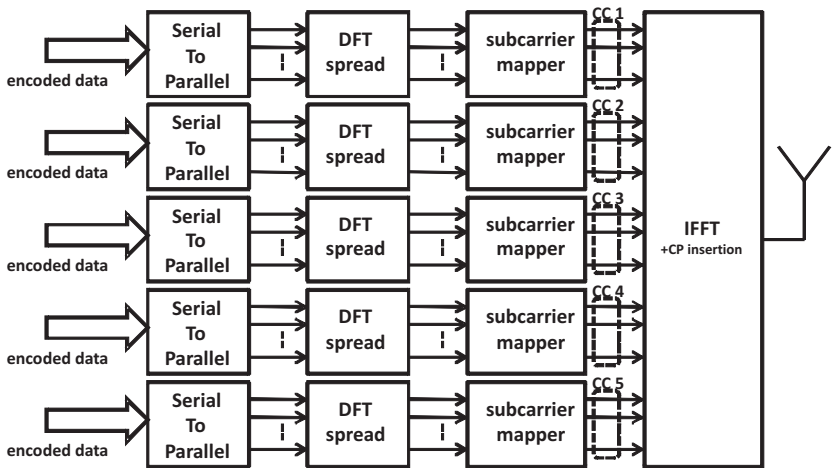

Figure 7.2: NxDFT-s-OFDM.

has an impact on the MAC layer: the logical transport channel needs re-design to cope with the different physical channel capability, thus leading to different specifications between the two technologies.

The NxDFT-s-OFDM solution is therefore preferable since it is fully compatible with Release 8. As shown in Figure 7.2, up to 5 Release 8-like transport blocks are independently DFT-spread before being mapped over the CCs. With the assumption of maintaining the same parametrization (i.e., subcarrier spacing) for each of the CCs, a single IFFT can be used to generate the time domain signal. With this solution, the transmissions over multiple CCs can be seen as parallel Release 8 transmissions, thus allowing link adaptation per CC. The issues related to the link adaptation process per CC will be discussed in Section 7.5. For each CC, non-contiguous allocation of the RBs on which the user data are scheduled has been approved with the aim of enhancing the scheduling flexibility. The RBs are grouped in a certain number of *clusters* before being mapped over disjoint sub-bands within the same CC (see Figure 7.3).

7.4 CM performance

SC-FDM has been selected as uplink modulation and coding scheme for LTE Release 8 mainly due to the advantageous backoff requirement in the transmit power amplifier. Unfortunately, the NxDFT-s-OFDM leads to multicarrier transmission and therefore breaks the low CM property of the single carrier

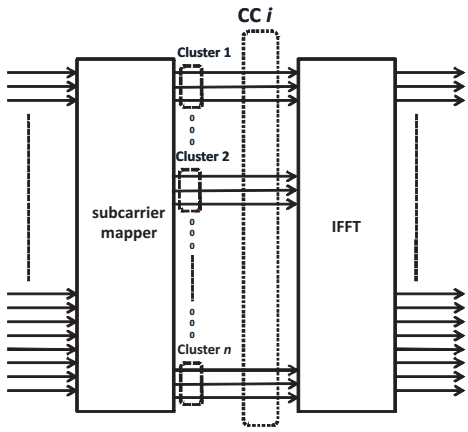

Figure 7.3: Clustered allocation of RBs in NxDFT-s-OFDM.

signal. In order to justify the adoption of NxDFT-s-OFDM for the uplink of LTE-A, the gain in terms of CM over OFDM should however be clear.

In this section, we evaluate the CM performance of NxDFT-s-OFDM considering different number of CCs. Results are obtained through Monte Carlo simulations, assuming the structure in Figure 7.2 with data encoded with 16QAM. An effective transmission bandwidth of 10 MHz is considered. The 600 subcarriers are split over 1, 2 or 5 CCs; in each CC, they are further divided in 1, 2 or 5 clusters which are randomly distributed over the effective 18 MHz bandwidth of a single CC.

In Figure 7.4, results are shown for different number of CCs as well as for OFDM. For the latter, only the single CC case is shown since its performance is not affected by the transmission over multiple CCs. As a general trend, the CM of NxDFT-s-OFDM increases with the number of CCs and the number of clusters. This means, a larger power back-off is required in case of transmission over several CCs to avoid the effect of non-linearities. However, a gain of around 0.2 dB is kept over OFDM even with $N = 5$. Furthermore, 5 CCs are likely to be assigned to non-power limited UEs in good SNR conditions, for which preserving a very low CM is not critical. Note that the clustered allocation of RBs over the same CC is highly detrimental for $N = 1$ (allocation over 5 clusters performs even worse that 2 CCs with 2 clusters), while this effect is considerably reduced when the number of CCs increases. Hence, for users transmitting with a single CC, e.g. on the cell edge, contiguous RB allocation should preferably be used.

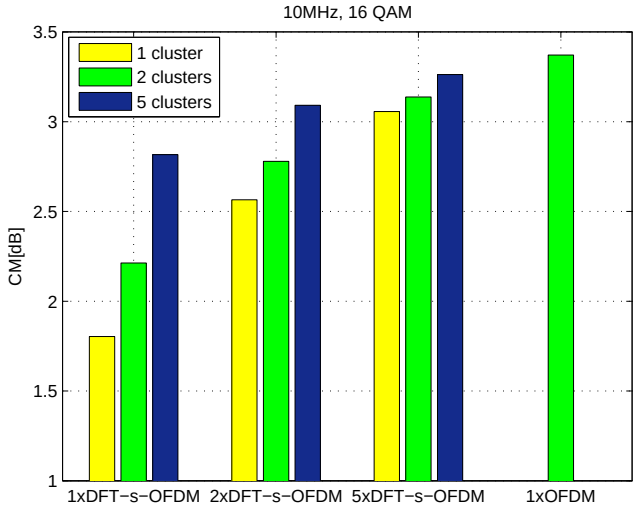

Figure 7.4: CM performance of NxDFT-s-OFDM and OFDM.

7.5 Bundling of link level parameters

The high spectral efficiency performance of the 3GPP radio access technologies is mainly due to the possibility of adapting the transmission parameters to the instantaneous channel conditions. HARQ, fast link adaptation and precoding in FDD mode rely on a feedback channel. MCS's indexes, ACK/NACK (A/N) messages and precoding matrix indicators increase however the feedback overhead in the downlink signaling. In LTE Release 8, a single CW is mapped over the whole transmission bandwidth, and thus only a single MCS index is fed back. In LTE-A it is assumed that each CW is mapped over a CC [7], and it is still under discussion whether the MCS index should be sent per CC or one for the whole user bandwidth. The first solution can make a better use of the frequency selectivity of the channel, but it also increases up to 5 times the feedback overhead. At the same time, also the HARQ process feedback can be made per CC or over the whole bandwidth. In the second case, all the CWs over the used CC set must be retransmitted even only one of them is incorrectly decoded. The following alternatives will be considered here:

1. *no bundling*: a single MCS field and A/N message per CC (Figure 7.5(a)). This solution allows to easily cope with the different channel gains over the CCs; however, it is the most expensive solutions in terms of feedback

overhead.

2. *HARQ bundling*: the MCS is still selected per CC, but the A/N message is sent per the whole used CC set (Figure 7.5(b)).

3. *HARQ/MCS bundling per Antenna*: a single MCS field and A/N message per the whole used CC set (Figure 7.5(c)).

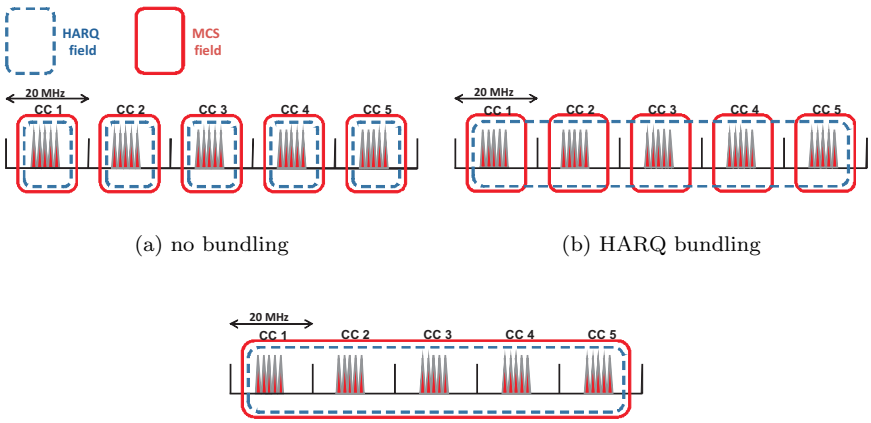

(a) no bundling

(b) HARQ bundling

(c) HARQ/MCS bundling

Figure 7.5: Bundling of HARQ and MCS fields.

In case of MCS bundling, the MCS to be used in the UE is computed as a function of the SNR values of the SRSs which are transmitted over multiple CCs. Since the data over multiple CCs are expected to experiment uncorrelated fading because of the frequency separation, the selected MCS might not be the one leading to successful transmission on all CCs, and hence force retransmission of all CWs. To avoid this problem, we propose the following alternative solutions:

- *time symbol based CW mixing*. The data belonging to a certain CW are permuted over different CCs on a time symbol basis, as shown in Figure 7.6(a). Since the mixing is performed on a CW basis, the CM of the signal is not affected.

- *data symbol based CW mixing*: The modulated symbols for each CW enter an interleaver block; data are written "row-wise" and read "column-wise". In this way, symbols belonging to each CW are mapped over different CCs (see Figure 7.6(b)). Since the interleaving operation is performed before the DFT, the CM properties of the transmit signals are not compromized.

By applying a *CW mixing* technique, the experienced channel gain is averaged over CWs transmitted by the antenna, and the selected MCS is a more valid predictor of the achievable throughput. Furthermore, the SNR-averaging provided by the CW mixing reduces the number of unnecessary retransmissions for HARQ bundling since the CWs mapped over different CCs have now instantanously the same probability to be correctly decoded.

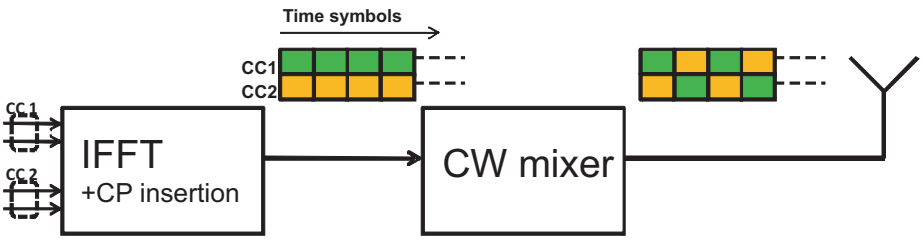

(a) time symbol based CW mixing

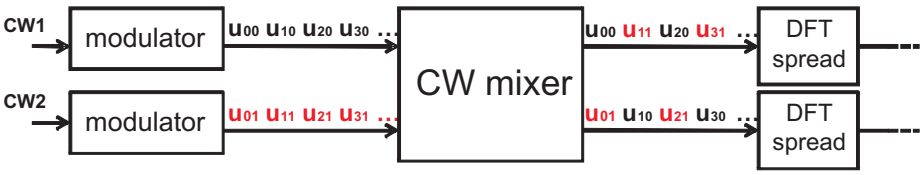

(b) data symbol based CW mixing

Figure 7.6: CW mixing strategies.

The feedback overhead per antenna required for supporting the aforementioned solutions is described in Table 7.2, assuming 10 MCS options (therefore requiring 4 bits of feedback for indexing plus 1 bit for A/N message). It is worth to notice that *HARQ/MCS bundling* keeps constant the feedback overhead over different numbers of CCs.

Regarding the precoded transmission, a single precoding matrix should be applied at least over the whole subcarrier set where the CW is mapped to preserve the low CM property of DFT-s-OFDM signals. When transmission over multiple CCs occurs, the precoding matrix can be selected per CC or over the whole transmission bandwidth (per BW). Assuming the 6 elements codebook for rank 1 transmission defined for 2 transmit antennas, the feedback overhead for the precoding is described in Table 7.2.

Table 7.1: Feedback overhead per antenna for link adaptation (bits per frame)

	1 CC	2 CCs	3 CCs	4 CCs	5 CCs
no bundling	5	10	15	20	25
HARQ bundling	5	9	13	17	21
HARQ/MCS bundling	5	5	5	5	5

Table 7.2: Feedback overhead per precoded rank 1 transmission (bits per frame)

	1 CC	2 CCs	3 CCs	4 CCs	5 CCs
precoding per CC	3	6	9	12	15
precoding per BW	3	3	3	3	3

Even though the UE may transmit on up to 5 CCs, it is preferable that its transmission bandwidth does not exceed 3 CCs. As noticed in [108], in the power limited uplink a wider transmission bandwidth capability does not necessarily contribute to an increase of the throughput because of the lower power spectrum density. In the numerical evaluation we will therefore consider transmission on up to 3 CCs.

7.5.1 Optimization for HARQ and turbo SIC receiver

As mentioned above, when HARQ bundling is performed, all the CWs have to be retransmitted in case one of them is not correctly decoded. Nevertheless, the receiver is aware of the eventual correct reception of one CW since its CRC is checked. This means, it can store the correct CW and remove its interference contribution from the wrong CW when both of them are retransmitted. The interference contribution on the CW which has not yet been correctly retrieved can hence be fully eliminated at the first inner iteration of the SIC algorithm, and the overall latency can be reduced. Of course, performance is also expected to improve since the SIC algorithm can rely on the correct CW at the previous transmission rather than on the retransmitted CW, which can be instantaneously affected by fading. Note that, in case of IR, the receiver has to be aware of the different puncturing patterns used at the transmitter, so that the CW which is re-encoded for interference elimination purpose can match with the re-transmitted one. This option has been applied in the following performance evaluation.

Table 7.3: Simulation parameters for the evaluation of transmission over multiple CCs.

Carrier frequency	2 GHz
Sampling frequency	92.16 MHz
Subcarrier spacing	15 KHz
Number of CCs	1, 2, 3
FFT size	6144
CP length	$5.2^a/4.68^b$ μs
Frame duration	14
Antenna configurations	2x2, 2x4
Channel Model	Typical Urban
User speed	3 kmph, 50 kmph
Pilot Overhead (Ov)	0%
Channel estimation	Ideal
MCS settings	QPSK: 1/6, 1/3, 1/2, 2/3 16QAM: 1/2, 2/3, 3/4 64QAM: 2/3, 4/5
Channel code	3GPP Rel.8 compliant Turbo code with basic rate 1/3
Turbo decoder iterations	8
BLER target	10%
HARQ retransmission strategy	IR
HARQ Max. number of retransmissions	4
HARQ SAW channels	6

[a] 1st and 8th OFDM/SC-FDM symbol in a subframe.
[b] $2^{th} - 7^{th}$ and $9^{th} - 14^{th}$ OFDM/SC-FDM symbols in a subframe.

7.5.2 Performance evaluation

The link level performance of the multiple CC transmission is evaluated using our LTE compliant MATLAB simulator. The main simulation parameters are gathered in Table 7.3. For simplicity, we limit our analysis to the 2 transmit antenna case. According to the 3GPP decision of avoiding precoded transmission for full rank, we set as test cases open loop rank 2 and precoded rank 1.

For this study we also consider perfect channel knowledge at the receiver.

Each CW is mapped over a single CC; this means, up to 6 CWs are transmitted in 3 CCs case and rank 2 transmission. Unless otherwise specified, an effective transmission bandwidth of 25 RBs per CC is considered. A Typical Urban channel model is used in the simulations. A 5 ms delay, corresponding to 10 transmission slots, is assumed between the selection of the MCS and the precoder in the BS and its application in the transmitter. A maximum of 4 retransmissions is considered for the HARQ algorithm, which uses the IR option.

Note that, when MCS bundling over multiple CCs is considered, the BLER target has to be modified in such way that each of the bundled CWs has the same BLER target of no bundling case. This can be done by defining an equivalent BLER target as follows:

$$BLER_{target,eq} = 1 - (1 - BLER_{target})^{N_{CC}} \tag{7.1}$$

where N_{CC} is the number of bundled CWs. By using $BLER_{target,eq}$ in the selection of the MCS to be used by the N_{CC} CWs, we ensure that each of the CWs preserves, in average, the desired $BLER_{target}$.

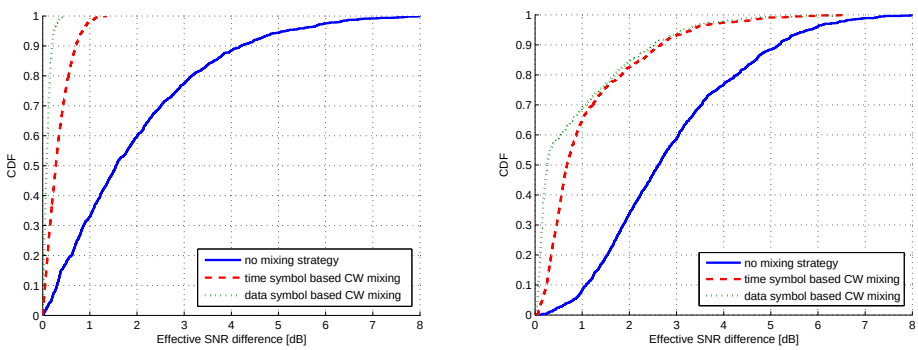

(a) 2 CCs

(b) 3 CCs

Figure 7.7: CDF of the effective post-detection data symbol SNR difference among multiple CCs.

Figure 7.7 shows the Complementary Distribution Function (CDF) of the difference of the effective post-detection data symbol SNR among multiple CCs.

The effective post-detection SNR is computed as in Eq.(A.3). As expected, the usage of a CW mixing technique considerably reduces the SNR difference between CCs thanks to its averaging effect. The benefit is more consistent for *data symbol based CW mixing* and especially for 2 CCs, since it performs a deeper permutation of the data across the CCs. Nevertheless, in terms of spectral efficiency performance, no relevant difference has been noticed between *data symbol based CW mixing* and *time symbol based CW mixing*. This is due to the limited set of 10 MCSs used in the simulations; it is reasonable to claim that the use of an extended MCSs set would highlight the further benefits of *data symbol based CW mixing*. In the next, we will simply refer to a generic CW mixing strategy.

Figure 7.8 shows the spectral efficiency performance of the HARQ bundling option assuming 2x2 rank 2, 2 CCs and linear MMSE receiver. Note that the position of the 2 CCs in the spectrum does not affect the link performance since the frequency separation between the data mapped over adjacent or disjoint CCs is much larger than the coherence bandwidth of the Typical Urban channel. No bundling results are also included for the purpose of comparison. In low SNR region, where retransmissions are more likely to occur, the high speed leads to a beneficial time diversity; this explains the better spectral efficiency performance of the results obtained with speed 50 kmph with respect to the 3 kmph one. At low speed the HARQ bundling leads to a loss of around 0.5 dB with respect to no bundling, and slightly reduced at 50 kmph. The CW mixing has negligible impact in the 50 kmph case, but allows to almost fully overcome the performance gap with no bundling for low speed. In high SNR region the behavior turns to be the opposite; the high speed leads of course to some spectral efficiency loss. Furthermore, the CW mixing results to be more advantageous in the 50 kmph case. No benefits are indeed visible at 3 kmph, where retransmissions are unlikely to occur.

The spectral efficiency performance of HARQ/MCS bundling is shown in Figure 7.9, still assuming linear MMSE receiver, and 3 kmph. For 2 CCs, the losses with respect to no bundling increase up to 2 dB. However, CW mixing allows to achieve approximately the same performance of only-HARQ bundling while saving a significant feedback overhead. In the 3 CCs case, the losses due to bundling increase up to 4 dB. The gain due to CW mixing is around 2 dB; however, in this case only-HARQ bundling still performs better. No relevant differences in the trends have been noticed at 50 kmph.

Similar considerations hold for the 2x4 case (see Figure 7.10). Note that here the losses due to the bundling are limited to 1.5 and 2 dB for 2 CCs and 3 CCs, respectively; this is because the added receive diversity smooths the effect of the channel fades, thus improving the post-detection SNR. As a consequence, the gap with no bundling results is further reduced when CW mixing is applied.

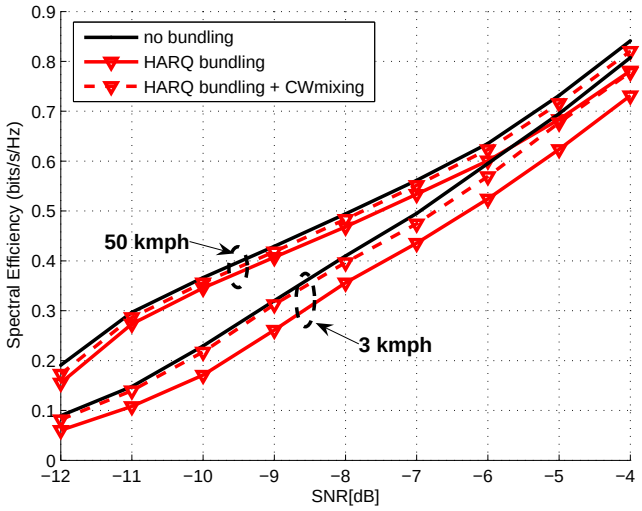

(a) behavior in low SNR region

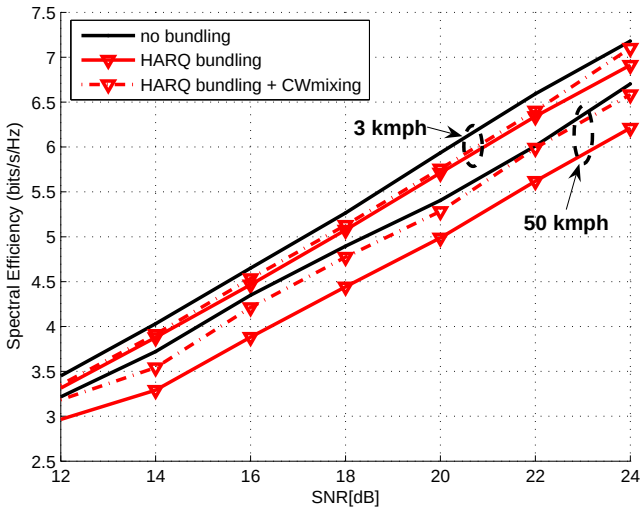

(b) behavior in high SNR region

Figure 7.8: HARQ bundling performance for 2 CCs and linear MMSE receiver for 2x2 rank 2 configuration, 3 kmph.

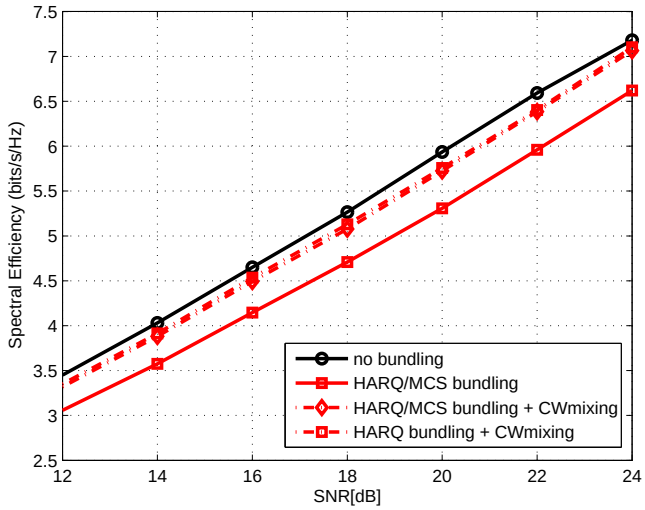

(a) 2 CCs

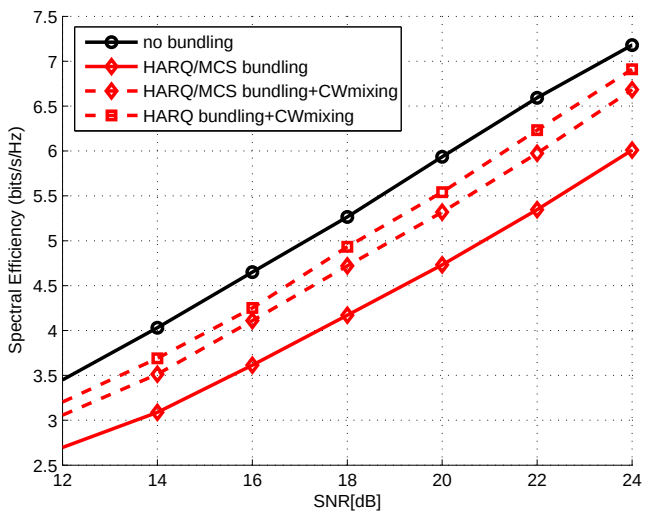

(b) 3 CCs

Figure 7.9: HARQ/MCS bundling performance with linear MMSE receiver for 2x2 rank 2 configuration, 3 kmph.

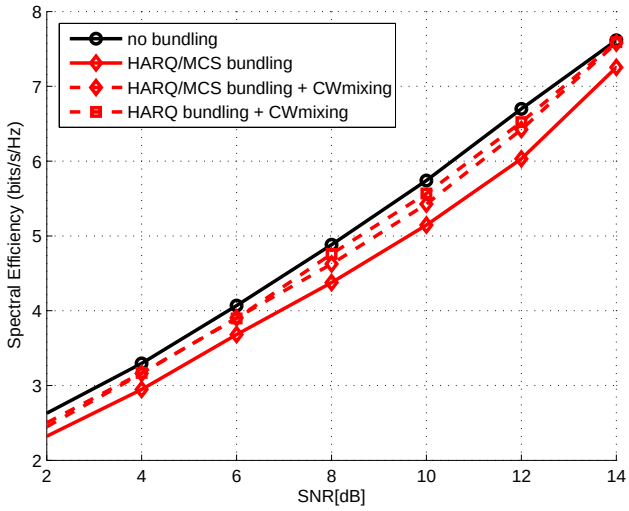

(a) 2 CCs

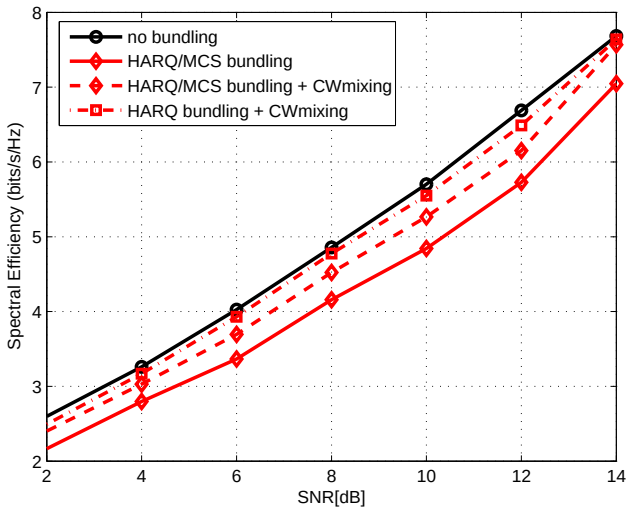

(b) 3 CCs

Figure 7.10: HARQ/MCS bundling performance with linear MMSE receiver for 2x4 rank 2 configuration, 3 kmph.

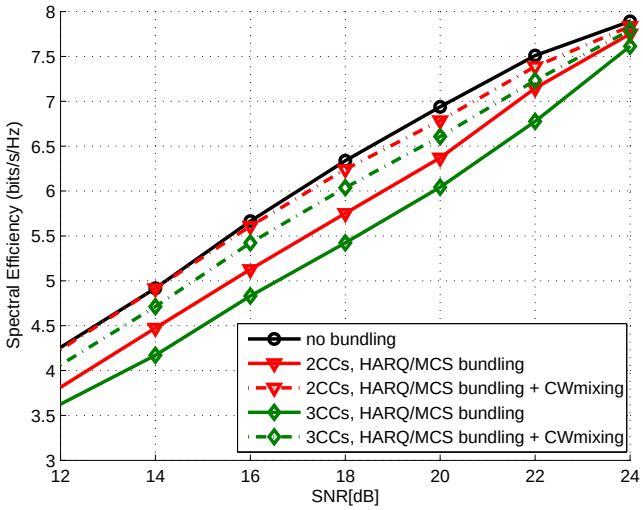

(a) 3 kmph

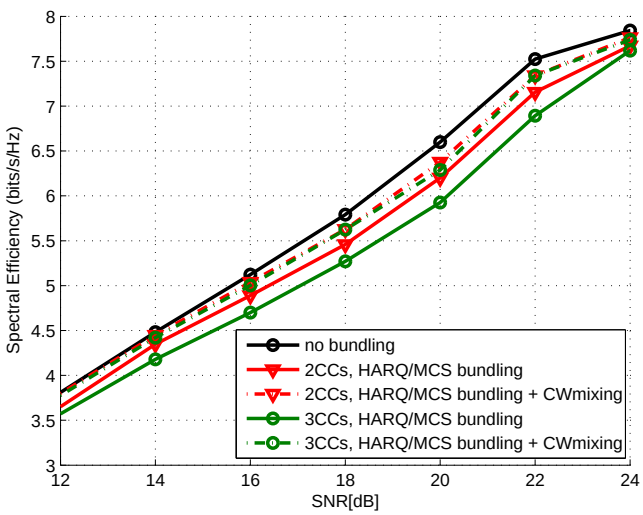

(b) 50 kmph

Figure 7.11: 2 CCs vs. 3 CCs performance with turbo SIC receiver for 2x2 rank 2 configuration.

Results obtained with turbo SIC receiver (2 iterations) and 2x2 rank 2 configuration are shown in Figure 7.11. The optimization introduced in subsection 7.5.1 has been applied. The HARQ/MCS bundling leads to a loss with respect to no bundling up to 1.8 dB and 2.3 dB for 2 CCs and 3 CCs, respectively. Its impact is hence reduced with respect to the linear MMSE receiver. CW mixing allows again to boost the performance, recovering most of the loss (2 dB). Hence for 2 CCs, we obtain approximately the performance of no bundling, while for 3 CCs the gap is within 1 dB. At 50 kmph, the losses of the HARQ/MCS bundling is reduced to 1 dB and 1.5 dB for 2 CCs and 3 CCs, respectively. Transmission over 2 CCs and 3 CCs shows here the same performance when CW mixing is applied.

It is worth to mention that the HARQ/MCS bundling for rank 2 transmission can be also applied on a spatial domain basis over the 2 CWs mapped on the same CC. In our paper [109], we have shown that the performance of bundling across multiple antennas is similar to the one obtained with bundling across multiple CCs when linear receivers are used. In case of turbo SIC receiver, bundling across multiple CCs performs better; the SNR averaging across multiple antennas is indeed detrimental, since turbo SIC has been shown to benefit from the instantaneous SNR imbalance between CWs. The detrimental effect of the SNR averaging over antennas is due to the fact that it works "inside the interference cancellation loop", whereas the SNR averaging over CCs works "outside the interference cancellation loop".

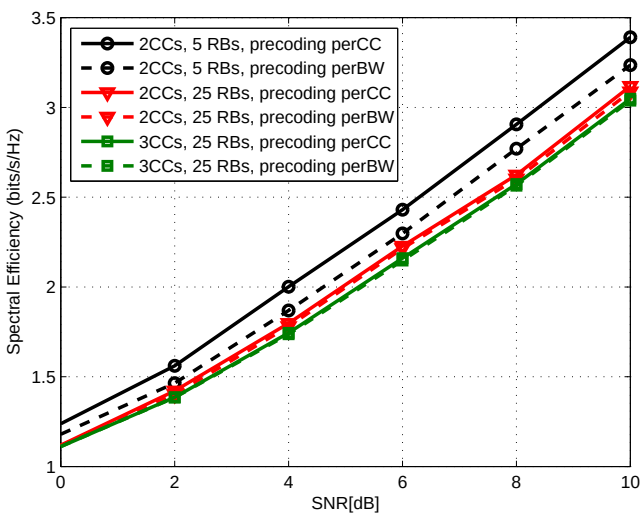

Figure 7.12: 2 CCs vs. 3 CCs, precoded 2x2 rank 1 performance, 3kmph.

Finally, the impact of precoding on a CC basis (per CC) or over the whole transmission bandwidth (per BW) is evaluated in Figure 7.12, assuming 2x2 rank 1 configuration. HARQ/MCS bundling combined with CW mixing is assumed. Together with the reference case of 25 RBs per CC, we consider also the case of an UE sending data over 5 RBs (i.e., around 900 kHz) per CC. In case of transmission over 2 CCs and 5 RBs per CC, the precoding per BW leads to a loss of around 0.7 dB with respect to the case of precoding per CC. Transmission over 25 RBs per CC shows poorer spectral efficiency, since the precoding matrix is selected by averaging the channel over a wider bandwidth, thus loosing frequency resolution. However, the performance gap between precoding per CC and precoding per BW is here negligible. Note that also for transmission over 3 CCs there is practically no difference.

7.6 Summary

In this chapter, we have focused on the transmission over multiple CCs in LTE-A uplink. The spectrum configuration as agreed in the 3GPP work item has been presented and NxDFT-s-OFDM has been introduced as a suitable air interface which is backward compatible with single CC technology as in LTE. In order to test the validity of this option for the uplink transmission, a CM evaluation of the NxDFT-s-OFDM signals has been carried out. The use of NxDFT-s-OFDM has been shown to require lower power derating than OFDM for both localized and clustered allocation of the RBs, even for transmission over 5 CCs. Since the transmission over multiple CCs is expected to dramatically increase the feedback overhead, we foresee the *bundling* of HARQ and MCS parameters over frequency. Two CW mixing strategies over CCs are proposed to improve the spectral efficiency performance when bundling is applied, while keeping a low feedback overhead. The losses due to the bundling of link level parameters are more consistent in a 2x2 rank 2 configuration and with a linear MMSE receiver; the gap with no bundling can be however reduced by adding diversity branches (2x4 configuration) or using a turbo SIC receiver. When combined with CW mixing, HARQ/MCS bundling over 2 CCs can achieve approximately the same performance of HARQ only bundling, with the advantage of a much lower feedback overhead. CW mixing also allows to obtain similar spectral efficiency when the bundling is performed over 2 and 3 CCs, and especially for high speed and turbo SIC receiver. In case of precoded transmission, the selection of the precoding matrix per CC is justified in case of small transmission bandwidth, otherwise a single precoding matrix can be adopted over the whole used CC set without significant performance degradation.

Chapter 8

Conclusion

Future generation mobile communication systems foresee the usage of efficient air interfaces, advanced MIMO techniques and wide spetrum allocation to achieve ambitious data rate targets. The physical layer design of the 4th generation systems has been studied in this dissertation. The uplink of LTE-A, based on SC-FDM technology, is assumed of main interest in this thesis. The integration of the main MIMO techniques such as spatial multiplexing, transmit diversity and precoding with a SC-FDM air interface is investigated with the aim of obtaining high spectral efficiency performance. The analysis of the results is based on link level simulations. Realistic features and impairments have been included in the evaluation in order to verify the feasibility of the proposed solutions for a real transceiver. In this chapter, the main findings of the work are summarized. The main recommendations and the suggestions for further studies are also provided.

8.1 Main Findings and Contributions

SC-FDM has been adopted as air interface for the uplink of the upcoming LTE-A systems since it exploits similar benefits of OFDM in terms of flexibility and multipath mitigation, at the same time leading to higher power efficiency. The cubic metric (CM) has been introduced as a reliable predictor of the backoff

which is needed in the power amplifier to avoid the intermodulation distortion. The lower CM of SC-FDM compared to OFDM allows the UE to operate at higher power, and therefore to extend the coverage.

The achievement of the uplink data rate target is only possible by using advanced MIMO techniques. The suitability of different MIMO algorithms for a SC-FDM air interface has been therefore investigated. A channel estimator based on cyclically shifted versions of the same CAZAC sequence to be sent by each transmit antenna has been designed. It is shown to introduce only little degradation with respect to the ideal channel knowledge when a Wiener Filter (WF) frequency interpolator is used in the receiver.

While the extension of the single transmit antenna scheme to open loop MIMO spatial multiplexing is straightforward, the same does not hold for more advanced MIMO technologies. Transmit diversity solutions based on Alamouti SFC over neighbouring subcarriers leads to SNR gain but also compromises the single carrier nature of the uplink signals. Even though the CM increase does not exceed 0.5 dB, the power efficiency reduction may be critical in power limited scenarios, where transmit diversity is more likely to be used. Alamouti STC over adjacent time symbols shows approximately the same link performance as SFC in a 2x4 configuration at low SNR and for both low and high speed when real channel estimation is considered. However, this solution has low flexibility due to the rigid time domain encoding. Starting from the time domain single carrier signals at each antenna, SFC solutions with low CM have been derived. They are shown to provide SNR gain over single transmit antenna solutions for small transport data blocks. For a low frequency selective channel, the low CM SFC scheme also outperforms STC in a 2x2 configuration. Transmit diversity algorithms for 4 transmit antennas have been shown not to be beneficial given the higher channel estimation error compared to 2 transmit antenna mode.

Precoded transmission in FDD mode relies on the availability of a feedback channel, whose capacity should be kept reasonably low. The main criteria for the design of an universal codebook of precoding matrices have been presented. Approaches based on SVD decomposition of the channel matrix are only valid for single stream transmission when the power balance among the transmit antennas is taken as a constraint, and may lead to high complexity in the matrix selection given the random-like nature of its entries. The codebook adopted for LTE downlink has been shown to be effective to obtain SNR gain over open loop transmission. However, it also increases the CM of the uplink signals in case of multi-stream transmission. A CM preserving codebook has been therefore derived through exaustive search considering the chordal distance as a main design metric. It has been shown to perform approximately the same as the LTE downlink codebook for different antenna correlation patterns. The low CM property can be broken for rank 3 transmission while still saving some

gain over the LTE downlink codebook. This is because rank 3 transmission is generally used by non power limited UEs. The single carrier nature of the uplink signals can however be kept only when WB precoding is applied. As a consequence, the precoded transmission results to be more suitable in an indoor office scenario given its higher coherence bandwidth.

The performance of SC-FDM has also been compared with OFDM to highlight the difference with the downlink when the used resources are the same. SC-FDM has been shown to be more sensitive to the noise than OFDM; this leads to lower spectral efficiency. The insertion of diversity branches is however beneficial for SC-FDM. Furthermore, the iterative detection also enhances the SC-FDM performance. Turbo receivers for single and multi-stream transmission have been proposed. The single stream turbo receiver is only suitable for SC-FDM since it reduces the noise enhancement issue of this air interface. The multi-stream turbo receiver improves the performance of both SC-FDM and OFDM given the removal of the interstream interference. The complexity of this solution can be kept limited by exploiting a CRC-checking strategy as well as by limiting the total number of turbo decoder iterations, with negligible impact on the coded performance. As an effect of the combined usage of receive diversity and turbo detection, SC-FDM can obtain the same spectral efficiency of OFDM in both single and multi-stream mode.

The impact of the transmission over multiple CCs on the link performance is also investigated. NxDFT-s-OFDM, which is the solution agreed within 3GPP to adapt SC-FDM to a spectrum structure with multiple CCs, has been shown to preserve lower CM than OFDM despite of an increase with respect to SC-FDM. The usage of multiple CCs also leads to an increase of the feedback overhead for HARQ, link adaptation and precoding parameters. The bundling of these parameters across multiple CCs reduces this overhead but also leads to poorer spectral efficiency performance. Two CW mixing strategies allowing to average the SNR gain over multiple CCs have been proposed. They have shown to leverage the link performance when bundling is applied, and therefore the same spectral efficiency of no bundling transmission can approximately be achieved.

8.2 Recommendations

The investigations carried out in this PhD work justify the adoption of SC-FDM as air interface for the uplink of the 4th generation mobile communication systems. It has been shown indeed that SC-FDM can obtain approximately the same performance of OFDM, at the same time maintaining higher power efficiency. Advanced MIMO techniques such as transmit diversity and precoding

have been shown to provide SNR gain and are therefore worth to be included in the upcoming standard.

Since the low CM property of the SC-FDM signal is particularly advantageous in power limited scenarios, traditional SFC where the Alamouti principle is applied over adjacent subcarriers should be discarded for the uplink. On the other hand, the inclusion of STC can be critical when an odd number of time symbols in a frame are used for data transmission. Since the derived low CM SFC scheme provides SNR gain over SIMO only for small transport data blocks, it can be considered as a valid solution for Uplink Control Information (UCI). Moreover, the inclusion of a time symbol encoded with low CM SFC in a frame can overcome the constraints of STC.

Since only WB precoding has to be considered for a SC-FDM based interface, precoding is particularly suitable for low time dispersive channels, or for transmission of small transport data blocks. However, rank 1 precoding is still worth to be applied over frequency selective channels as Typical Urban in case of low speed, since it shows he same performance as STC without any constraint on the number of time symbols in a frame.

Receive diversity and array gain should be exploited in a SC-FDM air interface, since they also reduce the noise enhancement of this technology. Moreover, turbo detection should definitely be supported in the receiver. It improves indeed the spectral efficiency performance in single stream transmission, while in multi-stream transmission the removal of the interstream interference allows to leverage the diversity gain of the multiple receive antennas. Finally, the robustness to the AGI makes the turbo detection particularly envisable in MU-MIMO mode.

When transmission over multiple CCs occurs, the bundling of link adaptation and HARQ parameters over 2 CCs together with CW mixing has to be considered to reduce the feedback overhead. For higher number of CCs the degradation of spectral efficiency performance is instead visible for full rank transmission and linear receiver, while bundling and mixing can still be applied for turbo SIC reception. Similarly, a single precoding matrix can be applied over the whole CC set in case of large data blocks to be sent.

8.3 Future work

In this section we address some potential guidelines to continue the investigations carried out in this PhD work.

It is known that wireless networks with high frequency reuse may be strongly affected by the intercell interference. In case of non-synchronized networks as commonly assumed in FDD mode, uplink and dowlink transmission of different cells may interfere each other. In the linear and non-linear receiver design we only considered the white noise and the co-channel interference as performance limiting factors, but the transceiver chain can be optimized by assuming realistic asynchronous inter-cell interferers. As mentioned in Chapter 5, the presence of uplink/dowlink asymmetric interferers may also severely affect the performance of precoded MIMO in TDD mode, since the channel estimated in the downlink may be considerably different from the uplink channel. It is worth to notice that the impact of the interference on a SC-FDM based air interface is expected to be less critical than in OFDM, since the IDFT operation in the receiver can spread a localized interference component over the whole transmission bandwidth, thus "whitening" it. This should be however carefully modeled and evaluated.

Moreover, in this study we only considered *short term* precoding, i.e. the selection of the precoding matrix is made depending on *quasi*-instantaneous channel conditions, assuming low speed. The feasibility of a long term precoding operation, based for instance over the channel covariance matrix, has to be evaluated and compared with the presented open and closed loop solutions.

Coordinated Multi-Point (CoMP) transmission [110] is also a candidate technology for MU-MIMO in LTE-A. In the uplink, it assumes that multiple UEs can be simultaneously detected by two or more cooperating BSs, thus achieving macro diversity. Linking the physical layer studies with the system level design is essential to fully appreciate the potentialities of this technology. For instance, the UEs to be paired in MU-MIMO mode can be selected depending on the expected link performance when precoding and non-linear detection are used, and not only on traditional SNR metrics. In that sense, the codebook of precoding matrices can be further optimized when designed jointly with the scheduling algorithm.

Finally, RF optimization for transmission over multiple CCs occurs is an essential part of the transceiver design. Analog and digital filters have to be designed assuming that each UE can transmit over multiple CCs; high Adjacent Channel Leakage Ratio (ACLR) in case of channel aggregation is therefore required.

Appendix A

Link simulator structure and features

The LTE/LTE-A link simulator has been developed together with other colleagues in Aalborg University and Nokia Siemens Networks. Its validation has been carried out in [23] and [45]. In this PhD project, further features have been added concerning the uplink MIMO as well as the transmission over multiple component carriers. The simulator is based on MATLAB script and C language. In this Appendix a general description of the transceiver chain is provided, as well as the implementation details of fast link adaptation and HARQ and the modeling of the Radio Frequency (RF) impairments.

A.1 Transceiver chain

The basic transceiver chain in the LTE/LTE-A link simulator is depicted in Figure A.1. Note that, in case of MIMO, the whole chain can be replicated and further blocks such as precoder, layer mapper or transmit diversity encoder are needed. The different MIMO solutions are discussed in the report. Here, we simply describe the common operations which are required for the transmission of any CW. At the beginning of the chain, the CW is generated as a collection of random bits. The size of the CW depends on the selected modulation and

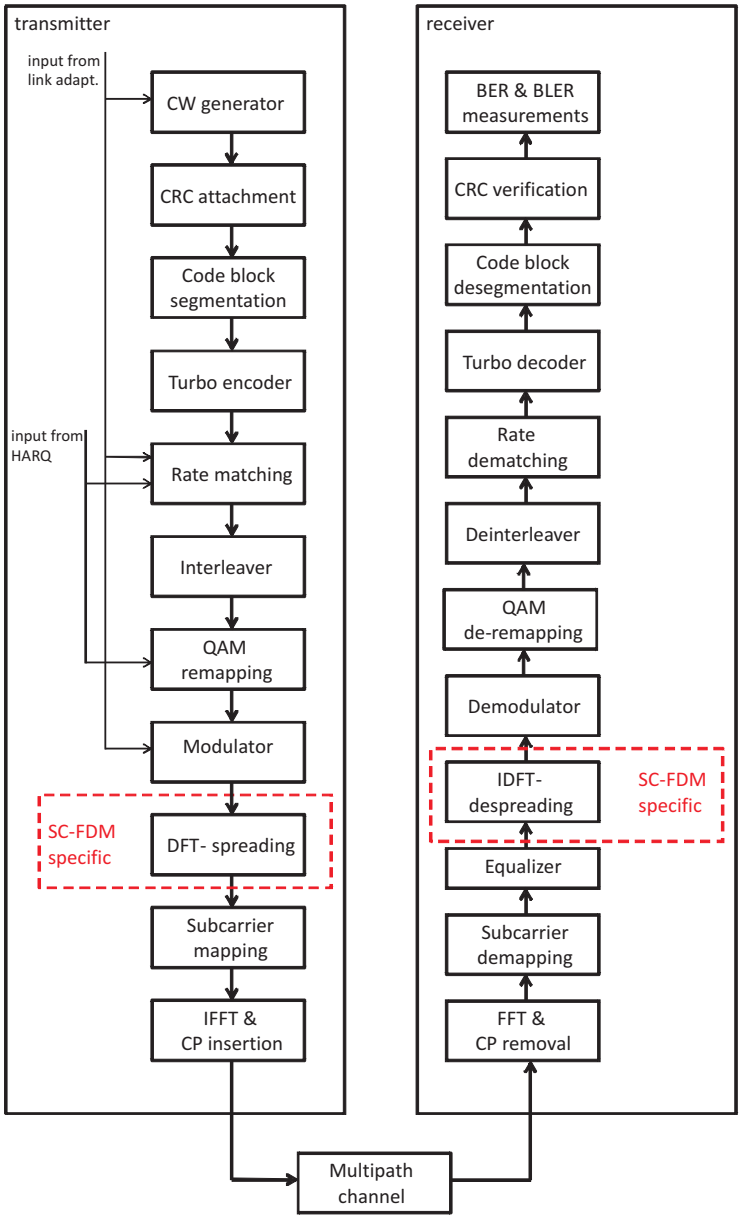

Figure A.1: LTE/LTE-A link level simulator.

coding scheme (MCS) which can be manually set, or communicated by the fast link adaptation module. Then, a Cyclic Redundancy Check (CRC) code is computed and appended at the end of the CW. According to the CW size and the maximum code block size, the CW may be split into several block. Each CW is subsequentely turbo encoded with a basic coding rate 1/3. This means, two parity bits are generated for each systematic bit. The rate matching block adjusts the bit rate according to the coding rate requirements. This is done by puncturing or repeating the input bit stream. Afterwards, the bit stream is interleaved and passed to the modulator, which maps them over data symbols belonging to BPSK, QPSK, 16QAM or 64QAM constellations. For QAM modulations, a remapping is performed to set the systematic bits at more reliable constellation points. In case of SC-FDM, a DFT spreading operation is applied over groups of symbols having size equal to the used subcarriers N_{sub}. Afterwards, the sets of N_{sub} samples are multiplexed with the pilot symbols, and mapped to the proper subcarriers. The traditional OFDM operations, i.e. IFFT and CP insertion, are therefore performed. Note that maximum code block size, puncturing and repeating patterns, modulation and interleaving are all set to be compliant with the 3GPP specifications [20].

At the receiver side, the reverse operations are carried out. The amplitude and phase-distortions introduced by the channel are compensated by the equalizer block. The demodulator generates a soft estimate of all the transmitted bits in the form of likelihood ratios, which are de-interleaved and fed to the turbo decoder. Issues concerning the computation of the likelihood ratios in OFDM and SC-FDM are faced in Section 3.5. The turbo decoder consists on two decoding stages exchanging iteratively soft information and separated by interleavers/de-interleavers. A max-log MAP suboptimal algorithm for each decoding stage is used to reduce the complexity with respect to the optimal MAP algorithm [111]. The resultant hard estimates of the systematic bits are then recombined in the original CW. The CRC-check verifies the correctness of the CW, so that the BLER statistics can be build. Similarly, the uncoded BER and coded BER are evaluated by comparing the transmit bit vector with the received one.

A.2 Fast Link Adaptation implementation

The Fast Link Adaptation, often referred as Adaptive Modulation and coding (AMC), is definitely one of the main features enabling efficient transmission in modern wireless networks. It allows to adapt at each time frame the amount of data to be sent to the instantaneous channel conditions by dynamically selecting the MCS at each transmission [16]. When the UE experiences poor radio link conditions, it will typically use low order MCSs (e.g., QPSK 1/6) to achieve

robustness to the noise and the channel fading; in case of a highly reliable channel it will use instead high order MCSs (e.g., 64QAM 4/5), allowing to leverage its throughput.

In our implementation, the Fast Link Adaptation module in the receiver selects for each CW the MCS to be used as the one leading to highest expected throughput with respect of a certain BLER target, i.e.

$$MCS_{sel} = arg\,max_i \{(1 - BLER_i) \times B_i \times ECR_i\} \tag{A.1}$$

subject to $BLER_i < BLER_{target}$, where B_i and ECR_i are the number of bits per symbol and the effective coding rate for the i-th MCS, respectively. The $BLER_i$ values for each MCS are obtained by mapping an effective Signal-to-Noise ratio (SNR) over AWGN curves [16]. The effective SNR is computed by exploiting an estimate of the SNR per each subcarrier obtained in a previous transmission.

For OFDM, the Exponential Effective SIR Mapping (EESM) model [112] is widely used for the computation of the effective SNR, which can be written as follows:

$$SNR_{eff} = -\beta \cdot ln \left(\frac{1}{N_{sub}} \sum_{k=0}^{N_{sub}-1} e^{-\frac{\lambda_k}{\beta}} \right) \tag{A.2}$$

where λ_k is the estimated data symbol SNR in the subcarrier k, β is a parameter which is estimated from extensive link level simulations for every MCS, and takes into account the sensitivity of the turbo decoder performance towards frequency selectivity.

In SC-FDM each data symbol is spread over the whole bandwidth by the DFT operation. This means, the effective SNR which is used in the BLER mapping corresponds to the data symbol SNR, which can be computed as follows [113]:

$$SNR_{eff} = \left(\frac{1}{\frac{1}{N_{sub}} \sum_{k=0}^{N_{sub}-1} \frac{\lambda_k}{\lambda_k+1}} - 1 \right)^{-1} \tag{A.3}$$

An Outer Loop Link Adaptation (OLLA) technique as described in [114] is also included to avoid incorrect decisions of the fast link adaptation module. The

aim of the OLLA is to stabilize the BLER target by adding an adaptive offset to the computed effective SNR, depending on whether the CW has been correctly detected. In case of correct detection, an up step size in the SNR domain is applied, otherwise a down step size.

A.3 Hybrid Automatic Repeat Request implementation

HARQ is a physical layer packet retransmission strategy which exploits the error detection capabilities of the 3GPP radio access technologies [18]. In LTE a cyclic redundancy code (CRC) is appended to the information bits of each CW to check if the detection process has been successful. In case of correct detection, an ACK message is sent to the UE through signaling, otherwise a NACK message is sent and the UE has to retransmit the CW. As mentioned in Chapter 1, HARQ reduces the latency between the retransmissions with respect to the traditional ARQ protocols at MAC layer. Two types of retransmission strategies are usually considered:

1. Chase combining (CCo): the same CW is used for both transmission and retransmissions. The *soft* values of the bits are stored and combined with the *soft* values of the re-transmitted CW. This is made with the aim of improving the reliability of the information bits.

2. Incremental redundancy (IR): in the transmitter different puncturing pattern as well as re-arrangements of the bits in the QAM constellation are applied to the re-transmitted CW. The soft combining is still applied at the receiver.

The IR option is expected to achieve higher gain than CCo, since besides the combining it also exploits some coding gain due to the retransmission of part of the punctured parity bits. Retransmissions are usually based on a Stop-and-Wait (SAW) protocol [115]. After a CW has been sent, the UE has to wait for the ACK/NACK message from the BS. In order to avoid idle periods due to pending ACK/NACK messages, the SAW protocol makes use of N parallel channels. Note that, when HARQ is used, the OLLA should only be applied at the first transmission [45].

A.4 Effect of radio-frequency imperfections in the transmitter

In a real transceiver chain, the baseband signal is fed to the radio-frequency (RF) front-end, which converts it to an analog signal oscillating at a certain carrier frequency and having a predefined power level. In the RF front end the non-linearity of the electronic components deteriorates the overall link performance with respect to the nominal baseband behaviour. The most common RF transceiver imperfections are the non-linear power amplifier, gain/phase imbalance, DC offset and phase noise. The effect of the RF impairments on the LTE uplink performance has been widely investigated in a previous PhD project [23]. The error vector magnitude (EVM) is considered as a direct measure of the signal quality, and it can be computed as follows:

$$EVM = \sqrt{\frac{\sum_{k=0}^{N_{sub}-1} |\mathbf{Z}[k] - \mathbf{R}[k]|^2}{\sum_{k=0}^{N_{sub}-1} |\mathbf{R}[k]|^2}} \cdot 100 \tag{A.4}$$

where $\mathbf{Z}[k]$ and $\mathbf{R}[k]$ are the kth complex baseband constellation point of the SC-FDM symbol and reference SC-FDM symbol, respectively. It has been shown that a white noise source generator with power equal to $10log_{10}(EVM)$ can fit the main RF imperfections in realistic EVM ranges (below 10%).

Appendix B

Channel Models

The realization of the multipath channel model is based on the implementation described in [116]. The channel models used in the link level studies in this dissertation are Typical Urban, Indoor office and SCMD. The Power Delay Profiles (PDPs) of the mentioned channels are shown in Table B.1, while their frequency correlation properties, obtained by DFT of the PDPs, are shown in Figure B.1.

The Typical Urban channel has a maximum delay spread of around 5 μs, turning to a coherence bandwidth of around 375 kHz (from inspection of the frequency correlation plot at value 0.6). As expected, the Indoor office channel model has a very low dispersivity, up to 200 ns and therefore the coherence bandwidth is much wider. SCMD channel model has instead a coherence bandwidth of around 1 MHz. All the presented channel shows good frequency correlation properties over a 20 MHz bandwidth, thus validating their usage in our simulations. Note that in the case of Typical Urban channel the frequency correlation properties are evaluated over a 60 MHz bandwidth. This is because this channel has also been used in the studies concerning the transmission over multiple CCs presented in Chapter 7. The suitability of this channel model for different FFT sizes is also tested through link level BLER studies, assuming SISO antenna configuration and an UE bandwidth of 300 subcarriers. As shown in Figure B.2, the BLER performance are not dependent on the selected FFT size (in particular, 20 MHz and 60 MHz cases are depicted).

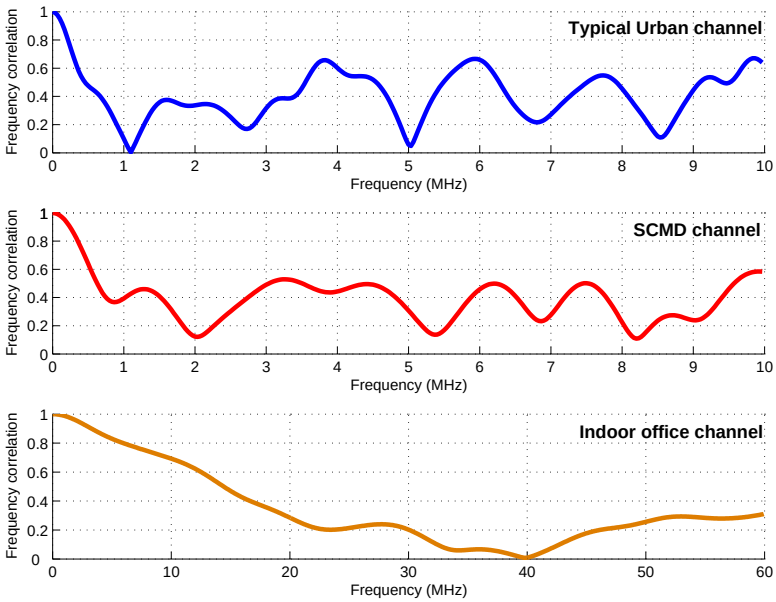

Figure B.1: Frequency correlation properties of the used channel models.

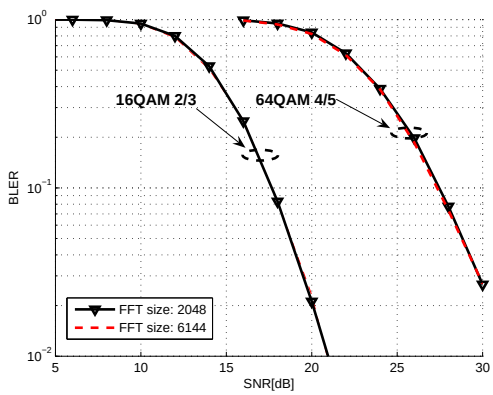

Figure B.2: BLER performance of SISO SC-FDM for Typical Urban channel, assuming UE bandwidth of 300 subcarriers and different FFT sizes.

Table B.1: PDP of the used channel models

N_p	Typical Urban		Indoor		SCMD	
	Delay(ns)	Power(dB)	Delay(ns)	Power(dB)	Delay(ns)	Power(dB)
1	0	-5.7	0	-2.2	0	-3
2	217	-7.6	5	-6.6	12.5	-5.22
3	512	-10.1	5	-2.1	25	-6.98
4	514	-10.2	5	-5.8	287.5	-4.27
5	517	-10.2	15	-3.3	300	-6.49
6	674	-11.5	15	-4.7	312.5	-8.25
7	882	-13.4	15	-4.1	200	-5.72
8	1230	-16.3	20	-8.2	212.5	-7.94
9	1287	-16.9	20	-3.0	225	-9.70
10	1311	-17.1	25	-5.2	662.5	-7.30
11	1349	-17.4	30	-7.0	685	-9.52
12	1533	-19.0	35	-4.6	697.5	-11.28
13	1535	-19.0	40	-6.8	812.5	-9.01
14	1622	-19.8	45	-8.6	825	-11.23
15	1818	-21.5	80	-10.0	837.5	-12.99
16	1836	-21.6	85	-12.1	925	-11.43
17	1884	-22.1	110	-12.4	937.5	-13.65
18	1943	-22.6	115	-11.8	950	-15.41
19	2048	-23.5	150	-20.4	-	-
20	2140	-24.3	175	-16.6	-	-

Appendix C

Evaluation of OFDMA/SC-FDMA in a multi-user scenario

In this appendix, we define a framework for the performance evaluation of OFDMA/SC-FDMA in a multi-user scenario. Scheduling solutions for OFDMA and SC-FDMA are discussed, and a simplified semi-analytical approach used to derive the results shown in Section 2.5 is also presented.

C.1 Channel Aware scheduling algorithms

Since OFDMA allows high freedom in resource allocation because no constraint on the contiguousness of the RBs is generally assumed, its optimal scheduling is based on a combinatorial comparison of all the possible allocations of RBs. Nevertheless, this solution is intractable because of its high computational complexity. A more practical greedy algorithm can be adopted [117], in which resources are allocated to the user that maximizes the marginal scheduling metric gain in each RB. Even for SC-FDMA the optimal scheduling solution is unapplicable. Here we propose a relatively low complex channel-aware scheduling algorithm for SC-FDMA, which is based on a recursive expansion of the

bandwidth to allocate to each user by starting from the maximum value of the scheduling metric. Considering as an input the matrix M, whose dimension is $[number\_of\_users, number\_of\_RBs]$ and whose entries represent all the user metrics for each RB, the steps of the proposed recursive maximum expansion (RME) algorithm are the following ones:

> [**Step 1**] Select the combination UE-RB with the highest metric value (UE_0-RB_0 in Figure C.1(a)); [**Step 2**] Assign RB_0 to UE_0; [**Step 3**] Expand the allocation in Step 2 for UE_0 both on the right- and left-hand side of M, until another UE with a better metric is found (UE_1 in Figure C.1(a)); [**Step 4**] Put UE_0 in idle mode; [**Step 5**] Repeat Steps 1-4 by searching for the maximum among the non-idled UEs (see Figure C.1(b)-(c)). Stop when all the UEs are idled or all RBs have been allocated; [**Step 6**] If not all RBs have been allocated, search for the UE with the maximum value of the metric among the remaining RBs; [**Step 7**] Check if one of the adjacent already assigned RBs belongs to the same UE found in Step 6; [**Step 8**] If the UE is not the same, delete this maximum from M and repeat Step 6. Otherwise, expand its allocation both on the right- and left-hand side of M until the contiguousness with the previous allocation is achieved on one side. Stop to expand on the other side whenever another (idled) UE having a higher metric value is found (see Figure C.1(d)); and [**Step 9**] Repeat Steps 6-8 until all RBs are allocated (see Figure C.1(e)).

C.2 Semi-analytical approach

Given the different nature of their signal generation as well as the different constraints in terms of resource allocation, OFDMA and SC-FDMA are expected to behave distinctly in a multi-user scenario. An evaluation of both access schemes performance can be done by focusing on their analytical behaviors or by means of system-level simulations. A fully-analytical approach becomes intractable though, if rigorously applied to a realistic scenario. As a consequence, in order to give our investigation a certain degree of generality and, at the same time, to keep it easily manageable, we opted for a trade-off between the two approaches. The evaluation has been therefore carried out following a semi-analytical approach. First, we simulate the scenario, i.e., generate user locations, fast fading channels, shadowing, path loss, etc. Then, based on the latter, we employ the scheduling algorithms described in Section C.1. Once the resource allocation is performed, the signal-to-noise ratio experienced by each user in the assigned

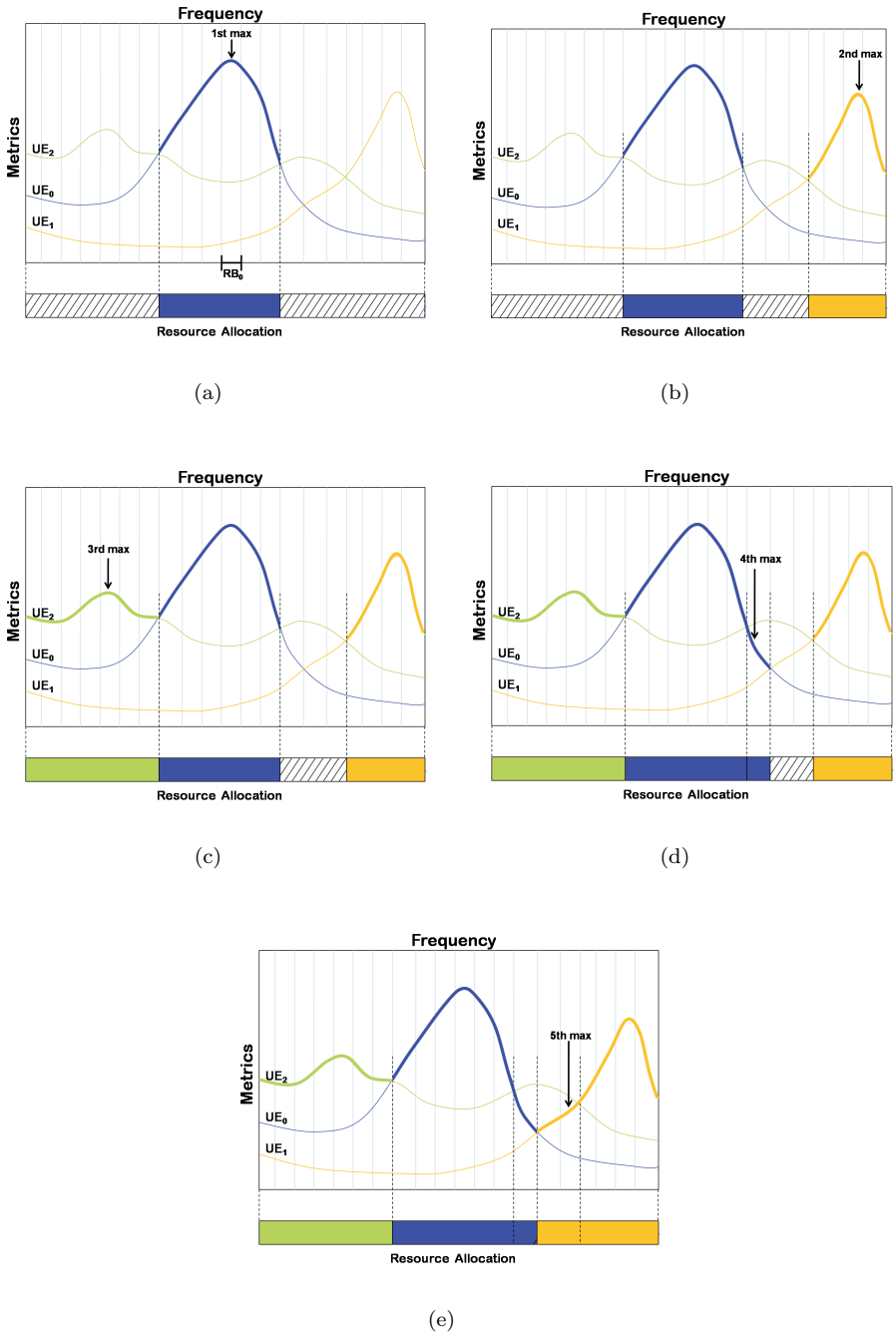

Figure C.1: RME scheduling algorithm for SC-FDMA, assuming 3 users.

resources is used in the analytical expressions below, in order to calculate the optimal spectral efficiency. In this way, we retrieve an upper bound that can give useful insights on the performance of the two access schemes.

We consider a simplified model where all UEs are assumed to transmit at the same power P_{max}, and where the transmit power per subcarrier of user j ($P_j^{(sub)}$) depends on the number of frequency resources allocated. For OFDMA, the data symbols are directly mapped over the subcarriers. Therefore, the maximum spectral efficiency of user j is simply obtained by summing up the maximum spectral efficiency values over the subcarriers within each RB assigned to that user. This gives:

$$S_{OFDMA,j}\left(P_{max}, I_{RB,j}\right) = \frac{1}{N_{RB}} \sum_{m \in I_{RB,j}} \frac{1}{N_{sub,RB}} \cdot \cdot \sum_{n \in N_{sub,RB}} log_2\left[1 + \gamma_{(m-1)N_{sub,RB}+n,j}\right] \quad \text{(C.1)}$$

where $N_{sub,RB}$ is the number of subcarriers per RB, $I_{RB,j}$ is the set of RBs assigned to user j, N_{RB} is the total number of RBs, and $\gamma_{k,j}$ is the SNR per subcarrier, defined as:

$$\gamma_{k,j} = \frac{P_j^{(sub)} \left|\mathbf{h}^j(k)\right|^2}{L_{loss,j}\left(\sigma_w^2 \Delta f\right)} \quad \text{(C.2)}$$

where $\left|\mathbf{h}^j(k)\right|^2$ is the channel gain of subcarrier k for user j, $L_{loss,j}$ is the path loss and shadowing term of user j, and Δf is the subcarrier spacing in Hz. Note that Eq.(C.1) implicitly assumes that a different modulation and coding scheme (MCS) can be used over each RB.

In SC-FDMA, the data detection is performed after the IDFT operation. Therefore, the upper spectral efficiency of a certain UE cannot be expressed as a linear sum of the upper spectral efficiencies over all the allocated RBs. The upper spectral efficiency of user j can instead be written as [118]:

$$S_{SC-FDMA,j}\left(P_{max}, I_{RB,j}\right) = \frac{|I_{RB,j}|}{N_{RB}} log_2\left[1 + \left(\frac{1}{\frac{1}{|I_{sub,j}|}\sum_{m \in I_{sub,j}} \frac{\gamma_{j,m}}{\gamma_{j,m}+1}} - 1\right)^{-1}\right] \quad \text{(C.3)}$$

where $|I_{RB,j}|$ is the number of RBs assigned to user j and $|I_{sub,j}|$ is the total number of subcarriers of user j[1]. It is worth to notice that in SC-FDMA an unique MCS can be used over the whole transmission bandwidth. These analytical expressions are used by the scheduler to compute the maximum spectral efficiency of each user in each RB. By means of these values, the scheduling metrics are calculated according, for instance, to the proportional fair (PF) criterion [17], which are then exploited by the scheduling algorithm. Finally, Eq.(C.1) and Eq.(C.3) are used in the final maximum spectral efficiency computation for each UE, given its assigned set of RBs.

[1]Eq. (C.1) and Eq. (C.3) have been obtained hypothesizing that the length of the CP is greater than the length of the discrete-time baseband channel impulse response, so that ISI and ICI are avoided.

Appendix D

Adaptive equalizer coefficients for the single stream turbo receiver

In this appendix, we derive analitically the forward and feedback coefficients for the adaptive equalizer in the single stream turbo receiver, which has been presented in Section 6.3.

In a SIMO system, the received signal at subcarrier k can be written as follows:

$$\mathbf{r}[k] = \mathbf{h}[k]\mathbf{d}[k] + \mathbf{w}[k] \tag{D.1}$$

where $\mathbf{h}[k]$ is the $N_R \times 1$ vector of the channel coefficients, $\mathbf{d}[k]$ is the transmit frequency sample, and $\mathbf{w}[k]$ is the noise vector.

Our goal is defining the forward coefficients $\mathbf{C}_{ff}$ and the feedback coefficient $\mathbf{C}_{fb}$ in the adaptive equalizer in order to minimize the mean square error between the transmit samples and their post-equalizer estimates. We therefore consider

the following optimization problem:

$$(\mathbf{C}_{ff}[k], \mathbf{C}_{fb}[k]) = arg\, min_{\mathbf{C}_{ff}[k], \mathbf{C}_{fb}[k]} E\left(\left|\mathbf{d}[k] - \mathbf{r}_{eq}[k]\right|^2\right) \tag{D.2}$$

for $k = 0, \cdots, N_{sub} - 1$, with the constraint

$$\frac{1}{N_{sub}} \sum_{q=0}^{N_{sub}-1} \mathbf{C}_{fb}[q] = 0. \tag{D.3}$$

We want to express the output of the adaptive equalizer as follows:

$$\mathbf{r}_{eq}[k] = \mathbf{C}_{ff}[k]\mathbf{r}[k] - \mathbf{C}_{fb}[k]\widehat{\mathbf{d}}[k] \tag{D.4}$$

where $\widehat{\mathbf{d}}$ is the available estimate of the transmit sequence. The cost function to minimize can be therefore expressed as

$$\varepsilon^2[k] = E\left(\left|\left(\mathbf{C}_{ff}[k]\mathbf{h}[k] - 1\right)\mathbf{d}[k] - \mathbf{C}_{fb}[k]\widehat{\mathbf{d}}[k] + \mathbf{C}_{ff}[k]\mathbf{w}[k]\right|^2\right) + \\ + \beta\left(\frac{1}{N_{sub}} \sum_{q=0}^{N_{sub}-1} \mathbf{C}_{fb}[q]\right). \tag{D.5}$$

Assuming that the transmit signals and their estimates are independent from the noise, we can rewrite Eq.(D.5) as

$$\varepsilon^2[k] = E\left(\left|\left(\mathbf{C}_{ff}[k]\mathbf{h}[k] - 1\right)\mathbf{d}[k] - \mathbf{C}_{fb}[k]\widehat{\mathbf{d}}[k]\right|^2\right) + \\ + \sigma_w^2 \left|\mathbf{C}_{ff}[k]\right|^2 + \beta\left(\frac{1}{N_{sub}} \sum_{q=0}^{N_{sub-1}} \mathbf{C}_{fb}[q]\right). \tag{D.6}$$

Since the samples of the soft estimates are independent due to the presence of

the bit-interleaver, we have:

$$E\left(\mathbf{d}[p]\mathbf{d}^*[q]\right) = \begin{cases} \sigma^2_{\widehat{d}} & if\ p = q \\ 0 & if\ p \neq q \end{cases} \tag{D.7}$$

where $\sigma^2_{\widehat{d}}$ is the variance of the estimated sequence. Eq.(D.6) can be therefore expressed as

$$\begin{aligned} \varepsilon^2[k] = \sigma^2_d \left|(\mathbf{C}_{ff}[k]\mathbf{h}[k] - 1)\right|^2 + \\ + \sigma^2_{\widehat{d}} \left(\left|\mathbf{C}_{fb}[k]\right|^2 - \mathbf{C}^H_{fb}[k]\mathbf{C}_{ff}[k]\mathbf{h}[k] - \mathbf{C}_{fb}[k]\mathbf{h}^H[k]\mathbf{C}^H_{ff}[k] + \mathbf{C}^H_{fb}[k] + \mathbf{C}_{fb}[k]\right) + \\ + \sigma^2_w \left|\mathbf{C}_{ff}[k]\right|^2 + \beta \left(\frac{1}{N_{sub}} \sum_{q=0}^{N_{sub}-1} \mathbf{C}_{fb}[q]\right), \end{aligned} \tag{D.8}$$

where σ^2_d is the variance of the transmit sequence. By setting $\frac{\delta\varepsilon^2[k]}{\delta C_{fb}[k]} = 0$ we have

$$\mathbf{C}_{fb}[k] = \mathbf{C}_{ff}[k]\mathbf{h}[k] - 1 - \frac{\beta}{\sigma^2_{\widehat{d}} N_{sub}}. \tag{D.9}$$

By applying the constraint in Eq.(D.3), we obtain

$$\beta = \sigma^2_{\widehat{d}} \left[\sum_{q=0}^{N_{sub}-1} \mathbf{C}_{ff}[q]\mathbf{h}[q] - N_{sub}\right]. \tag{D.10}$$

The optimum coefficients of the feedback filter are therefore given by

$$\mathbf{C}_{fb}[k] = \mathbf{C}_{ff}[k]\mathbf{h}[k] - \frac{1}{N_{sub}} \sum_{q=0}^{N_{sub}-1} \mathbf{C}_{ff}[q]\mathbf{h}[q]. \tag{D.11}$$

Similarly, setting $\frac{\delta\varepsilon^2[k]}{\delta \mathbf{C}_{ff}[k]} = 0$ yields:

$$\mathbf{C}_{ff}[k]\left[\left(\sigma_d^2 - \sigma_{\widehat{d}}^2\right)\|\mathbf{h}[k]\|^2 + \sigma_w^2\right] = \mathbf{h}^H[k]\left(\sigma_d^2 - \frac{\sigma_{\widehat{d}}^2}{N_{sub}}\sum_{q=0}^{N_{sub}-1}\mathbf{C}_{ff}[q]\mathbf{h}[q]\right), \tag{D.12}$$

where $\|\cdot\|$ denotes the Euclidean norm. Let us introduce now the following auxiliary variables:

$$\mathbf{P}[k] = \frac{\mathbf{h}^H[k]}{\left(\sigma_d^2 - \sigma_{\widehat{d}}^2\right)\|\mathbf{h}[k]\|^2 + \sigma_w^2} \tag{D.13}$$

$$\mu = \frac{1}{N_{sub}}\sum_{q=0}^{N_{sub}-1}\mathbf{P}[q]\mathbf{h}[q]. \tag{D.14}$$

The forward coefficients can be expressed as:

$$\mathbf{C}_{ff}[k] = \left(\sigma_d^2 - \frac{\sigma_{\widehat{d}}^2}{N_{sub}}\sum_{q=0}^{N_{sub}-1}\mathbf{C}_{ff}[q]\mathbf{h}[q]\right)\mathbf{P}[k]. \tag{D.15}$$

By defining

$$\lambda = \sigma_d^2 - \frac{\sigma_{\widehat{d}}^2}{N_{sub}}\sum_{q=0}^{N_{sub}-1}\mathbf{C}_{ff}[q]\mathbf{h}[q], \tag{D.16}$$

from Eq.(D.14) and Eq.(D.15) it follows that

$$\frac{1}{N_{sub}}\sum_{q=0}^{N_{sub}-1}\mathbf{C}_{ff}[q]\mathbf{h}[q] = \lambda\mu. \tag{D.17}$$

It is therefore straightforward to notice that

$$\lambda = \frac{\sigma_d^2}{1 + \sigma_{\widehat{d}}^2 \mu}. \tag{D.18}$$

Hence, we finally obtain

$$\begin{aligned}\mathbf{C}_{ff}[k] &= \frac{\sigma_d^2}{1 + \sigma_{\widehat{d}}^2 \mu} \frac{\mathbf{h}^H[k]}{\left(\sigma_d^2 - \sigma_{\widehat{d}}^2\right) \|\mathbf{h}[k]\|^2 + \sigma_w^2} = \\ &= \frac{\sigma_d^2}{1 + \frac{\sigma_{\widehat{d}}^2}{N_{sub}} \sum_{q=0}^{N_{sub}-1} \frac{\|\mathbf{h}[q]\|^2}{\left(\sigma_d^2 - \sigma_{\widehat{d}}^2\right) \|\mathbf{h}[q]\|^2 + \sigma_w^2}} \frac{\mathbf{h}^H[k]}{\left(\sigma_d^2 - \sigma_{\widehat{d}}^2\right) \|\mathbf{h}[k]\|^2 + \sigma_w^2}.\end{aligned} \tag{D.19}$$

Bibliography

[1] S. M. Redl, M. K. Weber, and M. W. Oliphant, *GSM and Personal Communications Handbook*. Artech House, 1998.

[2] P. Rysavy, "Mobile Broadband: EDGE, HSPA, and LTE," *Online material URL: http://www.itu.int/ITU-D/imt-2000/index.html*, September 2006.

[3] A. J. Viterbi, *CDMA: Principles of Spread Spectrum Communication*. Prentice Hall PTR, 1995.

[4] H. Holma and A. Toskala, *WCDMA for UMTS*. Wiley, 2001.

[5] ——, *HSDPA/HSUPA for UMTS*. Wiley, 2006.

[6] ——, *LTE for UMTS: OFDMA and SC-FDMA Based Radio Access*. Wiley, 2009.

[7] "Requirements for further advancements for E-UTRA LTE-Advanced," 3rd Generation Partnership Project, Tech. Rep. TR 36.913, V8.0.0, 2008.

[8] "LTE Physical Layer - General Description (Release 8)," 3rd Generation Partnership Project, Tech. Rep. TS 36.201, V8.2.0, 2008.

[9] L. Hanzo, M. Munster, B. Choi, and T. Keller, *OFDM and MC-CDMA for Broadband MultiUser Communications, WLANs and Broadcasting*. John Wiley - IEEE Press, 2003.

[10] H. G. Myung, J. Lim, and D. J. Goodman, "Single carrier FDMA for uplink wireless transmission," *IEEE Vehicular Technology Magazine*, vol. 2, no. 3, pp. 30–38, September 2006.

[11] "Text proposal for TR 36.814 on uplink transmission scheme," 3GPP, TSG-RAN WG1 Meeting #55bis,, Tech. Rep. R1-090532, January 2009.

[12] G. J. Foschini, "Layered space-time architecture for wireless communication in a fading environment when using multi-element antennas," *Bell Labs Technical Journal*, pp. 41–59, October 1996.

[13] I. E. Telatar, "Capacity of multi-antenna Gaussian channels," *European Transactions on Telecommunications*, vol. 10, no. 6, pp. 585–595, November 1999.

[14] A. Dabak, S. Hosur, and R. Negi, "Space time block coded transmit antenna diversity scheme for WCDMA," *IEEE Wireless Communications and Networking Conference*, vol. 3, pp. 1466–1469, September 1999.

[15] J. Winters, "On the capacity of radio communication systems with diversity in a Rayleigh fading environment," *IEEE Transactions on Communications*, vol. 5, no. 5, pp. 871–978, June 1987.

[16] A. Krishnamoorthy, Y. Blankenship, P. Sartori, K. Baum, and B. Classon, "Enhanced Link Adaptation methods for wireless multi-carrier systems," *IEEE 65th Vehicular Technology Conference, VTC2007-Spring*, pp. 1911–1915, April 2007.

[17] C. Wengerter, J. Ohlhorst, and A. von Elbwart., "Fairness and Throughput Analysis for Generalized Proportional Fair Frequency Scheduling in OFDMA," *IEEE 61th Vehicular Technology Conference, VTC2005-Spring*, pp. 1903–1907, June 2005.

[18] F. Frederiksen and T. E. Kolding, "Performance and modeling of WCDMA/HSDPA transmission/H-ARQ schemes," *IEEE 56th Vehicular Technology Conference, VTC2002-Fall*, pp. 472–476, September 2002.

[19] B. E. Priyanto, H. Codina, S. Rene, T. B. Sørensen, and P. Mogensen, "Initial performance evaluation of DFT-spread OFDM based SC-FDMA for UTRA LTE uplink," *IEEE 65th Vehicular Technology Conference, VTC2007-Spring*, pp. 3175–3179, April 2007.

[20] "Multiplexing and channel coding," 3rd Generation Partnership Project, Tech. Rep. TR 25.212, V8.0.0, 2007.

[21] "Performance of localized and distributed SC-FDMA," 3GPP, TSG-RAN WG1 Meeting #44, Tech. Rep. R1-060540, February 2006.

[22] S. Han and J. Lee, "An overview of peak-to-average power ratio reduction techniques for multicarrier transmission," *IEEE Wireless Communications*, vol. 12, no. 2, pp. 56–65, April 2005.

[23] B. E. Priyanto, *Air Interfaces of Beyond 3G Systems with User Equipment Hardware Imperfections.* PhD dissertation, Aalborg University, 2008.

[24] "LTE Cubic Metric," 3GPP, TSG-RAN4 Meeting #38, Tech. Rep. R4-060179, February 2006.

[25] "Comparison of PAR and Cubic Metric for Power De-rating," 3GPP, TSG-RAN4 Meeting #31, Tech. Rep. R4-040367, May 2004.

[26] H. Sari, G. Karam, and I. Jeanclaude, "Frequency-domain equalization of mobile radio and terrestrial broadcast channels," *IEEE Global Telecommunication Conference*, vol. 1, pp. 1–5, November 1994.

[27] J. Proakis, *Digital Communications,* 4th *edition.* Mc-Graw Hill, 2001.

[28] "Deployment aspects," 3rd Generation Partnership Project, Tech. Rep. TR 25.943, V6.0.0, 2005.

[29] D. Falconer, S. Ariyavisitakul, A. Benyamin-Seeyar, and B. Eidson, "Frequency domain equalization for single-carrier broadband wireless systems," *IEEE Communication Magazine*, vol. 40, no. 4, pp. 58–66, April 2002.

[30] W. Wang, T. Ottosson, M. Sternadt, A. Ahlen, and A. Svensson, "Impact of Multi-User Diversity and Channel Variability on Adaptive OFDM," *IEEE 58th Vehicular Technology Conference, VTC2003-Fall*, vol. 1, pp. 547–551, October 2003.

[31] "Winner II Channel Models," Tech. Rep. Winner II Deliverable 1.1.2 V 1.0 IST-4-027756, September 2007.

[32] C. Oestges and B. Clerckx, *MIMO Wireless Communications: from Real-World Propagation to Space-Time Code Design.* Academic Press, 2007.

[33] A. Paulraj, D. Gore, R. Nabar, and H. Bolckskei, "An overview of MIMO communications - a key to gigabit wireless," *Proceedings of the IEEE*, vol. 92, pp. 198–218, February 2004.

[34] R. Prasad, M. I. Rahman, S. Das, and N. Marchetti, *Single- and Multi-carrier MIMO transmission for Broadband Wireless Systems.* River Publishers, 2009.

[35] R. Heath and A. Paulraj, "Switching between multiplexing and diversity based on constellation distance," *Proceedings on Allerton Conference on Communciation, Control and Computing*, October 2000.

[36] P. Mogensen, W. Na, I. Kovacs, F. Frederiksen, A. Pokhariyal, K. Pedersen, T. Kolding, K. Hugl, and M. Kuusela, "LTE Capacity Compared to the Shannon Bound," *IEEE 65th Vehicular Technology Conference, VTC2007-Spring*, pp. 1234–1238, April 2007.

[37] "Layer Mapping for UL SU-MIMO in LTE-Advanced," 3GPP, TSG-RAN WG1 Meeting #56, Tech. Rep. R1-091102, February 2009.

[38] Q. Li and N. Ramesh, "Channel coding performance in CDMA2000 systems," *IEEE Emerging Technologies Symposium: Broadband, Wireless Internet Access*, 2000.

[39] I. Medvedev, B. Bjerke, R. Walton, J. Ketchum, M. Wallace, and S. Howard, "A Comparison of MIMO Receiver Structures for 802.11N WLAN - Performance and Complexity," *IEEE 17th International Symposium on Personal, Indoor and Mobile Radio Communications*, pp. 1–5, September 2006.

[40] H. Lee, B. Lee, and I. Lee, "Iterative detection and decoding with an improved V-BLAST for MIMO-OFDM systems," *IEEE Journal on Selected Areas in Communications*, vol. 24, no. 3, pp. 504–513, March 2006.

[41] Y. Li, "Pilot-symbol-aided channel estimation for OFDM in wireless systems," *IEEE Transactions on Vehicular Technology*, vol. 49, no. 4, pp. 1207–1215, 2000.

[42] B. Popovic, "Generalized chirp-like polyphase sequences with optimum correlation properties," *IEEE Transactions on Information Theory*, vol. 38, no. 4, pp. 1406–1409, July 1992.

[43] "Uplink Reference Signal in EUTRA," 3GPP, TSG-RAN WG1 Meeting #46bis, Tech. Rep. R1-062642, October 2006.

[44] P. Hoeher, S. Kaiser, and P. Robertson, "Two-dimensional pilot-symbolaided channel estimation by Wiener filtering," *IEEE International Conference on Signal Processing*, vol. 3, no. 3, pp. 1845–1848, April 1997.

[45] W. Na, *MIMO Techniques in UTRA Long Term Evolution.* PhD dissertation, Aalborg University, 2007.

[46] "System Level Evaluation of Synchronous and Asynchronous Hybrid Automatic Repeat Request (HARQ) for Uplink Single Carrier FDMA (SC-FDMA)," 3GPP, TSG-RAN WG1 Meeting #45, Tech. Rep. R1-061215, May 2006.

[47] S. Alamouti, "A simple transmit diversity technique for wireless communications," *IEEE Journal on Selected Areas in Communications*, vol. 16, no. 8, pp. 1451–1458, October 1998.

[48] B. Vucetic and J. Yuan, *Space-Time Coding.* Wiley, 2003.

[49] V. Tarokh, H. Jafarkhani, and A. Calderbank, "Space-Time Block Codes from Orthogonal Designs," *IEEE Transactions on Information Theory*, vol. 45, no. 5, pp. 1456–1467, July 1999.

[50] H. Jafarkhani, "A quasi-orthogonal space-time block code," *IEEE Transactions on Communications*, vol. 49, no. 1, pp. 1–4, January 2001.

[51] A. Laufer and Y. Bar-Ness, "Full Rate Space Time Codes for Large Number of Transmitting Antennas with Linear Complexity Decoding and High Performance," *IEEE Information Theory Workshop*, October 2009.

[52] E. Dahlman, S. Parkvall, J. Skold, and P. Beming, *3G Evolution: HSPA and LTE for Mobile Broadband (2nd ed.).* Academic Press, 2008.

[53] M. Rupp and C. Mecklenbrauker, "On extended Alamouti schemes for space-time coding," *The 5th International Symposium on Wireless Personal Multimedia Communications*, vol. 1, pp. 115–119, 2002.

[54] B. Vrigneau, J. Letessier, P. Rostaing, L. Collin, and G. Burel, "Statistical comparison between max-dmin, max-SNR and MMSE precoders," *Fortieth Asilomar Conference on Signals, Systems and Computers, 2006. ACSSC '06*, pp. 1611–1614, 2006.

[55] G. Golub and C. Loan, *Matrix Computation (3rd ed.).* Johns Hopkins University Press, Baltimore, MD, USA, 1996.

[56] P. Sampath, H. Stoica and A. Paulraj, "Generalized linear precoder and decoder design for MIMO channels using the weighted MMSE criterion," *IEEE Transaction on Communications*, vol. 49, no. 12, pp. 2198–2206, December 2001.

[57] A. Scaglione, P. Stoica, S. Barbarossa, G. Giannakis, and H. Sampath, "Optimal designs for space-time linear precoders and decoders," *IEEE Transaction on Signal Processing*, vol. 5, no. 5, pp. 1051–1064, May 2002.

[58] H. Määttänen, O. Tirkkonen, and K. Hugl, "Orthogonalizing transmission in MIMO with linear receiver and finite MCS set," *IEEE Wireless Communications and Networking Conference*, pp. 522–527, April 2008.

[59] G. Berardinelli, L. A. Maestro Ruiz de Temiño, T. B. Sørensen, P. Mogensen, and K. Pajukoski, "On the Feasibility of precoded Single User MIMO for LTE-A Uplink," *Journal of Communications*, vol. 4, pp. 155–163, April 2009.

[60] E. Sengul, H. Park, and E. Ayanoglu, "Bit-Interleaved Coded Multiple Beamforming with Imperfect CSIT," *IEEE Transactions on Communications*, vol. 57, no. 5, pp. 1505–1513, May 2009.

[61] A. Gersho and R. Gray, *Vector Quantization and Signal Compression.* Norwell, MA: Kluwer Academic, 1992.

[62] D. J. Love and R. W. Heath, "Limited feedback unitary precoding for orthogonal space-time block codes," *IEEE Transaction on Signal Processing*, vol. 53, no. 1, pp. 64–73, January 2005.

[63] ——, "Limited feedback unitary precoding for spatial multiplexing systems," *IEEE Transaction on Information Theory*, vol. 51, no. 8, pp. 2967–2976, August 2005.

[64] D. J. Love, R. W. Heath, and T. Strohmer, "Grassmannian beamforming for multiple-input multiple-output wireless systems," *IEEE Transaction on Information Theory*, vol. 49, no. 10, pp. 2735–2747, October 2003.

[65] O. Tirkkonen, K. Hugl, and Y. Teng, "Two-Tx Precoding Codebooks for Variable Spatial Correlation," *IEEE International Conference on Communications, ICC '09*, pp. 1–6, June 2009.

[66] P. Griffiths and J. Harris, *Principles of Algebraic geometry.* Wiley, 1978.

[67] S. Zhou and B. Li, "BER criterion and codebook construction for finite-rate precoded spatial multiplexing with linear receivers," *IEEE Transaction on Signal Processing*, vol. 54, no. 5, pp. 1653–1665, May 2006.

[68] "Codebook design for precoded MIMO," 3GPP, TSG-RAN WG1 Meeting #42, Tech. Rep. R1-060672, February 2006.

[69] R. Samanta and R. W. Heath, "Codebook Adaptation for Quantized MIMO Beamforming Systems," *Conference Record of the Thirty-Ninth Asilomar Conference on Signals, Systems and Computers*, pp. 376–380, November 2005.

[70] D. J. Love, R. W. Heath, V. K. N. Lau, D. Gesbert, B. D. Rao, and M. Andrews, "An overview of limited feedback in wireless communication systems," *IEEE Journal on Selected Areas in Communications*, vol. 26, no. 8, pp. 1341–1365, October 2008.

[71] B. Clerckx, Y. Zhou, and S. Kim, "Practical Codebook Design for Limited Feedback Spatial Multiplexing," *IEEE International Conference on Communications, ICC '08*, pp. 3982–3987, May 2008.

[72] R. Nabar, H. Bolcskei, V. Erceg, D. Gesbert, and A. Paulraj, "Performance of multiantenna signaling techniques in the presence of polarization diversity," *IEEE Transactions on Signal Processing*, vol. 50, no. 10, pp. 2553–2562, October 2002.

[73] "Codebook Design for E-UTRA MIMO Pre-coding," 3GPP, TSG-RAN WG1 Meeting #46, Tech. Rep. R1-062016, September 2006.

[74] "Final Report of 3GPP TSG RAN WG1 #56bis v1.0.0," 3GPP, Tech. Rep. R1-091671, March 2009.

[75] A. Householder, "Unitary Triangularization of a Nonsymmetric Matrix," *Journal of the ACM (JACM)*, vol. 5, pp. 339–342, October 1958.

[76] J. Kermoal, L. Schumacher, K. Pedersen, P. Mogensen, and F. Frederiksen, "A stochastic MIMO radio channel model with experimental validation," *IEEE Journal on Selected Areas in Communications*, vol. 20, no. 4, pp. 1211–1226, 2002.

[77] H. Sampath, S. Talwar, J. Tellado, V. Erceg, and A. Paulraj, "A fourth-generation MIMO-OFDM broadband wireless system: design, performance, and field trial results," *IEEE Communications Magazine*, vol. 40, no. 9, pp. 143–149, 2002.

[78] H. Asplund, J. Medbo, B. Goransson, J. Karlsson, and J. Skold, "A simplified approach to applying the 3GPP spatial channel model," *17th IEEE International Symposium on Personal, Indoor and Mobile Radio Communications (PIMRC '06)*, pp. 1–5, September 2006.

[79] "Discussion on Uplink SU-MIMO for LTE-Advanced," 3GPP, TSG-RAN4 Meeting #56, Tech. Rep. R1-090616, February 2009.

[80] H. Asplund, J.-E. Berg, F. Harrysson, J. Medbo, and M. Riback, "Propagation Characteristics of Polarized Radio Waves in Cellular Communications," *IEEE 66th Vehicular Technology Conference, VTC2007-Fall*, pp. 839–843, September 2007.

[81] Y. Zhao, R. Adve, and T. J. Lim, "Precoding of orthogonal STBC with channel covariance feedback for minimum error probability," *15th IEEE International Symposium on Personal, Indoor and Mobile Radio Communications*, vol. 1, no. 1, pp. 503–507, 2004.

[82] "UL-MIMO with Antenna Gain Imbalance," 3GPP, TSG-RAN WG1 #55bis, Tech. Rep. R1-090327, January 2009.

[83] "Consideration on rank 3 codebook design for UL SU-MIMO in LTE-A," 3GPP, TSG-RAN WG1 #58, Tech. Rep. R1-090357, August 2009.

[84] G. Lebrun, T. Ying, and M. Faulkner, "MIMO transmission over a time-varying TDD channel using SVD," *Electronic Letters*, vol. 37, no. 22, pp. 1363–1364, October 2001.

[85] G. Lebrun, J. Gao, and M. Faulkner, "MIMO transmission over a time-varying channel using SVD," *IEEE Transactions on Wireless Communications*, vol. 4, no. 2, pp. 757–764, March 2005.

[86] "MIMO OFDM in the TDD mode," Wireless World Research Forum, White Paper available at www.ww-rf.org, Tech. Rep.

[87] "Non-codebook-based Precoding for Uplink transmission," 3GPP, TSG-RAN WG1 #56, Tech. Rep. R1-090943, February 2009.

[88] L. Bahl, J. Cocke, F. Jelinek, and J. Raviv, "Optimal decoding of linear codes for minimizing symbol error rate," *IEEE Transactions on Information Theory*, vol. 20, no. 2, pp. 284–287, March 1974.

[89] B. Hu, I. Land, L. Rasmussen, R. Piton, and B. Fleury, "A Divergence Minimization Approach to Joint Multiuser Decoding for Coded CDMA," *IEEE Journal on Selected Areas in Communications*, vol. 26, no. 3, pp. 432–445, April 2008.

[90] C. Berrou, A. Glavieux, and P. Thitimajshima, "Near Shannon limit error-correcting coding and decoding: Turbo-codes." *IEEE International Conference on Communications, ICC '93*, vol. 26, pp. 1064–1070, May 1993.

[91] C. Douillard, M. Jezequel, C. Berrou, A. Picart, P. Didier, and A. Glavieux, "Iterative correction of intersymbol interference: Turbo Equalization," *European Transactions on Telecommunications*, vol. 6, no. 5, pp. 507–511, September 1995.

[92] B. Hochwald and S. Brink, "Achieving Near-Capacity on a Multiple-Antenna Channel," *IEEE Transactions on Communications*, vol. 51, no. 3, pp. 389–399, March 2003.

[93] Y. de Jong and T. Willink, "Iterative Tree Search Detection for MIMO Wireless Systems," *IEEE 56th Vehicular Technology Conference, VTC2002-Fall*, vol. 2, pp. 1041–1045, September 2002.

[94] C. Laot, R. Le Bidain, and D. Leroux, "Low-Complexity MMSE Turbo Equalization: A Possible Solution for EDGE," *IEEE Transactions on Wireless Communications*, vol. 4, pp. 965–974, May 2005.

[95] W. Ryan, "A Turbo Code Tutorial," *http://www.ece.arizona.edu/ ryan/.*

[96] D. Raphaeli and Y. Zarai, "Combined turbo equalization and turbo decoding," *IEEE Communications Letters*, vol. 2, no. 4, pp. 107–109, April 1998.

[97] C. Navarro Manchón, L. Deneire, P. Mogensen, and T. B. Sørensen, "On the Design of a MIMO-SIC Receiver for LTE Downlink," *IEEE 68th Vehicular Technology Conference, VTC2008-Fall*, pp. 1–5, September 2008.

[98] F. Vogelbruch and S. Haar, "Improved soft ISI cancellation for turbo equalization using full soft output channel decoder's information," *IEEE Global Telecommunication Conference*, vol. 3, pp. 1736 – 1740, October 2003.

[99] N. Benvenuto and P. Bisaglia, "Parallel and successive interference cancellation for MC-CDMA and their near-far resistance," *IEEE 58th Vehicular Technology Conference, VTC2003-Fall*, vol. 2, pp. 1045–1049, October 2003.

[100] A. Nakajima and F. Adachi, "Iterative joint PIC and 2D MMSE-FDE for Turbo-coded HARQ with SC-MIMO Multiplexing," *IEEE 63th Vehicular Technology Conference, VTC2006-Spring*, vol. 5, pp. 2503–2507, May 2006.

[101] P. Luethi, A. Burg, S. Haene, D. Perels, N. Felber, and W. Fichtner, "VLSI implementation of a high-speed iterative sorted MMSE QR decomposition," *IEEE International Symposium on Circuits and Systems (ISCAS 2007)*, pp. 1421–1424, May 2007.

[102] F. Edman and V. Owall, "A scalable pipelined complex valued matrix inversion architecture," *IEEE International Symposium on Circuits and Systems (ISCAS 2005)*, vol. 5, pp. 4489–4492, May 2005.

[103] H. Kim, W. Zhu, Bhatia, J. Karim Mohammed, A. Shah, and B. Daneshrad, "A Practical, Hardware Friendly MMSE Detector for MIMO-OFDM Based Systems," *EURASIP Journal on Advances in Signal Processing*, January 2008.

[104] "Uplink multiple access for LTE-Advanced," 3GPP, TSG-RAN WG1 Meeting #53bis, Tech. Rep. R1-082609, July 2008.

[105] L. G. U. Garcia, K. I. Pedersen, and P. Mogensen, "Autonomous component carrier selection: interference management in local area environments for LTE-Advanced," *IEEE Communications Magazine*, vol. 47, no. 9, pp. 110–116, September 2009.

[106] S. Kumar, Y. Wang, N. Marchetti, I. Kovacs, K. Pedersen, and P. Mogensen, "Spectrum Load Balancing for Flexible Spectrum Usage in Local Area Deployment Scenario," *3rd IEEE Symposium on New Frontiers in Dynamic Spectrum Access Networks, 2008. DySPAN 2008*, pp. 1–5, 2008.

[107] K. Takeda, S. Nagata, Y. Kishiyama, M. Tanno, H. Higuchi, and M. Sawahashi, "Investigation on Optimum Radio Parameters Design in Layered OFDMA for LTE-Advanced," *IEEE 69th Vehicular Technology Conference, VTC2009-Spring*, pp. 1171–1175, May 2008.

[108] "UL Transmission Bandwidth in LTE-Advanced," 3GPP, TSG-RAN WG1 Meeting #56, Tech. Rep. R1-090899, February 2009.

[109] G. Berardinelli, T. B. Sørensen, P. Mogensen, and K. Pajukoski, "Transmission over Multiple Component Carriers in LTE-A Uplink," *IEEE Wireless Communication Magazine, to be published.*

[110] S. Venkatesan, "Coordinating Base Stations for Greater Uplink Spectral Efficiency in a Cellular Network," *IEEE 18th International Symposium on Personal, Indoor and Mobile Radio Communications, PIMRC 2007*, pp. 1–5, 2007.

[111] J. Vogt and A. Finger, "Improving the max-log-MAP turbo decoder," *IEEE Electronic Letters*, vol. 36, no. 23, pp. 1937–1939, November 2000.

[112] "System-level evaluation of OFDM - further considerations," 3GPP, TSG-RAN WG1 Meeting #35, Tech. Rep. R1-031303, November 2003.

[113] S. Tingting, Z. Shidong, and Y. Yao, "Capacity of single carrier systems with frequency-domain equalization," *Proceedings of the IEEE 6th Circuits and Systems Symposium on Emerging Technologies: Frontiers of Mobile and Wireless Communication*, vol. 2, pp. 429–432, June 2004.

[114] M. Nakamura, Y. Awad, and S. Vadgama, "Adaptive control of link adaptation for high speed downlink packet access (HSDPA) in W-CDMA," *The 5th International Symposium on Wireless Personal Multimedia Communications*, vol. 2, pp. 382–386, October 2002.

[115] S. Kallel, "Efficient stop-and-wait type II hybrid ARQ scheme," *Electronic Letters*, vol. 28, no. 12, pp. 1097–1098, July 1992.

[116] L. Schumacher, J. Kermoal, F. Frederiksen, K. Pedersen, A. Algans, and P. Mogensen, "Mimo Channel Characterization," IST Project, IST-1999-11729, METRA Deliverable, Tech. Rep., February 2001.

[117] K. Kim, Y. Han, and S. Kim, "Joint Subcarrier and Power Allocation in Uplink OFDMA Systems," *IEEE Communication Letters*, vol. 6, no. 9, pp. 526–528, July 2005.

[118] J. Lim, H. G. Myung, K. Oh, and D. J. Goodman, "Channel-Dependent Scheduling of Uplink Single Carrier FDMA Systems," *IEEE 64th Vehicular Technology Conference, VTC2006-Fall*, pp. 1–5, September 2006.